NASA CONTRACTOR REPORT 166270

Study of Aerodynamic Technology for Single-Cruise-Engine V/STOL Fighter/Attack Aircraft

Final Report

Leon Mark
Rockwell International

CONTRACT NAS2-11002
February 1982

NASA CONTRACTOR REPORT 166270

Study of Aerodynamic Technology for Single-Cruise-Engine V/STOL Fighter/Attack Aircraft

Final Report

Leon Mark
Rockwell International
4300 E. Fifth Avenue
Columbus, Ohio 43216

Prepared for
Ames Research Center
under Contract NAS2-11002

National Aeronautics and
Space Administration

Ames Research Center
Moffett Field, California 94035

GREENVALT

T-38A

FOREWORD

This study of aerodynamic technology for single-cruise-engine V/STOL fighter/attack aircraft was conducted by Rockwell International from June 1981 through February 1982. The research study was sponsored by the United States Navy and the National Aeronautics and Space Administration under NASA Ames Research Center Contract NAS2-11002. The technical monitor was Mr. D. A. Durston of NASA Ames. Mr. M. W. Brown of the Naval Air Systems Command and Mr. J. H. Nichols, Jr. of the Naval Ship Research and Development Command supported the study.

The Rockwell Project Manager for this Phase I study effort was Mr. Leon Mark. The author wishes to acknowledge the assistance provided by Messrs. D. A. Durston, W. P. Nelms, and T. Gregory of NASA Ames and Messrs. J. D. Richardson, E. E. Kerrigan, D. R. Cichy, C. J. Carney, K. L. Irwin, D. C. Curtin, and E. F. Bonner of Rockwell International.

For the sake of clarity and understanding United States customary units have been used throughout in lieu of SI (Systeme Internationale) units. A conversion table is provided in the Symbols-Nomenclature section, page xiii for those who wish to use metric units.

CONTENTS

CONTENTS Continued

CONTENTS Continued

SUMMARY

During the past ten years a large number of configurations and concepts have been offered as solutions to the supersonic Vertical/Short Take Off and Landing (V/STOL) aircraft design problem. One of the most systematic efforts was conducted under the joint auspices of NASA Ames and the David Taylor Ship Research and Development Center and reported in Reference 1. The aircraft concepts investigated were all two-cruise-engine designs. Aerodynamic uncertainties were defined, and four models built to provide the aerodynamic data base necessary to resolve the uncertainties. The present study was undertaken to broaden the scope of these studies to include other advanced aerodynamic/propulsive concepts and their unique characteristics and uncertainties. This will provide a more complete aerodynamic data base for advanced fighter aircraft design.

Two supersonic V/STOL configurations have been conceived, refined, sized to a particular mission scenario, and analyzed in detail. The results of these analyses are presented herein. Also presented are the uncertainties that arose in predicting key aerodynamic characteristics and aero/propulsion interactions of these configurations. Finally a research program is proposed to resolve these uncertainties.

The configurations studied featured fore and aft thrust augmenting ejectors in a single large chord clipped delta wing. They evolved from advanced design studies Rockwell International has been conducting for the past several years on VTOL, STOL and CTOL fighter concepts.

These configurations were developed on the Rockwell Configuration Development System (CDS). Key conventional flight features of both configurations include a washout twist optimized for the supersonic cruise condition, an enlarged radius on the highly swept (subsonic) wing leading edge, and an automatic camber input with the wing trailing edge flap which is used for trim of the unstable airframe. In addition, the alternate configuration features a blunt trailing edge wing behind the aft augmenter which is treated to minimize its base drag.

Subsequent to the conceptual development, the aircraft were sized to meet all of the NASA guidelines and to accomplish 150 n.mi. Vertical Take Off (VTO) and 300 n.mi. Short Take Off (STO) Deck Launched Intercept (DLI) missions. The aircraft carried two long range Advanced Intercept Air-to-Air Missiles (AIAAMs) on the VTO mission and four AIAAM's on the STO mission. All missiles were semi-submerged on the fuselage.

Once the configurations were developed and sized, a detailed aerodynamic analysis was conducted on the Aerodynamic Preliminary Analysis System (APAS II). Performance sensitivities were evaluated to determine those parameters that contributed most significantly to the success of the designs. Available experimental data and/or empirical analyses were used to quantify the certainty with which the key parameters could be

predicted. From these investigations the most significant uncertainties were determined to be:

Base drag of two-dimensional blunt bases (subsonic-transonic-supersonic).

Wave drag of configurations with substantial lateral volume.

High angle of attack stability and control characteristics.

Canard trimmer-wing leading edge-inlet interference.

Drag-due-to-lift of variable camber configurations.

Effectiveness of wing tip mounted vertical tails on wings with highly swept leading edges.

High inlet operation at high angle of attack

- Effect of canopy proximity
- Effect of fuselage shape
- Effect of wing root shielding.

STOL aerodynamic characteristics of thrust augmenters.

In order to resolve these uncertainties, it is proposed to conduct wind tunnel tests from low subsonic speeds to M = 2.0 on a full span sting mounted model consisting of:

A common fuselage, inlet, and vertical tails

Two wings (baseline and alternate)

A forward fuselage plug at the inlet

An alternate canopy shape

Deflectable elevons, ailevators, and rudders

Three elevon sets - short chord, extended chord and blunt trailing edge

An all moveable canard at two longitudinal locations

Vertical tails on the wing tips or fuselage mounted

Forward fuselage strakes

Three trailing edge shape modifications on the alternate wing.

Wing leading edge vortex flap

An alternate forebody shape

SYMBOLS-NOMENCLATURE

a	-	Longitudinal Acceleration ~ Ft/Sec.^{2}	
a.c.	-	Aerodynamic Center	
AR	-	Aspect Ratio	
b	-	Wing Span	
c	-	Chord	
$\bar{c}$	-	Mean Aerodynamic Chord	
C_D	-	Drag Coefficient	$= \frac{D}{q\ S_{Ref}}$
C_{D_F}	-	Skin Friction Drag Coefficient	
C_{D_i}	-	Drag-Due-to-Lift Coefficient	
C_{D_0}	-	Zero Lift Drag Coefficient	
C_f	-	Flat Plate Skin Friction Coefficient	
C_{f_e}	-	Equivalent Skin Friction Coefficient	
C_ℓ	-	Rolling Moment Coefficient	$= \frac{\ell}{q\ S_{Ref}\ b}$
C_L	-	Lift Coefficient	$= \frac{L}{q\ S_{Ref}}$
C_m	-	Pitching Moment Coefficient	$= \frac{m}{q\ S_{Ref}\ \bar{c}}$
C_n	-	Yawing Moment Coefficient	$= \frac{n}{q\ S_{Ref}\ b}$
C_Y	-	Side Force Coefficient	$= \frac{Y}{q\ S_{Ref}}$
C.G.	-	Center of Gravity	

D	-	Drag ~ Pounds
D_1	-	Mutual Deflection of Inboard Flaps or Elevons ~ Degrees
D_2	-	Mutual Deflection of Outboard Flaps or Ailevators ~ Degrees
F.F.	-	Form Factor
g	-	Acceleration Due to Gravity ~ 32.2 ft/sec.^{2}
G.W.	-	Gross Weight ~ Pounds
ℓ	-	Rolling Moment ~ Ft-Pounds
ℓ	-	Length ~ Ft.
L	-	Lift ~ Pounds
L/D	-	Lift-to-Drag Ratio
m	-	Pitching Moment ~ Ft-Pounds
M	-	Mach Number
MAC	-	Mean Aerodynamic Chord ~ In.
n	-	Yawing Moment ~ Ft-Pounds
p	-	Roll Rate ~ Rad/Sec.
q	-	Dynamic Pressure ~ Pounds/Ft.^{2}
		(or) Pitch Rate ~ Rad/Sec.
r	-	Yaw Rate ~ Rad/Sec.
R_N	-	Reynolds Number
S	-	Area ~ Ft.^{2}
S_{Ref}	-	Reference Area ~ Ft^2 (usually = S_W)
S_W	-	Wing Area ~ Ft.^{2}
S_{Wet}	-	Wetted Area ~ Ft.^{2}

SYMBOLS-NOMENCLATURE (Continued)

T	-	Thrust
t/c	-	Thickness to Chord Ratio
T/W	-	Thrust to Weight Ratio
TOGW	-	Takeoff Gross Weight ~ Pounds
V	-	Freestream Velocity ~ Knots or Ft/Sec.
W	-	Weight ~ Pounds
W/S	-	Wing Loading ~ Pounds/Ft.^{2}
Y	-	Side Force ~ Pounds
α	-	Angle of Attack ~ Degrees
β	-	Sideslip Angle ~ Degrees
γ	-	Flight Path Angle ~ Degrees
δ_a	-	Roll Control Deflection = Differential Deflection of Outboard Ailevators ~ Degrees (Primary purpose of outboard surfaces or "ailevators" is for roll control; however, at low speeds, the ailevators can be mutually deflected for pitch control)
δ_e	-	Pitch Control Deflection = Mutual Deflection of Inboard Elevons ~ Degrees (Primary purpose of inboard surfaces or "elevons" is for pitch control; however, they can be deflected differentially for roll control)
δ_D	-	Augmenter Diffuser Half Angle
δ_M	-	Mean Augmenter Flap Deflection ~ Degrees
δ_r	-	Rudder Deflection ~ Degrees
ϕ	-	Bank Angle ~ Degrees
ϕ	-	Augmentation Ratio $= \frac{\text{Lift}}{\text{Nozzle Gross Isentropic Thrust}}$
θ	-	Pitch Attitude ~ Degrees

SYMBOLS-NOMENCLATURE (Continued)

λ - Taper Ratio

$\Lambda_{L.E.}$ - Leading Edge Sweep Angle ~ Degrees

$\Lambda_{c/4}$ - Quarter Chord Sweep Angle ~ Degrees

Metric Conversion Factors

Quantity	SI Units	Multiply by	To Obtain FPSR Units	Multiply by	To Obtain SI Units
Mass (M)	kg	6.852 (-2)	slug	1.459 (+1)	kg
Length (L)	m	3.281	ft	3.048 (-1)	m
Density (ρ)	kg/m^3	1.940 (-3)	$slug/ft^3$	5.155 (+2)	kg/m^3
Temperature (T)	°C + 273 °K	1.8	°F + 460 °R	5.556 (-1)	°C + 273 °K
Velocity (V)	m/sec km/hr	3.281 6.214 (-1)	ft/sec mi/hr	3.048 (-1) 1.609	m/sec km/hr
Force (F)	N kg m/sec^2	2.248 (-1)	lb slug ft/sec^2	4.448	N kg m/sec^2
Work Energy (J)	Nm (joule, J)	7.376 (-1)	slug ft^2/sec^2 Btu	1.356	Nm (joule)
Power (W)	Nm/sec (watt, W)	7.376 (-1) 1.341 (-3)	slug ft^2/sec^3 hp (550 ft lb/sec)	1.356 7.456 (+2)	Nm/sec (watt)
Pressure (p)	N/m^2 (pascal, Pa)	2.088 (-2)	slug/ft sec^2 lb/ft^2	4.788 (+1)	N/m^2 (pascal)
Specific Energy, etc	Nm/kg	1.076 (+1)	ft lb/slug	9.290 (-2)	Nm/kg
Gas Constant	Nm/kg °K	5.981	ft lb/slug °R	1.672 (-1)	Nm/kg °K
Coef. of Viscosity (μ)	kg/m sec	2.088 (-2)	slug/ft sec	4.788 (+1)	kg/m sec
Kinematic Viscosity (ν)	m^2/sec	1.076 (+1)	ft^2/sec	9.290 (-2)	m^2/sec
Thermal Conductivity (k)	N/sec °K	1.249 (-1)	lb/sec °R	8.007	N/sec °K
Heat Transfer Coefficient	N/m sec °K	3.807 (-2)	lb/ft sec °R	2.627 (+1)	N/m sec °K

LIST OF FIGURES

LIST OF FIGURES (CONTINUED)

LIST OF FIGURES (CONTINUED)

LIST OF FIGURES (CONTINUED)

LIST OF TABLES

1.0 INTRODUCTION

1.1 BACKGROUND

In 1972 Rockwell International was awarded a contract to build two prototypes of a supersonic V/STOL fighter using an innovative thrust augmenting ejector concept in the wings and canards. This concept folded the lifting system into a compact package suitable for supersonic flight and provided a far more benign temperature and pressure footprint than that experienced with pure thrust lifting systems. Augmenter research on similar concepts has been pursued by the NASA Ames Research center. The NASA Ames Research Center was tasked with the development of V/STOL technology in 1976, and in 1977 sponsored several studies, References 1-1 through 1-5, of V/STOL fighter attack aircraft to identify areas requiring further research. The basic objective was to fill in the aerodynamic data base for design of successful high speed V/STOL aircraft. These studies produced moderately large twin engine concepts. In order to broaden the aerodynamic data base, studies of smaller single-cruise engine concepts were commissioned by the Navy and the NASA Ames Research Center in June of 1981 to investigate the aerodynamic technology associated with several different concepts. The Navy/Marines have been operating a subsonic V/STOL aircraft for over 10 years, and have been investigating means to expand the mission and speed capabilities of V/STOL aircraft. Recent Navy studies, Reference 1-6, have shown advantages in dispersal and sortie rate for V/STOL aircraft from carriers, as well as improved close support capability from land bases.

1.2 OBJECTIVES

The objectives of the Phase I effort as reported herein were to:

1. Identify and analyze two unique high performance single-cruise engine V/STOL concepts that have the potential to fulfill the Navy fighter/attack role.

2. Estimate the aerodynamic, propulsion and performance characteristics of these configurations and assess the aerodynamic and aero/propulsion interaction uncertainties requiring additional research.

3. Define a wind tunnel model and test program to explore these uncertainties, and provide a high quality data base for design and evaluation of future high speed V/STOL and conventional aircraft configurations.

1.3 SCOPE

Two V/STOL configurations were studied. Both configurations used ejector thrust augmenters as the VTOL lifting system. The forward augmenters were oriented differently for the two configurations. The

baseline configuration used a spanwise forward augmenter similar to the aft augmenter, while the alternate configuration used a chordwise forward augmenter in the wing root. This led to differences in wing planform and airfoil shape. The fuselage and vertical tails were identical for both configurations. The configurations were refined during the conceptual design, and the unique advantages of each were explored. Emphasis, during the study, was placed on conceptual design and aerodynamic and propulsion analysis. Sufficient supporting work in weights, structures, avionics and controls was undertaken only to ensure credibility of the concepts. Likewise emphasis was placed on the development of conventional flight performance and STOL performance was studied to the extent necessary to assure credible assessment of the capability and that the capability was adequate to meet mission requirements.

1.4 STUDY PLAN

The major elements of the study plan consisted of defining the design requirements, selecting and refining the configuration concepts, sizing the configurations, analyzing the configurations, determining the aerodynamic and aero/propulsion uncertainties, and formulating a research program. A task flow diagram of this effort is depicted on Figure 1-1.

The conceptual design process was initiated with a definition of the V/STOL fighter/attack aircraft design requirements. The guidelines listed in the Statement of Work (SOW) were supplemented by supersonic (DLI) design missions, long range AIAAM weapons, an avionics suite, STOL capability, structural design limits, and other design criteria considered necessary to the realistic design of an aircraft.

In consideration of the guidelines and design requirements, single-cruise-engine V/STOL fighter/attack aircraft conceptual arrangements were input to the Rockwell Configuration Development System (CDS). This approach permitted a rapid development of the candidate configuration three-view around known components: cockpit, fixed equipment, engines, VTOL system, landing gear, etc. The system determined wetted areas and volume plots from which friction drag and wave drag were assessed. Candidate designs were formulated from two directions. The baseline concept utilized dual spanwise thrust ejector augmenters. The alternate concept began with Rockwell super-cruiser fighter configurations, and integrated a single spanwise thrust ejector augmenter combined with a chordwise augmenter to attain the V/STOL performance capability. The configurations were refined using the CDS analysis and design change capability along with linear lifting surface programs to minimize wave drag and drag due-to-lift. The refined baseline concept was selected for performance sizing. This step required design layouts of two different sized aircraft using the same cockpit and equipment and with sufficient detail to perform aerodynamic, propulsion, and weight analyses.

Using these geometric, aerodynamic, propulsion, and weights data, the concept was scaled to meet the mission and maneuvering requirements as well as the V/STOL requirements. This procedure involved the use of a vehicle sizing and performance evaluation program, which scales the

variable components of the aircraft while accounting for the corresponding changes in the aerodynamic, propulsion, and weight characteristics. The design load factor, flight design weight definition, and structural state-of-the-art factors were also inputs.

The resulting aircraft, sized as small as possible to meet all of the requirements, were then analyzed on the APAS II system, Reference 1-7. This system analyzes the complete longitudinal and lateral-directional stability and control characteristics of the configuration. The analysis includes wave drag due to lift, and wing leading edge and tip vortex effects.

Comparison of these analyses were made with selected analyses using the USAF DATCOM, Reference 1-8, and other semi-empirical methods. Sensitivities to various aerodynamic characteristics were determined, and areas of uncertainty defined. A wind tunnel model and test program were then conceived to evaluate all of these uncertainties throughout the speed range anticipated for the aircraft.

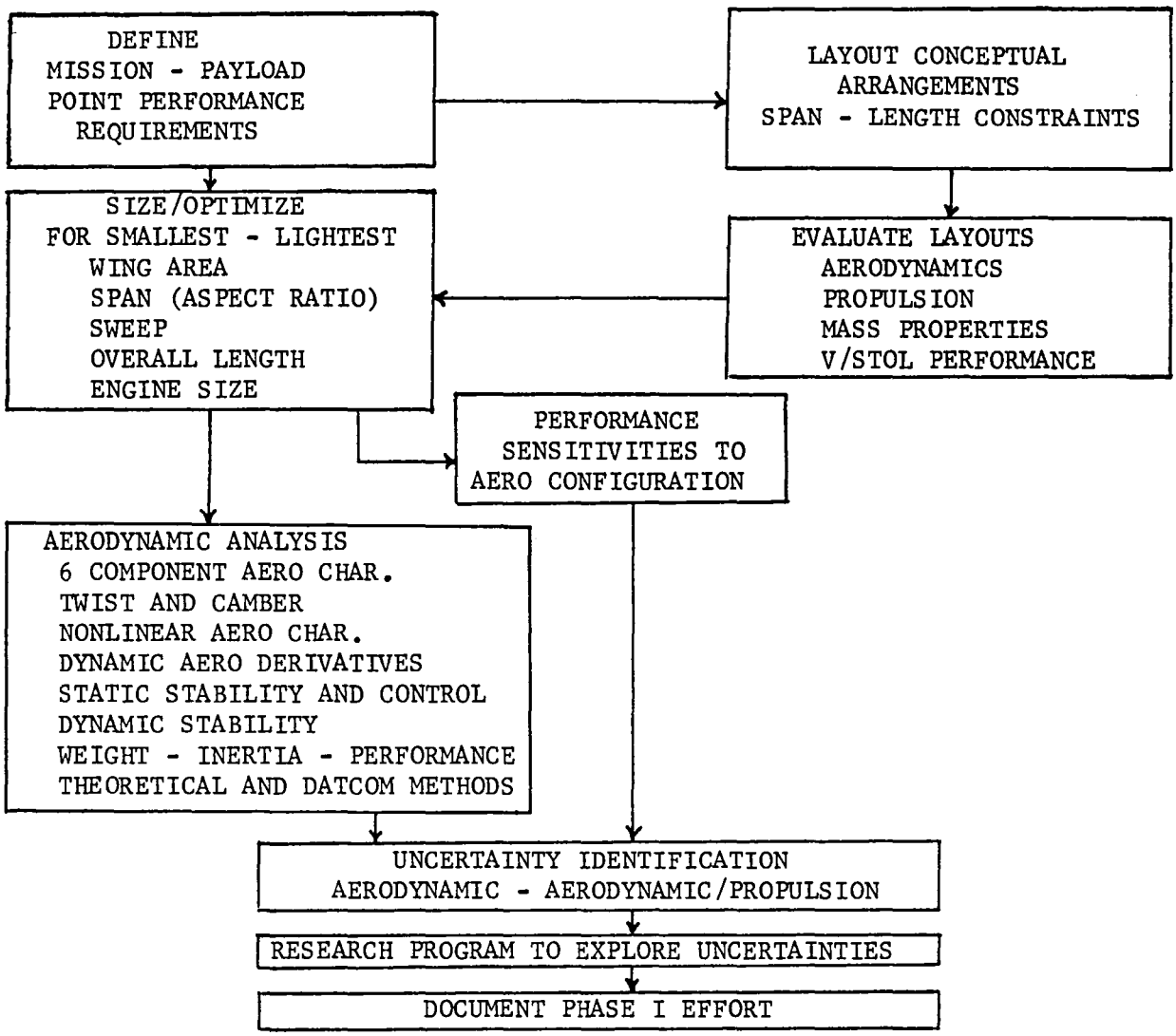

Figure 1-1 Phase I Task Flow

2.0 AIRCRAFT DESIGN

2.1 GUIDELINES

The capabilities desired of the configuration concept were outlined in the contract statement of work as:

High performance, single-cruise engine, VSTOL fighter/attack aircraft.

Supersonic dash capability with sustained Mach number capability of at least 1.6.

Operational from land and from ships smaller than CVs without catapults and arresting gear (good STO capability).

Sustained load factor of 6.2 at Mach 0.6, 10,000 feet altitude at 88 percent VTOL gross weight.

Specific excess power at 1G (PS1G) of 900 fps at Mach 0.9, 10,000 foot altitude at 88 percent VTOL gross weight.

VTOL gross weight of approximately 15,000 to 30,000 pounds.

STO sea-based gross weight = VTOL gross weight plus approximately 8,000 to 10,000 pounds.

Notes:
1. Techniques such as a ski jump may be proposed to achieve the STO requirements. Design implications imposed by such a mode of operation shall be considered.
2. The foregoing guidelines do not reflect future aircraft mission performance or operational usage requirements.

Other guidelines which must be set in order to uniquely define a point design are mission radius and armament loading. These items define the fuel load and ultimately the aircraft size. The missions selected to size the aircraft were a 1.6M run in 150 n.mi. VTO DLI mission and a 1.6M, 300 n.mi. STO DLI mission. The armament selected consisted of two long range AIAAM missiles for the VTO mission and four AIAAMs for the STO mission. Contracted and in-house operations analysis studies indicated the desirability for the 300 n.mi. supersonic DLI mission with long range missiles.

2.2 DESIGN PHILOSOPHY

The underlying design philosophy for this supersonic V/STOL fighter was to keep it as lightweight and simple as possible and still meet all of the aforementioned design guidelines. The number of configuration variables such as leading and trailing edge high lift devices, variable

ramp engine inlets, etc., were minimized. The advanced state-of-the-art in materials and structures projected for the 1995 time period were incorporated. The large chord, highly swept wing provided a relatively thick structure while presenting a relatively thin wing to the airstream (three to four percent t/c) for low wave drag.

High maneuvering performance was maintained through the low wing loading (45 lbs/ft^2) and relatively high thrust loading with maximum afterburner (1.5 T/W). Ejector thrust augmenters provided good vertical lift performance by augmenting the intermediate thrust 50 percent, while providing a low temperature and low pressure footprint. The single large chord, high swept, thin lifting surface provided a very low level of wave drag. Although it had significantly more surface area than previously considered wing-canard configurations, the friction drag in pounds was no greater due to the high Reynolds number provided by the long chord. This low friction drag and light wing loading allowed moderately high lift to drag ratios (about 11) to be achieved with the aspect ratio 1.8 wing. This is compatible with data shown for the AVRO Vulcan in Reference 2-1. The high leading edge sweep also allowed an oversized wing leading edge radius to be incorporated with little wave drag penalty. This relatively large leading edge radius (at the wing tip) provides about 90 percent leading edge suction at cruise conditions.

Synergism was incorporated wherever possible. For instance, the center of gravity was moved as far aft of the aerodynamic center (unstable) as possible to aid VTO balance and to provide an increasing camber (trailing edge down elevon deflection) with increasing angle of attack. At zero angle of attack no elevon deflection is required to trim so there is no camber drag penalty.

2.3 CONCEPT FORMULATION

Rockwell International has had on-going Independent Research and Development (IR and D) programs directed toward the development of high performance V/STOL and CTOL fighter/attack aircraft. About 10 years ago one of these V/STOL concepts was selected for prototyping by the United States Navy and designated the XFV-12A. This concept featured thrust augmenting ejectors in the wings and canards of a supersonic interceptor. The ejectors, as mentioned above, augment the engine intermediate thrust about 50 percent and provide a cool, low pressure footprint, as shown on Figure 2-1. This relatively benign footprint is very desirable for shipboard operations and makes operation from unprepared land bases more feasible than direct or vectored thrust concepts. A significant amount of contracted research and IR and D have contributed to the understanding of augmenter phenomena and to their practical applications.

IR and D and contracted research studies have also been conducted throughout this time period on the continued evolution of high performance V/STOL fighter/attack aircraft designs using the thrust augmenter wing concept. These studies, along with full and model scale reingestion evaluations, led to the incorporation of an inlet on top of the fuselage as shown on the advanced wing-canard configuration (-026E) of Figure 2-2.

The reingestion studies indicated that very little of the reingestion was coming from the auxiliary inlet on top of the fuselage. Concern over the conventional performance of such an arrangement was with the body cross flow, nose vortices, and canard-fuselage juncture effects on the quality of the airflow at the inlet. A small scale model wind tunnel test showed that a leading edge strake on the canard, illustrated on the -026E sketch on Figure 2-2, shielded the inlet from these undesirable flow fields and provided performance comparable to underfuselage inlets. Thus, the inlet was mounted on top of the fuselage for both baseline and alternate configurations.

This continuing IR and D effort led to the blended wing concept (-035C), as shown on Figure 2-2. This latter concept placed the wings and canards of earlier concepts in the same plane and connected them with structure to make a single lifting surface. This concept significantly reduced the wave drag of the entire configuration. The blended wing concept also permitted the use of simpler, lighter, higher performance rectangular augmenters. This was the baseline configuration proposed for this study. An alternate arrangement of the forward augmenter in a chordwise orientation to take advantage of the NASA Ames research on the chordwise augmenter was added.

High angle of attack wind tunnel tests were conducted, during the interval between the Reference 8-4 proposal submittal and contract award, with small models similar to the proposed baseline and alternate configurations. The favorable inputs from the wing tip mounted vertical tail of the baseline aircraft appeared to be lost at very low angles of attack. Therefore, the wing tip verticals were replaced with a highly swept wing tip similar to that on the alternate proposal configuration. Although the aerodynamic characteristics were better behaved, both aircraft exhibited pitch-up at high (30 degrees) angles of attack. However, both aircraft eventually (35 to 40 degrees of attack) exhibited a strong stable pitch down tendency from stall to 90 degrees angle of attack. These data and concerns as to the flexibility and related aeroelastic effects of these highly swept wing tips led finally to the modified wing tips of the study configurations, shown in Figure 2-2. In light of the wind tunnel data, it was decided to limit the relaxed static stability margin to about 5 percent MAC unstable to ensure the availability of pitch down control throughout the angle of attack range of zero to 90 degrees. This reduces the gain available from the camber input by the trailing edge elevon, and is probably a little conservative.

During the study, analyses were conducted to optimize the wing twist and camber. For the subsonic case they were both rather severe. It was decided to compromise in favor of the optimum supersonic twist, since the primary mission contained significant supersonic cruise. The camber was not incorporated, since the blunt subsonic leading edge provided good leading edge suction through most of flight envelope; some camber is introduced at subsonic speeds through the trailing edge (elevon) trim. It is noted that the baseline outboard panel is swept 65 degrees while the entire alternate configuration leading edge is swept 60 degrees.

For vertical takeoff the lift center must be compatible with the center of gravity location for 5 percent instability in the conventional flight mode. At the same time it was desired not to exceed 50 percent of the engine efflux to the smaller forward augmenter. In order to meet these diverse requirements the baseline aft augmenter was moved from its normal position at the aft flap toward the center of the wing chord. The alternate aircraft did not require this modification, since its forward chordwise augmenter could be located further forward than the spanwise forward augmenter of the baseline configuration. Pitch reaction controls were added to both configurations to provide a range of acceptable center of gravity locations for vertical takeoff (VTO). Obtaining the specification required VTO simultaneous control with only the thrust ejector augmenters, resulted in a single center of gravity location for maximum VTO performance. The pitch reaction controls increased vertical takeoff capability while keeping the simultaneous control power in reserve.

Moving the baseline aft augmenter forward allowed a more conventional shallow trailing edge angle than could be realized with the aft augmenter location. The aft augmenter arrangements have characteristically used a small amount of bluntness, about 1/2 to 1 percent of the wing chord, to relieve the otherwise steep trailing edge angle. The base drag for this amount of trailing edge bluntness is very small as shown in References 2-2 and 2-3, since the blunt trailing edge is immersed in the boundary layer. The alternate configuration uses a much larger blunt base to reduce the trailing edge angle substantially. Research conducted by the contractor and others, Reference 2-4, shows that the drag of significantly blunt based airfoils can be greatly reduced by trailing edge treatment such as splitter plates. It is anticipated that the base drag can be eliminated by the proper combination of trailing edge treatments. It is also expected, based on past research, that the blunt based elevon will exhibit increased control effectiveness over that estimated.

The latest, baseline and alternate, configurations in this continuing evolution are shown on Figure 2-2. These aircraft were initially scaled out at 29,000 pounds. Conceptual analyses indicated they would easily exceed the 150 nautical mile (n.mi.) vertical takeoff (VTO) Deck Launched Intercept (DLI) mission, and the 300 n.mi. Short Takeoff (STO) mission. A version of the baseline aircraft was scaled down on the Rockwell Configuration Development System (CDS), keeping the fuselage nose and cockpit the same and varying the rest of the airplane. Using these two sizes of the baseline aircraft, a parametric evaluation was conducted in order to select a near optimum. The scale one engine had a sea level tropical day thrust rating of 24,000 pounds, and the scale one wing area was 684 square feet (-20 point on Figure 2-3). The smaller design had a 20,000 pounds thrust (scale .833) engine with a wing area .833 of the larger (-22 point on Figure 2-3). These two aircraft established the scaling factors that permitted excursions in scaling from .7 to 1.1 size.

The resulting matrix of aircraft all sized to perform the 150 n.mi. Deck Launched Intercept mission are presented in Figure 2-3. Two limit lines have been superimposed upon the matrix. The vertical takeoff limit

defines the minimum engine and wing sizes for vertical takeoff. The 300 n.mi. STO mission requirement utilizes the maximum fuel capacity of each aircraft. This capacity is defined primarily by the wing size since the fuselage capacity does not change. The STO limit represents the smallest wing that will support the radius requirement. A baseline aircraft was selected, as shown on Figure 2-3, within these limits at a wing scale of .76 and engine scale of .83 to allow for some growth during the more detailed preliminary analysis. This initial baseline had a design takeoff weight of 23,900 pounds. The same engine fuselage and wing size were used for both configurations. As detailed weights were determined, the aircraft grew slightly, the baseline to 25,025 pounds and the alternate to 24,300 pounds. Since some growth capability had been allowed for, they did not have to be resized.

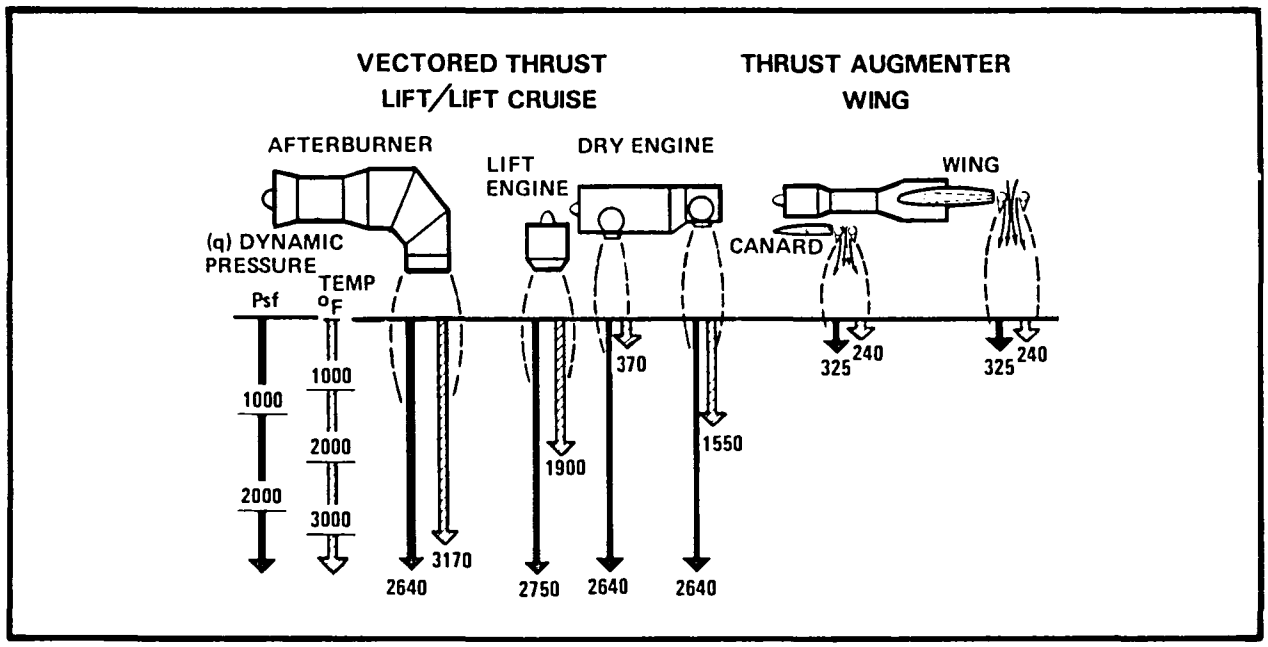

Figure 2-1 Footprint Comparison

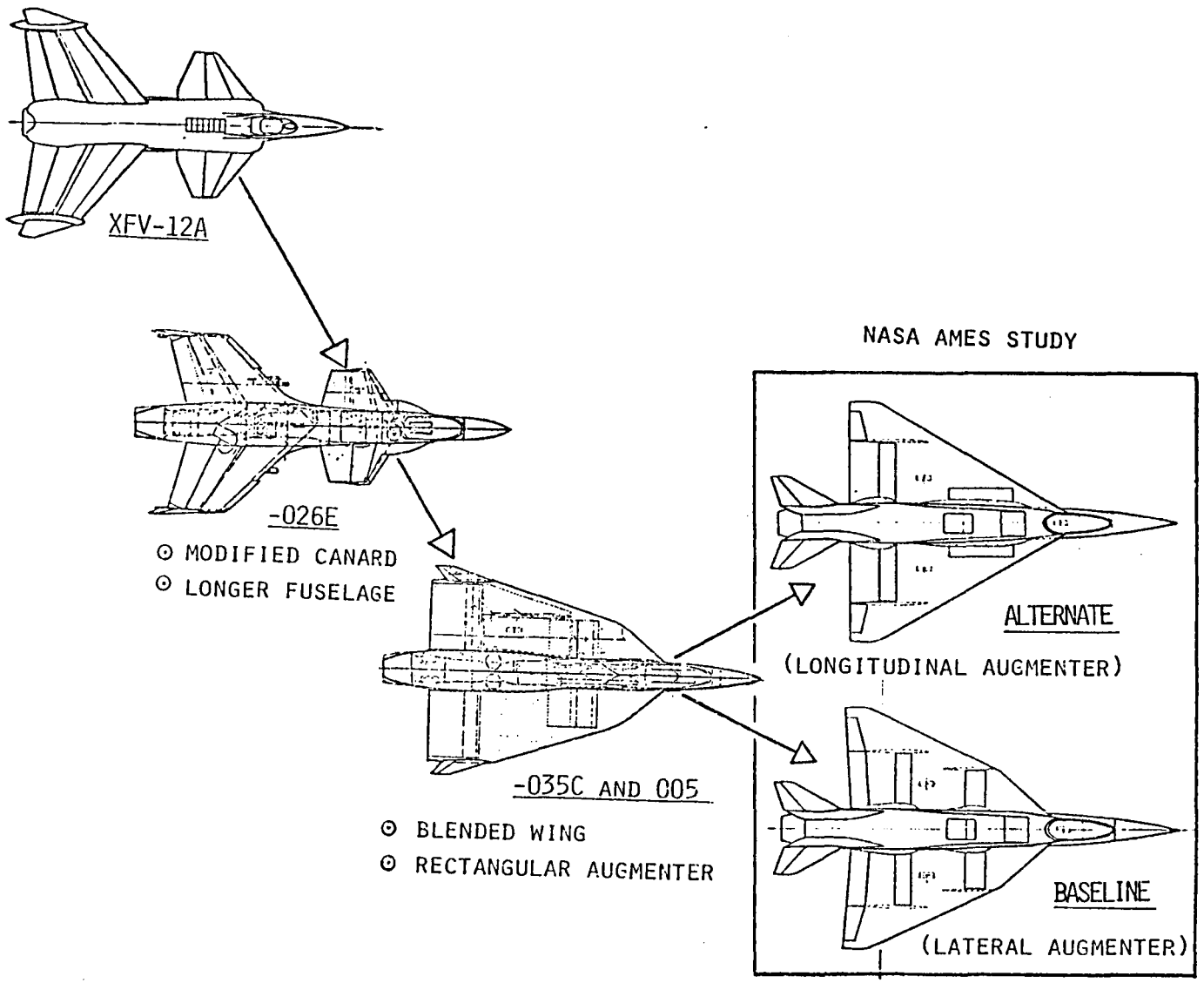

Figure 2-2 Design Evolution

⊙ -20 -22 PRELIMINARY DESIGNS USED FOR SCALING

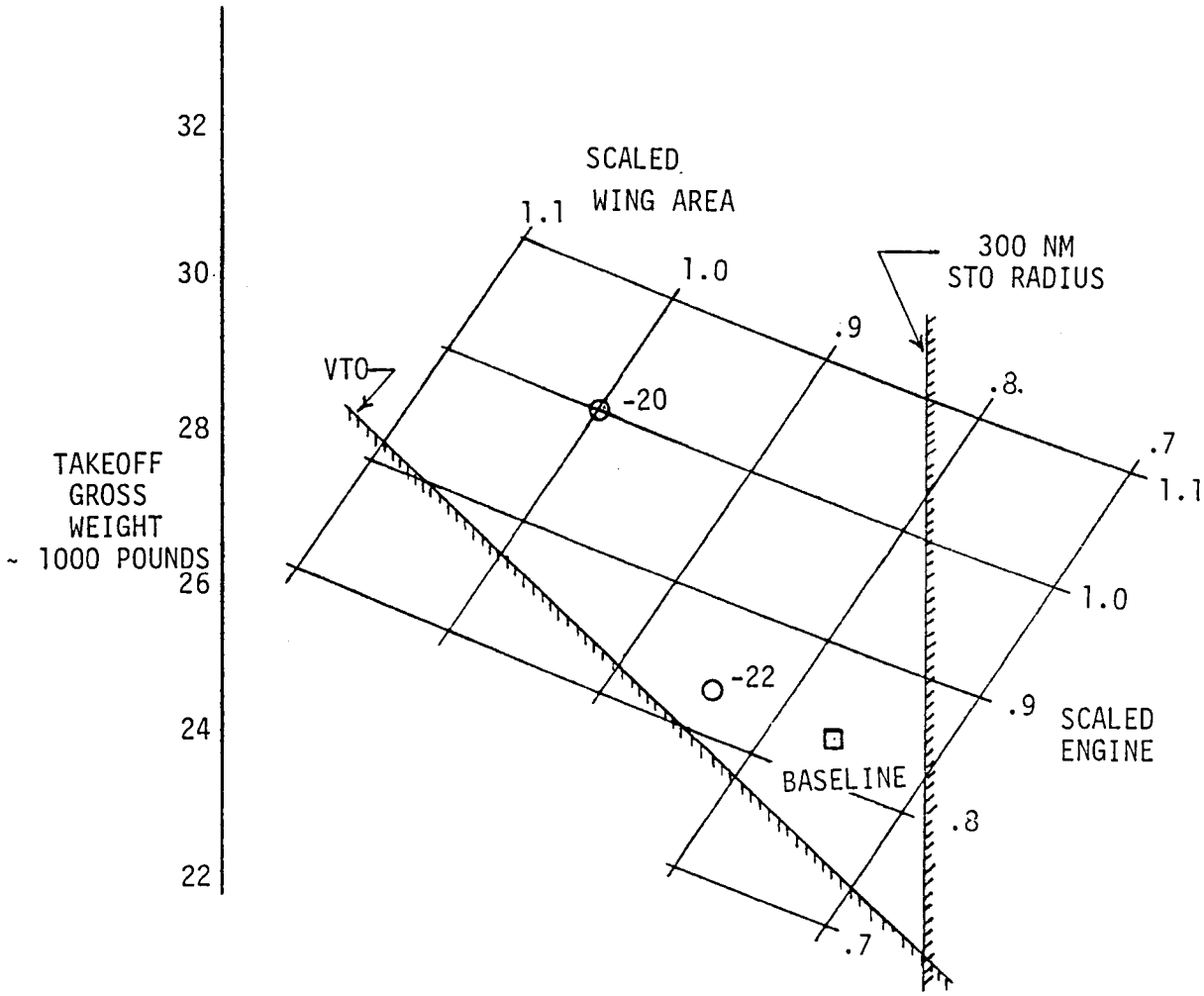

Figure 2-3 Aircraft Sizing Carpet Plot

3.0 AIRCRAFT DESCRIPTION

3.1 AIRCRAFT DESCRIPTION

3.1.1 Baseline Configuration

The exterior arrangement of the baseline aircraft is illustrated in Figure 3-1 and is designated 141-023Q. A definition of the wing outer panel twist (about the 65 percent chord element) is shown in Figure 3-2.

3.1.2 Inboard Profile

The fuselage exterior lines including the vertical stabilizers are identical for both the baseline (-023Q) and alternate (-002F) configurations. Powerplant location and most of the augmenter ducting installations are identical for both configurations. The differences exist primarily in the forward augmenter primary flow manifolding which would not effect the exterior fuselage lines. The fuselage inboard profile is illustrated in Figure 3-3 and is designated 84884-002F-1.

3.1.3 Alternate Configuration

The exterior arrangement of the alternate aircraft is illustrated in Figure 3-4 and is designated 84884-002F. A definition of the wing outer panel twist for this alternate configuration is shown in Figure 3-5.

3.1.4 Armament

Nine store stations have been allocated for both the baseline and alternate V/STOL configurations. Since the fuselage contours of both versions are identical, the fuselage store stations are likewise identical, as are the wing tip mounted SRAAM rail stations. The intermediate wing stations (3R, 3L as shown in Figure 3-6) differ in wing spanwise location due to wing planform and augmenter endplate differences. The baseline intermediate wing stations are located at WS 108 and the alternate locations are further inboard at WS 80. Two additional outboard wing stations (one per side) may be possible on the alternate configuration -002F.

The advanced weapons depicted (Figure 3-6) are as follows:

AIAAM	-	Advanced Intercept Air-Air Missile
AMRAAM	-	Advaned Medium Range Air-Air Missile
SRASM	-	Short Range Air - Surface Missile
SRAAM	-	Short Range Air-Air Missile

The HARPOON is an existing air-surface missile intended for anti-shipping use while HARM is an anti radiation (RADAR) misssile which is now under hardware development.

Space is available on the upper fuselage for two upward ejection, semi-submerged AAM stations and would be valuable assets to relatively small fighters such as the subjects of this study. Practical application of this concept would, however, require prior development and flight test to determine satisfactory ejection/separation envelopes. A related upward ejection study is underway at Rockwell International, entitled "Low Level Delivery System," under USAF Contract F08635-80-C-0307.

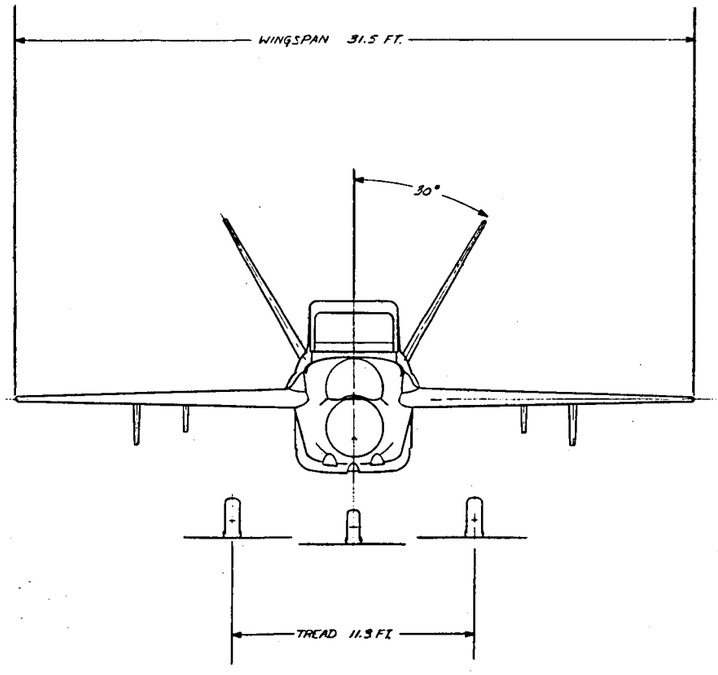

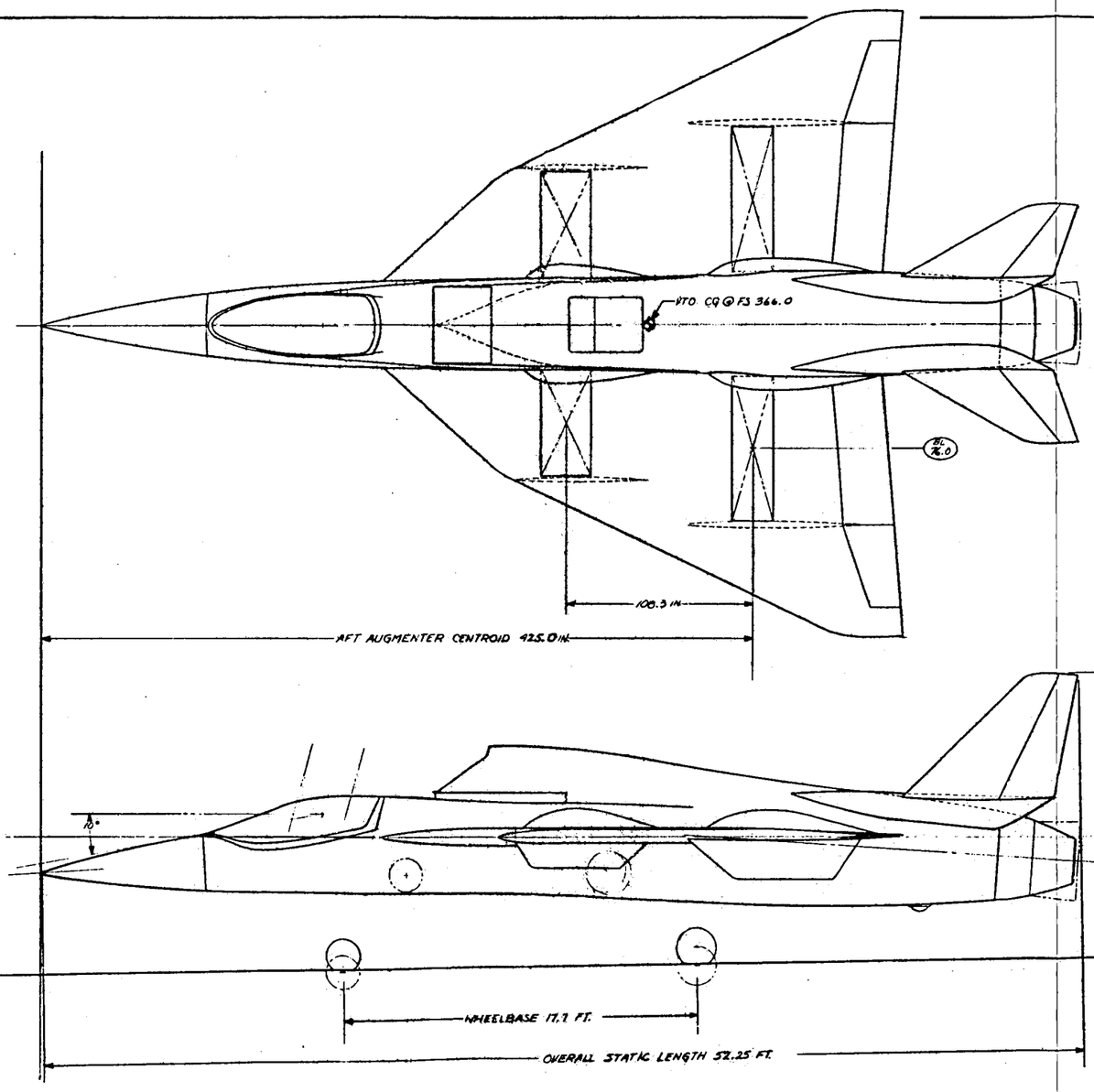

BASELINE AIRCRAFT GEOMETRY

			WING	VERT. STAB.
AREA	(REF) SQ. FT.		541.	36.7
	(EXPOSED) SQ. FT.		422.9	--
ASPECT RATIO			1.8	1.41
SPAN		FT.	31.5	7.2
TAPER RATIO	(INBOARD/OUTBOARD)		.715/.164	.33
CHORD	(CENTERLINE)		329.2	--
	(ROOT)	IN.	301.0	92.2
	(TIP)	IN.	38.5	30.6
	(MAC)	IN.	241.6	66.5
SWEEP	(LE)	DEG.	48/64	41.6
THICKNESS RATIO	(ROOT)		.038	.04
	(TIP)		.034	.04
DIHEDRAL		DEG.	0	60
INCIDENCE		DEG.	0	0
TWIST (WASHOUT)		DEG.	-4	0

AUGMENTER GEOMETRY

		FWD	AFT
A_2 - INLET AREA	(SQ. IN.)	1945	2161
A_2/A_Q - INLET AREA RATIO		14.0	20.5
ℓ/d - DIFFUSER LENGTH TO THROAT WIDTH RATIO		1.6	1.5
AR - ASPECT RATIO		2.2	3.6

SCALE 1/40	DWN E. KERRIGAN	Rockwell International Corporation North American Aircraft Division Columbus, Ohio 43216
FSCM NO. 89372	DATE 12-18-81	
	MODEL N/A	
BASELINE V/STOL FIGHTER (LATERAL-FORWARD AUGMENTER)		141-0230

FIG. 3-1
3-3/3-4

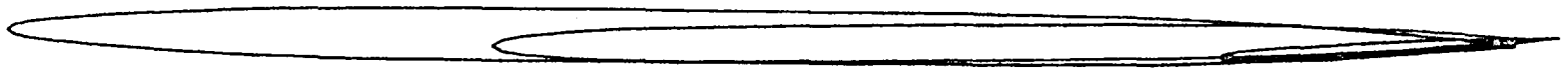

LEADING EDGE RADIUS = .235 INCH CONSTANT

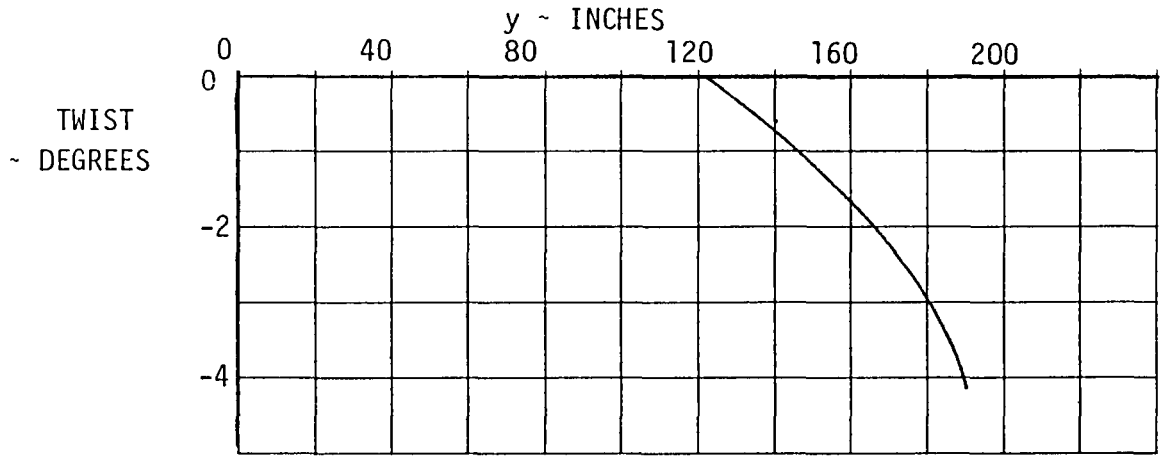

Figure 3-2 Twist Distribution for Baseline Configuration

FS 0 · FS 100.0 · FS 135.0 · FS 171.0 · FS 202.9 · FS 300.0 · FS 342.2 · FS 359.1 · FS 450.5 · FS 482.6 · FS 573.1 · FS 578.5

20°

CENTERBODY DEPLOYED TO VTOL POSITION (TYPICAL - 4 PLACES)

AUXILIARY INLET

MOST AFT CG. FS 575.1 WL -3.9

P&W TYPE L-230588 90° CLAMSHELL DIVERTER

FS 627.2

EJECT. CLEARANCE 30 in

INLET AREAS
CAPTURE: 1106 SQ.IN.
THROAT: 990 SQ.IN

FRP

10°

FRP

1° THRUST

FWD PITCH TRIM/CONTROL NOZZLE

STRUT COMPRESSED DURING RETRACTION

FS 521.4

AFT PITCH TRIM/CONTROL NOZZLE

STRUTS BOTTOMED, TIRES FLAT

STATIC GROUND LINE (-1°)

ADVANCED INTERCEPT AIR/AIR MISSILE WITH LAU-92 LAUNCHER

FS 182.0

20 x 6.6-10

FS 377.8

AERO I-C 200 GAL ℄ TANK (ALTERNATE TO AIAAM)

24 x 8-12

.62 SCALE V8051 ADVANCED P&W TURBOFAN

ENGINE MOUNTED ACCESSORY DRIVE

SCALE 1/20	DWN E. KERRIGAN	Rockwell International Corporation North American Aircraft Division Columbus, Ohio 43216
FSCM NO. 89372	DATE 15 DEC. 1981	
	MODEL N/A	
FUSELAGE INBOARD PROFILE SHOWING KEY INSTALLATION DETAILS (141-0230 SIMILAR)		84884-002F-1

FIG. 3-3

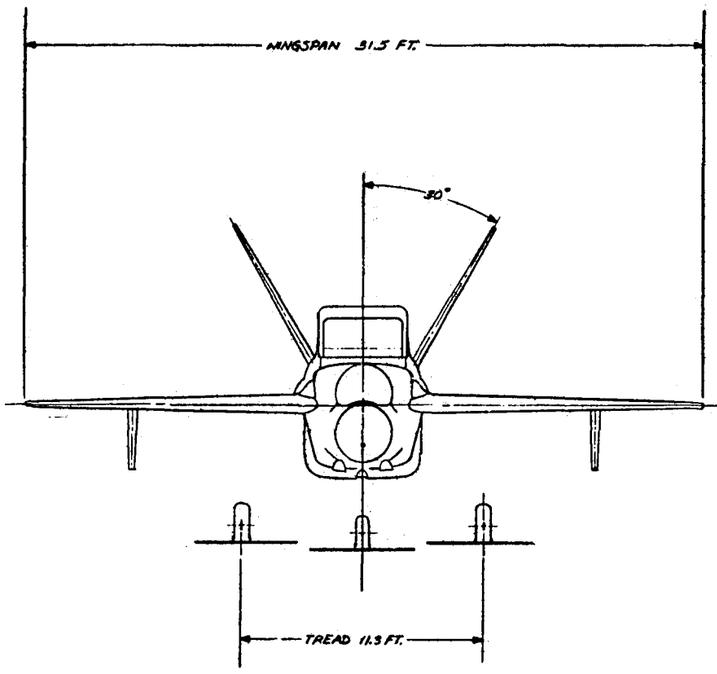

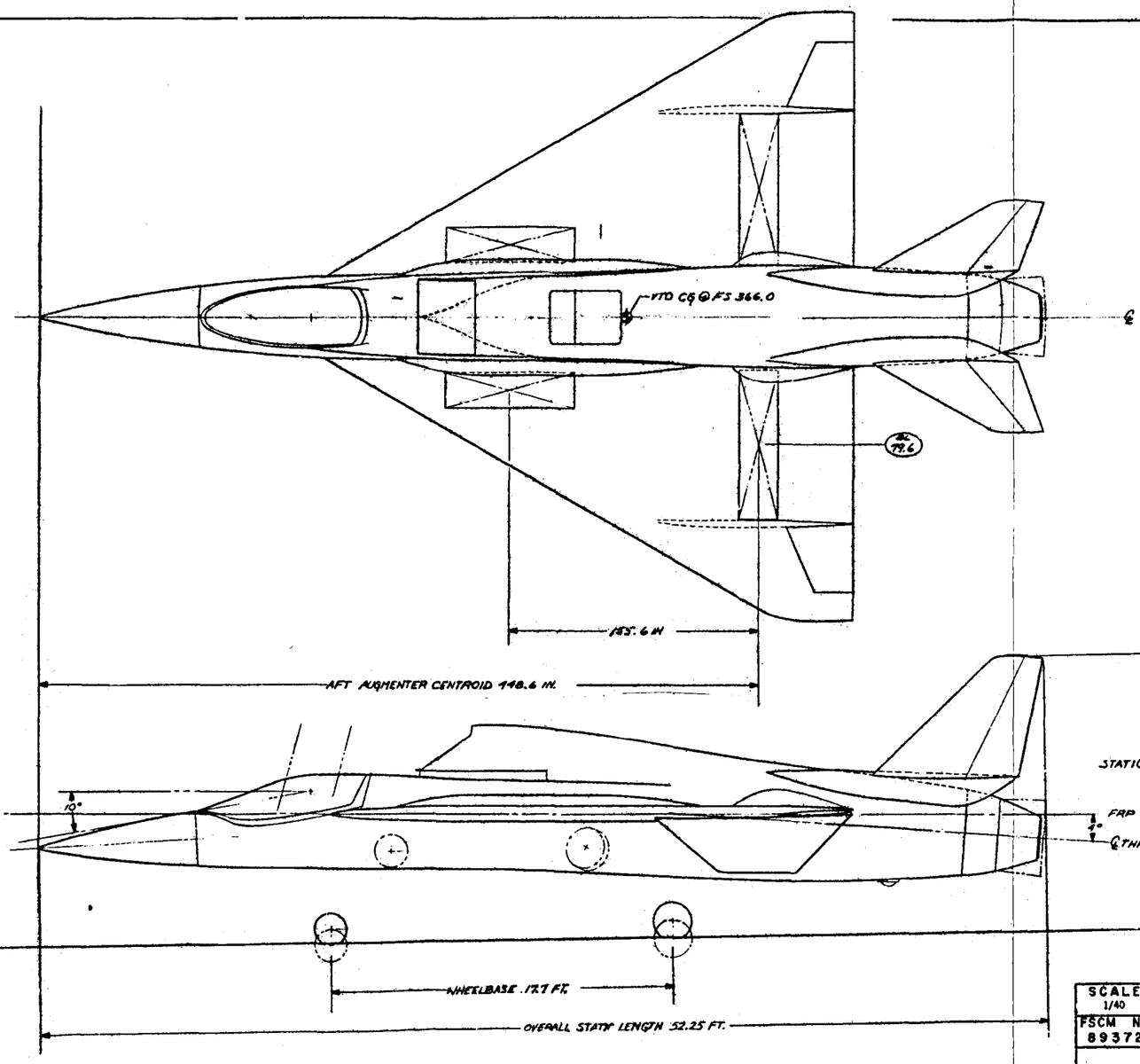

ALTERNATE AIRCRAFT GEOMETRY

			WING	VERT. STAB.
AREA	(REF)	SQ. FT.	548.	36.7
	(EXPOSED)	SQ. FT.	416.3	--
ASPECT RATIO			1.8	1.41
SPAN		FT.	31.5	7.2
TAPER RATIO			.21	.32
CHORD	(CENTERLINE)		372.5	--
	(ROOT)	IN.	323.0	92.
	(TIP)	IN.	45.0	39.6
	(MAC)	IN.	251.6	65.5
SWEEP	(LE)	DEG.	60	41.6
THICKNESS RATIO:	(ROOT)		.038	.04
	(TIP)		.034	.04
DIHEDRAL		DEG.	0	60
INCIDENCE		DEG.	0	0
TWIST	(WASHOUT)	DEG.	-3	0

AUGMENTER GEOMETRY

			FWD.	AFT
A_2	- INLET AREA	(SQ. IN.)	1760.	2312.
A_2/A_0	- INLET AREA RATIO		12.5	22.0
L/D	- DIFFUSER LENGTH TO THROAT WIDTH RATIO		1.4	1.5
AR	- ASPECT RATIO		3.6	3.7

SCALE 1/40	DWN E. KERRIGAN	Rockwell International Corporation North American Aircraft Division Columbus, Ohio 43216
FSCM NO. 89372	DATE 12-18-81	
	MODEL N/A	
ALTERNATE V/STOL FIGHTER (LONGITUDINAL FORWARD AUGMENTER)		84884-002F

FIG 3-9
3-8/3-9

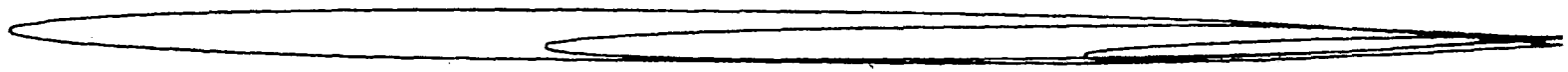

LEADING EDGE RADIUS = .235 INCH CONSTANT

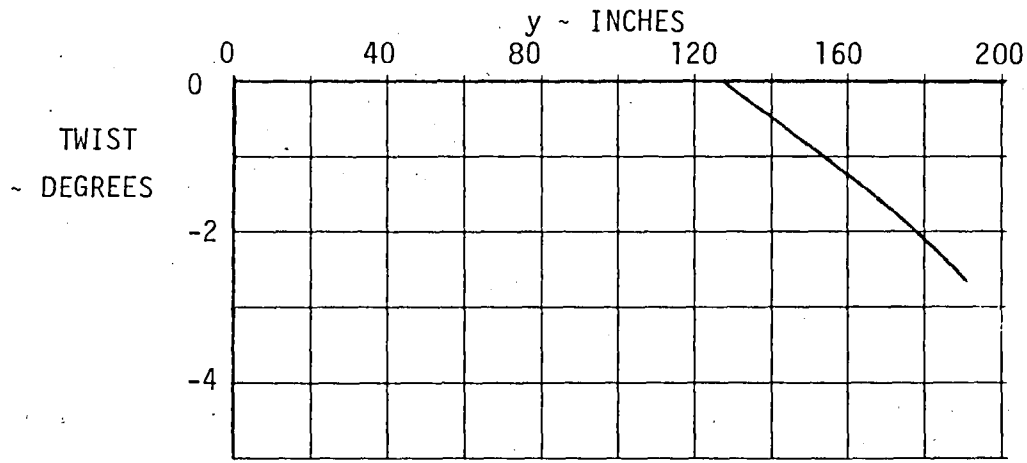

Figure 3-5 Twist Distribution for Alternate Configuration

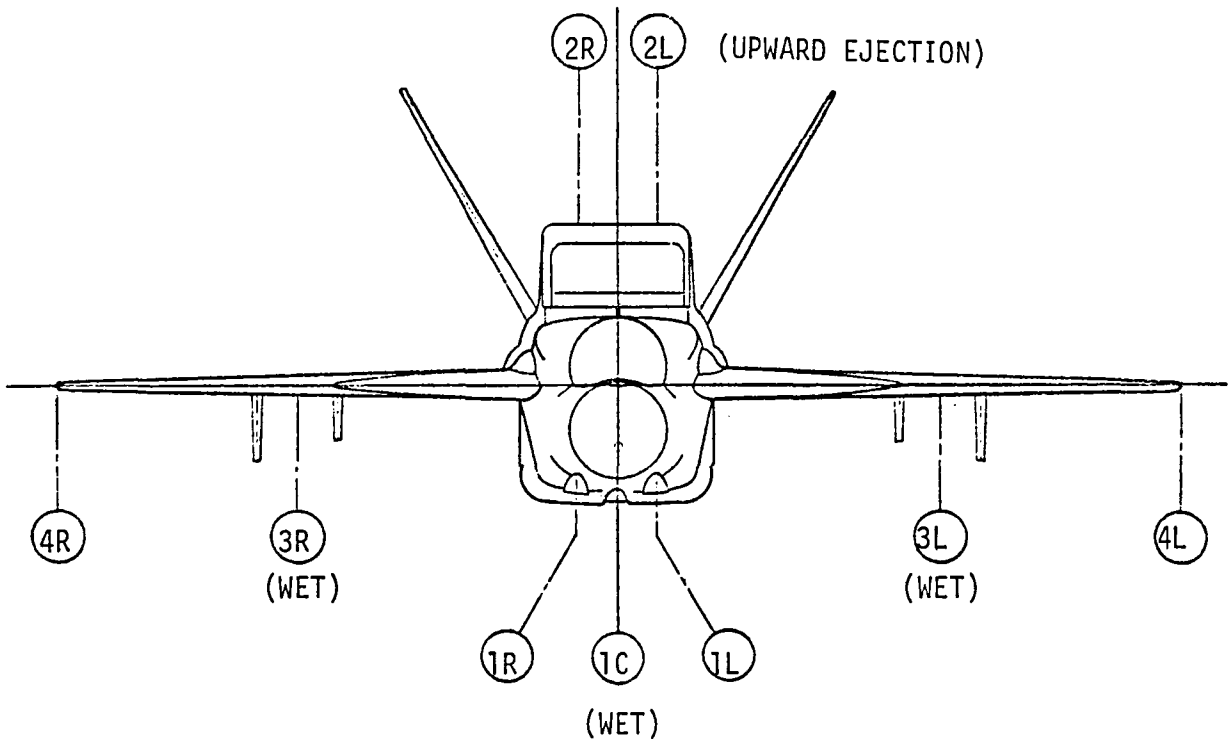

STORE \ STATION	4R	3R	2R	1R	1C	1L	2L	3L	4L
AIAAM		(X)	X	X	X	X	X	(X)	
AMRAAM		(X)	X	X	X	X	X	(X)	
SRASM		X						X	
HARPOON		X			X			X	
HARM		X						X	
SRAAM	X								X
200 GAL. EXT. TANK		X			X			X	

(X) DENOTES AAM NOT SEMI-SUBMERGED

Figure 3-6 Store Station Allocations

3.2 MASS PROPERTIES

3.2.1 Weight Estimation Basis

The methods used in estimating the structural weight are based on a series of empirical weight estimation routines developed by NAAO-Columbus and reviewed with the Weight Control Branch personnel at Naval Air Systems Command. These methods incorporate a data base from existing aircraft and allow for state-of-the art adjustment based upon related design studies. Input data consist of structural criteria, dimension data, functional design requirements, and adjustment factors to allow for special conditions. Adjustment factors to allow for special conditions are predominantly concerned with the assessment of unique configurations and the application of advanced materials and advanced construction concepts.

Adjustments for uniqueness of configuration, such as wing arrangement and thrust augmented lifting surfaces, are based on the actual hardware component weights of the XFV-12A airplane. The wing arrangement interacts with the fuselage in a manner which results in a relatively lightly loaded fuselage. This is accounted for in the fuselage weight estimation by reducing the statistical GN_Z value by 15 percent. A final correction factor of .962 is then applied to the fuselage weight estimation for specific calibration to the XFV-12A fuselage weight. In order to reflect the proper materials utilization, three basic categories of fuselage weight have been established on the basis of XFV-12A actual weights. These categories are: (1) steel and miscellaneous (canopy, mech., paint, etc.) structure that was designed by load and other requirements with no specific temperature effects (approximately eight percent), (2) "cool" structure (aluminum, etc., approximately 56 percent) and (3) "hot" structure (titanium, etc., approximately 36 percent). Weight estimation methods for thrust augmented lifting surfaces have been published in a Society of Allied Weight Engineers Conference Paper No 1163 and have also been discussed with NAVAIR Weight Control Branch personnel.

Adjustments for utilization of advanced materials and advanced construction concepts are primarily keyed to the classification of "cool" and "hot" structures; "hot" structures requiring material utilization consistent with specific temperature levels.

For advanced composites applications, weight reductions over metal designs are estimated which incorporate present day graphite/epoxy technology payoffs and projected improvements for the 1995 time period. Present day graphite/epoxy technology payoffs have been demonstrated on current aircraft and documented in numerous design studies, with typical results shown in column one of Table 3-1. The indicated weight reductions have been achieved in the face of current design criteria which limits design ultimate strains to levels substantially below the failure capability of the basic composite material. These limitations have been necessary because of wide scatter in material properties, effect of strain concentrations, environmental degradation, etc.

Additional weight reductions projected for the 1995 time period are shown in column two of Table 3-1. These projections are based on a conservative assessment of anticipated payoffs resulting from a substantial ongoing and planned government funded effort directed at improving the structural efficiency of advanced composites. A number of these programs are directed at increasing the design strain level of composite structures through a reduction in basic material properties scatter, reduction in material properties sensitivity to moisture and increased resistance to impact damage. Other programs will result in an increased use of integral structures. For fuselage structures additional weight reductions will result from an increased exploitation of postbuckling strength. For wing structures, in particular, an NADC sponsored program is directed at the development of high strain design concepts with a goal of an additional weight reduction of 20 percent. Recently completed NADC funded conceptual design studies of high strain wing structures have shown weight savings over current composite wing designs of over 20 percent for subsonic patrol aircraft and 7.5-10 percent for fighter/attack aircraft. In view of these concentrated development efforts, this contractor's projection of a maximum total additional weight reduction of six percent may well be exceeded.

TABLE 3-1

PROJECTED COMPOSITE TECHNOLOGY REDUCTIONS FOR THE 1995 TIME PERIOD

	1 Current Composite Technology Weight Reductions Over Metal Design	2 Projected Improvements Over Current Technology	(1) x (2) Advanced Composite Technology Weight Reduction Over Metal Design
Wing Box	20% (.8)	6% (.94)	25% (.75)
Fuselage (Non-Temp. Affected)	20% (.8)	5% (.95)	24% (.76)
Vertical	20% (.8)	6% (.94)	25% (.75)
Landing Gear Structure	0%	0%	0%
Air Induction System	10% (.9)	5% (.95)	15% (.85)

The weight estimation of augmenter components, thrust transfer system and "hot" fuselage structure is based on XFV-12A component weights, modified for advanced construction concepts, such as superplastic forming/diffusion bonding, and modified for advanced material applications, such as fiber reinforced advanced titanium (FRAT) composites. There are currently several titanium alloys under development

at the Rockwell International Science Center which exhibit high creep strength to 1200°F, which will be adequate for the 1180°F gas temperature encountered in this study. In addition, titanium aluminide alloys have been under development of the Air Force Materials Laboratory since 1972 for applications in the 1200-1500°F range.

In the Propulsion Group, a sustained growth in basic gas turbine engine thrust-to-weight ratios has been observed over the past two decades. This growth rate has been projected by the engine manufacturer in his estimate of the 1990 era engine weight. The engine manufacturer has also forecast the diverter weight based on his experience on the XFV-12A and development work accomplished since that time. Very nominal state-of-the-art improvements have been incorporated in the remainder of the Propulsion Group.

Several technological improvements are discussed in the Aircraft Systems section of this report. Significant weight savings will be available over the next 15 years in the following areas:

Avionics Systems - Application of modular avionics packaging, digital mechanizations, and micro electronics produce significant savings. For example, processor weights and displays and controls reflect the 1995 time period. Sharing of common power supplies, multiplexing, use of high voltage DC (270 VDC) for basic power, and use of active elements for phased array radar antennas also reduce weight.

Flight Control Systems - Utilization of digital fly-by-light flight control system interfaced with advanced direct drive actuators incorporating the advantages of 8000 psi hydraulics as noted in the next paragraph.

Lightweight Hydraulic System - Use of high pressure hydraulic (8000 psi) to achieve reductions in system weight and space requirements. The increased pressure allows a reduction in actuator piston areas with a resulting reduction in flow demand for the same horsepower capability. Weight and size of distribution lines, pumps, reservoirs, etc., can be reduced.

High Voltage DC (HVDC) Electrical Sytem - This technology improvement produces (a) a reduction of maintenance, cost, and weight in the generating package, (b) reduction of weight in the distribution wiring, and (c) a significant reduction of volume and weight of the avionic power supplies.

3.2.2 Weight Balance and Inertia

Baseline - A weight breakdown for the baseline aircraft is shown on Table 3-4 using the MIL-STD 1374 weight summary form. Table 3-2 below presents the centers of gravity and moments of inertia for the baseline aircraft for several loading conditions.

TABLE 3-2

BASELINE CONFIGURATION BALANCE AND INERTIA ESTIMATE

	USABLE FUEL LOAD	WEIGHT	X FS	Z WP	I_{xx} ROLL	I_{yy} PITCH	I_{zz} YAW	I_{xz} PROD.
VTOGW	5,641	25,025	365.8	-0.6	10,235	86,692	92,886	143
COMBAT G.W.	2,638	22,022	365.8	-2.5	8,028	86,665	91,282	139
LANDING G.W.	691	20,075	368.6	-5.0	7,621	85,567	90,408	523
OWE	0	18,184	374.8	-3.8	7,190	82,874	88,118	551

NOTE: 1. All store loads (2) AIAAMS (1200 Lbs.), except OWE

2. Inertia Units are shown in Slug-Ft.^{2}

Alternate - The weight breakdown for the alternate aircraft is shown on Table 3-5 using the MIL-STD 1374 weight summary form. Table 3-3 below presents the centers of gravity and moments of inertia for several loadings of the alternate aircraft.

TABLE 3-3

ALTERNATE CONFIGURATION BALANCE AND INERTIA ESTIMATE

	USABLE FUEL LOAD	WEIGHT	X FS	Z WP	I_{xx} ROLL	I_{yy} PITCH	I_{zz} YAW	I_{xz} PROD.
VTOGW	5,350	24,300	365.9	-0.6	9,938	84,180	90,195	139
COMBAT G.W.	2,434	21,384	365.8	-2.8	7,795	84,154	88,637	135
LANDING G.W.	663	19,613	368.9	-5.1	7,446	83,598	88,327	511
OWE	0	17,750	375.1	-3.9	7,018	80,896	86,015	538

NOTE: 1. All store loads (2) AIAAMS (1200 Lbs.), except OWE

2. Inertia Units are shown in Slug-Ft.^{2}

TABLE 3-4

BASELINE CONFIGURATION WEIGHT SUMMARY

MIL-STD 1374

	DLI VTO	DLI STO	CAP	F.E.	INTER-DICTION	SS
TOTAL STRUCTURE	(9133)					
WING GROUP	4118					
TAIL GROUP -HORIZONTAL	-					
-VERTICAL + END PLATES	563					
BODY GROUP	2951					
ALIGHTING GEAR GROUP-MAIN	805					
-NOSE	194					
-ARREST	-					
ENGINE SECTION OR NACELLE GROUP	50					
AIR INDUCTION SYSTEM	452					
PROPULSION GROUP	(5373)					
ENGINE (AS INSTALLED)	3287					
GEAR BOXES AND DRIVES	125					
PITCH PIPES	111					
COOLING AND DRAIN PROVISIONS	30					
ENGINE CONTROLS	30					
STARTING SYSTEM	116					
LUBRICATING SYSTEM	-					
FUEL SYSTEM	427					
THRUST DIVERTER	238					
THRUST TRANSFER	816					
EPU INST'L.	193					
FIXED EQUIPMENT	(3223)					
FLIGHT CONTROLS GROUP	634					
INSTRUMENT GROUP	70					
HYDRAULIC AND PNEUMATIC GROUP	244					
ELECTRICAL GROUP	367					
AVIONICS GROUP	1144					
ARMAMENT GROUP	130					
FURNISHINGS GROUP	276					
AIR CONDITIONING GROUP	348					
HANDLING GROUP	10					
TOTAL WEIGHT EMPTY	17729	17729	17729	17729	17729	17729
CREW	(180)	(180)	(180)	(180)	(180)	(180)
FUEL	(5723)	(8982)	(11702)	(11702)	(11702)	(10342)
UNUSABLE	82	82	82	82	82	82
USABLE INTERNAL	5641	8900	8900	8900	8900	8900
USABLE EXTERNAL	-	-	2720	2720	2720	1360
200 GAL. EXT. TANKS + PYLONS/RACKS	(-)	(-)	(624)	(624)	(624)	(212)
HYDRAZINE	(56)	(56)	(56)	(56)	(56)	(56)
OIL	(20)	(20)	(20)	(20)	(20)	(20)
ARMAMENT	(1314)	(2628)	(2628)	(2008)	(4803)	(3230)
LAUNCHERS	114	228	228	408	408	494
AIAAMS (2)/(4)/(4)	1200	2400	2400			
MRAAM (4)				1200		
SRAAM (2)				400	400	400
SRASM (4)/HARPOON (2)					4000	2336
EQUIPMENT	(3)	(3)	(3)	(3)	(3)	(3)
1ST AID KIT	3	3	3	3	3	3
TOTAL USEFUL LOAD	7296	11869	15213	14593	17393	14043
TAKE-OFF GROSS WEIGHT	25025	29598	32942	32322	35122	31772
FLIGHT DESIGN GROSS WEIGHT	22769					
LANDING DESIGN GROSS WEIGHT	22622					

TABLE 3-5

ALTERNATE CONFIGURATION WEIGHT SUMMARY

MIL-STD 1374

	DLI VTO	DLI STO	CAP	F.E.	INTER-DICTION	SS
TOTAL STRUCTURE	(8633)					
WING GROUP	3620					
TAIL GROUP-HORIZONTAL	-					
-VERTICAL + END PLATES	482					
BODY GROUP	3042					
ALIGHTING GEAR GROUP-MAIN	795					
-NOSE	192					
-ARREST	-					
ENGINE SECTION OR NACELLE GROUP	50					
AIR INDUCTION SYSTEM	452					
PROPULSION GROUP	(5456)					
ENGINE (AS INSTALLED)	3287					
GEAR BOXES AND DRIVES	125					
PITCH PIPES	88					
COOLING AND DRAIN PROVISIONS	30					
ENGINE CONTROLS	30					
STARTING SYSTEM	116					
LUBRICATING SYSTEM	-					
FUEL SYSTEM	427					
THRUST DIVERTER	238					
THRUST TRANSFER	922					
EPU INST'L.	193					
FIXED EQUIPMENT	(3206)					
FLIGHT CONTROLS GROUP	627					
INSTRUMENT GROUP	70					
HYDRAULIC AND PNEUMATIC GROUP	239					
ELECTRICAL GROUP	367					
AVIONICS GROUP	1144					
ARMAMENT GROUP	130					
FURNISHINGS GROUP	276					
AIR CONDITIONING GROUP	348					
HANDLING GROUP	5					
TOTAL WEIGHT EMPTY	17295	17295	17295	17295	17295	17295
CREW	(180)	(180)	(180)	(180)	(180)	(180)
FUEL	(5432)	(8307)	(11027)	(11027)	(11027)	(9667)
UNUSABLE	82	82	82	82	82	82
USABLE INTERNAL	5350	8225	8225	8225	8225	8225
USABLE EXTERNAL	-	-	2720	2720	2770	1360
200 GAL.EXT.TANKS + PYLONS/RACKS	(-)	(-)	(624)	(624)	(624)	(212)
HYDRAZINE	(56)	(56)	(56)	(56)	(56)	(56)
OIL	(20)	(20)	(20)	(20)	(20)	(20)
ARMAMENT	(1314)	(2628)	(2628)	(2008)	(4808)	(3230)
LAUNCHERS	114	228	228	408	408	494
AIAAMS (2)/(4)/(4)	1200	2400	2400			
MRAAM (4)				1200		
SRAAM (2)				400	400	400
SRASM (4)/HARPOON (2)					4000	2336
EQUIPMENT	(3)	(3)	(3)	(3)	(3)	(3)
1ST AID KIT	3	3	3	3	3	3
TOTAL USEFUL LOAD	7005	11134	14538	13918	16718	13368
TAKE-OFF GROSS WEIGHT	24300	28489	31833	31213	34013	30663
FLIGHT DESIGN GROSS WEIGHT	22160					
LANDING DESIGN GROSS WEIGHT	21970					

3.3 STRUCTURAL DESIGN

3.3.1 Materials

Based on the experience gained from the production of the prototype XFV-12A vehicle, it may be stated that a current technology base exists for construction of augmenter components for use in the 800-1000°F temperature range and that the titanium alloys provide the most efficient structural materials from a strength/weight standpoint in this temperature range.

The augmenter designs presented in this study are predicated on the use of mixed flow temperatures of 1180°F. Recent developments of titanium alloys and Fiber Reinforced Advanced Titanium (FRAT) have produced materials with characteristics which show a high potential for achieving high creep strength and oxidation resistance to 1200°F.

Composite Materials - Graphite reinforced composite material has been considered as the principal candidate material for construction of major portions of the wing and fuselage structure in the proposed designs. Based on experience gained from tethered flight testing of the prototype XFV-12A vehicle, it has been demonstrated that the temperature of primary aluminum wing and fuselage structure located in close proximity to augmenter ducts containing 900°F gas may be maintained below 250°F with a relatively small amount of thermal insulation material and cooling air flow. Current graphite/epoxy composite materials retain most of their strength at temperatures up to 250°F. Graphite/bismaleimide composite materials, for use up to 450°F, are now reaching production status and are amenable with current composites manufacturing facilities in that graphite/epoxy cure cycles and tooling can be utilized for fabrication. Emerging graphite/polimide materials have the capability to extend the useful operating temperatures to the 500-600°F range. The philosophy employed in selecting materials for these designs is therefore to replace the aluminum structure currently existing in corresponding areas of the XFV-12A prototype with graphite/epoxy, graphite/bismaleimide, or graphite/polyimide construction to the extent possible, and to provide sufficient insulation of the 1180°F gas ducting to prevent excessive heating of the composite structure.

The application of graphite epoxy advanced composites to major aircraft components such as fuselages and lifting surfaces has demonstrated a weight savings of approximately 20 percent over corresponding metal designs. Thus far the potential weight savings by the use of advanced composites has been somewhat inhibited by the necessity of limiting the working strain level to a fraction of its full capacity. These limitations have been required in part to compensate for scatter in design due to moisture. However, further advances in composite technology are now feasible which will result in additional weight advantage and which will be derived from planned government programs in the following areas:

- increased graphite/epoxy strength allowables through reduction in material scatter;

- increased laminate strain level capacity through use of special design/manufacturing techniques and the characterization of the effect of defects;

- reduced strength degrading effect of impact damage through characterization of the nature and propagation of damage and employment of material forms with increased resistance to damage;

- improved capability for in-the-field detection of damage through development of NDT systems which allow rapid interrogation of large areas of aircraft structure;

- increased structural efficiency of thin-skin composite construction through utilization of available postbuckling strength and comprehensive evaluation of postbuckling behavior; and

- increased laminate resistance to moisture degradation through fiber treatment and resin development.

Development of metal matrix materials with particular emphasis on landing gear applications, and the development of graphite/polyimides for use in the 300°F-500°F temperature range offer additional weight savings potential.

3.3.2 Fuselage Structure

The fuselage structure contemplated in this study is conventional with the exception of the materials applications previously described. The structural arrangement consists of longerons interconnected with fuselage frames and internal shear webs along with a stressed skin exterior cover. Key frames would be colocated with points of concentrated loads such as the radome pressure bulkhead, ejection seat support, landing gear trunnions, engine moments, wing carry-through and external weapons launchers. The vertical stabilizer surfaces would be supported by two dorsal booms connected to aft fuselage primary structure and spanning the engine diverter valve hot section.

Engine Accessibility - A structured door is located beneath the engine between fuselage stations 443 and 541 which contains the lower diverter valve transition ducting. The ducting extends forward to two quick disconnect expansion bellows located at fuselage station 447. Engine and accessory access is provided by removal of this lower door which will expose 78 percent of the engine lower semi-cylinder.

Engine Removal - A door panel is located aft of fuselage station 541 extending to station 578.5 which would be designed as secondary structure and which covers the lower half of the afterburner chamber. This quick disconnect panel would be removed in conjunction with the forward structural door for engine removal. The upper diverter valve ducting would remain in place in the upper fuselage without being disconnected from the wing aft augmenter duct feed connections. This feature is provided by unclamping the upper diverter valve manifold from the engine at engine frames located immediately fore and aft of the diverter valve.

The engine is then lowered approximately two inches after repositioning the engine/inlet duct seal and then moved aft 36 inches on a standard engine handling trailer such as the AIRLOG 4000A. The complete engine, including diverter valve and afterburner, is then clear of the station 443 lower frame and can be lowered on the handling trailer for transport away from the aircraft. Engine installation would be the reverse of the removal procedure.

Maintainability - Great emphasis should be placed during the fuselage structural design to provide quick release type access doors adjacent to systems components which must be serviced or scrutinized frequently. Coordination between structures and systems design engineering can provide a colocation of components and doors to limit quick access provisions to further limit their corresponding weight penalties. Direct natural access areas such as those provided by the landing gear wells would also be exploited for frequent servicing and maintenance of systems components.

3.3.3 Wing Structure

The modified delta and delta geometry of the baseline and alternate configurations, respectively, are generally ideal for structural design which results in high structural efficiency. The long chords permit relatively large physical wing thickness (ten inches at wing station 33) which provides efficient box depth and large wing volume for fuel and augmenter ducting, while limiting the wing thickness ratio to approximately four percent. The moderate aspect ratio and surface loading characteristic of delta designs also contribute favorable to structural efficiency.

The large interruption in wing surface skins and additional structural concessions required to accommodate the augmenters do, however, detract from the structural efficiency maximum potential of the delta planform. This augmenter equipped delta planform endures as an efficient combination, given the V/STOL mission of the design.

The wing structure contemplated is similar in approach for both the baseline and alternate configurations. The wing inboard panel contains the augmenters and extends from an inboard rib at wing station 28, which is attached to fuselage frames, to wing station 121 (baseline) and 128 (alternate). The inboard panel would contain structural boxes located forward and aft of the augmenters which provide structural continuity to a major rib at wing station 121 or 128. These sectional torque boxes in the inboard panel react torsional loads imposed by the trailing edge surfaces and the wing outer panel. Wing bending loads are reacted primarily in the aft box.

The aft augmenter in the baseline configuration is located considerably further forward in the wing than is the augmenter in the alternate version. As a result, the baseline wing would be equiped with an additional auxiliary torque box section extending spanwise and located between the augmenter aft diffuser surface and the trailing edge flap.

3.4 FLIGHT CONTROLS

3.4.1 Hover

The control concept for maneuvering and trim in hover utilizes the primary lift (augmented thrust) vectors, Modulation of the lift magnitude and direction from each augmenter produces the moments for control and vertical height control. In pitch, the primary lift vectors are supplemented by a reaction control system. Figure 3-7 pictorially summarizes the hover control concept.

As seen in Figure 3-7 moment control is accomplished by deflecting the Coanda flaps toward or away from one another to decrease or increase, respectively, ejector lift magnitude. Thus, pitch control moment and roll control moment are developed by fore and aft or left and right differential deflection of the augmenter diffuser flaps. Height control is provided by simultaneous operation of all diffuser flaps, with the diffuser flaps opening for increased lift and closing for lift reduction.

Lift vector direction is provided by deflecting the diffuser flaps of an augmenter in the same direction to direct the efflux from the nozzles as well as the induced flow. In this case, the diffuser angle is approximately constant or it can be varied to account for changes in augmentation ratio with mean flap deflection. Therefore, yaw control in hover is accomplished by differential mean flap deflection of the aft augmenters as shown in Figure 3-7.

The above aircraft control concept by use of augmenter lift vectors was utilized on the XFV-12A V/STOL prototype. By analysis and limited tethered hover data, it was shown to be a feasible concept. Figure 3-8 shows the XFV-12A tethered hover moment data acquired at NASA Langley. The aircraft was also "flown" by the pilot untethered but suspended from an overhead cable. He demonstrated very precise position control with this system.

In addition to the use of differential fore and aft augmenter diffuser flap deflection for pitch control, a fore and aft reaction control nozzle is employed as indicated in Figure 3-7. The reaction control purpose is to augment the pitching moment available from the ejectors and to provide an additional moment source when the surface diffusers are operating near their maximum deflections. A forward and aft nozzle are incorporated so that all pitching moment inputs from the reaction control system add to the total lift (downward thrusting).

Maneuvering of the aircraft in hover is accomplished through control of aircraft attitude. Fore and aft translation and lateral translation, therefore, are performed by pitching and rolling, respectively, to a constant attitude. For the case of fore and aft translation, an incremental mean flap deflection of the augmenters can also be used to provide the force or lift vector rotation to translate the aircraft. Thus, it is intended that the pitch and roll control system

will incorporate an attitude hold mode to facilitate translational maneuvering by aircraft attitude.

The basic airframe longitudinal and lateral dynamic modes are unstable in the hover flight regime. A stability augmentation system will provide the stabilization required.

3.4.2 STOL/Conversion

The transition from hover to conventional flight is accomplished by deflecting the augmenter flaps to low deflections followed by complete augmenter flap retraction. The flap commanded mean rate required determined from transition time history studies of the XFV-12A is from 1-4°/sec. As the flap deflections reach approximately 25° initiation takes place of the thrust diversion from the augmenters to the engine main rear nozzle. Completion of thrust diversion is accomplished prior to complete retraction of the flaps. The functioning of the pitch, roll, and yaw control during transition flight varies as a function of mean flap deflection. As the mean flap deflection decreases from the hover deflection (approximately 90°) the fore and aft flaps of each augmenter gradually change from a diffuser deflection mode to a mean flap mode, as illustrated in Figure 3-9. The movement of the augmenter flaps thus revert toward conventional deflection operation as the conventional speed range is approached. For example, when the mean flap deflection is approximately 40° the lateral control function on the aft augmenter consists of differential mean flap deflection with very little diffuser angle change.

The longitudinal (forward) augmenter for the alternate configuration is operated differently in the transition or STOL regime. As the mean flap of the aft (chordwise) augmenter deflects to lower positions, the center nozzles and aft end-door is retracted into the forward wing surface at the start of the transition when the hover flap deflection range terminates. As the thrust diversion phase begins, the forward augmenter continues the retraction to a closed position.

The outboard ailevators and rudders are deflected normally at all flight regimes including hover. In this way no phasing in and out of ailevator and rudder deflections during the transition is required. These surfaces become effective as the dynamic pressure increases and vice versa and augment the control power available at the higher end of the transition speed range. During the thrust diversion phase as the augmenters are retracting the ailevators, elevons, and rudders provide the control and stability augmentation functions.

When the aircraft are conducting STOL operations, the mean flap deflection can be selected at any value required. The flaps are also capable of high rates, due to hover control requirements, so that discrete flap changes can be commanded to facilitate rapid thrust vectoring encountered in shipboard flat deck or ski-jump takeoffs. Pitch, roll, and yaw control deflection schedules are set by the commanded mean flap deflection angle as in transition flight.

3.4.3 Conventional Flight

The conventional flight regime employs the inboard control surfaces as elevons (primarily pitch - supplement roll) as in the transition mode. The outboard surfaces are used as ailevators (primarily roll - supplement pitch) and the rudders are used for yaw control. The outboard ailevators include the pitch function to produce the control power required at high angle of attack. The stabilization functions are delegated to the elevons for pitch, ailevators for roll, and rudders for yaw.

Since the aircraft, aerodynamically, is designed to be statically unstable in pitch at subsonic speeds, the stabilization system as in the hover and transition flight modes, must provide the static and dynamic stability. The aircraft is designed to be statically stable lateral-directionally and will require no static stability augmentation. The dynamic oscillatory stability is also stable but will require stability augmentation to product satisfactory lateral-directional damping and modal charactersitics throughout the flight envelope.

3.4.4 Control System Concept

The control of a V/STOL fighter aircraft has requirements that span a large spectrum of variables including utilizing the propulsion system as part of the primary controls. Therefore, the most efficient control system becomes an integrated propulsion control - flight control system. The aircraft will use a triple redundant, digital fly-by-light control system. By utilizing integrated control concepts, greater control accuracy can be obtained while eliminating unnecessary thrust modulation or demands. The computer system will command integrated digital direct drive actuators using high pressure hydraulics. Linear direct drive actuators will be used for control surfaces such as ailevators, elevons, and rudders, and rotary hingeline direct drive actuators shall be used on thrust augmenters and similar surfaces requiring large surface travels.

The use of the integrated direct drive actuator with the control electronic and sensors inbedded in the body of the actuator, make possible the transmission of digital signals directly from the computer to the actuator and signals can be transmitted either electrically or optically making possible a true fly-by-light control.

Inputs to the flight computers will be provided from triplex transducing signals to provide the pilots command. Rate and acceleration inputs are provided by cone-configured, distributed, skewed axis gyros and accelerometers. Triplex inputs from the propulsion system and air data system will also be provided.

The propulsion flight integrated control system will be designed as a single multivariable control unit with a primary goal of minimizing propulsion or thrust requirements, thereby reducing fuel requirements while increasing engine life. The multivariable control approach will also provide the optimum approach to provide artificial stability in all six degrees of freedom.

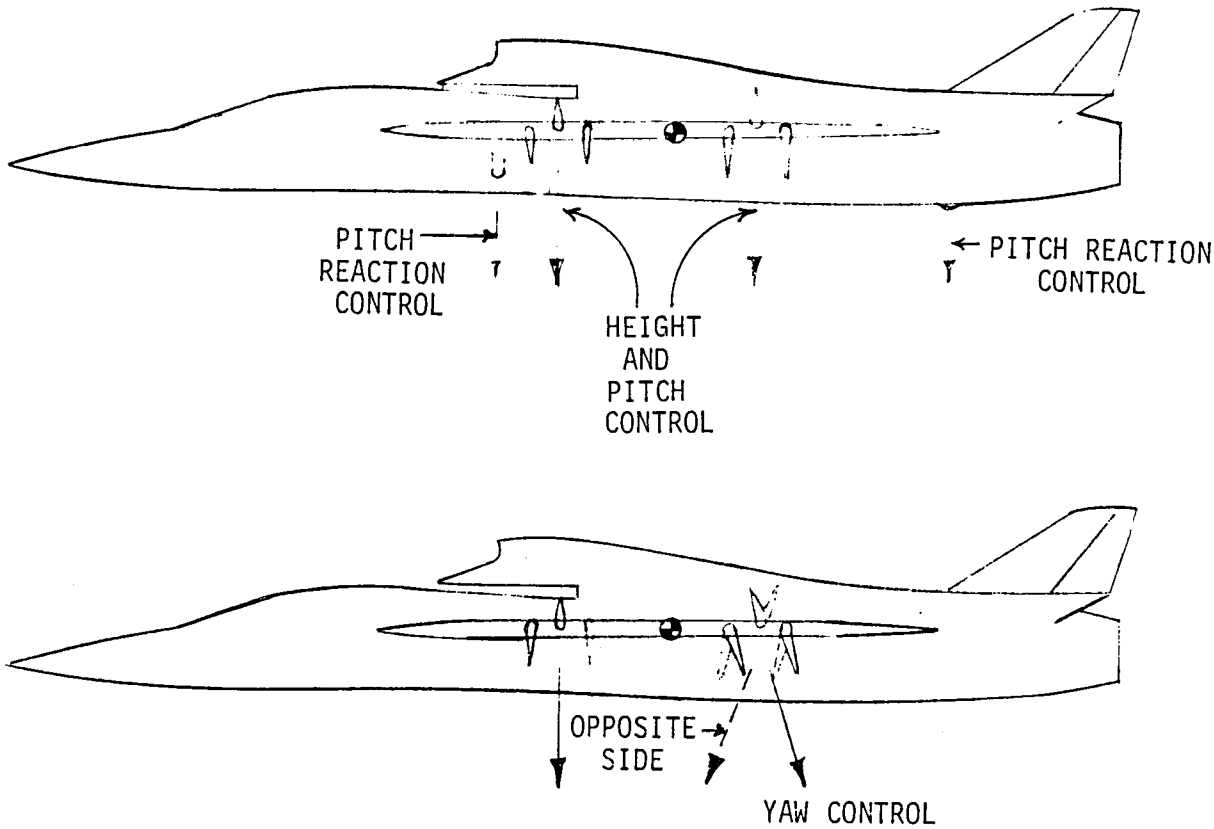

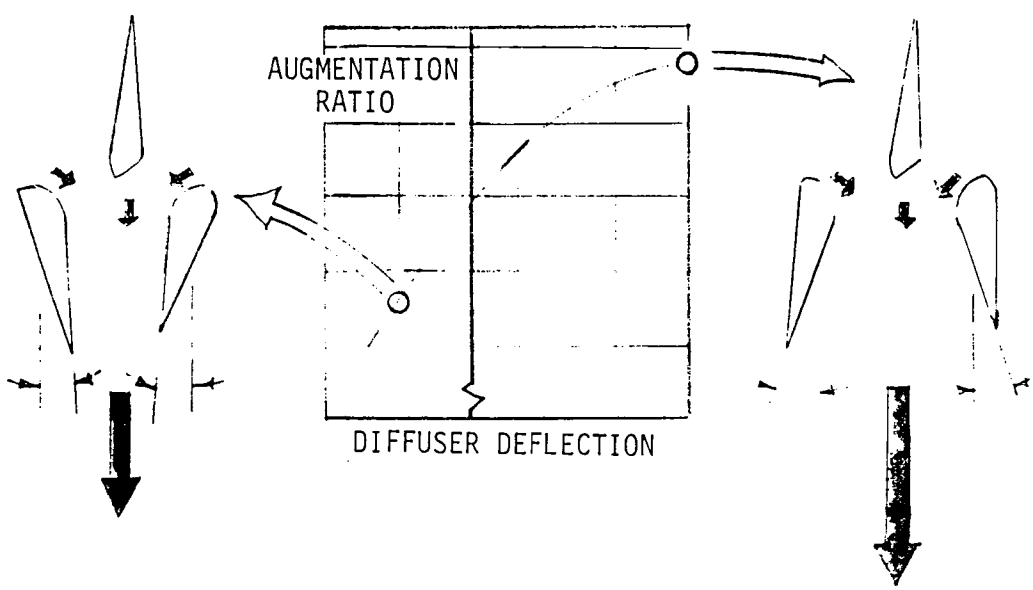

Figure 3-7 Hover Control Concept

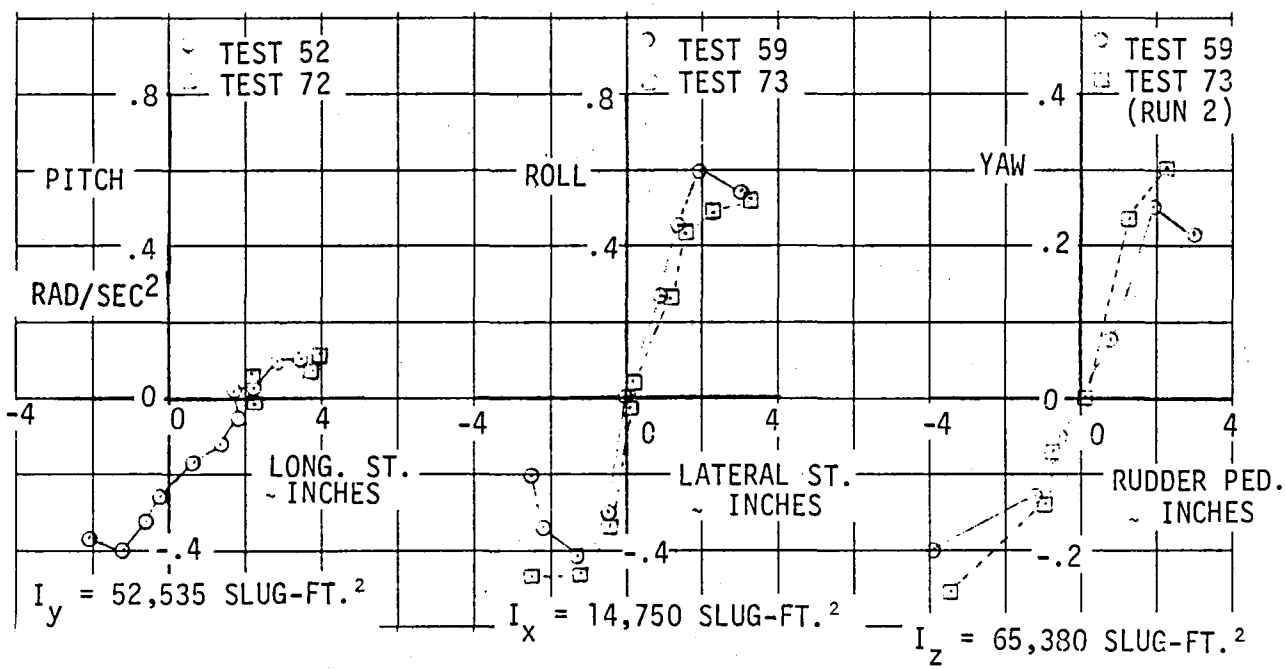

Figure 3-8. XFV-12A Control Response

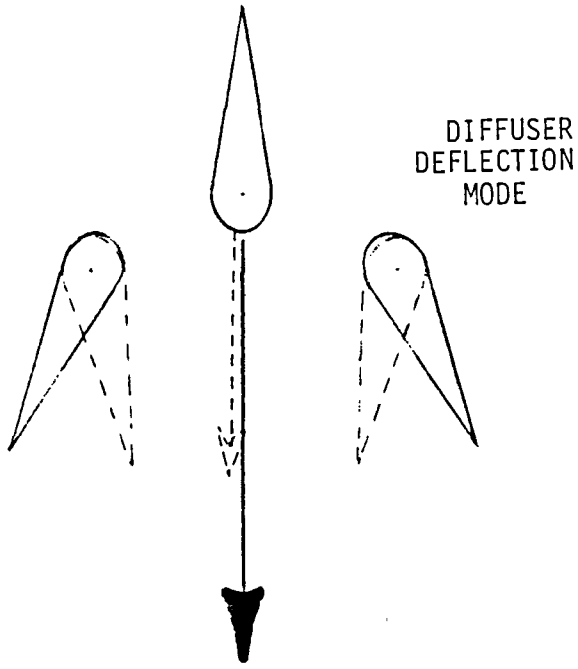

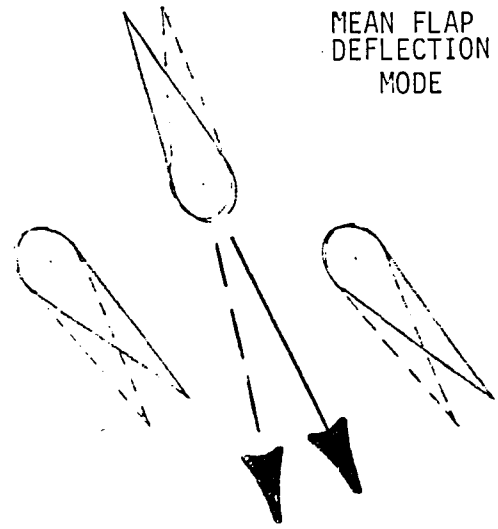

Figure 3-9 Pitch, Roll, and Yaw Mode Change With Commanded Mean Flap Deflection

3.5 SUBSYSTEMS

3.5.1 Electrical

The electrical system will be designed to generate and distribute the type, quantity and quality of electric power demanded by the on-board utilization systems. The primary electrical general system concept selected will be a 270 VDC. The 270 VDC generator will be a brushless, permanent magnet (PM) unit utilizing the latest high energy Samarium-Cobalt permanent magnet material and high permeability laminations. All rectification and filtering will be integral to the generator and with the generators cooling medium. The high efficiency of this design, typically 90 percent, will result in a minimum of power extraction from the main engine and hence reflect the maximum impact on engine fuel economy and a resultant aircraft lift cycle cost.

Secondary electric power will be provided by static DC/AC, DC/DC or AC/DC converters as required by the primary electric power and utilization systems. The latest technology advancements in high voltage, high power transistor, SCR and power MOSFET devices will be utilized in the above converters. With 270 VDC as the input power to the DC/DC Swtiching Mode Regulator converters, optimum weight can be achieved by the conversion devices. Bi-directional DC/DC converters will be installed where reverse current and voltage characteristics are desired, e.g., 270 VDC primary system with a 28 VDC emergency battery. Here during normal operation the converter will be operating in a 270/28 VDC regulated model, upon emergency the current flow is reversed and the battery provides regulated 270 VDC to the main emergency bus via the bi-directional converter operating in the 28-270 VDC mode.

With the aircraft designed for fly-by-wire, the need exists for the availability of redundant electric power for the flight control systems. In this application, triple redundancy will be provided by (1) the primary engine driven generator, (2) an Emergency Power Unit (EPU) driven generator and (3) a battery. The engine driven unit has been described above. The EPU driven generator will be a high speed, PM generator installed on the common rotor shaft of the EPU, i.e., operating at EPU rotor speed. This configuration offers the latest concept in lightweight EPU design. The installation of an on board EPU, therefore, provides the aircraft with electric power to be used for ground maintenance in addition to the in-flight emergency and/or backup power source. The battery system will be a battery/charger combination utilizing the latest battery concepts, e.g., Sealed Lead Acid (SLA) or Lithium Thionyl Chloride. The use of a battery charger precludes the need for scheduled maintenance and offers the optimum in life cycle cost reduction.

The electrical distribution system will use a fiber optic multiplex data bus with a centralized computer processor. Solid state power controllers will be utilized to preclude the need for circuit breakers and control switching devices. The computer controls and monitors the

power distribution system and interfaces with the generating systems control unit to coordinate the load switching and bus controls.

Brushless motors will be used wherever motor application is required to minimize maintenance and provide minimum life cycle cost.

3.5.2 Hydraulics

Power for operation of the various control system power components is provided by a LHS (light weight) high pressure, 8000 psi, hydraulic system. The hydraulic system, coupled with use of rotary direct drive valve modulars, rotary hydraulic power cylinders, and rotary feedback transducers, are presently being evaluated. This actuation concept is expected to reduce volume by as much as 80 percent and weight by 40 percent, as compared to current fly-by-wire systems.

The weight and space saved by the hydraulics system alone is being demonstrated in the current LHS (light weight hydraulics) advanced development and test program being conducted at Rockwell International-Columbus. The direct drive valve and LHS has successfully been demonstrated in the lab and in flight testing.

3.5.3 Environmental Control System

The Environmental Control System (ECS) provides cockpit pressurization, ventilation, heating and cooling. Additional ECS functions include avionics cooling and pressurization, and windshield rain, ice and fog clearing. The availability of 270 VDC electrical power and aircraft fuel for a heat sink permit the utilization of a vapor cycle refrigeration system as an advanced technology ECS system. The vapor cycle system has a higher coefficient of performance than an air cycle system and requires less power for operation. Installed weight of the system will be significantly less based on using high speed, Samarium Cobalt PM, 270 VDC motor(s) to drive the freon compressor and using the aircraft fuel for the heat sink.

Avionics heat dissipation normally represents about 75 percent of the total cooling load for the ECS system. The application of 270 VDC primary electric power will reduce the avionics cooling load by 12 percent and a corresponding ECS weight reduction of 9.5 percent based on an air cycle ECS configuration. Changing from air cycle to vapor cycle cooling will further reduce ECS weight by an additional 14.4 percent. Secondary benefits resulting from the use of a vapor cycle ECS and its reduced power requirements are less power extracted from the main propulsion engine, improved specific fuel consumption, lower takeoff gross weight for a given mission requirement and reduced life cycle cost.

3.5.4 Fuel System

The fuel system will be contained in three fuselage fuel tanks of bladder construction along with integral wing tanks. Motive flow fuel pumps will be installed on the engine accessory drive and will provide

high pressure flow to tank mounted ejector pumps. If required for proper mission performance, electric boost pumps will also be added. The fuel transfer pumps, and boost pumps when installed, will be of a brushless design for high reliability and maintainability. These electric pumps will be of the plug type wherein maintenance will be simplified to provide ready access to the motor, etc., for repair without the need for draining or disturbing the tank. Fuel line fittings will be of the ferrule end tube design with self locking flexible connectors. The connectors will have an integral electrical bonding capability to ensure automatic bonding.

3.5.5 Avionics

The avionics system will be a light weight integrated system primarily for intercept from combat air patrol and deck-launched intercept, staged from an air-capable ship. It will also provide targeting for a surface launched air-targeted (SLAT) missile and be capable of air-to-surface attack. The avionics suite will provide weapon control, navigation, communications, identification, electronic warfare, and subsystems monitoring and control, Table 3-6. The weight predictions noted in Table 3-6 assume that the normal weight increase(s) that would accompnay these functional improvements are offset by the utilization of advanced system power supplies, e.g., 270 VDC input to switching mode regulators. The projected advanced avionic power supplies would have an efficiency of 80 percent and comprise only 20-25 percent of the volume and weight utilizing the advanced 270 VDC switching mode regulator technology. The minimized weight and volume of each avionic system not only have an impact on reduced life cycle cost (LCC) of each system but also impact the total aircraft weight and LCC by the requirement for less cooling and input power as noted in previous sections of this report.

System flexibility will accommodate new weapons and requirements. Redundancy and multi-path mode configuration will enhance mission availability. Modular packaging with multiple standard modules at system, subsystem, and sensor levels will make it feasible to maintain the hardware with the minimal number of spares and logistics support. Maintenance at operational level will consist of replacement of weapons replaceable assemblies, fault-isolated by built-in test.

TABLE 3-6

AVIONICS PREDICTIONS FOR V/STOL PROJECTED TO 1995

HARDWARE	WEIGHT (LBS)	VOLUME (FT^3)
CNI		
UNH	18	.30
Secure Voice	10	.12
IFF (W/coder)	18	.27
Data Link	17	.15
TACAN	32	.61
Radar Alt.	8	.10
ADF	7	.30
Heading Ref.	3	
Aids		
HUD	50	.98
MFD	30	.74
MMD	30	.60
ICS	18	---
Funct. Gen.	28	.97
HSI	14	.21
Armament Control	30	.75
Carrier Landing	27	.33
Sensors		
Radar	300	5.00
Inertial	38	.63
ECM		
ALR	60	1.0
Dispensers	61	.78
Interface Units	36	
Data Processing	50	1.20

3.5.6 Crew Station

Escape System - The basic functions of the escape system are to boost, separate, recover, and survive. This advanced automatic aircrew escape system is capable of crewman recovery from 0 to 600 KEAS and altitudes from 0 to 50,000 feet. It has a bi-modal system to provide the shortest time sequence, dependent upon speed at time of emergency onset, to full personnel parachute inflation towards enhancing crewman recovery capability with the aircraft under adverse attitude, low altitude and angle of dive situations. This escape system incorporates a device to provide warning indication for advising the crew of the escape potential for a given situation. Further, for a specific area where the crew member recognizes a catastrophic aircraft failure and reacts in sufficient time for successful egress, automatic ejection will occur. Figure 3-10 depicts the sequence operation. For emergency aircraft evacuation this ejection seat would have a multi-mode sequence comprised primarily of two separate subsystems, the ejection system, and the recovery system.

The ejection system would encompass a crewman packaging sequence and a propulsion system to accomplish egress from the cockpit. Upon initiation of the egress system, a passive/positive restraint system for both arms and legs would be activated to prevent flailing injuries during high speed ejections. If the aircraft is in an adverse or uncontrolled flight condition at ejection, extremities restraint is beneficial at much lower speeds. This packaging sequence should occur within less than .3 second.

In the recovery system, parachute arrangement is the key to successful recovery. Therefore, it will be located on the seat, permitting deployment prior to seat-man separation. This arrangement allows flexibility in choosing the parachute deployment time and provides for optimization considering speed-altitude situation. The configuration permits use of inflating personnel parachute to effect positive seat-man separation in a clean manner plus precludes seat-man/parachute interference or collision. This multi-mode system will provide for seat stability control at low speed by the immediate deployment of the personnel parachute. At high speed and/or altitude conditions, a drogue chute will be deployed initially to hold seat in an upright attitude for stable-deceleration control to a speed/altitude safe for personnel parachute deployment.

Performance in the new generation fighter will generate sustained load factors which exceed the pilot's ability to withstand the associated "G" forces and to permit him to fully use his aircraft throughout the flight envelope with a conventional upright seat system. Maximum pilot's tolerance to sustain G load factor in a conventional upright seat is in the range of seven to eight G's for a period not exceeding two minutes. For sustained G's exceeding three minutes the tolerance level is in the four to five G range. Tolerance limitations are influenced by difficulty in breathing and chest pains.

The use of a two position reclining seat in the cockpit area would have the potential to substantially improve the pilot's ability to make full use of the maneuver performance which will be inherent in the advanced fighter aircraft design. Use of the reclined body position would have significant influence on minimizing detrimental physiological effects during air combat maneuvers, by providing the pilot with load factor protection for short periods. The recline seat also would have the potential for improving pilot performance at moderate G levels by removing the need for vigorous straining exercises to maintain perceptual and cognitive functions. For example, weapon release phases under simulated combat conditions have indicated that the load factor levels are generally in the range of three to five G. The reclined seat, therefore, has the potential to provide the pilot with the physiological edge for better performance.

Reclining the seat should provide the pilot with an incremental increase in tolerance level in the range of two to four G's and with prudent selection of the inclined seat back angle the maximum tolerance capability should be in the range of nine to 12 G's. In providing the aircraft with a cockpit configuration for high acceleration capability, the basic element is a seat which is capable of articulating in some fashion to a reclined position and thus reorienting the pilot with respect to the airplane resultant load factor vector. This position allows acceleration to be applied transverse to the pilot's axis thus resulting in a significant reduction in height of the hydrostatic column between the heart and carotid artery (blood supply system to the head), and to the lower extremities. Thus, eye level blood arterial pressure can be maintained and venous pooling reduced. Acceleration applied transverse to the pilot's spine is the position a human can accept higher G loadings. Some degree of acceleration protection provided to the pilot by the recline seat may be sacrificed by supporting the head to provide forward vision. It may be necessary to change the headrest angle which would result in elevating the head slightly. This would negate to some extent the load vector/arterial axis advantage gained by reclining. Raising the pilot's head as noted would enable the viewing of all primary displays and tracking aids under acceleration load factor. Rockwell has been studying the reclining seat concept and has selected the fixed seat for the present.

Those areas of the two position seat configuration which would require more thorough investigation in the realm of high "G" cockpit environment are:

a. Ejection capability/requirements under high acceleration.

b. Location/position of ejection controls for high acceleration applications.

c. Requirements necessary for emergency egress in supine position.

d. Supine articulation pivot position, shoulder versus back.

e. Supine seat - cockpit controls integration.

f. System egress and recovery mode configuration.

For the present concept Rockwell has selected the fixed seat concept.

Canopy - The cockpit is enclosed by a one-piece, clamshell, aft-hinged windshield/canopy (consisting of a polycarbonate transparency attached to a peripheral frame structure) that seals against fuselage longeron sills and by an aft bow-frame located just aft of the escape clearance envelope. The transparency will provide the desired resistance to bird strikes during subsonic operations. The windshield/canopy is easily jettisoned by the pilot or ground rescue personnel. Pyrotechnically initiated thrusters react against the forward portion of the canopy frame, rotating it up and aft until it unlocks from the aft hinges and is carried aft to provide clearance for emergency escape. The HUD combiner plane and the hard-panel glare shield provide adequate wind-blast protection during deck/ground-handling/taxi modes and during emergency flight operations after inadvertent canopy loss. The hard-panel glare shield may be easily unfastened and removed for easy maintenance. An important point, the canopy shall not delay egress of the seat from the cockpit. Therefore, the canopy shall either be jettison, cut, or penetrated by the seat during an emergency egress.

Vision - In a vertical takeoff and landing (VTOL) aircraft, the critical function of pilot operation at the different attitudes is of primary concern. The pilot must be afforded excellent visiblity and comfort so that he can operate his aircraft in the liftoff and touchdown maneuvers. The unique problem facing VSTOL operations is the necessity to maximize pilot vision while still maintaining a good supersonic area distribution. Forward quadrant vision angle of ten degrees in conjunction with overside vision of 40 degrees is provided per MIL-STD-850 for operation during liftoff and touchdown as well as transition. Low attitude angles are obtained during powered lift approach, thus providing good forward and side vision to maintain contact with the landing platform.

Displays-Controls - Cockpit CRT-type displays/instruments and primary and secondary controls are located and arranged for maximum efficiency and visual/tactile access during all normal and emergency flight modes and restraint conditions. All manually operated controls are located on either the right or left side of the cockpit, leaving the center area unobstructed for maximum display utilization. Adequate clearances permit rapid normal or emergency ingress/egress or safe escape throughout the subsonic flight envelope. The wide-angle heads-up display (HUD) provides the primary display of flight control, navigation, weapon delivery, energy mananagement, and selected threat-situation information. Other CRT-type displays are located on each side of and below the HUD to provide the necessary radar/E-O sensor, mission data, the aircraft subsystems status, and warning/caution/advisory displays. Primary controls and high-priority manual functions are located for access within reach limits and leg lengths of the pilot population under consideration.

The cockpit configuration is one that is designed to provide an efficient one crewmember arrangement that will be responsive to the functional and operational requirements for this type of noted air vehicle. Certainly the cockpit geometry can be arranged to accommodate the third through the 98th percentile male pilot (utilizing either Air Force or Navy Pilot population data). In addition, consideration has been given to the utilization of the female population as pilots. Current studies on the subject have indicated that for those cockpits sized to the male pilot population the 50th through the 95th female population can be accommodated. With further evaluation being conducted, it is realistic to assume that the lower female population range can also be accommodated.

Inlet Position - No interference of the egressing seat and the top mounted inlet is expected. High speed ejections would be the area of concern since the seat upon entering the airstream would be pitching aft. Initial assessment indicates that at high dynamic Q, the stable seat would in less than 50 miliseconds after egress from the cockpit have moved vertically at least two feet while moving aft 5-1/2 inches. At low speed the seat moves up and forward.

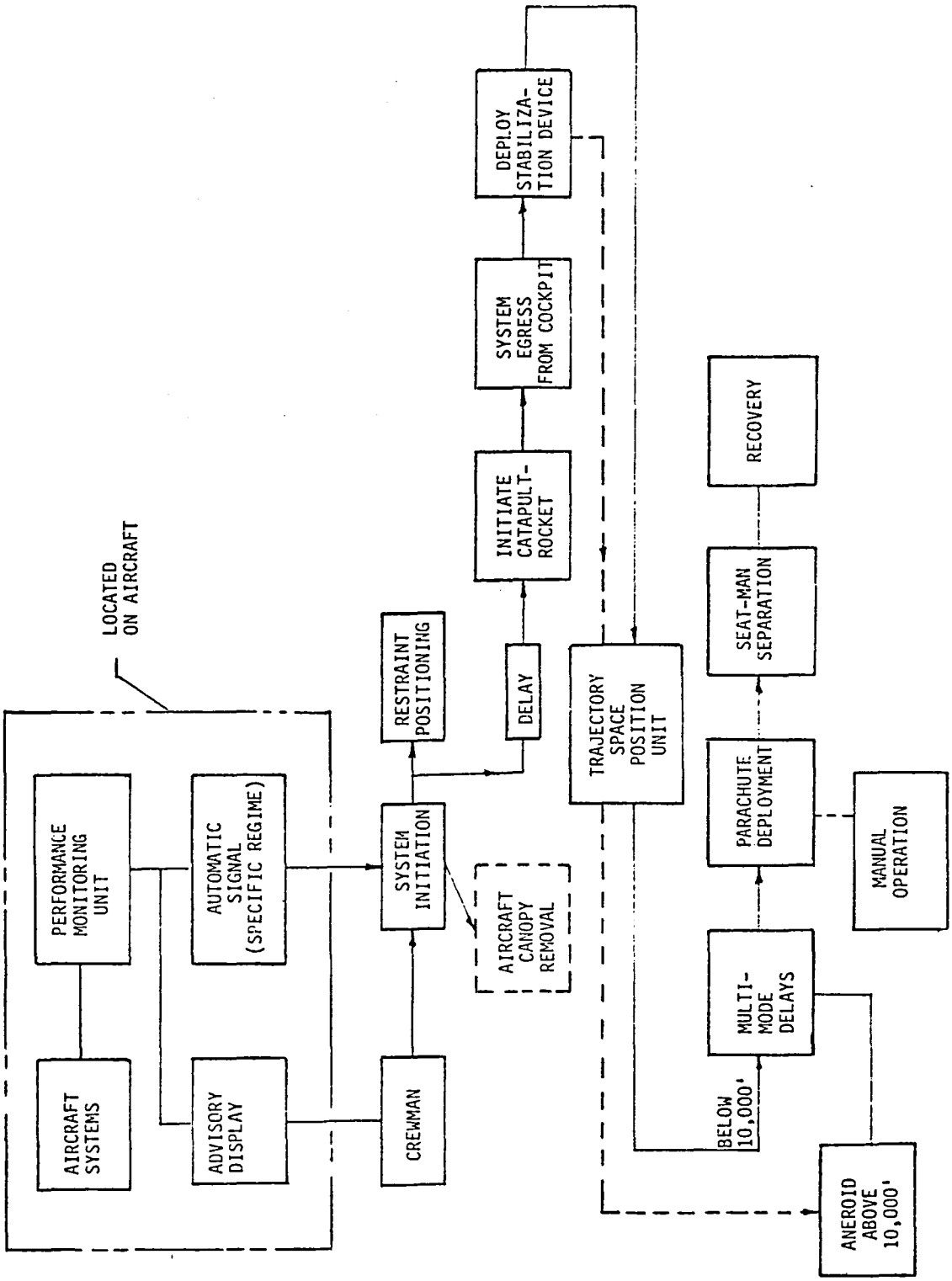

Figure 3-10 Escape System Diagram

4.0 AERODYNAMIC CHARACTERISTICS

4.1 BASELINE LONGITUDINAL CHARACTERISTICS - CONVENTIONAL FLIGHT

4.1.1 Drag

This section presents the drag characteristics of the baseline configuration along with a discussion of the methods used in the estimation of the drag. Trim drag data are based on a C.G. located at station 366.

Zero-Lift Drag - The zero-lift drag of the configuration is divided into the following categories:

- Skin Friction Drag
- Wave Drag
- Propulsion Installation Drag
- Store Drag

The skin friction drag was estimated using the NASA Delta Method of Reference (4-1), which is an empirical technique based on a correlation of measured drag data for both military aircraft and advanced concepts.

In this method the skin friction is calculated by summing the skin friction of the individual components and applying a correlation factor based on actual versus calculated drag data. The expression is:

$$C_{D_F} = 1.284 \sum C_f \left(\frac{S_{Wet}}{S_{Ref}}\right) F.F.$$

and

$$C_f = C_{f_{inc}} \left(\frac{C_f}{C_{f_{inc}}}\right)$$

where

$C_{f_{inc}}$, flat plate friction coefficient, is a function of Reynolds number and transition location (assumed to be at leading edge for this analysis), and the term $(C_f/C_{f_{inc}})$ is the ratio of compressible to incompressible skin friction.

The F.F. or form factor, which is based on a correlation of isolated body and wing low speed drag with their calculated flat plate drag, is a function of fineness ratio or thickness ratio. The 1.284 factor is the correlation factor between actual and calculated drag for fighter/attack type aircraft.

Figure 4-1 presents a detailed breakdown of the wetted area distribution of the configuration, and Table 4-1 presents the skin friction drag buildup for M=0.60 at 30,000 feet altitude. The miscellaneous drag item is the result of the 1.284 correlation factor noted above. The skin friction drag coefficient value of .01172 is small

TABLE 4-1

BASELINE CONFIGURATION
SKIN FRICTION BUILDUP

M = 0.60 ALTITUDE = 30,000 FEET S_{REF} = 541.0 FT.^{2}

Component	Wetted Area ~ S_{Wet} ~ Ft^2	Characteristic Length ~ ℓ ~ Ft.	Reynolds Number ~ R_N	Form Factor F.F.	C_f	$\Delta C_{D_F} = \frac{F.F. \times C_f \times S_{Wet}}{S_{Ref}}$
Fuselage	751.00	48.20	8.22×10^7	1.213	.00206	.00345
Wing	855.8	18.55	3.16×10^7	1.130	.00237	.00421
Wing End Plates - Fwd	27.42	5.54	9.4×10^6	1.130	.00286	.00016
Wing End Plates - Aft	81.4	7.58	1.29×10^7	1.130	.00272	.00046
Vertical Tails	147.4	5.55	9.5×10^6	1.130	.00286	.00088
Miscellaneous	-	-	-	-	-	.00256

Total S_{Wet} = 1863.02 Ft.^{2} Total C_{D_F} = .01172

$$C_{f_e} = \frac{.01172 \times 541.0}{1863.02} = .0034$$

because of the large wing area, and the large wing chord which results in a high Reynolds number and a low flat plate friction coefficient.

The wave drag at supersonic speeds was calculated by the contractor's Configuration Development System (CDS), Reference 4-2, which utilizes a far field linearized approach where the wave drag of a configuration is the average of the wave drag of a series of equivalent bodies of revolution. The equivalent bodies are based on area distributions determined by a series of oblique cuts inclined at the given Mach angle. A cross-sectional area distribution buildup for the baseline configuration is shown on Figure 4-2.

The transonic wave drag variation was calculated with the NASA Delta Method which was then faired into the supersonic results discussed above.

Figure 4-3 presents the propulsion installation drag increments. The propulsion installation drag includes those items which are either independent of power setting, such as the boundary layer diverter drag and the inlet bleed drag, or those associated with a "reference" engine operating condition, such as the spillage drag for the inlet at the critical mass flow ratio. The nozzle afterbody drag for the nozzles in the full-open position normally also falls in this category; however, in this instance the nozzle afterbody drag is not included in the drag. The spillage drag increment from critical inlet operation and the nozzle afterbody/base drag are included in the engine thrust data.

Figure 4-3 also presents the drag increments associated with the carriage of two and four Advanced Intercept Air-to-Air Missiles (AIAAM). The missiles are carried semi-submerged on the fuselage. Additional store installation subsonic drag data (drag areas) are shown on Table 4-2.

TABLE 4-2

STORE INSTALLATION SUBSONIC DRAG AREAS

Store Installation			Drag Area ~ $\Delta C_D S$ ~ Ft.^{2}
No.	Store	Carriage	
2	AIAAM	Semi-Submerged	.43
4	AIAAM	Semi-Submerged	.56
2	SRAAM	Pylon	.36
2	HARPOON	Pylon	1.42
4	SRASM	Pylon	1.11
2	200 Gallon Tanks	Pylon	1.06

Figure 4-4 presents the total zero lift drag coefficient variation with Mach number at 30,000 ft altitude for the clean configuration. This includes the skin friction drag, the wave drag, and the propulsion installation drag.

Drag-Due-to-Lift - The estimated drag-due-to-lift for the total configuration is based on 100 percent suction plus corrections to account for suction losses and associated edge vortex forces. These corrections were obtained from References 4-3 and 4-4 and are incorporated in the Aerodynamic Preliminary Analysis System II, Reference 1-7, used to determine the drag-due-to-lift. Typical results are shown on Figure 4-5 which presents the drag due to lift for zero (0) and 100 percent suction at M = 0.6, and the estimated values for the aircraft with zero flap deflection and with the flap deflected for trim. At a lift coefficient of .2 which corresponds to subsonic cruise, approximately 80 percent suction is indicated for the untrimmed case, and 100 percent suction for the trimmed case. The trim drag-due-to-lift is less than the untrimmed (zero flap deflection) because the airplane is unstable and requires a positive flap deflection (camber) for trim.

The variation of trimmed induced drag with Mach number is shown on Figure 4-4 for different trimmed lift coefficients as a function of Mach number. Trim drag polars for 0.3, 0.6, 0.9, 1.2, and 1.6 Mach number are presented on Figure 4-6. These data are for a C.G. location of Fuselage Station 366. The lift-to-drag ratio (L/D) as a function of trimmed lift coefficient is shown on Figure 4-7 for 0.60 and 1.60 Mach numbers at 10,000 feet and 50,000 feet, respectively. A maximum L/D of 10.7 is shown for the subsonic case while a value of 5.1 is indicated for the supersonic condition.

4.1.2 Lift and Pitch Characteristics

This section presents the estimated longitudinal characteristics of the baseline configuration. All pitching moment and trim data are for a C.G. located at Fuselage Station 366. The characteristics were generated using the Aerodynamic Preliminary Analysis System II (APAS), Reference (1-7), which was developed by the contractor under NASA contract NAS1-15674. High angle of attack data were evaluated using the contractor's High Lift Estimation Program and the USAF DATCOM, Reference (1-8).

Linear Data - The aspect ratio of the baseline wing is 1.83 and the leading edge sweep is 48.1° outboard. This geometry results in nonlinear lift and pitching moment curves at the higher angles of attack due to wing tip and leading edge vortex effects. In the angle of attack range of 0 to 5 degrees the data are relatively linear, however, Figure 4-8 presents the variation of lift curve slope and static margin, measured in the linear region, versus Mach number. The aircraft is approximately three percent MAC unstable at the subsonic Mach number, and 11 percent stable at the higher supersonic Mach numbers. The aircraft becomes stable at .92 Mach number.

Lift and Pitching Moment - The variation of lift with angle of attack and pitching moment with lift are shown on Figures 4-9 through 4-13 for an angle of attack range of 0 to 20 degrees and several control surface deflections. Data are presented for from 0.30 to 1.60 Mach numbers. Figure 4-9 presents the data at 0.30 Mach number. The vortex lift at the higher angles of attack is apparent with the lift at 20 degrees angle of attack approximately 25 percent higher than the slope at zero angle of attack would indicate. The aircraft is unstable throughout the α range with the configuration becoming less unstable with increasing α, demonstrating that the center of vortex lift is aft of the center of the linear or potential lift. The vehicle also has a positive pitching moment at zero lift. Data are also shown for control surface deflections of $+20^{\circ}$ on the inboard surface or elevons and zero on the outboard surfaces or ailevators, and for $+20^{\circ}$ on both surfaces. Both the elevons and the ailevators will be mutually deflected for pitch control at high angles of attack at subsonic speeds. Positive deflections are required for trim because of the unstable airframe.

Data at 0.60 and 0.90 Mach numbers are presented on Figure 4-10 and 4-11 for elevon deflections of +5 and +10 degrees. Positive deflections are required for trim in both cases, although for 0.90 Mach number, the positive pitching moment at zero lift is the primary reason for the positive deflection requirement.

Characteristics at 1.20 and 1.60 are shown on Figures 4-12 and 4-13 for -5 and -10 degrees elevon deflection. The aircraft is stable at these conditions and negative control surface deflections are required for trim. For -10 degrees deflection the trim C_L's are .53 and .29 at 1.20 and 1.60 Mach number. A trim lift coefficient of approximately .1 is required at altitude for these Mach numbers at the combat gross weight.

The variation of control effectiveness with Mach number is shown on Figure 4-14 for inboard flaps or ailevators deflected. Data at lower Mach numbers are also shown for both the inboard and outboard surfaces deflected.

Maximum Lift - The variation of trimmed maximum lift with Mach number is shown on Figure 4-15. The low speed value, which is for +20 degrees deflection on both inboard and outboard surfaces, was estimated with the contractor's high lift estimation program. The Mach number variation was estimated with Reference (1-8).

Damping in Pitch - The pitch damping variation with Mach numbers is shown on Figure 4-16 for low angles of attack. These data were generated with the Reference (1-7) program.

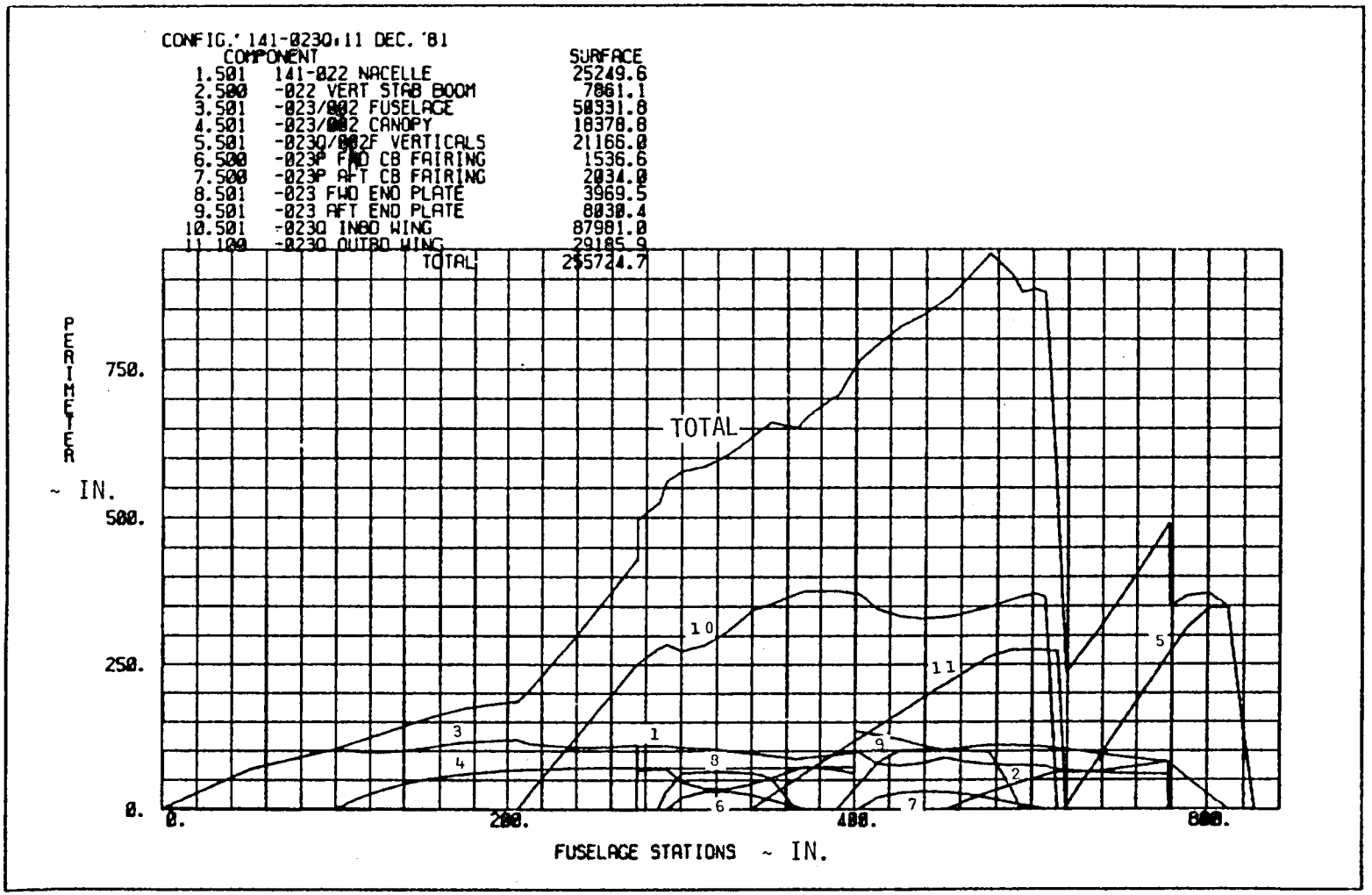

Figure 4-1 Baseline Configuration Wetted Area Distribution

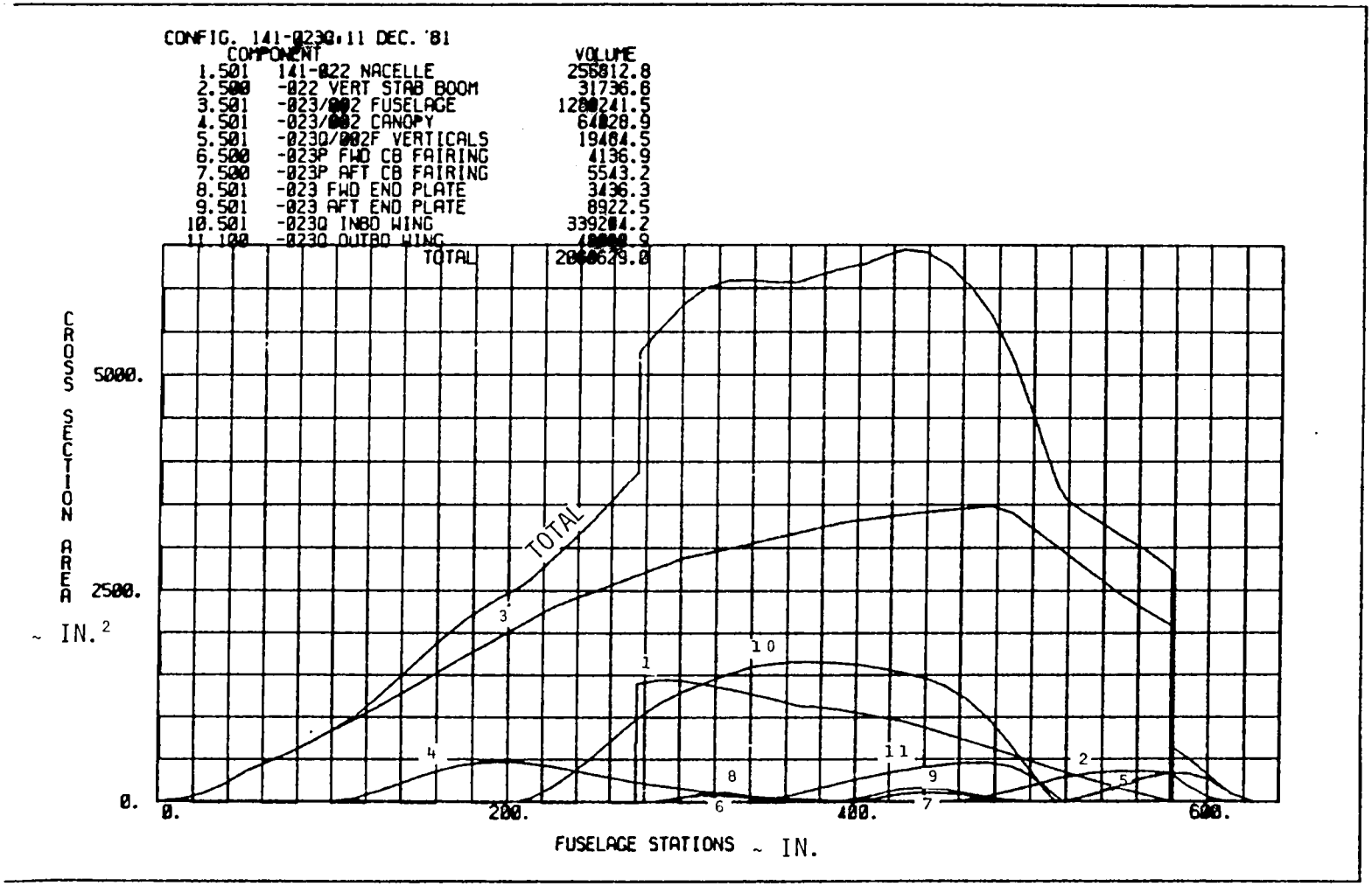

Figure 4-2 Baseline Configuration Cross Sectional Area Variation

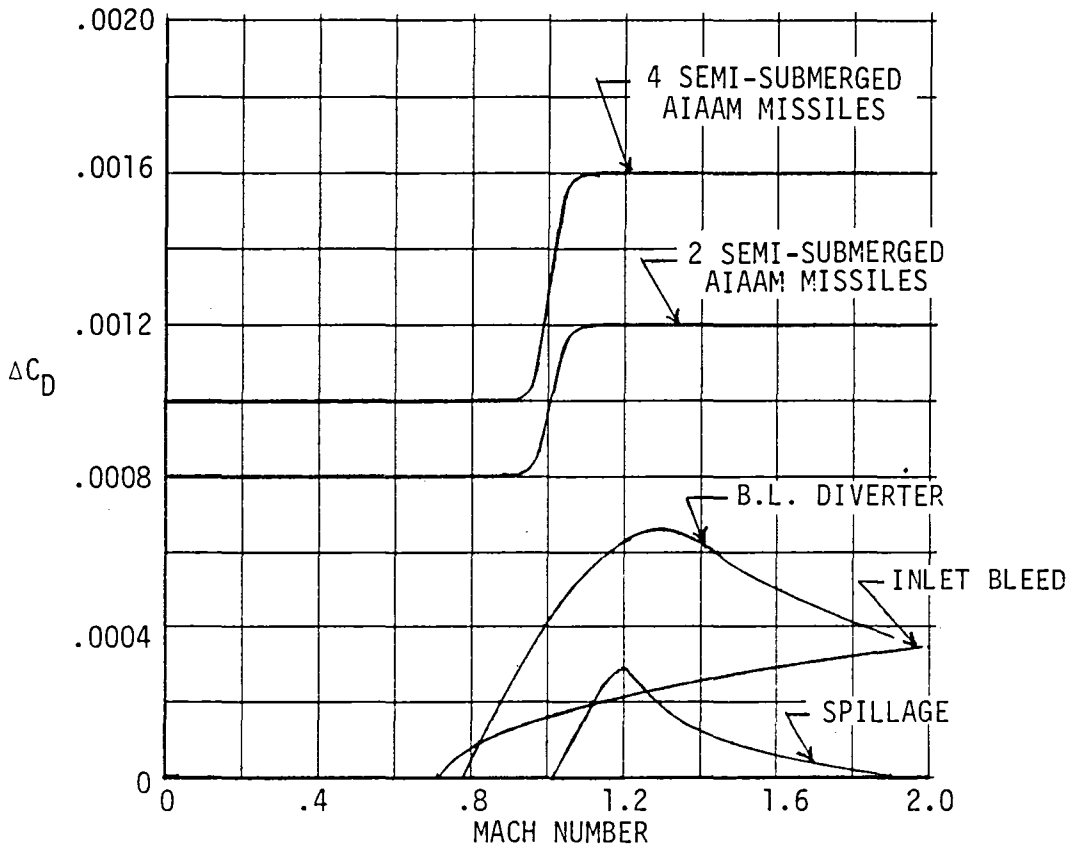

Figure 4-3 Propulsion and Store Installation Drag Increment Variation with Mach Number

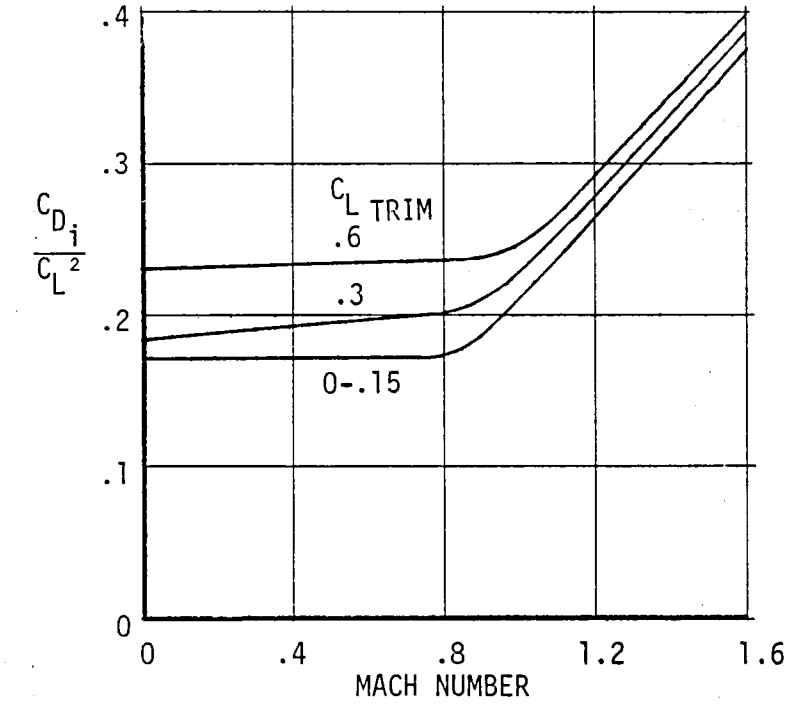

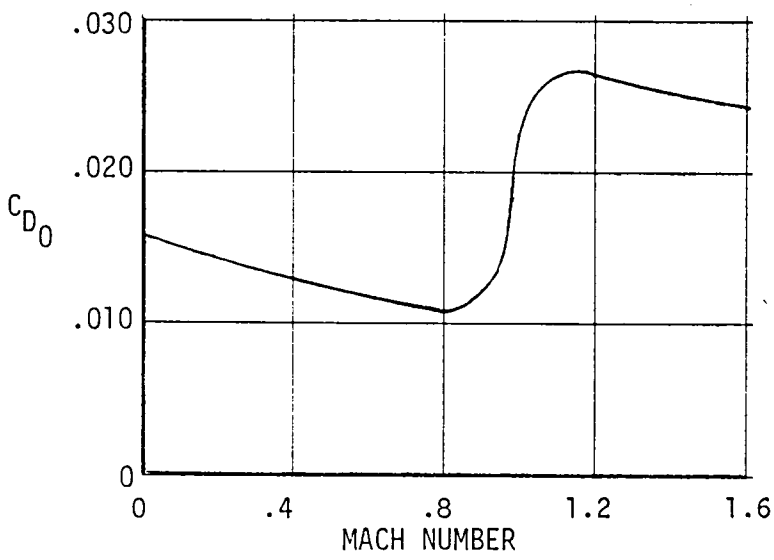

Figure 4-4 Baseline Configuration Drag Characteristics

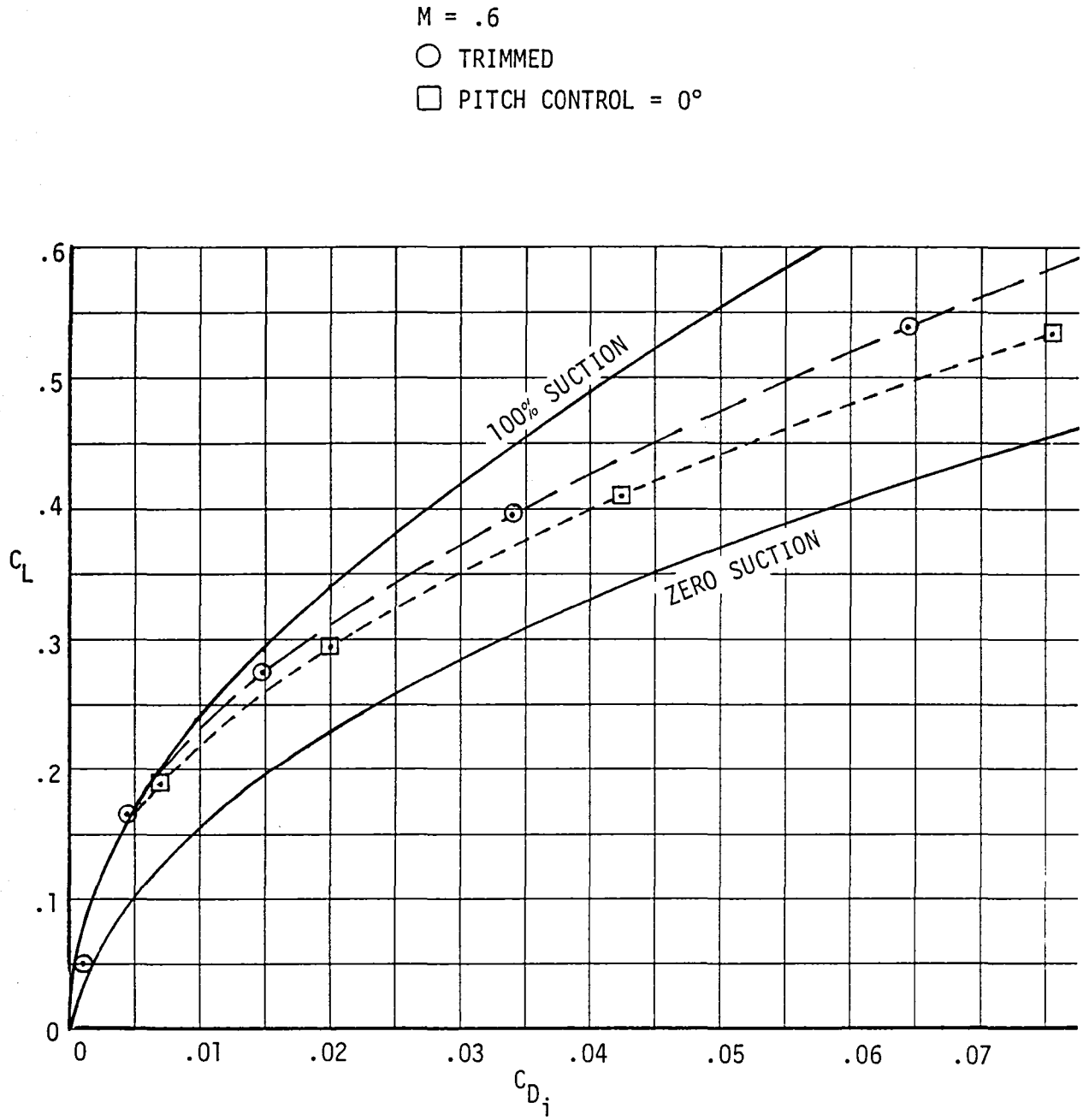

Figure 4-5 , Effect of Trim on Induced Drag

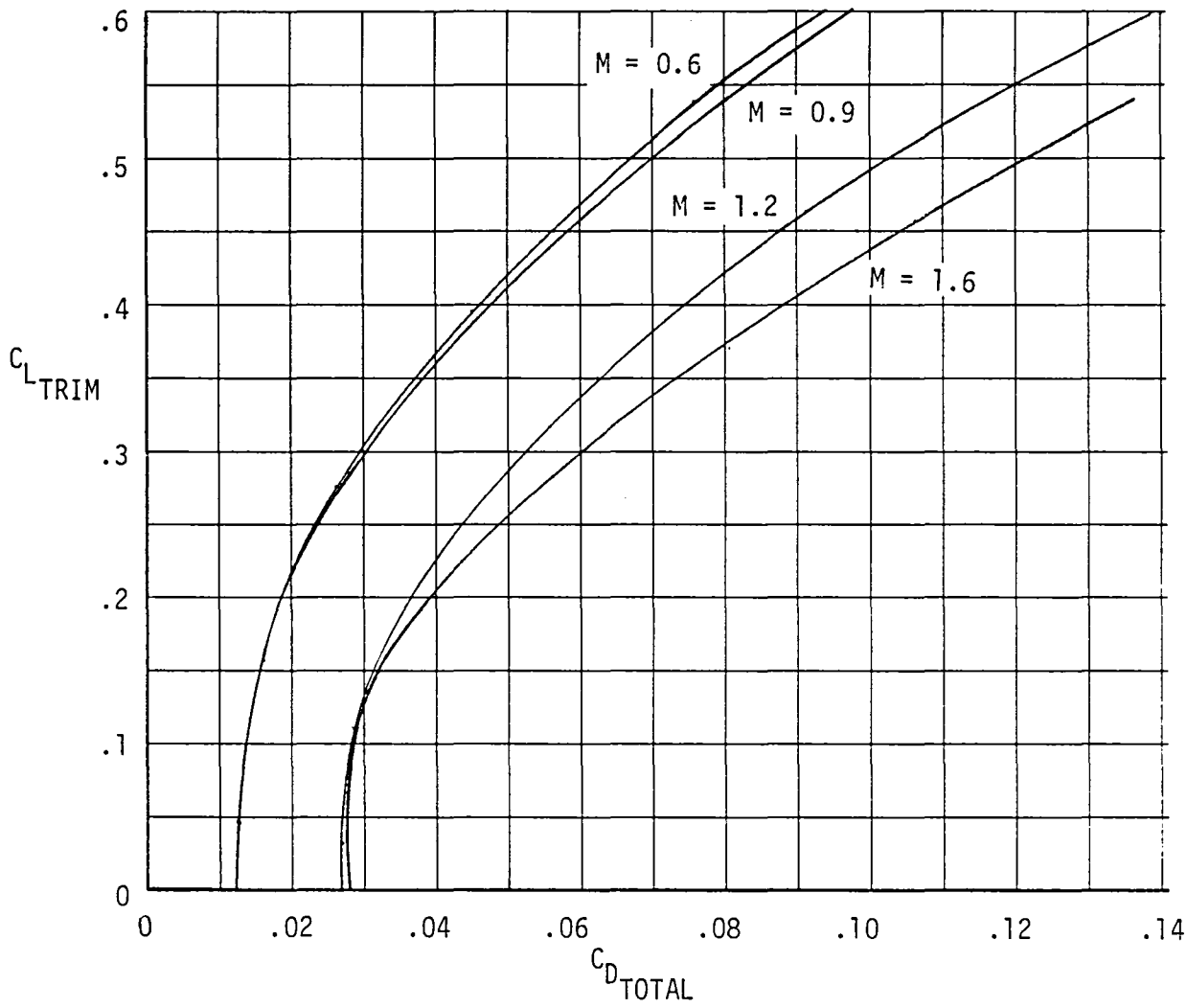

Figure 4-6 Baseline Configuration Trim Drag Polars

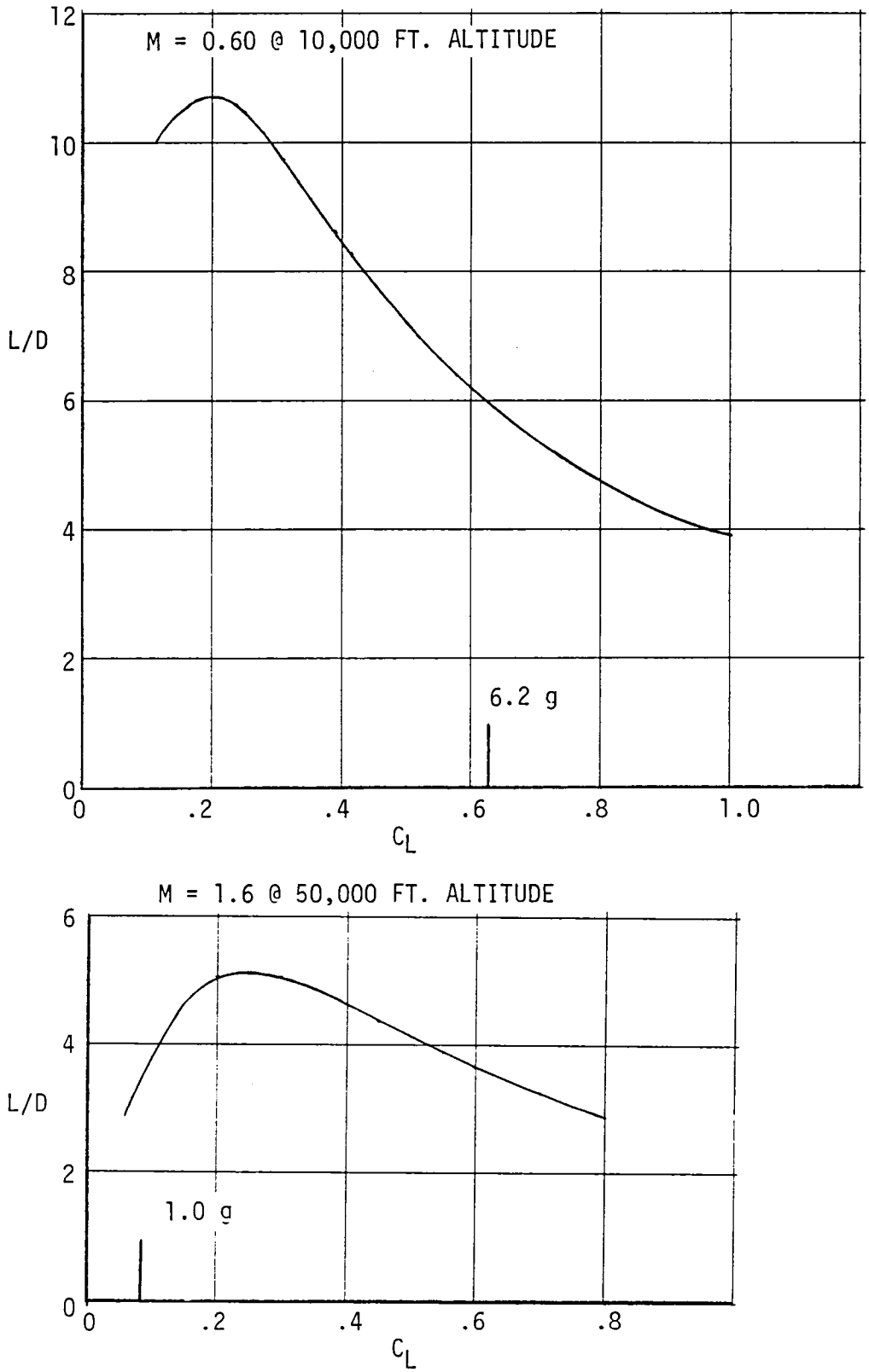

Figure 4-7 Baseline Configuration Aerodynamic Efficiency

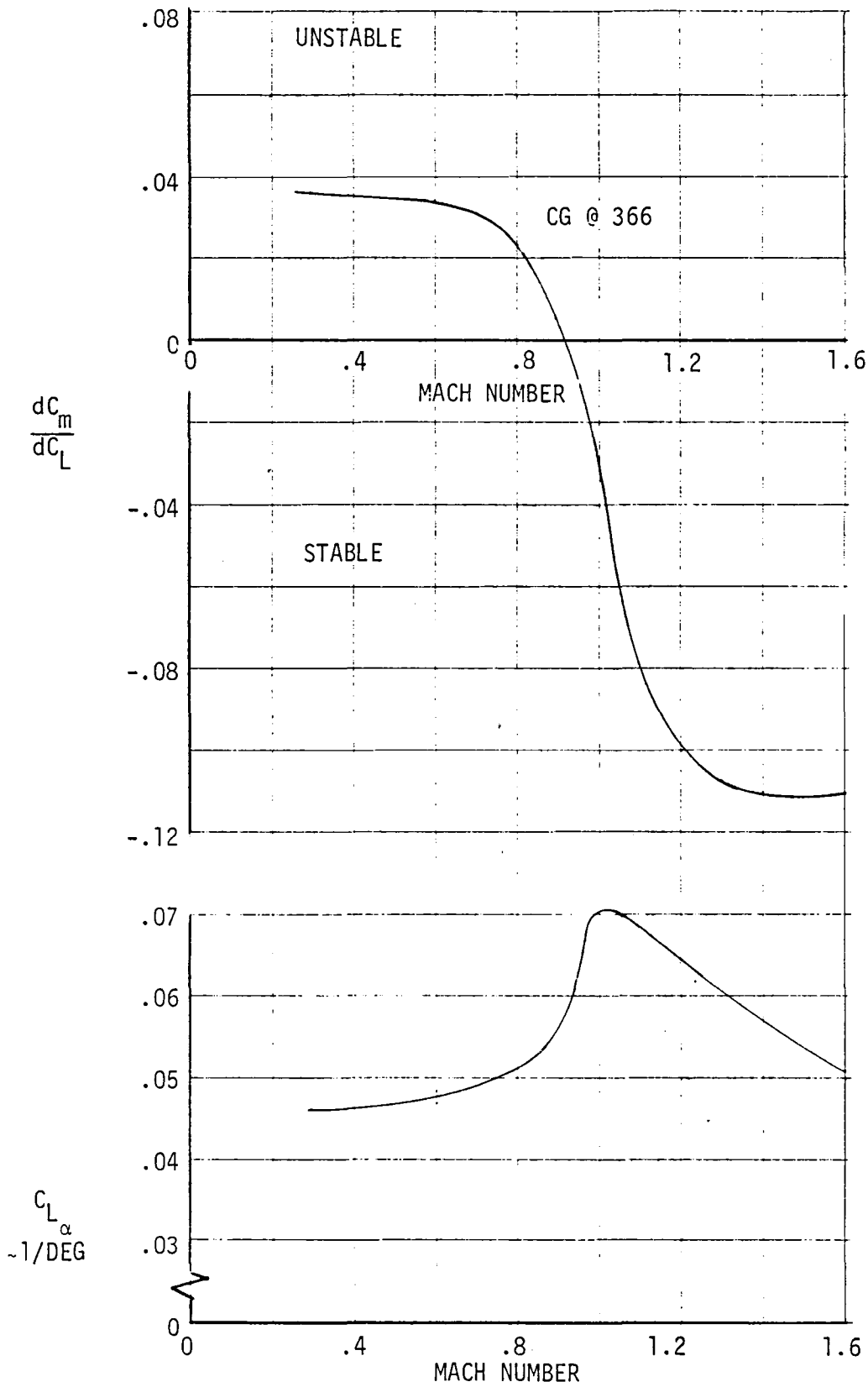

Figure 4-8 Baseline Configuration Longitudinal Characteristics ~ Zero Flap Deflection

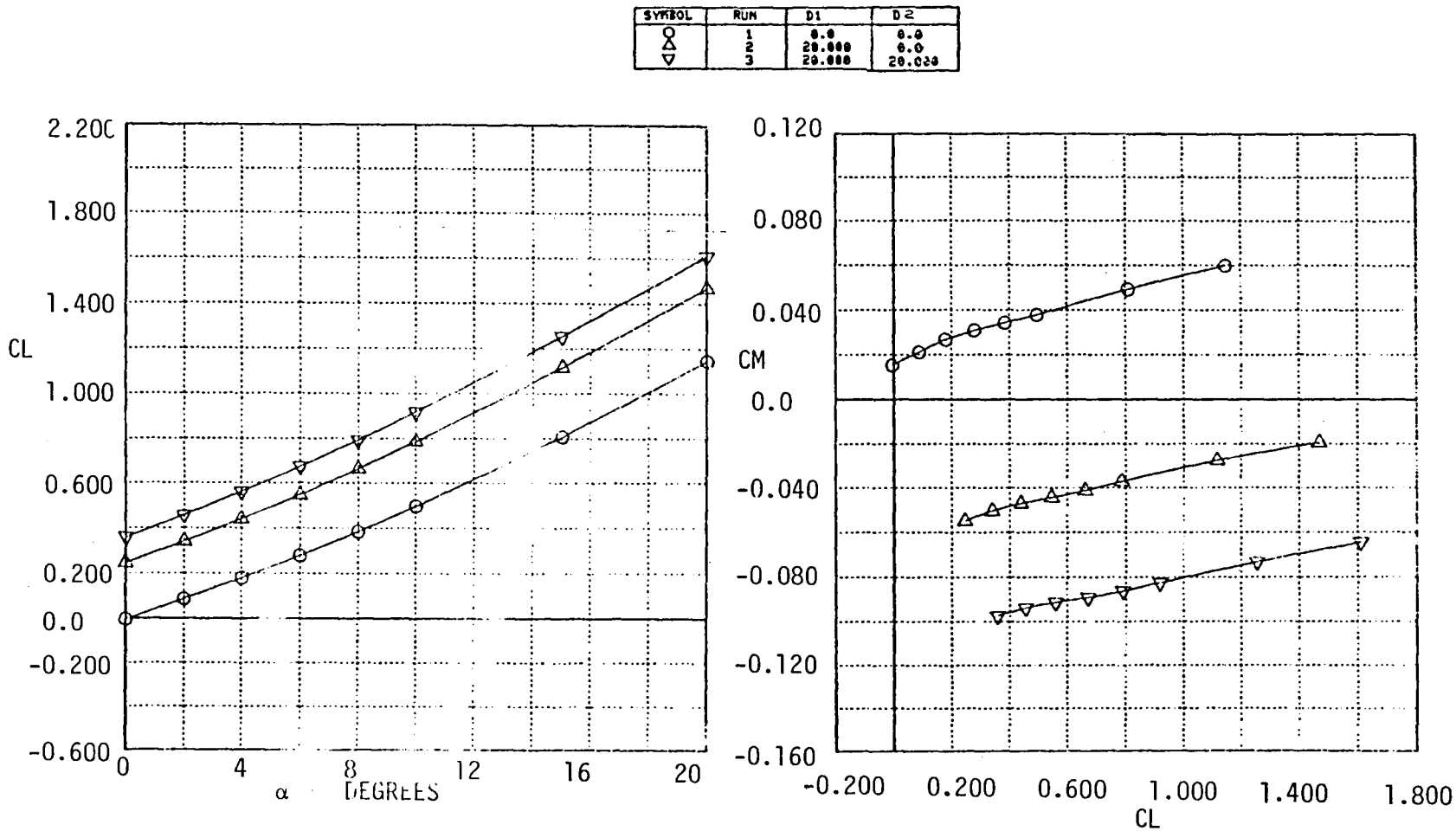

Figure 4-9a. Baseline Configuration, C_L vs α @ M = 0.3

Figure 4-9b. Baseline Configuration, C_L vs C_M @ M = 0.3

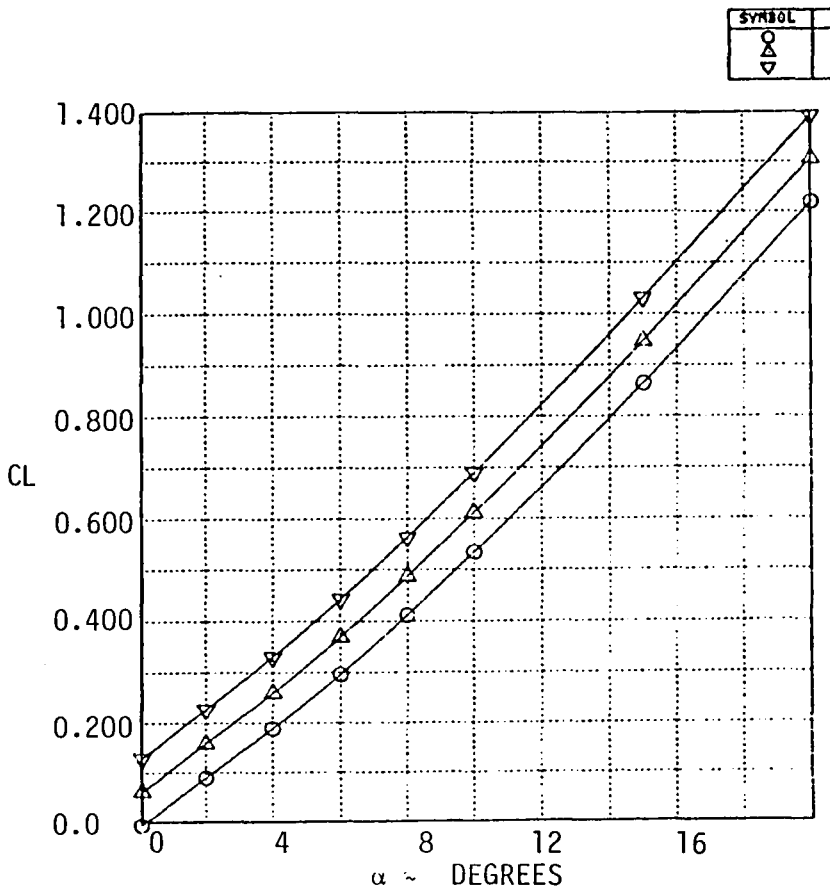

Figure 4-10a. Baseline Configuration, C_L vs α @ M = 0.6

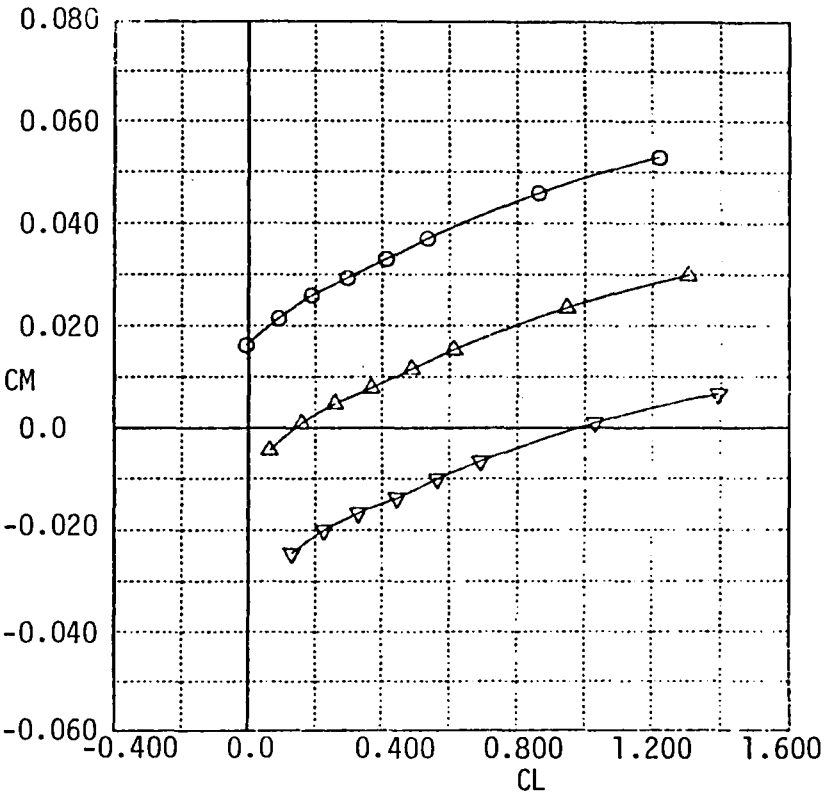

Figure 4-10b. Baseline Configuration, C_M vs C_L @ M = 0.6

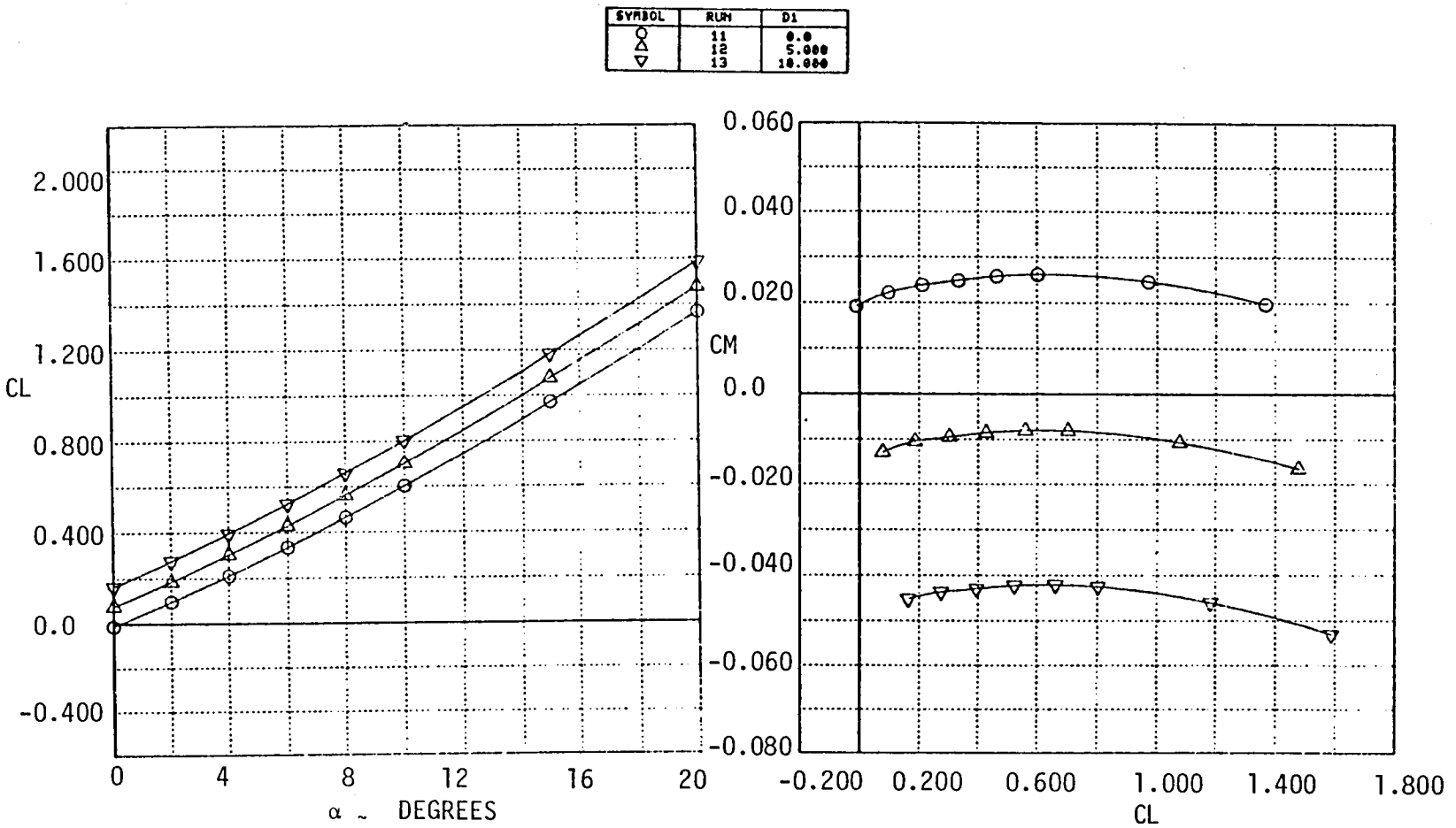

Figure 4-11a. Baseline Configuration, C_L vs α @ M = 0.9

Figure 4-11b. Baseline Configuration, C_M vs C_L @ M = 0.9

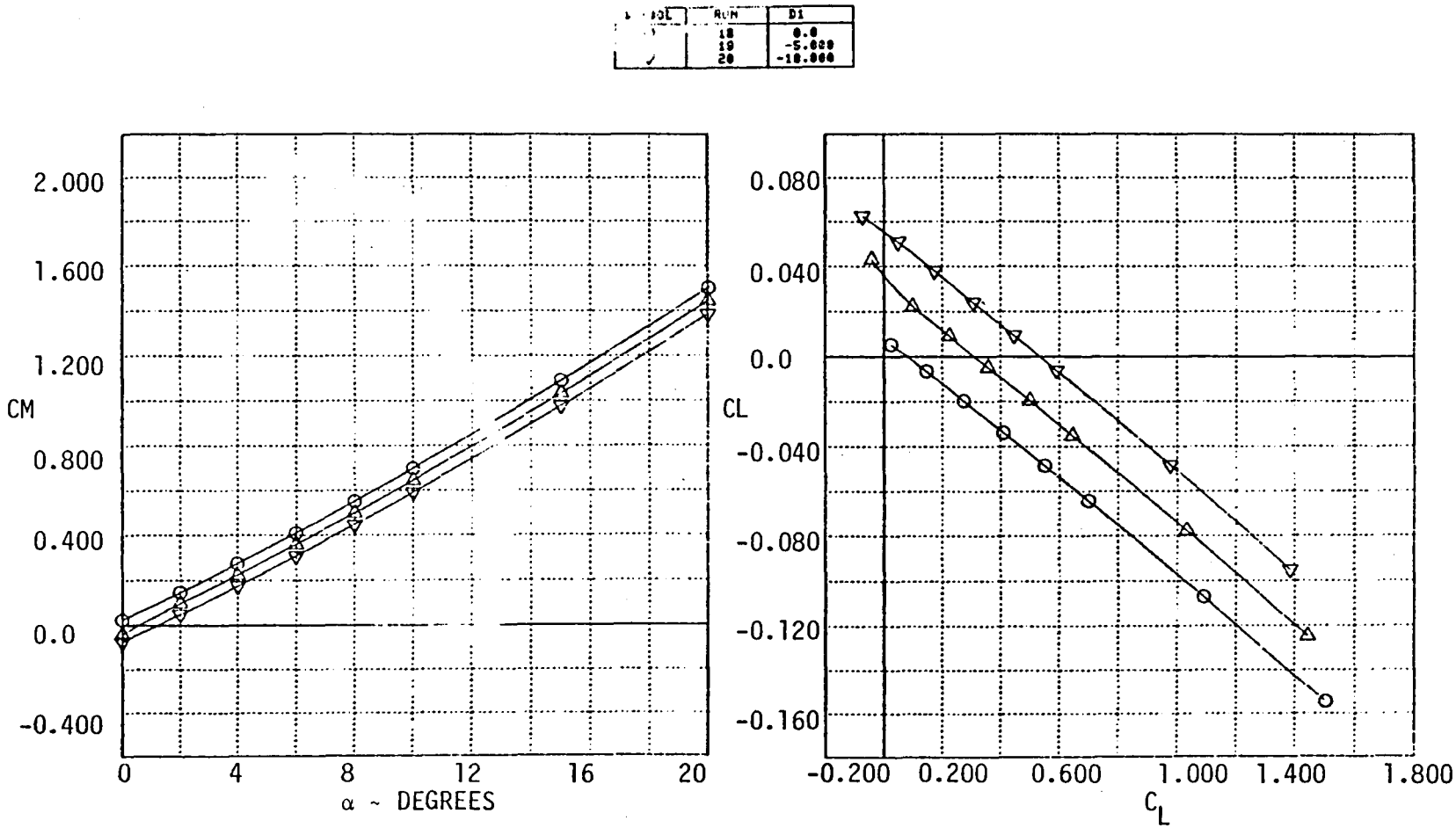

Figure 4-12a. Baseline Configuration, C_L vs α @ M = 1.2

Figure 4-12b. Baseline Configuration, C_M vs C_L @ M = 1.2

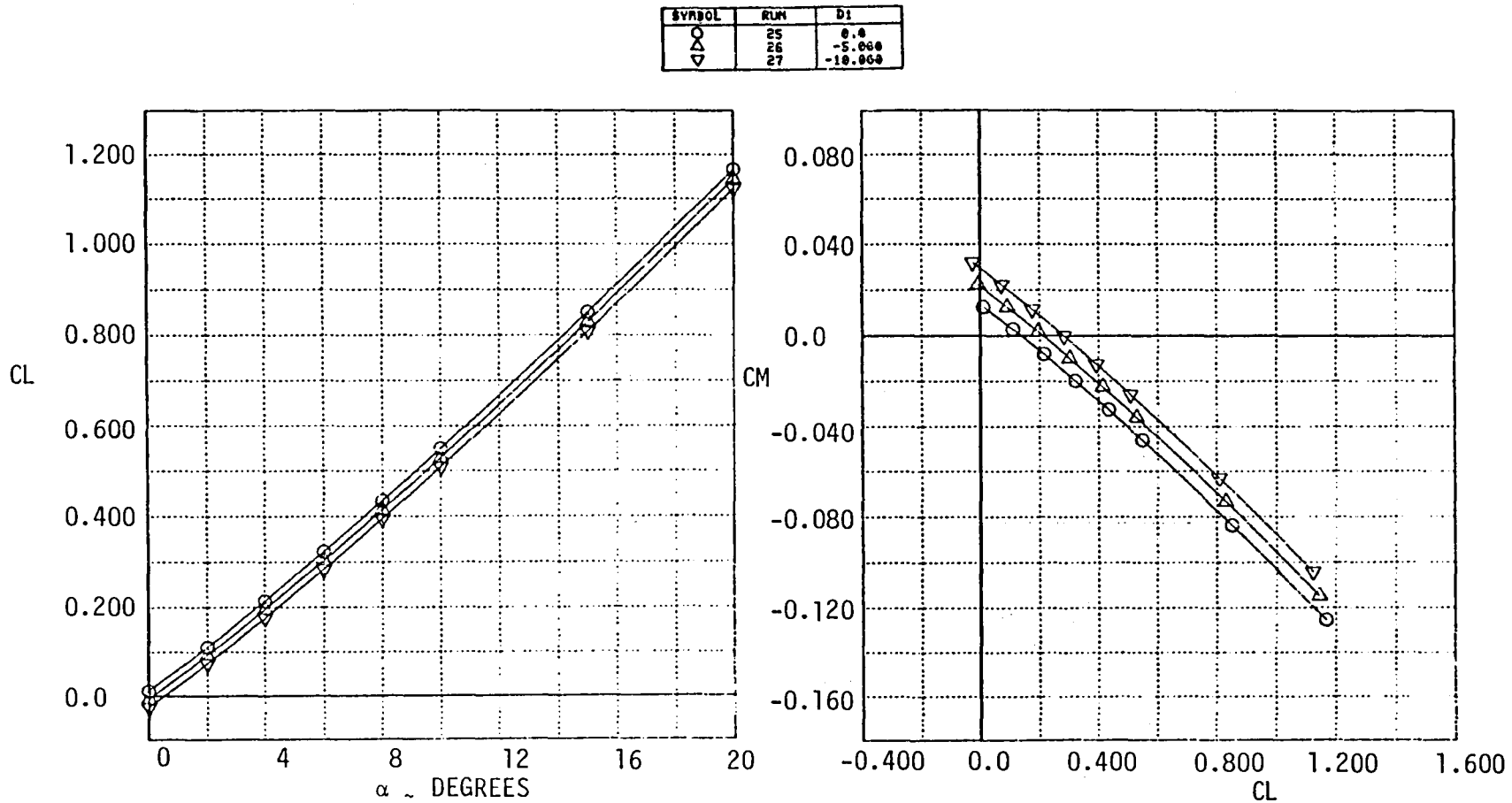

Figure 4-13a. Baseline Configuration, C_L vs α @ M = 1.6

Figure 4-13b. Baseline Configuration, C_M vs C_L @ M = 1.6

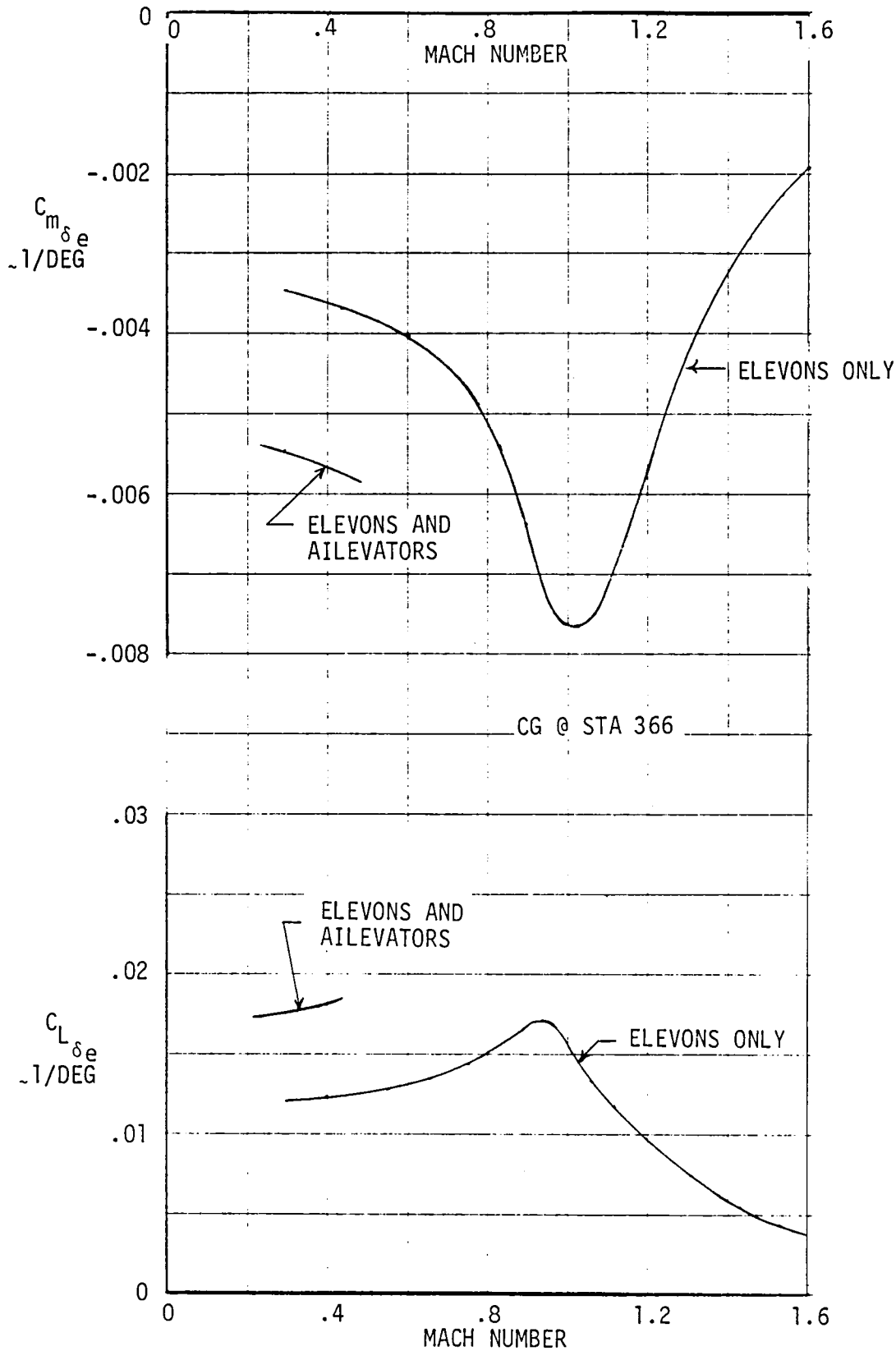

Figure 4-14 Baseline Configuration Longitudinal Control Effectiveness

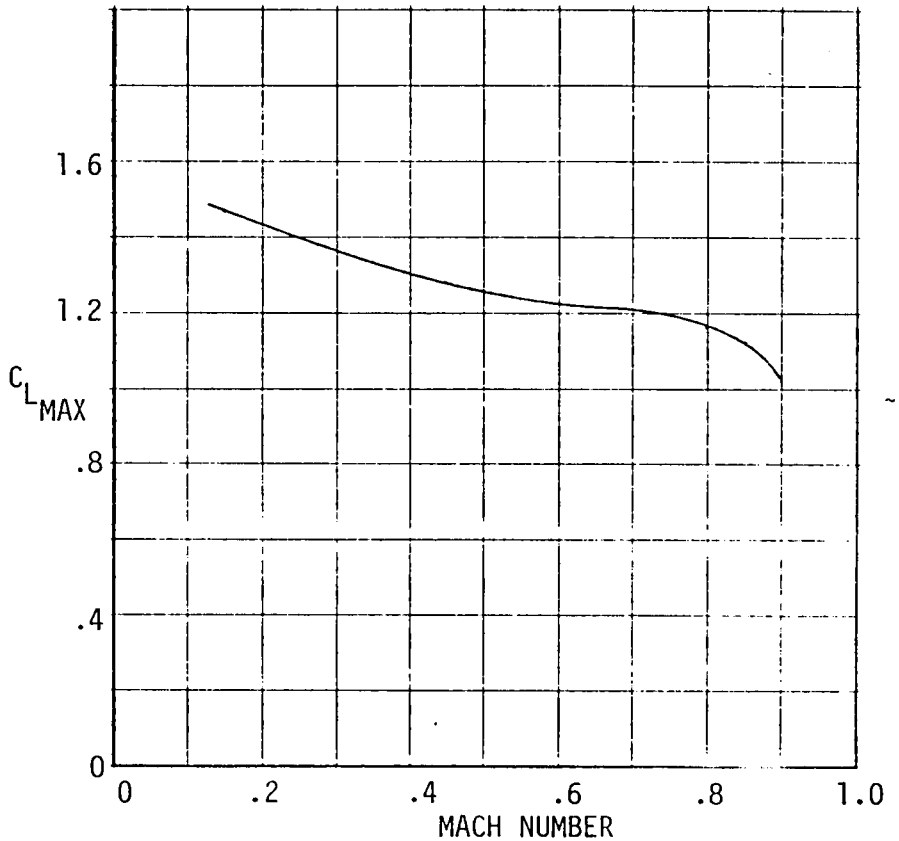

Figure 4-15. Baseline Configuration Subsonic Trimmed $C_{L_{Max}}$

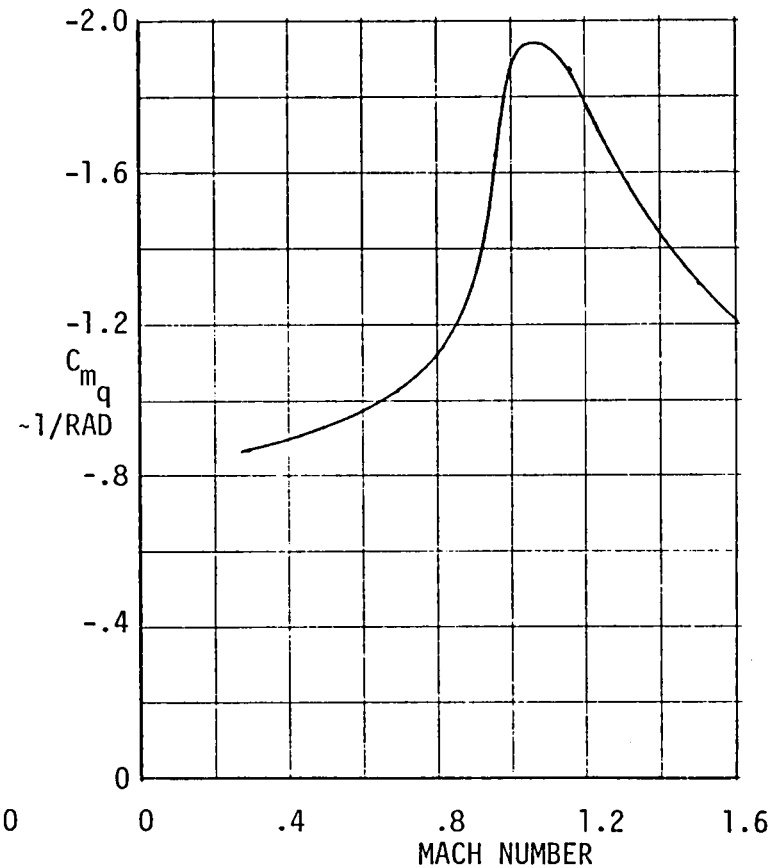

Figure 4-16. Baseline Configuration Pitch Damping

4.2 BASELINE CONFIGURATION LATERAL-DIRECTIONAL CHARACTERISTICS IN CONVENTIONAL FLIGHT

4.2.1 Stability

Lateral-directional aerodynamic characteristics in conventional flight were evaluated throughout the Mach range using the Aerodynamic Preliminary Analysis System II (APAS), Reference 1-7. The variation of static directional stability with Mach number at zero angle of attack is presented in Figure (4-17) for the rigid airplane. The level of stability is considered satisfactory such that the flexible configuration will be stable. The twin vertical tails are canted outboard 30 degrees to contribute to both pitch and yaw stability and are in a good position to provide control for recovery from unusual attitudes. The variation of directional stability with sideslip and angle of attack is presented in Figure (4-18) at M = .6 through M = 1.6. The directional stability is linear with sideslip but has some nonlinear variation with α.

Baseline configuration aero characteristics due to roll rate and yaw rate are shown in Figures (4-19) and (4-20). These data reflect good rigid levels for the preliminary design. Further analysis is required to evaluate the effects of flexibility.

4.2.2 Control

Directional control is provided by rudders in the twin verticals. Primary lateral control is provided by the wing outboard trailing edge flap. These flaps are used to supplement the pitch control and are thus dubbed ailevators. The wing inboard trailing edge flaps are used to supplement lateral as well as provide the primary pitch control and are dubbed elevons. The data presented in Figure 4-21 are for an antisymmetric deflection of one degree on each surface of the ailevator. Adequate roll response is generated to meet specification roll response requirements. Rudder effectiveness for 30 percent chord, full span rudders is shown in Figure 4-22. Deflection of the twin rudders results in some rolling moment input; however, the rolling moment does not appear to be significantly greater than for a single vertical of equal area on the centerline.

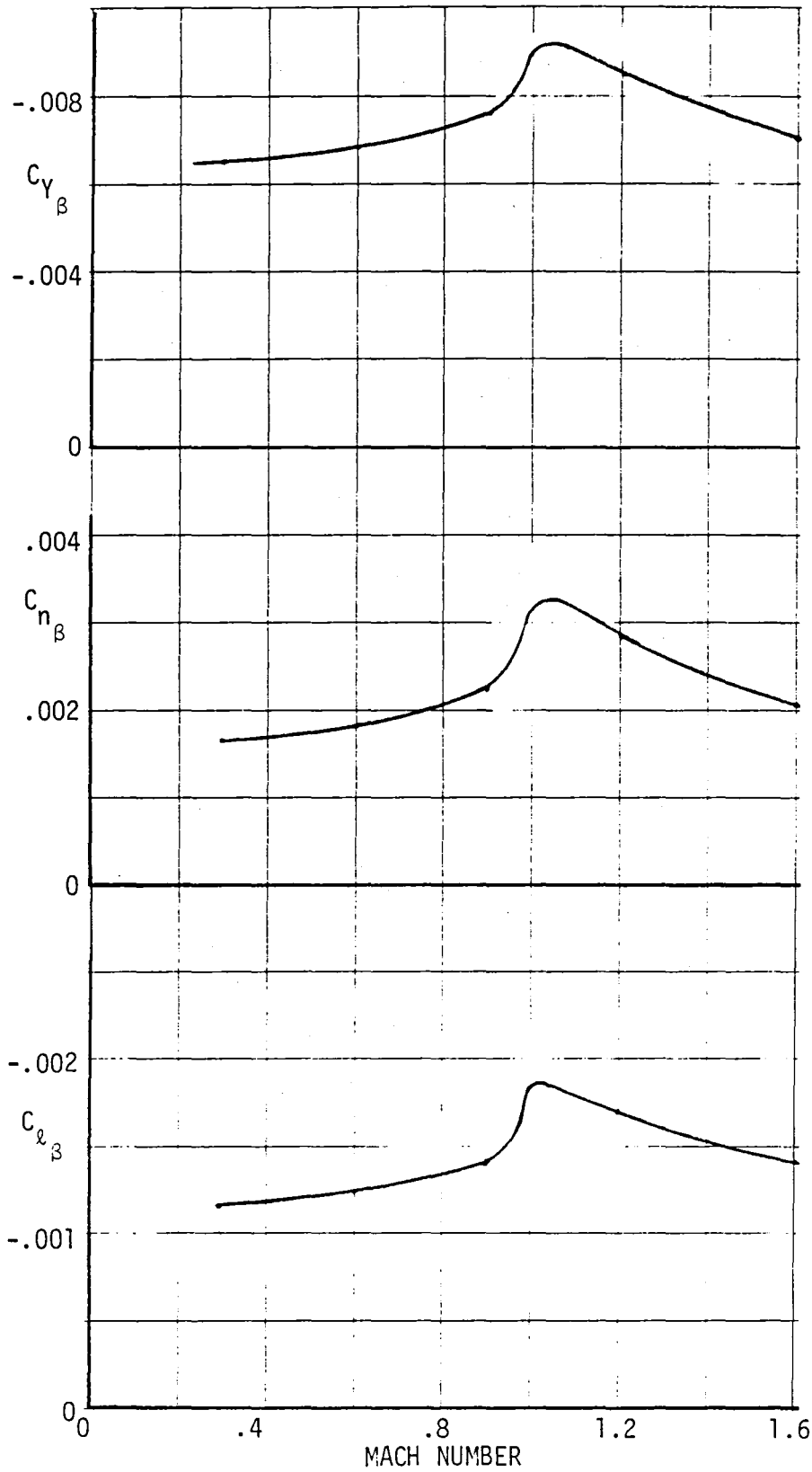

Figure 4-17 Baseline Configuration Static Directional Stability

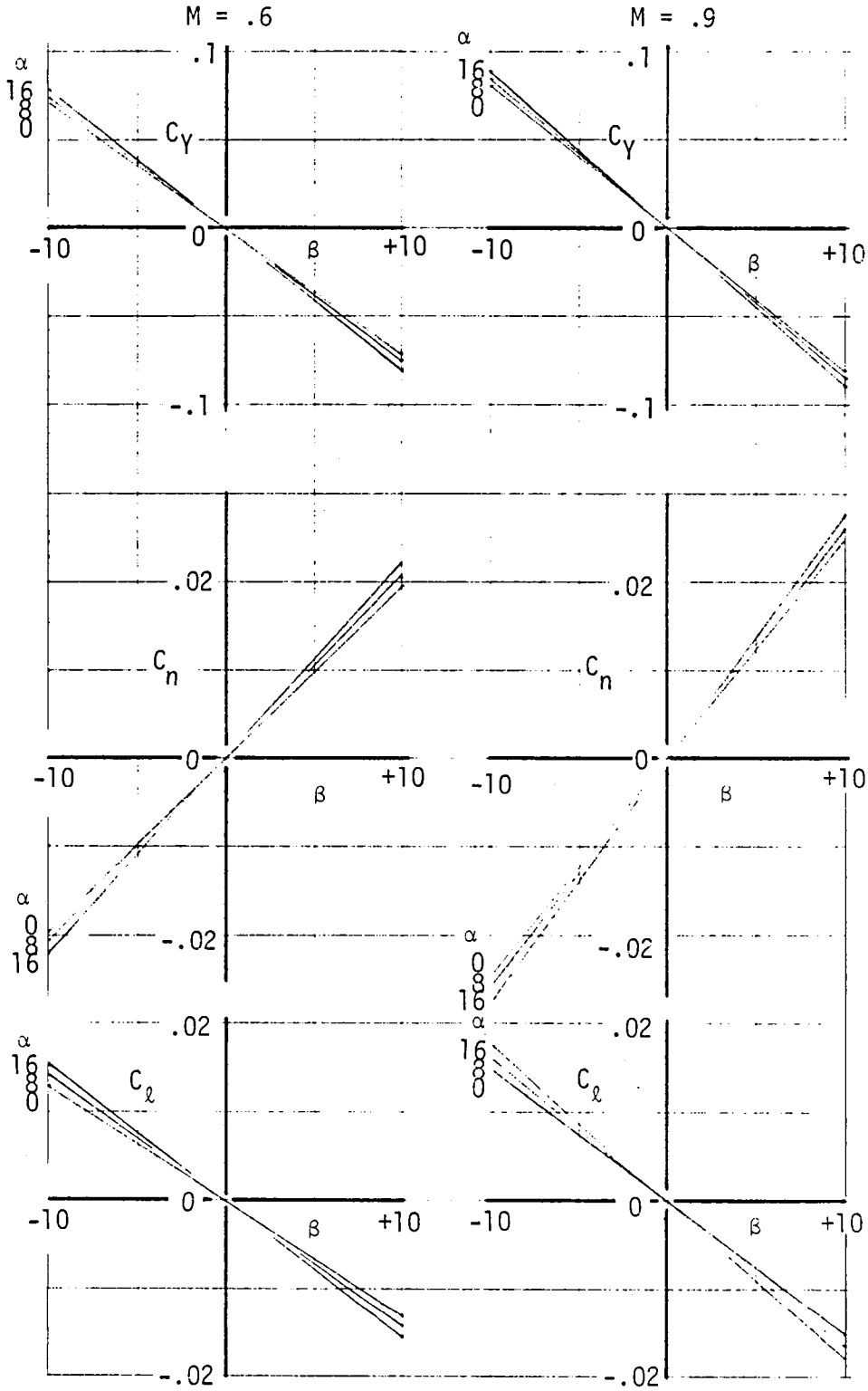

Figure 4-18a Baseline Configuration Directional Stability

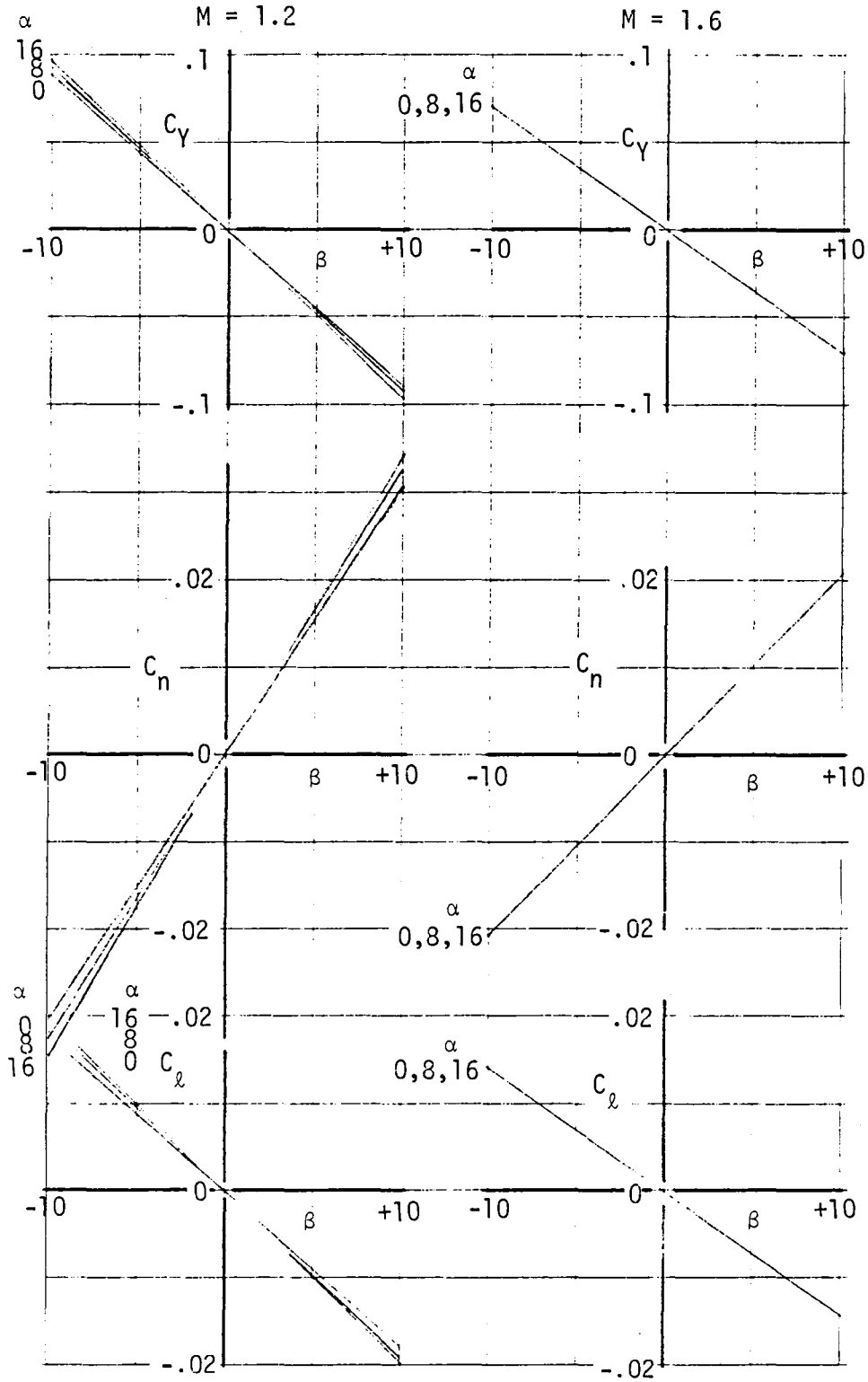

Figure 4-18b Baseline Configuration Directional Stability

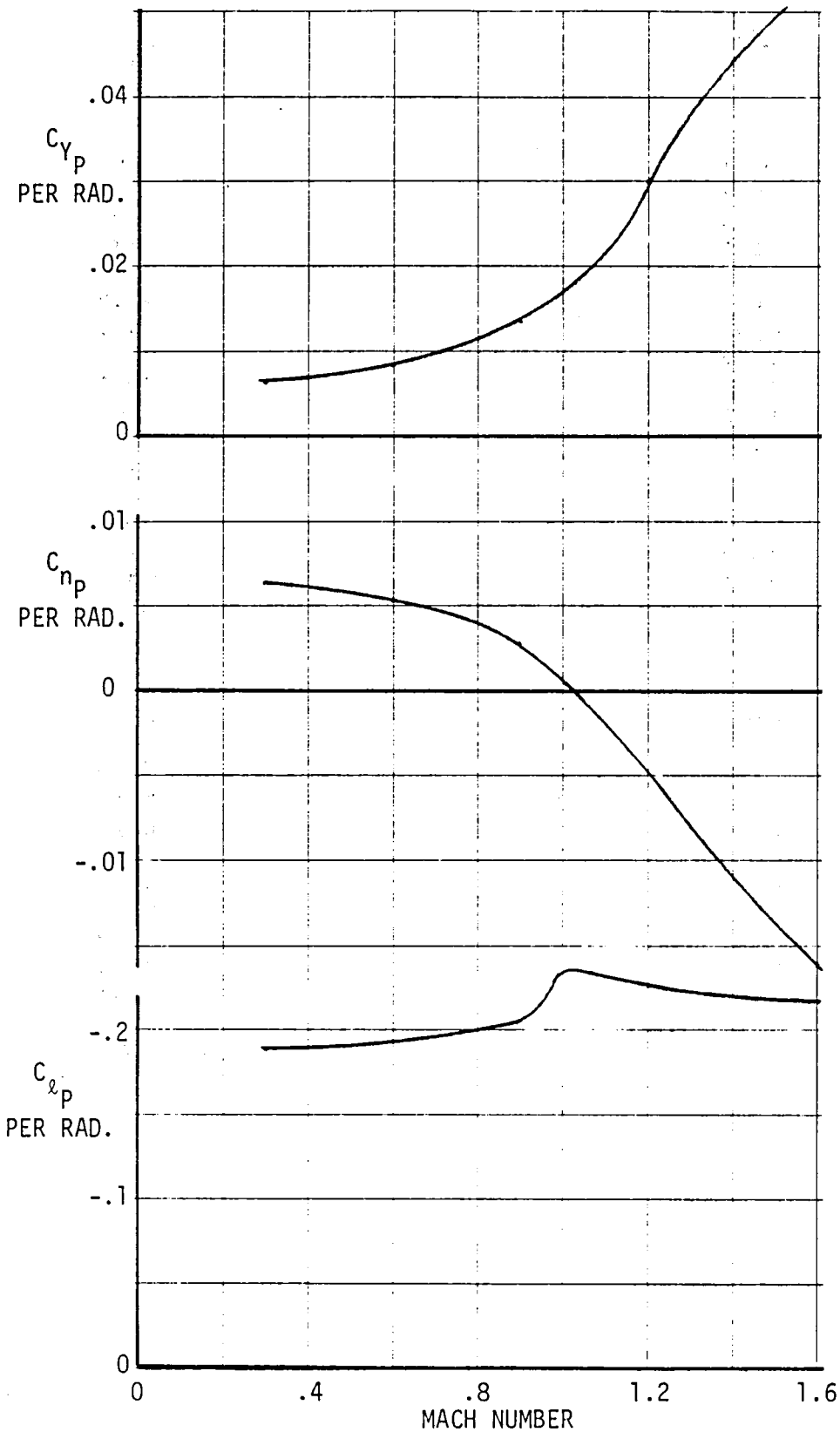

Figure 4-19 Baseline Configuration Rotary Derivatives

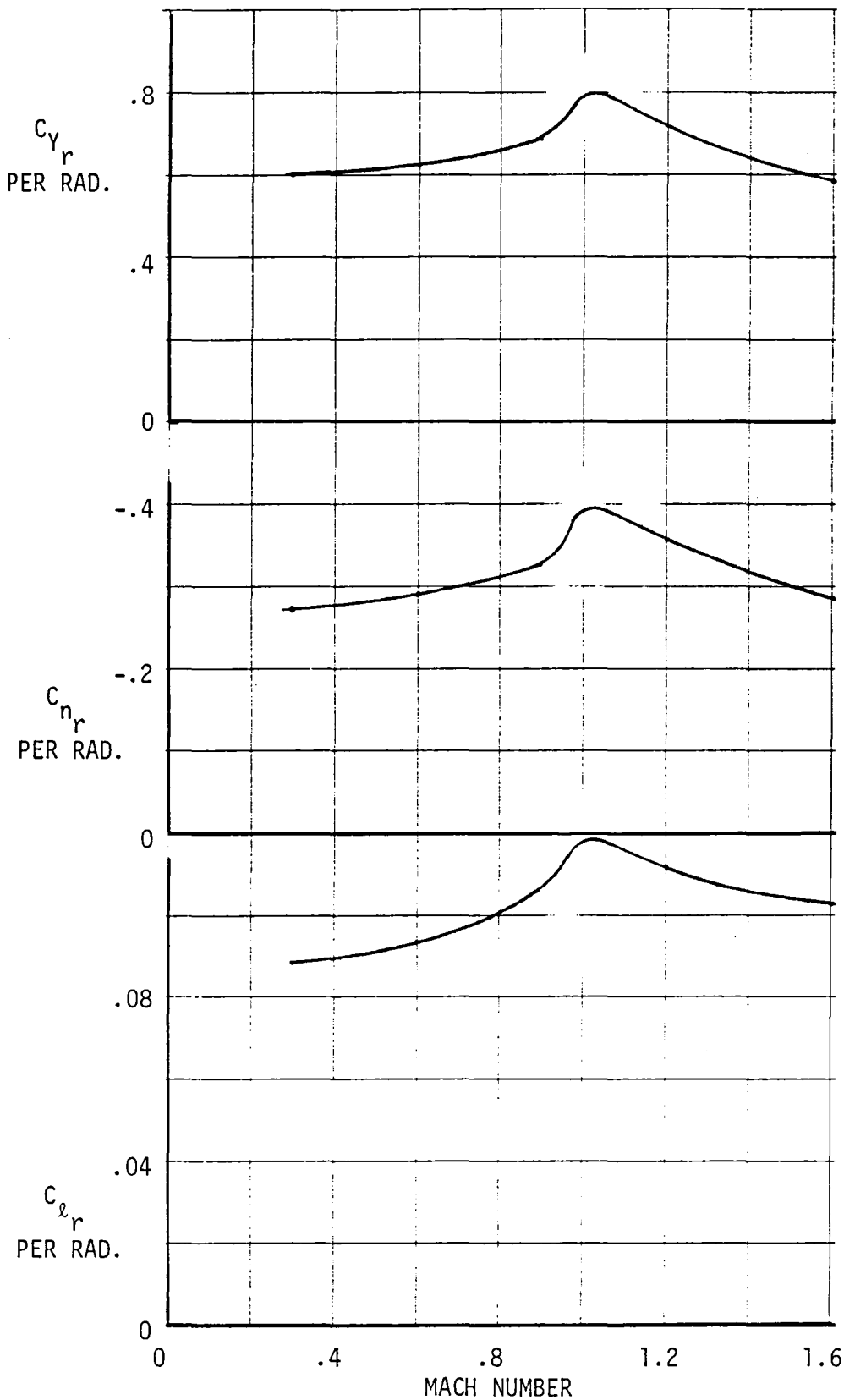

Figure 4-20 Baseline Configuration Yaw Rate Derivatives

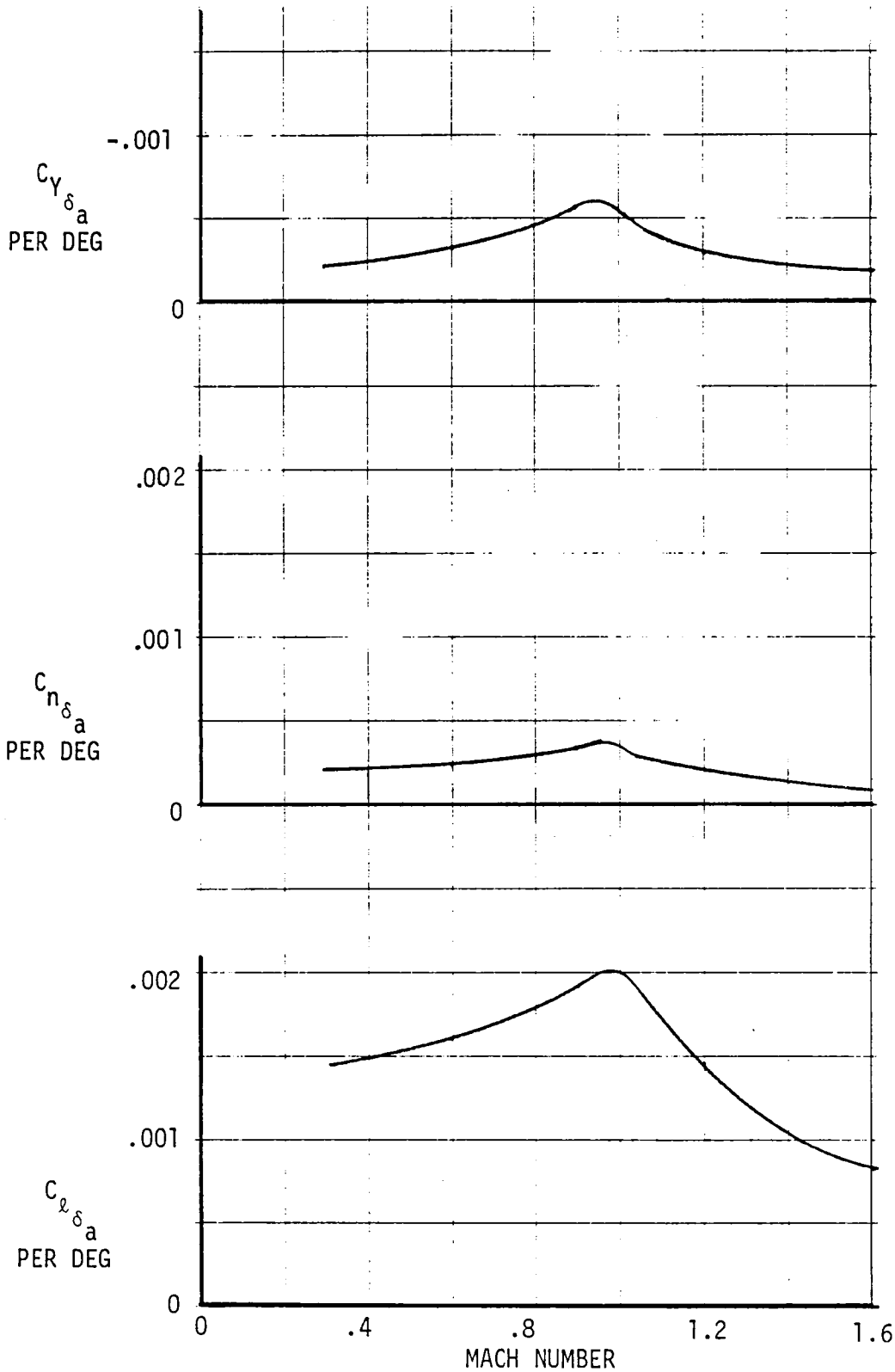

Figure 4-21 Baseline Configuration Lateral Control Effectiveness

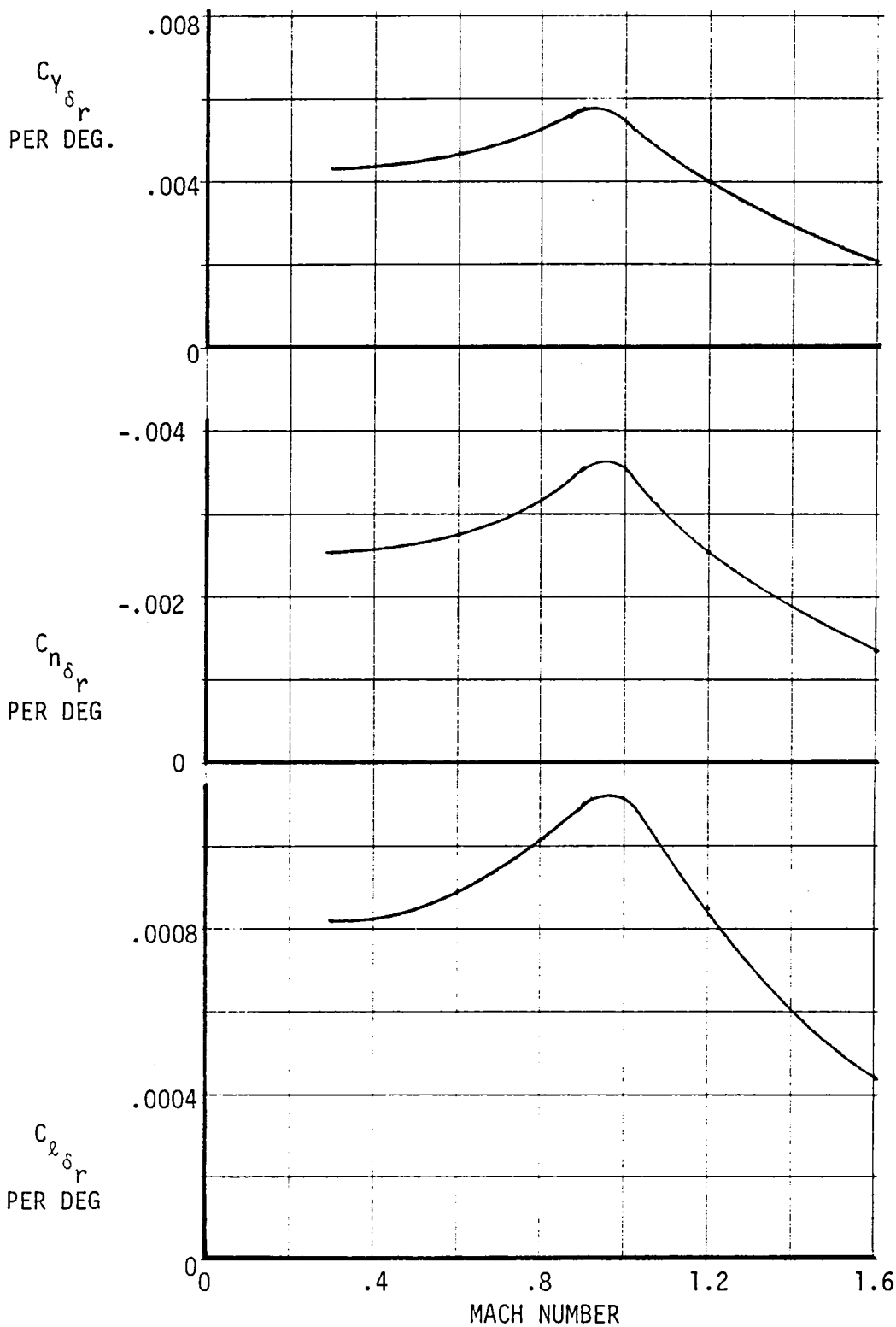

Figure 4-22 Baseline Configuration Rudder Effectiveness

4.3 BASELINE STOL/CONVERSION AND HOVER CHARACTERISTICS

STOL/Conversion - From previous augmenter tests conducted by this contractor it has been observed that for a given augmenter angle and airplane angle of attack lift is a linear function of dynamic pressure. The intercept of this curve at q = 0 is simply $\phi T \sin(\alpha + \delta)$, while the slope of the curve may be calculated from potential aerodynamic theory assuming unseparated flow condition. At very high dynamic pressures (low momentum coefficients) flow separation does occur, however, these flight conditions are not of interest in the STOL/conversion analysis.

Airplane drag is calculated from a modification of the momentum coefficient term in the classical jet flap induced drag equation,

$$C_{D_i} = \frac{C_L^2}{\pi AR + 2\phi C_\mu}$$

plus terms that account for recovered thrust and ram drag. In equation form, the resultant wind axis drag is given by

$$C_D = -r\phi C_\mu + \frac{C_L^2}{\pi AR + 2\phi C_\mu} + \frac{\dot{m}U_\infty}{qS} + C_{D_0}$$

The ram drag term is determined from engine airflow and augmenter secondary mass flow ratios. The recovery factor (r) was evaluated by comparing the drag equation with the known augmenter force at zero dynamic pressure.

The essential problem then is to calculate the circulation lift coefficient since the lift due to direct thrust is known from augmentation ratio and nozzle thrust characteristics.

The circulation lift was calculated using simple horseshoe vortices distributed over the wing, body, and flap components that make up the augmenter wing configuration. The trailing legs of the vortices were deflected relative to the wind axis system to account for wake deflection. In general, this deflection angle was the average of the flap angle setting relative to the wing chord plane. For the configurations of this study forty to fifty vortices were used to represent the STOL configuration.

From wind tunnel tests on closely spaced tandem augmenters it has been determined that a loss in lift occurs relative to the sum of the lift of the individual augmenters, as shown in Section 4.7. For this study it was assumed that the portion of the aft augmenter directly behind a forward augmenter is half as effective as the aft flap system would be in undisturbed flow. The rationale for the .5 factor follows from the linear theory result that the upper and lower surface contribute equally to the lift.

With the above estimation of lift and drag coefficients the STOL performance can be obtained as a function of velocity, angle of attack and augmenter setting. For the baseline configuration the STOL performance is

shown in Figure 4-23 and 4-24 for augmenter settings of 25° and 50°, respectively. It is noted from Figure 4-23 that an unaccelerated lift of 34,000 pounds can be developed at 100 to 120 knots.

Hover Ground Effect - The ground effect on hover lift of the XFV-12A based on test results obtained from wind tunnel tests and from tether tests conducted at NASA Langley is presented in Figure (4-25). At static height a small net lift loss was experienced which rapidly gave way to an increase in buoyancy as the landing gear extended. Additional data and discussion are presented in Section 4.7. At the point of full landing gear extension the lift increased to a buoyancy of 1.07 times the free air lift. Wind tunnel data indicated the buoyancy of the XFV-12A increased the lift approximately ten percent at the peak. During restrained tether tests at NASA Langley the XFV-12A experienced a one percent loss in lift at 20 to 25 feet above ground. During takeoff it is anticipated the lift loss will be insignificant because of the spring effect of the gear between the static height and full extension. Furthermore, there is adequate thrust margin for control so that small changes in lift due to ground effect will hardly be noted. It is anticipated that the baseline configuration will have similar ground effect on lift. It is noted that the vertical takeoff gross weight is defined by the lift, control, and vertical acceleration capability in free air. Langley restrained tethered tests at 35 feet above the ground, 0.2 scale model static pressure instrumentation, and smaller scale model tests specifically designed to measure suckdown, all showed no such effect. The VTO gross weight determination is enumerated in Section 6.1.

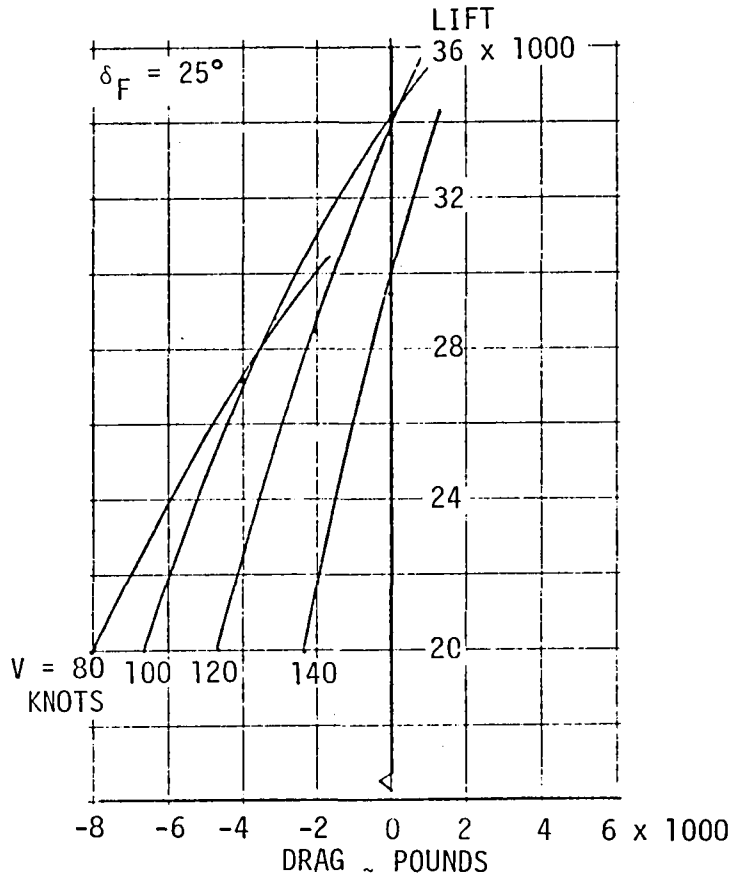

Figure 4-23. Baseline Configuration STOL Aero Characteristics

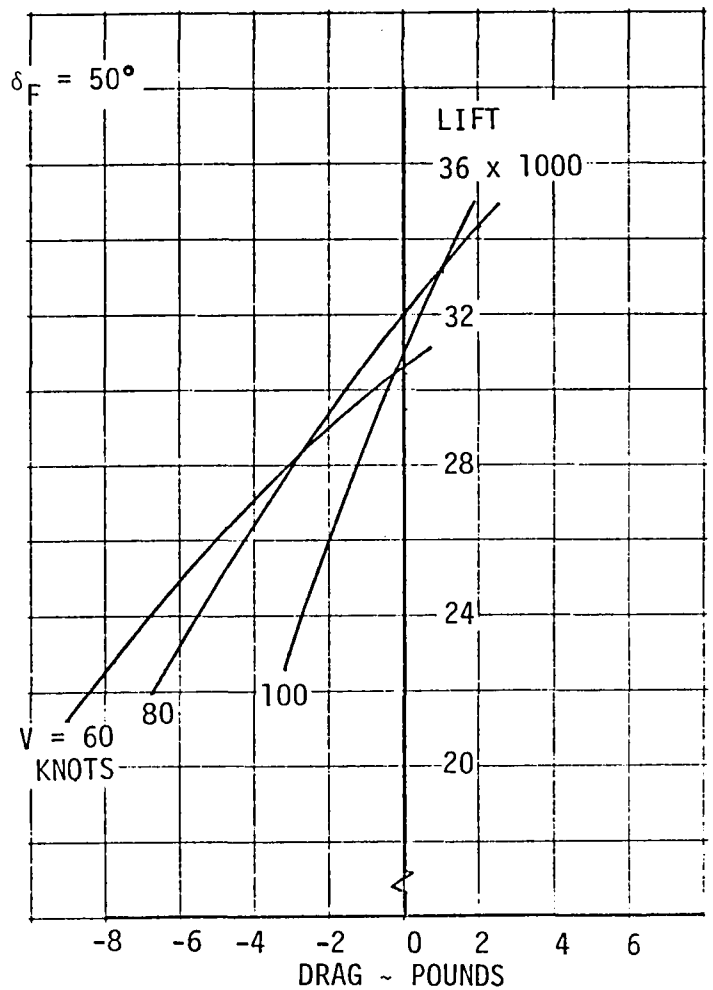

Figure 4-24. Baseline Configuration STOL Aero Characteristics

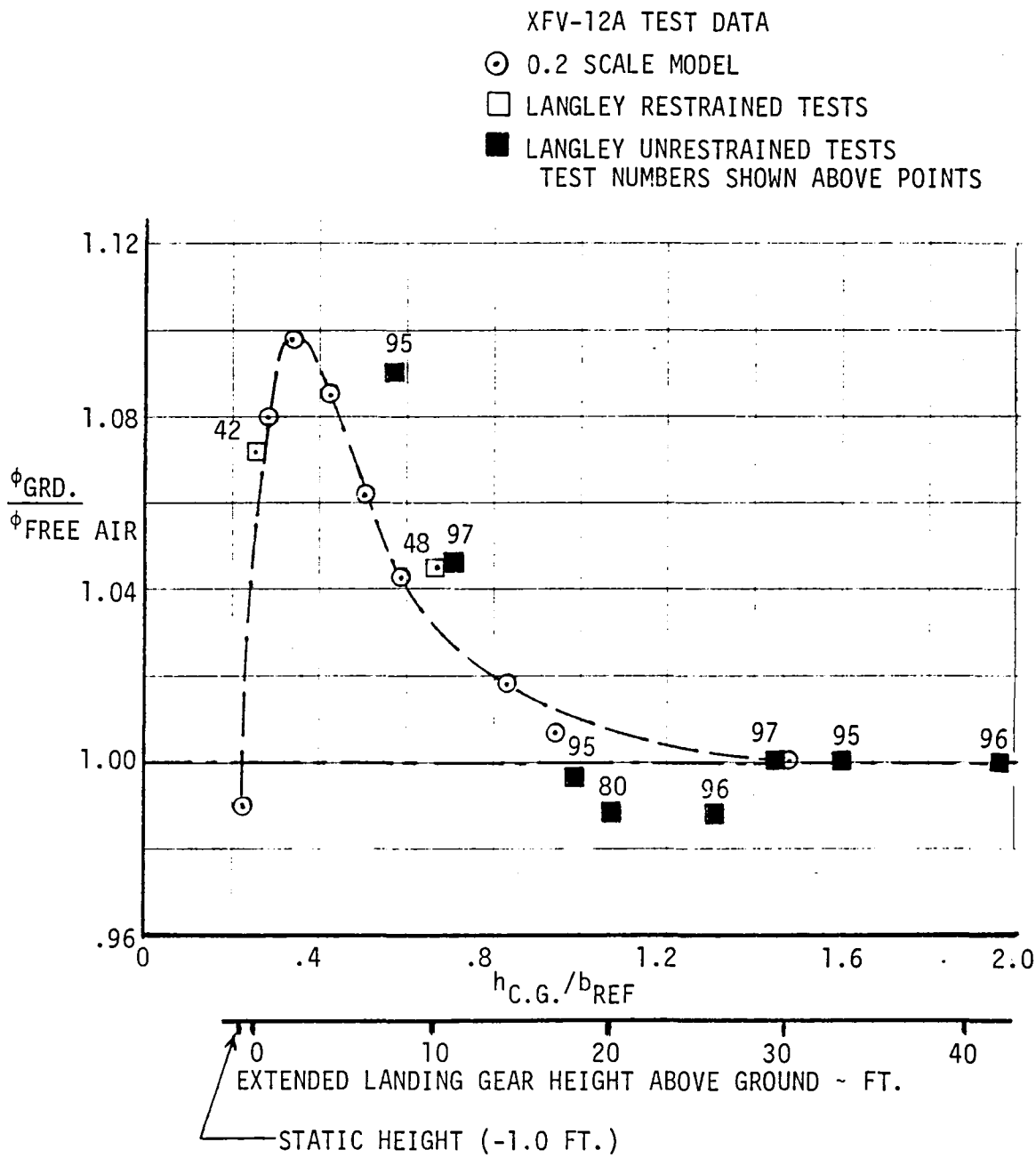

Figure 4-25 Ground Effect on Lift

4.4 ALTERNATE LONGITUDINAL CHARACTERISTICS - CONVENTIONAL FLIGHT

4.4.1 Drag

This section presents the drag characteristics of the alternate configuration. The methods used in estimating the drag are discussed in Section 4.1.1 and they are identical to those utilized in calculating the baseline drag. The alternate configuration features a blunt wing trailing edge behind the augmenter. This portion of the trailing edge span is configured to eliminate the base drag throughout the design speed range as discussed in Section 2.3. Wave drag estimates, using far field theory, included a trapezoidal stream tube aft of the inboard portion of the wing span extending to infinity. All trim drag data are based on a C.G. located at station 366.

Zero Lift-Drag - Figure 4-26 presents a detailed breakdown of the wetted area distribution for the alternate configuration, and Table 4-3 skin friction buildup for M = 0.60 at 30,000 feet altitude. The cross section area distribution buildup is shown on Figure 4-27.

The propulsion installation drag increments and the store drag increments are the same as for the baseline aircraft. These data are presented on Figure 4-3.

The total zero lift drag coefficient variation with Mach number for the clean configuration is shown on Figure 4-28 for an altitude of 30,000 feet.

Drag-Due-to-Lift - Figure 4-28 also presents the variation with Mach number of drag due to lift for different trimmed lifts and trim drag polars for selected Mach numbers are presented in Figure 4-29. All trim drag data are for a reference C.G. location of 366. The variation of L/D with lift for 0.60 and 1.60 Mach numbers at 10,000 and 50,000 feet altitude, respectively, is shown on Figure 4-30. Maximum L/D's of 10.4 and 5.3 are shown. The trimmed lifts for the 6.2 g maneuvering condition at 10,000 feet and 1 g flight at 50,000 feet are also noted.

4.4.2 Lift and Pitch Characteristics

This section presents the estimated longitudinal characteristics of the alternate configuration. All pitching moment and trim data are based on a C.G. located at station 366. The methods employed in estimating the longitudinal characteristics of the alternate configuration are noted in Section 4.1.2.

Linear Data - The variation with Mach number of lift curve slope and stability, measured over an angle of attack range of 0 to 5 degrees, is presented on Figure 4-31. The airframe is approximately five percent unstable at the low speeds and ten percent stable at the higher speeds. Neutral stability occurs at 0.94 Mach number.

TABLE 4-3

ALTERNATE CONFIGURATION
SKIN FRICTION DRAG BUILDUP

M = 0.60 ALTITUDE = 30,000 FEET S_{REF} = 548.0 FT.^{2}

Component	Wetted Area ~ S_{Wet} ~ Ft^2	Characteristic Length ~ ℓ ~ Ft.	Reynolds Number ~ R_N	Form Factor F.F.	C_f	$\Delta C_{D_F} = \frac{F.F. \times C_f \times S_{Wet}}{S_{Ref}}$
Fuselage	751.00	48.21	8.22×10^7	1.213	.00206	.00341
Wing	829.00	21.10	3.60×10^7	1.130	.00232	.00395
Wing End Plates	81.40	7.58	1.29×10^7	1.130	.00272	.00045
Vertical Tails	147.40	5.55	9.5×10^6	1.130	.00286	.00087
Miscellaneous	-	-	-	-	-	.00243

Total S_{Wet} = 1808.8 Ft.^{2} Total C_{D_F} = 0.01111

$$C_{f_e} = \frac{.0111 \times 548.0}{1808.8} = .00337$$

Lift and Pitching Moment - The variation of lift with angle of attack and pitching moment with lift for several control surface deflections are presented on Figures 4-32 through 4-36 at selected Mach numbers. The Mach 0.30 data (Figure 4-32) are for both inboard and outboard control surfaces (elevons and ailevators) deflected while the data for the other Mach numbers are for only the elevons deflected. Because of the stability variation with Mach number, positive control surface deflections at subsonic Mach numbers and negative deflections at supersonic Mach numbers are shown.

Both inboard and outboard surfaces are used at the very low speeds because of the need to trim to high lifts with the basic airframe instability. At higher subsonic Mach numbers, control requirements are reduced because the airframe is less unstable, and the control effectiveness is higher; therefore, only the inboard control surfaces are required.

At supersonic Mach numbers the control requirement increases and the effectiveness reduces, but there is sufficient control effectiveness to trim to lift coefficient well above the approximately 0.10 value required for level flight at altitude. Figure 4-37 summarizes the variation of control effectiveness with Mach numbers.

Maximum Lift - The variation of trimmed maximum lift with Mach number is shown in Figure 4-38. The low speed data is based on control surface deflections of +20 degrees on both the inboard and outboard wing trailing edge control surfaces.

Damping in Pitch - The variation of pitch damping with Mach number is shown on Figure 4-39.

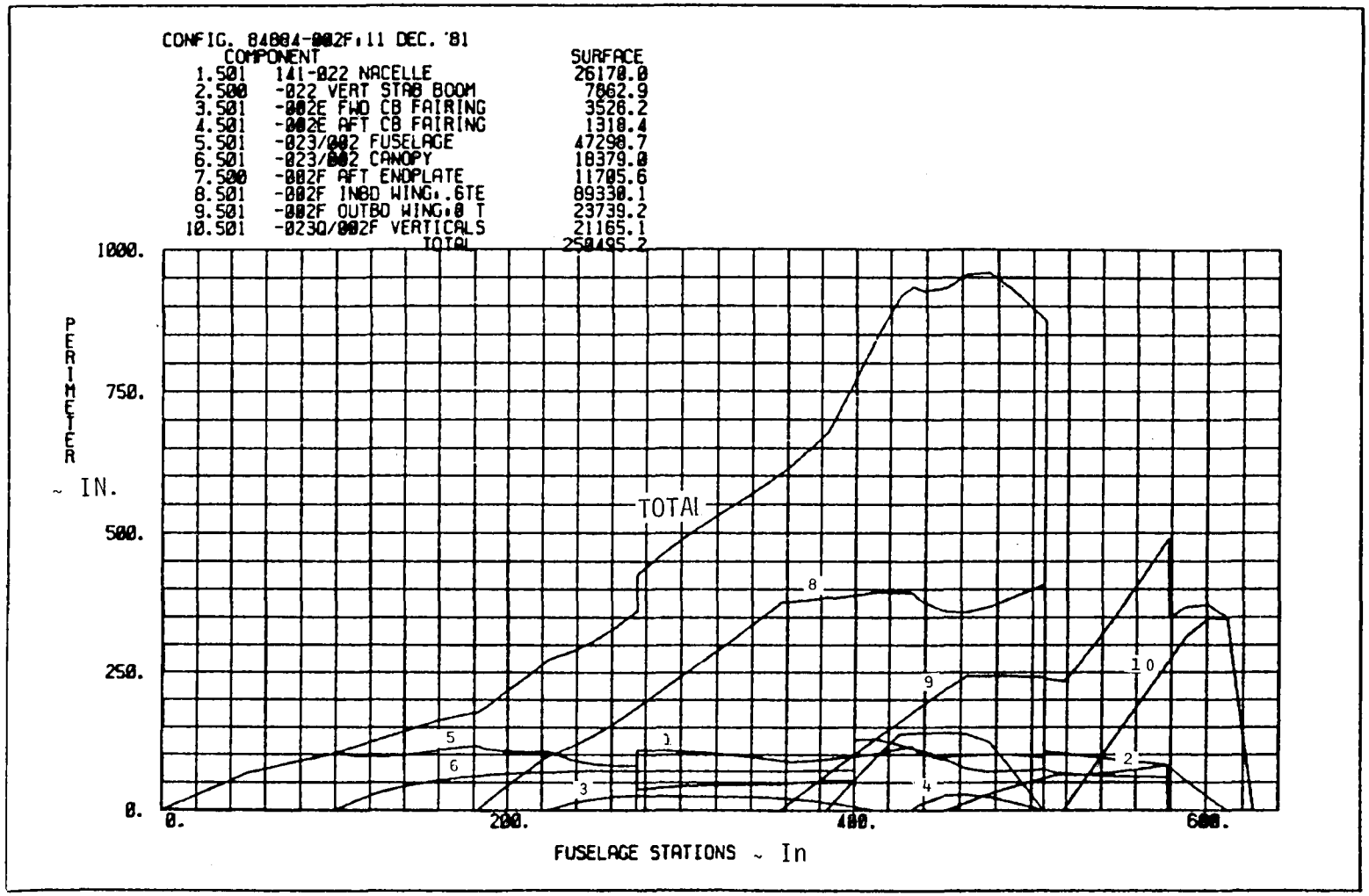

Figure 4-26 Alternate Configuration Wetted Area Distribution

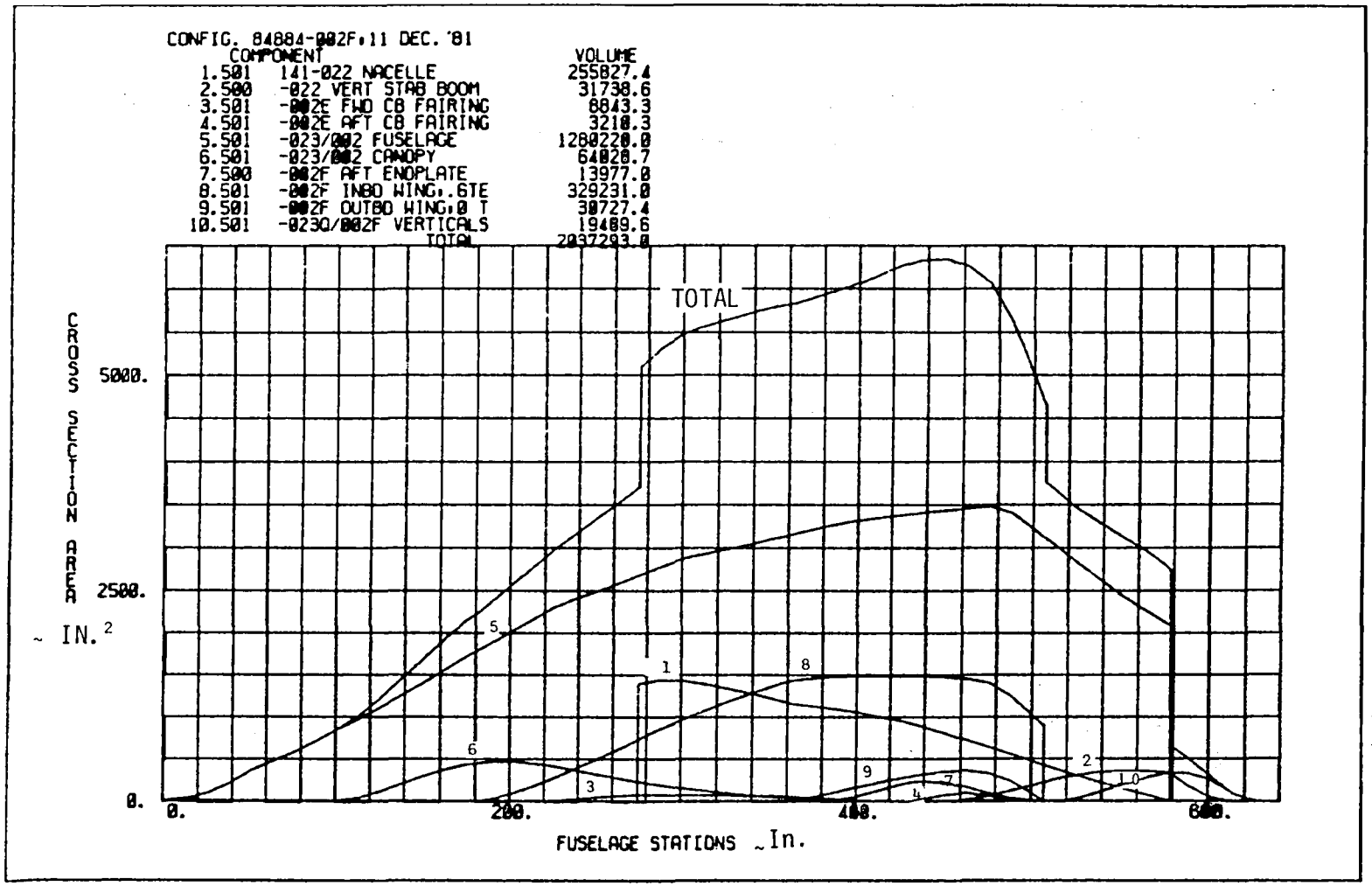

Figure 4-27 Alternate Configuration Cross Sectional Area Distribution

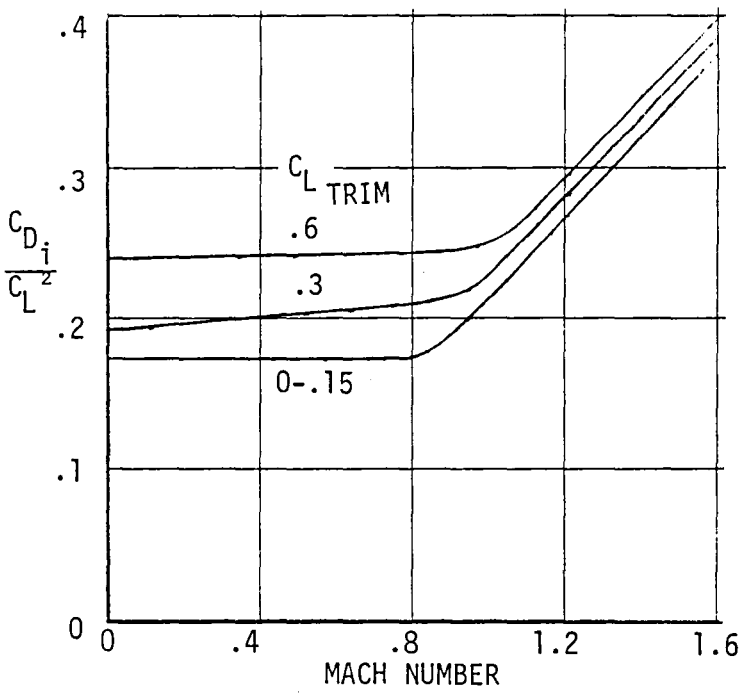

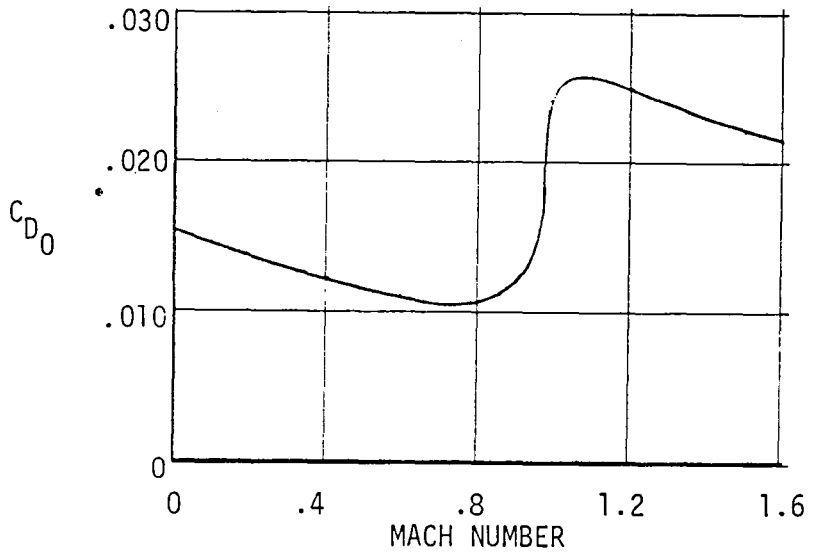

Figure 4-28 Alternate Configuration Drag Characteristics

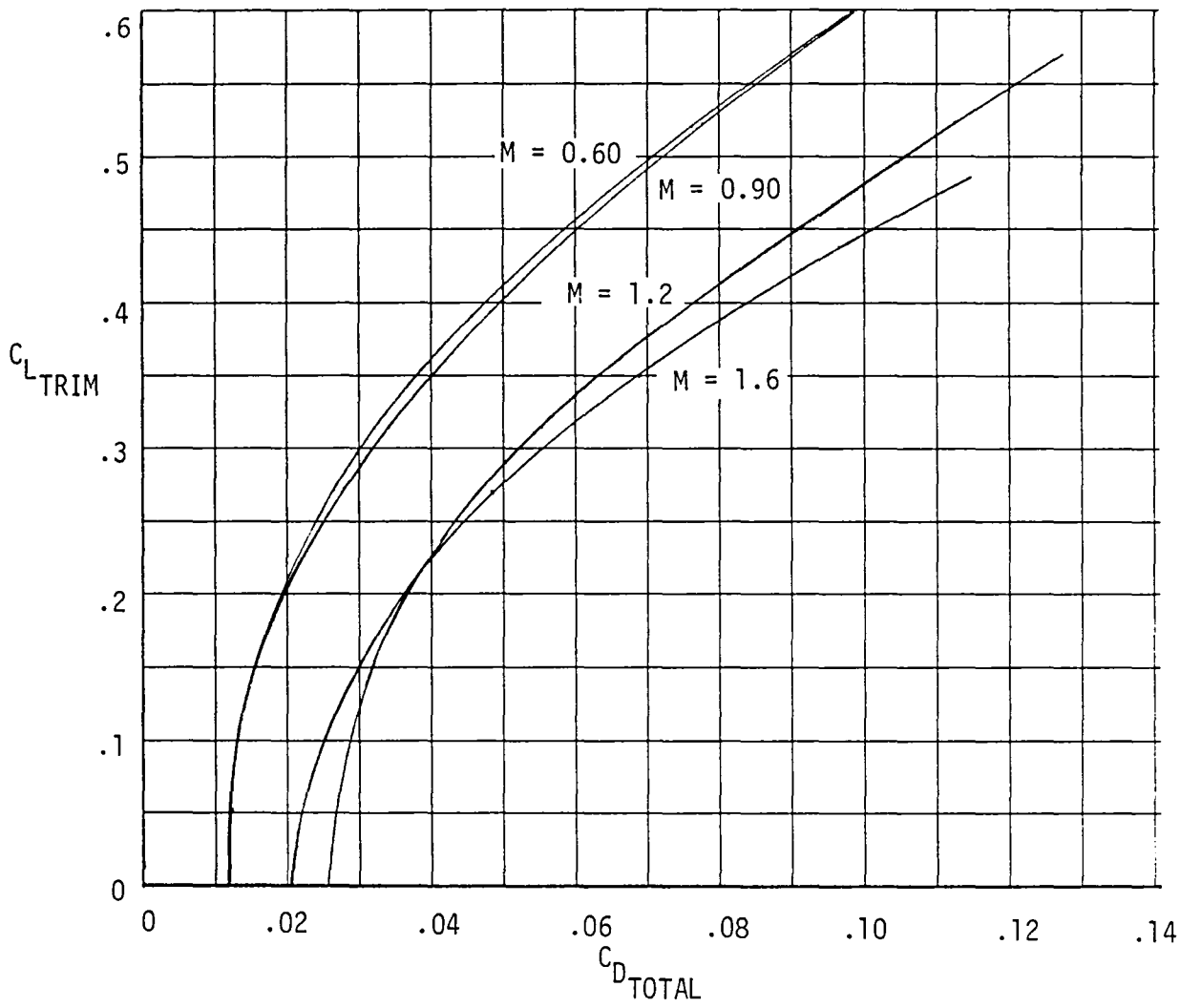

Figure 4-29 Alternate Configuration Trim Drag Polars

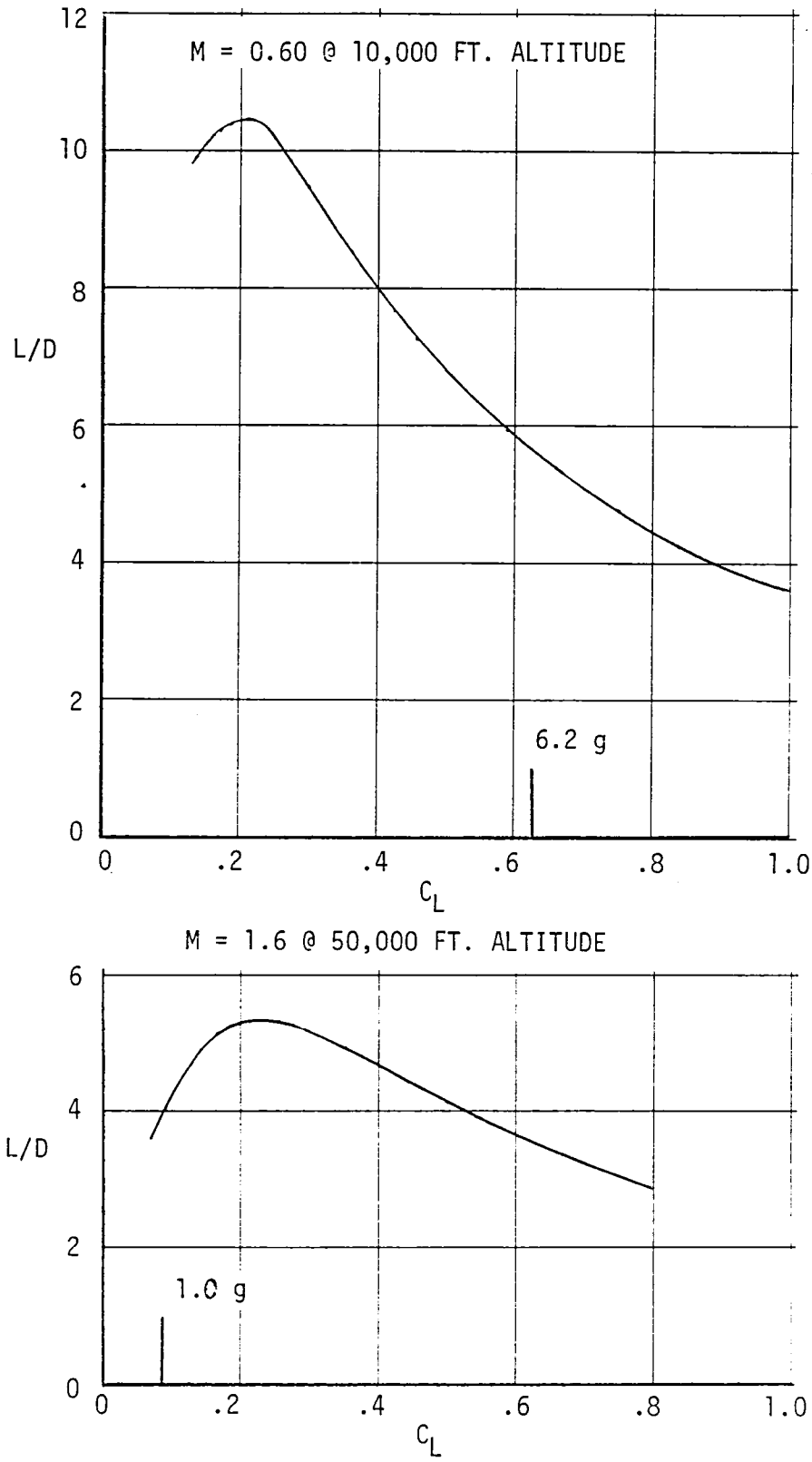

Figure 4-30 Alternate Configuration Aerodynamic Efficiency

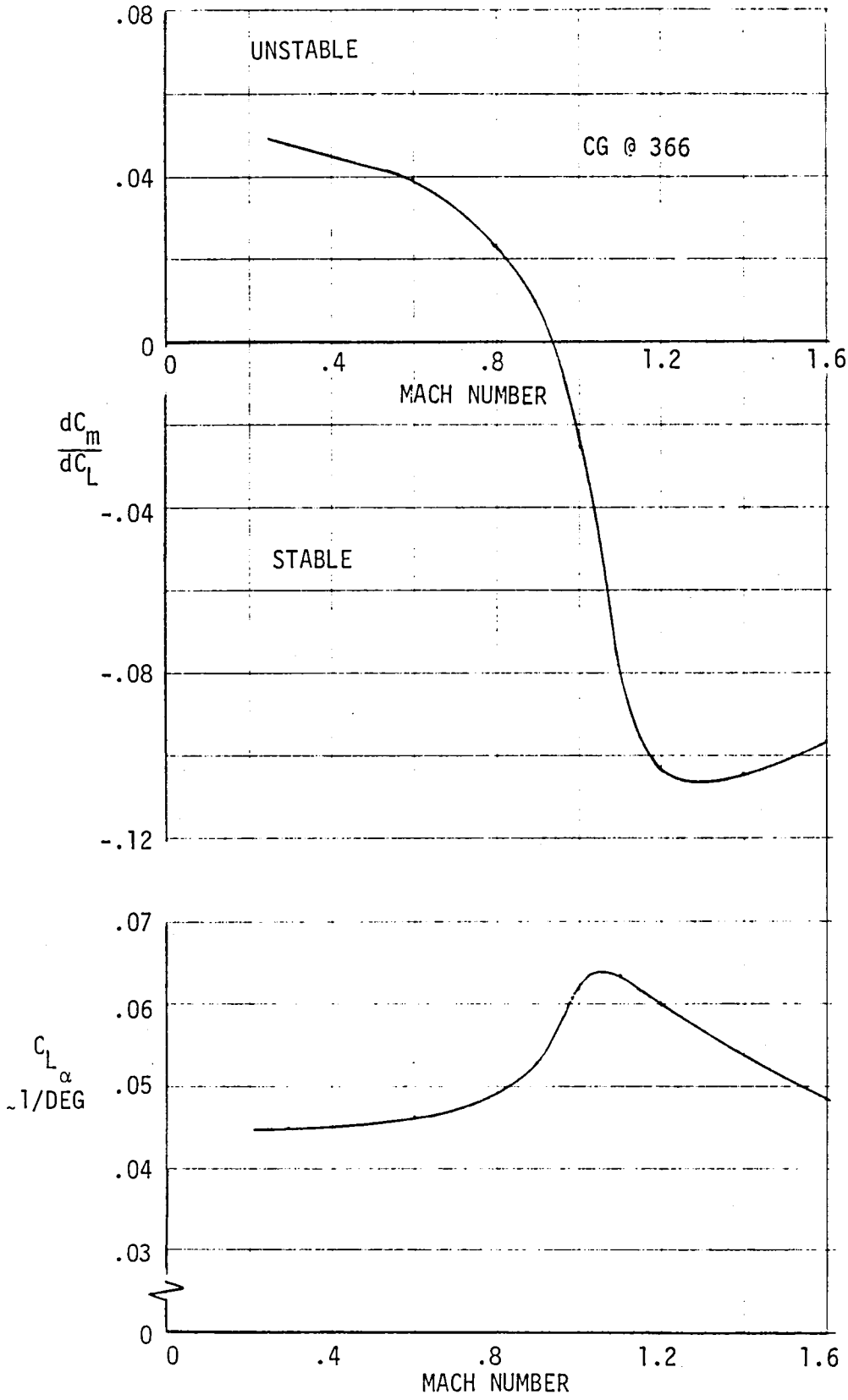

Figure 4-31 Alternate Configuration Longitudinal Characteristics ~ Zero Flap Deflection

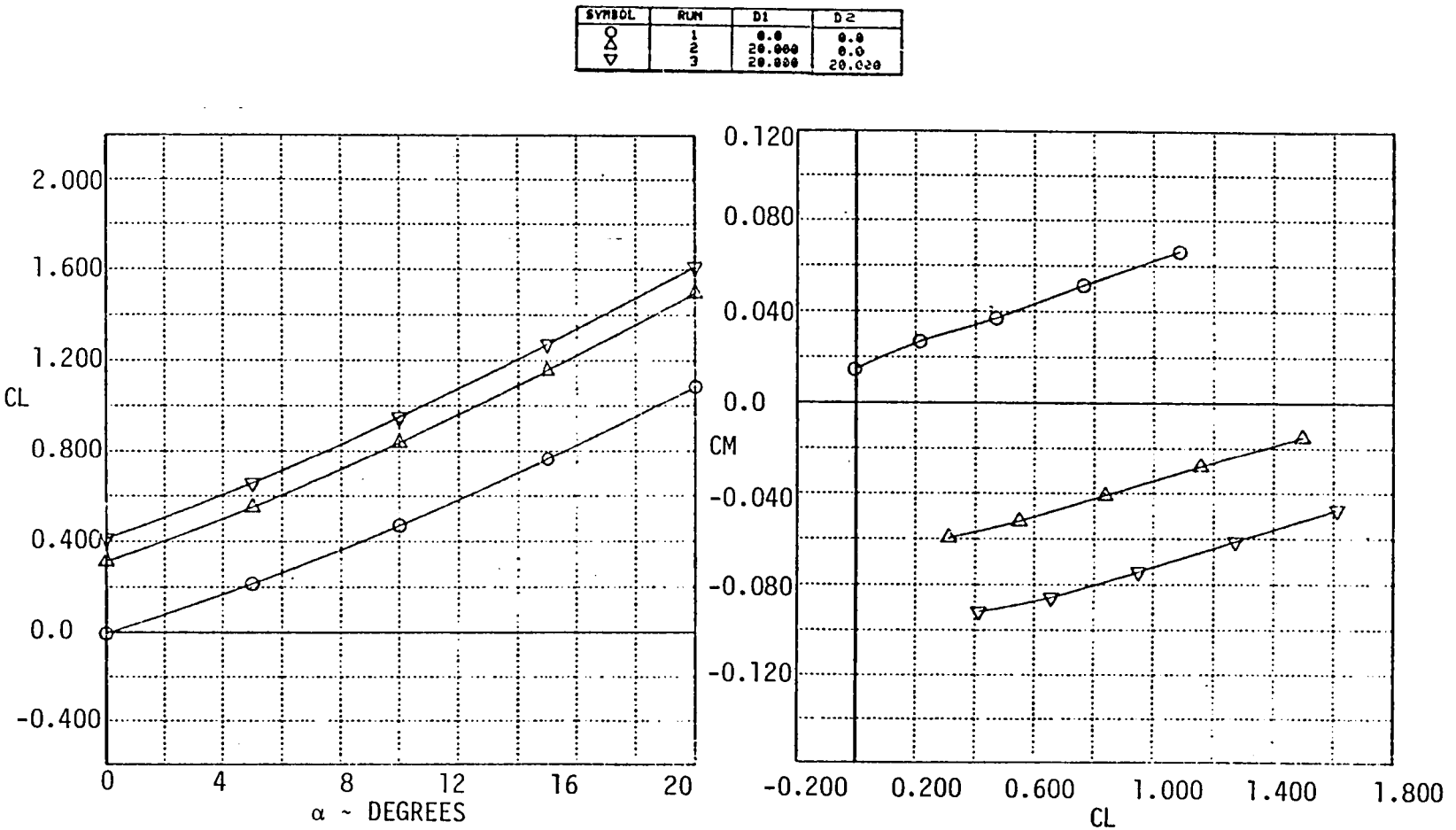

Figure 4-32a. Alternate Configuration, C_L vs α @ M - 0.3

Figure 4-32b. Alternate Configuration, C_M vs C_L @ M = 0.3

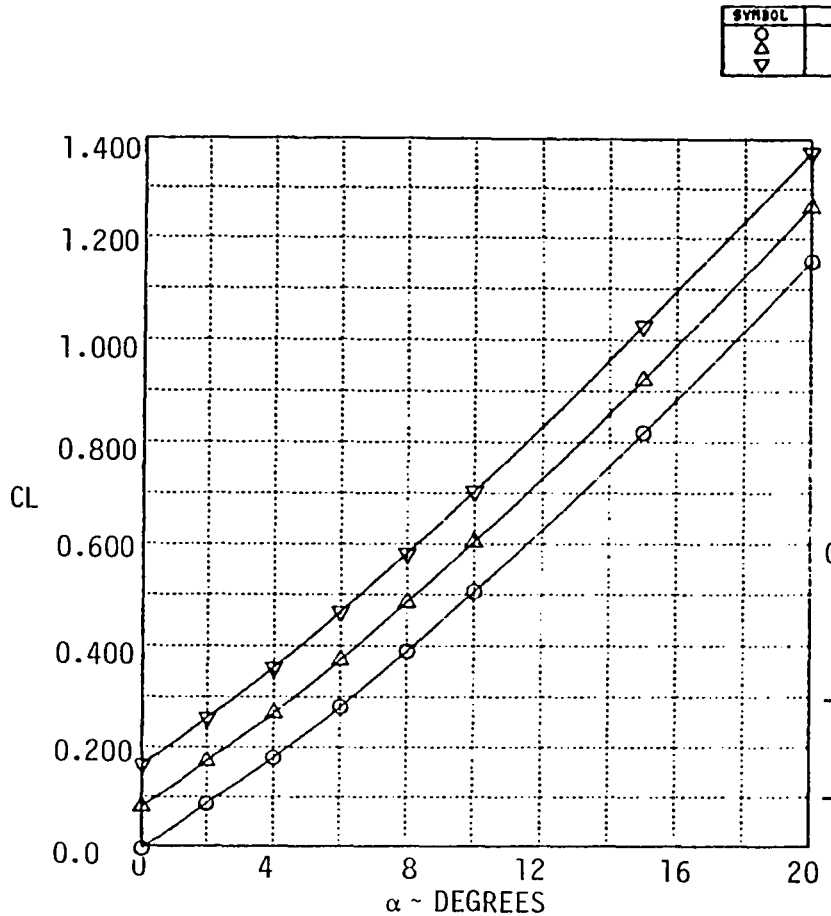

Figure 4-33a. Alternate Configuration, C_L vs α @ M = 0.6

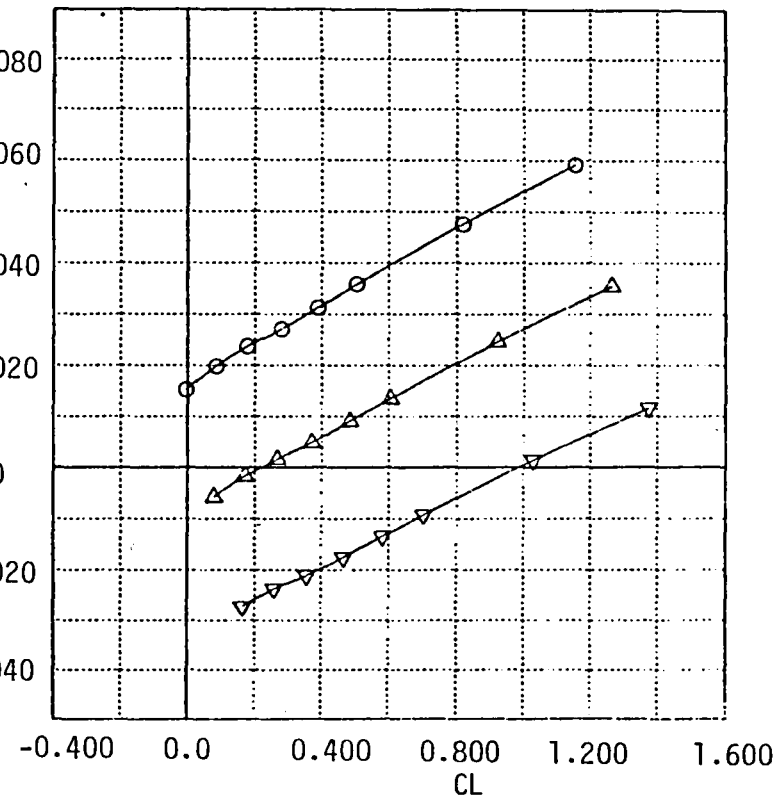

Figure 4-33b. Alternate Configuration, C_M vs C_L @ M = 0.6

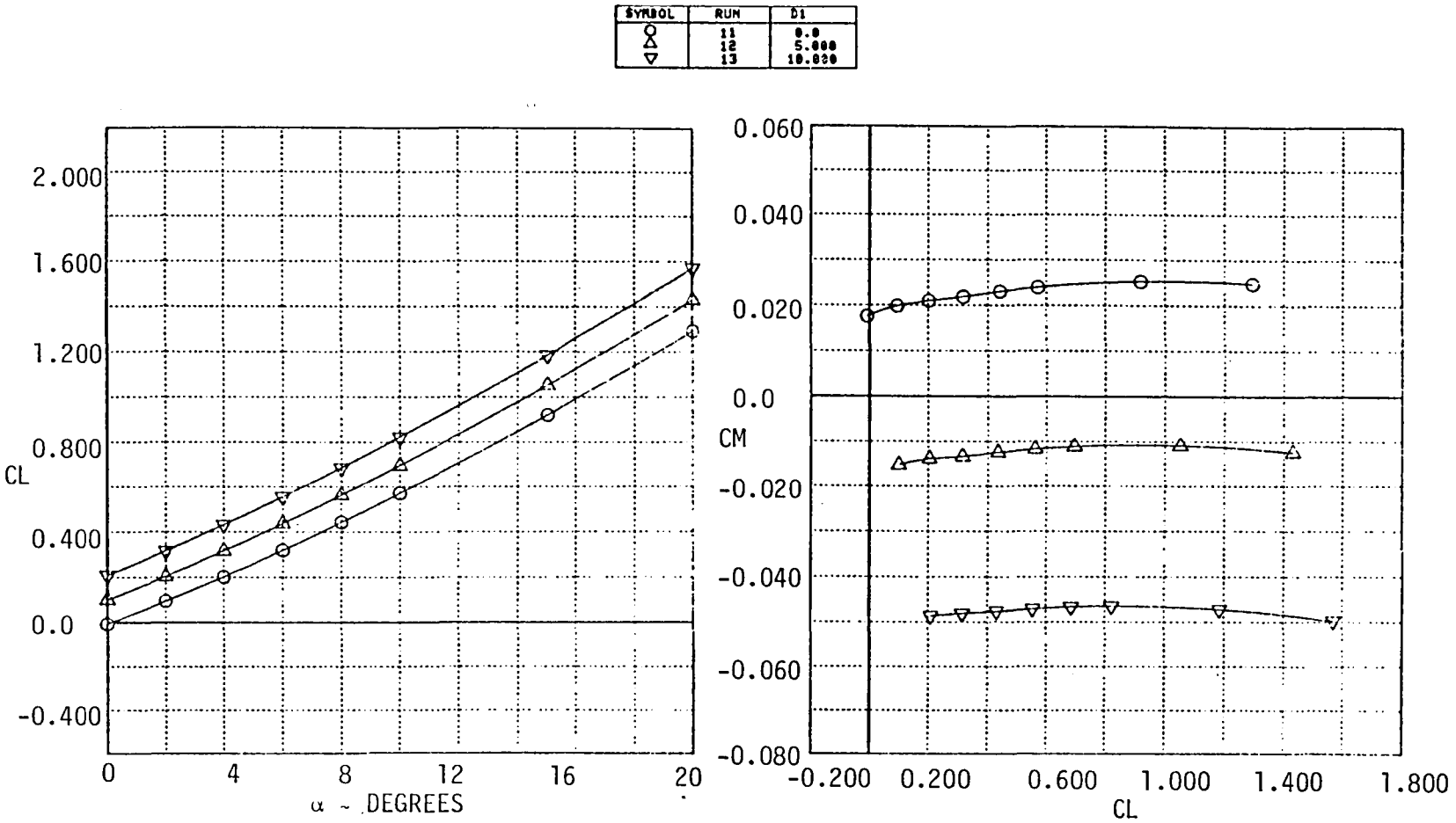

Figure 4-34a. Alternate Configuration, C_L vs α @ M = 0.9

Figure 4-34b. Alternate Configuration, C_M vs C_L @ M = 0.9

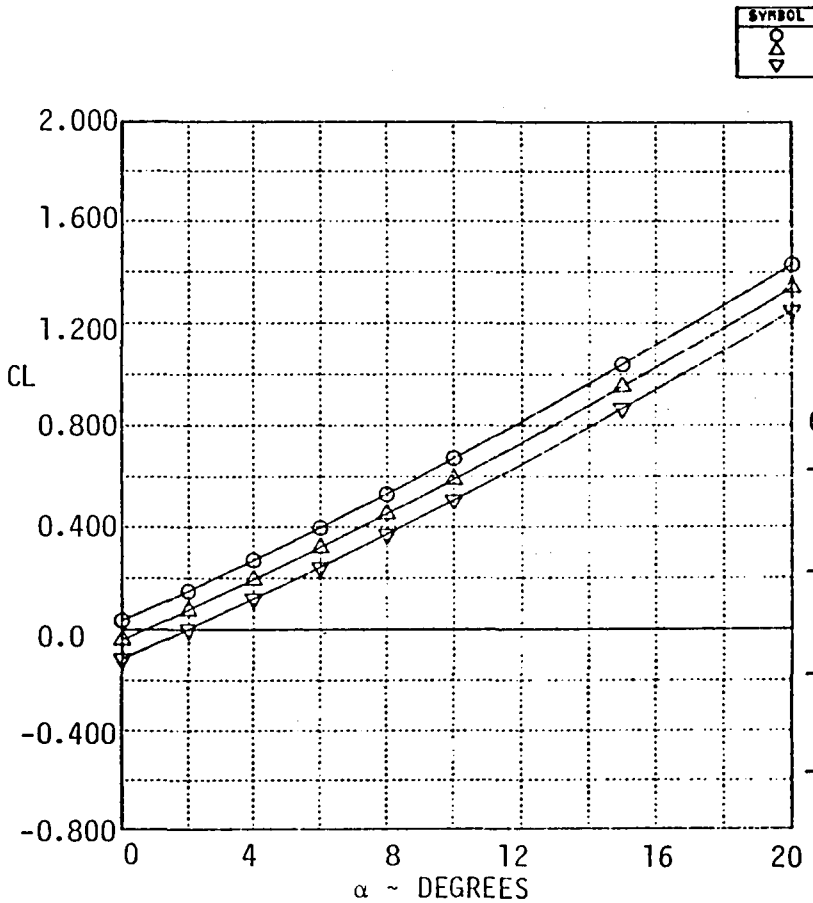

Figure 4-35a. Alternate Configuration, C_L vs α @ M = 1.2

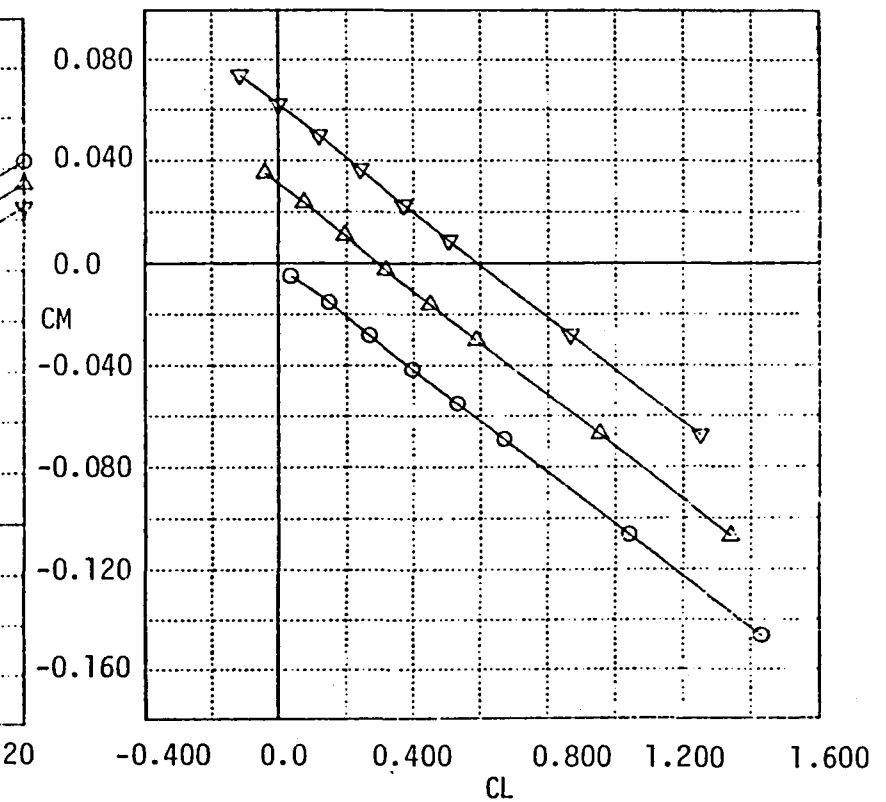

Figure 4-35b. Alternate Configuration, C_M vs C_L @ M = 1.2

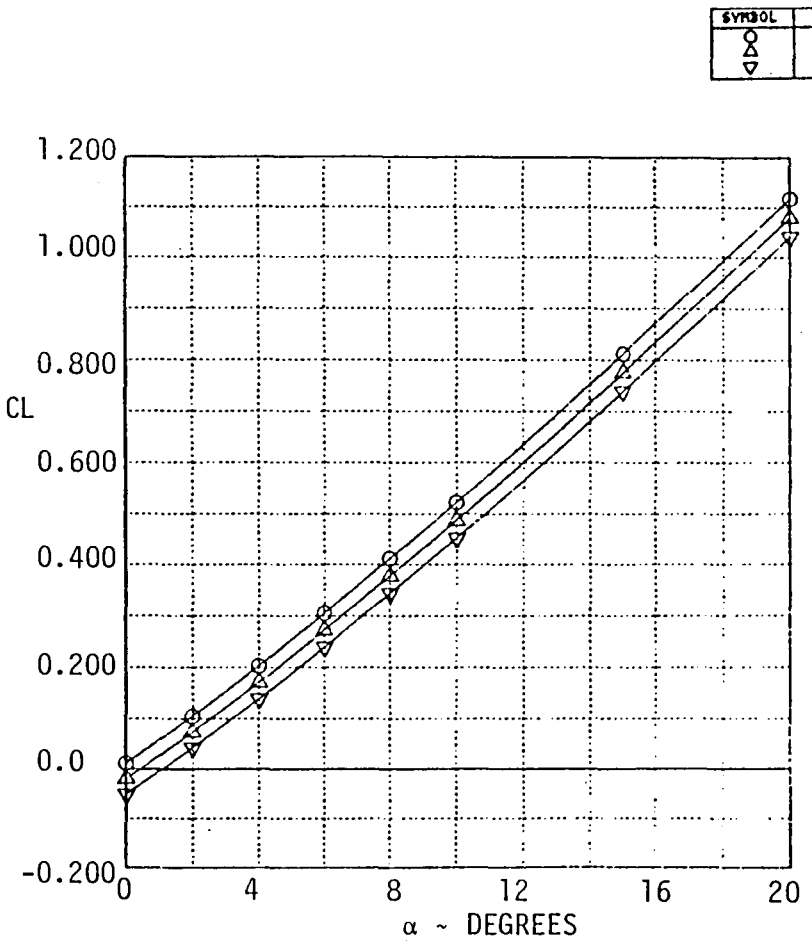

Figure 4-36a. Alternate Configuration, C_L vs α @ M = 1.6

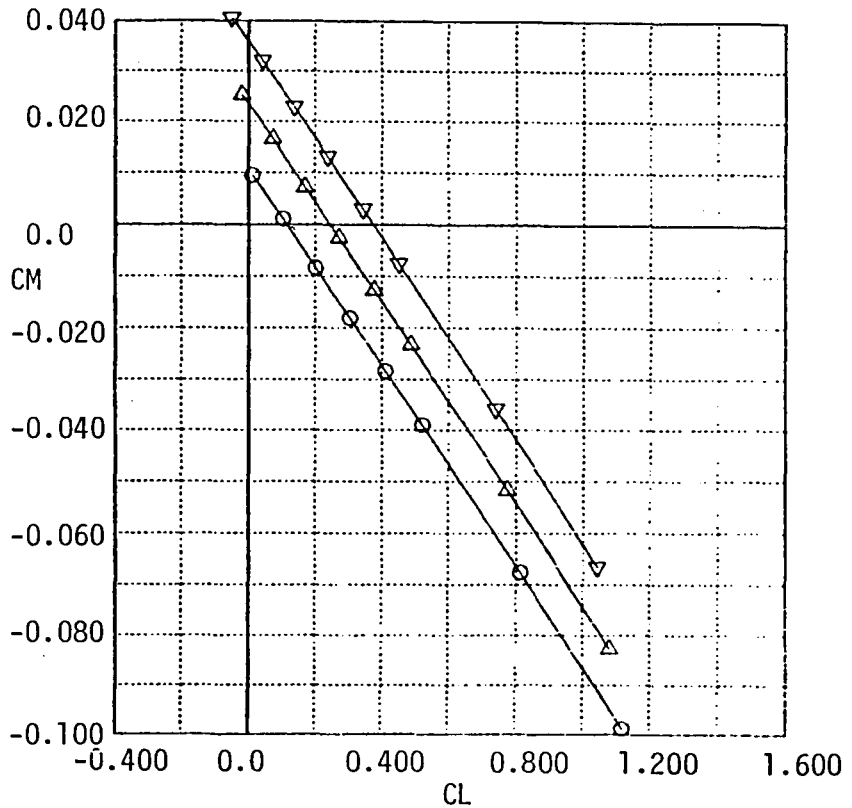

Figure 4-36b. Alternate Configuration, C_M vs C_L @ M = 1.6

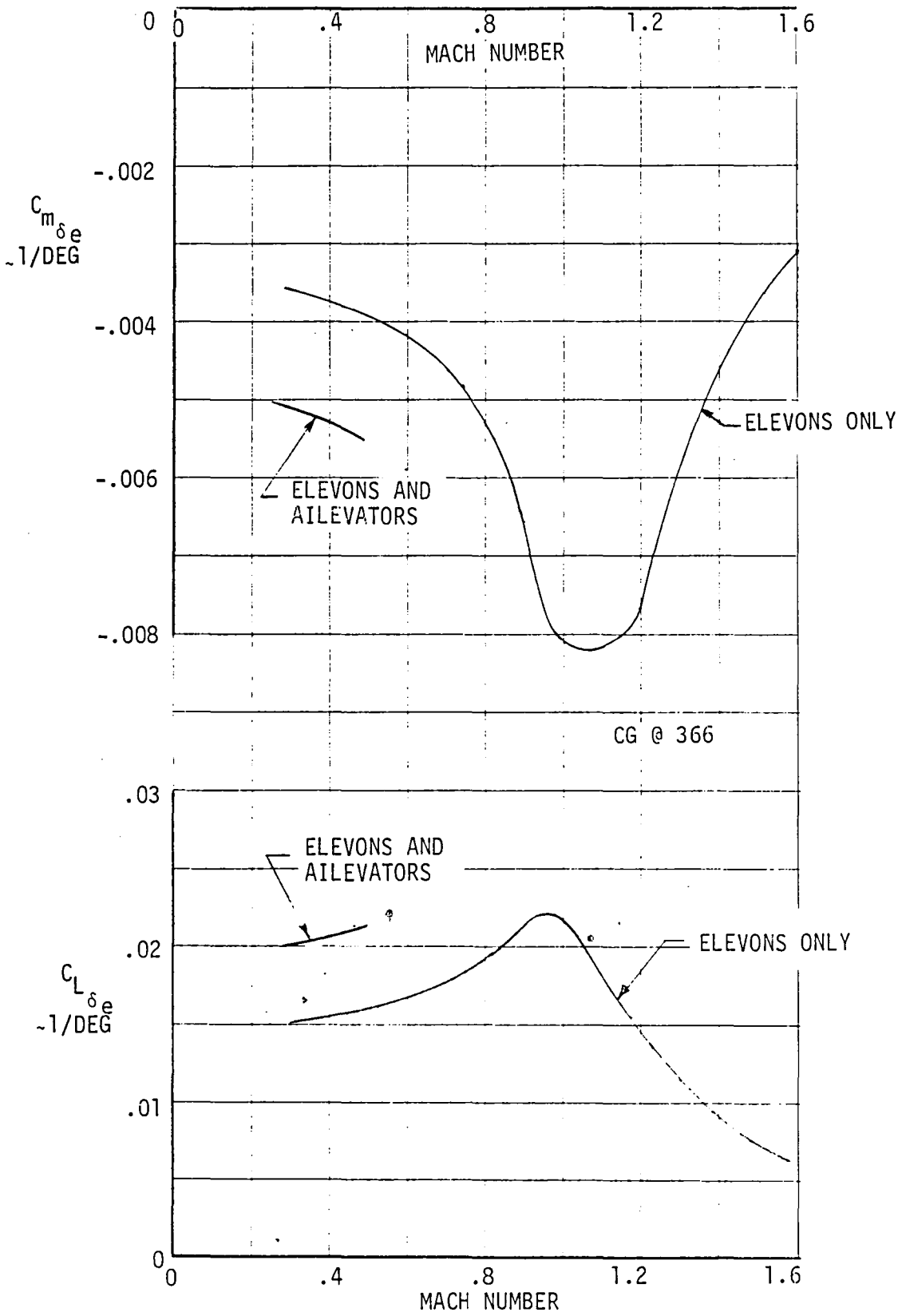

Figure 4-37 Alternate Configuration Longitudinal Control Effectiveness

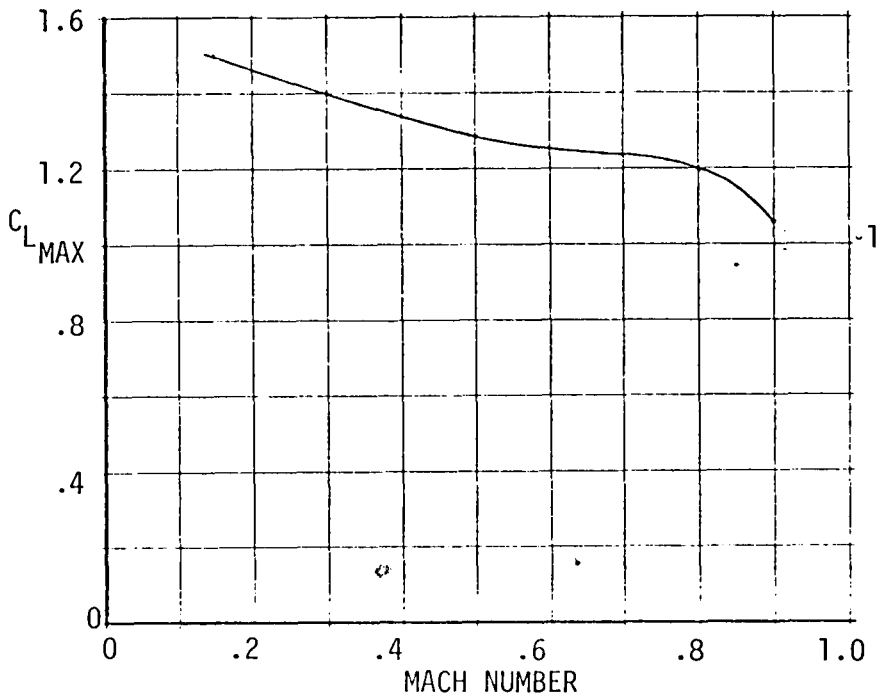

Figure 4-38. Alternate Configuration Subsonic Trimmed $C_{L_{Max}}$

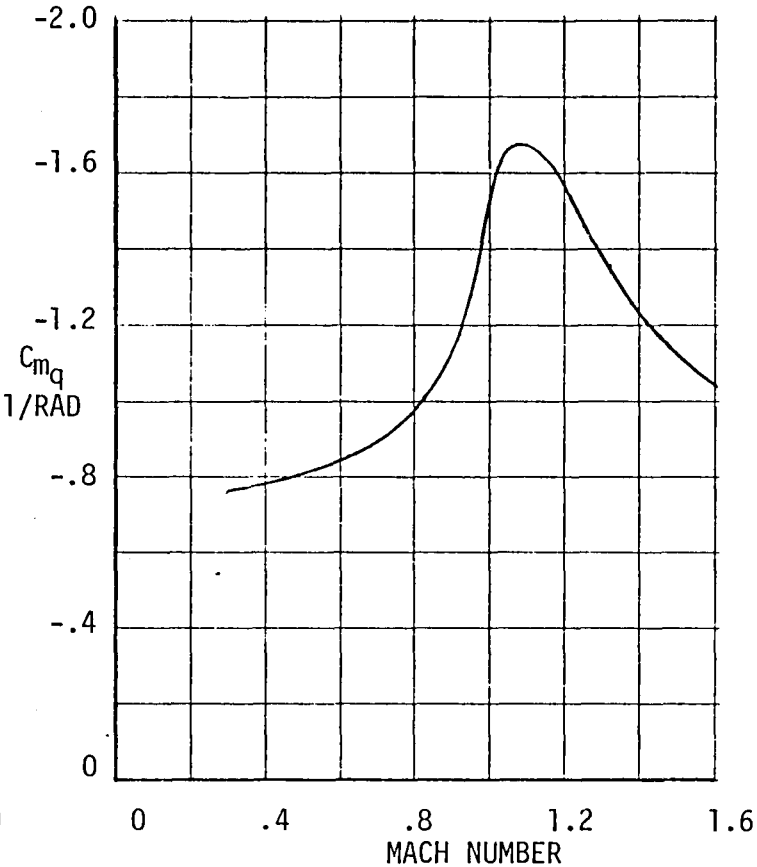

Figure 4-39. Alternate Configuration Pitch Damping

4.5 ALTERNATE CONFIGURATION LATERAL-DIRECTIONAL CHARACTERISTICS IN CONVENTIONAL FLIGHT

4.5.1 Stability

Lateral-directional aerodynamic characteristics of the alternate configuration are presented in Figure 4-40 through 4-45. Examination of the data and comparison with the baseline configuration reveals the two airplanes have similar side force and directional stability characteristics, however, the alternate airplane has significantly lower dihedral effect. The effect of the lower dihedral effect is an uncertainty at this point and will require further study. The trend of lower dihedral effect is to cause a greater possibility for spiral instability which can be corrected by varying the wing dihedral angle. Further analysis would be required to determine the desired dihedral angle. The planform change from baseline to alternate has very little effect on roll damping as shown in Figure 4-42 but does have noticeable effect on the cross derivative roll due to yaw rate presented in Figure 4-43. The lower cross derivative of the alternate configuration can be attributed to the lower dihedral effect.

4.5.2 Control

The alternate configuration has the same type trailing edge flap controls as the baseline configuration (rudder ailevators and elevons). Ailevator control effectiveness data are shown in Figure 4-44.

Rudder characteristics are shown in Figure 4-45 and are very much like the baseline aircraft data.

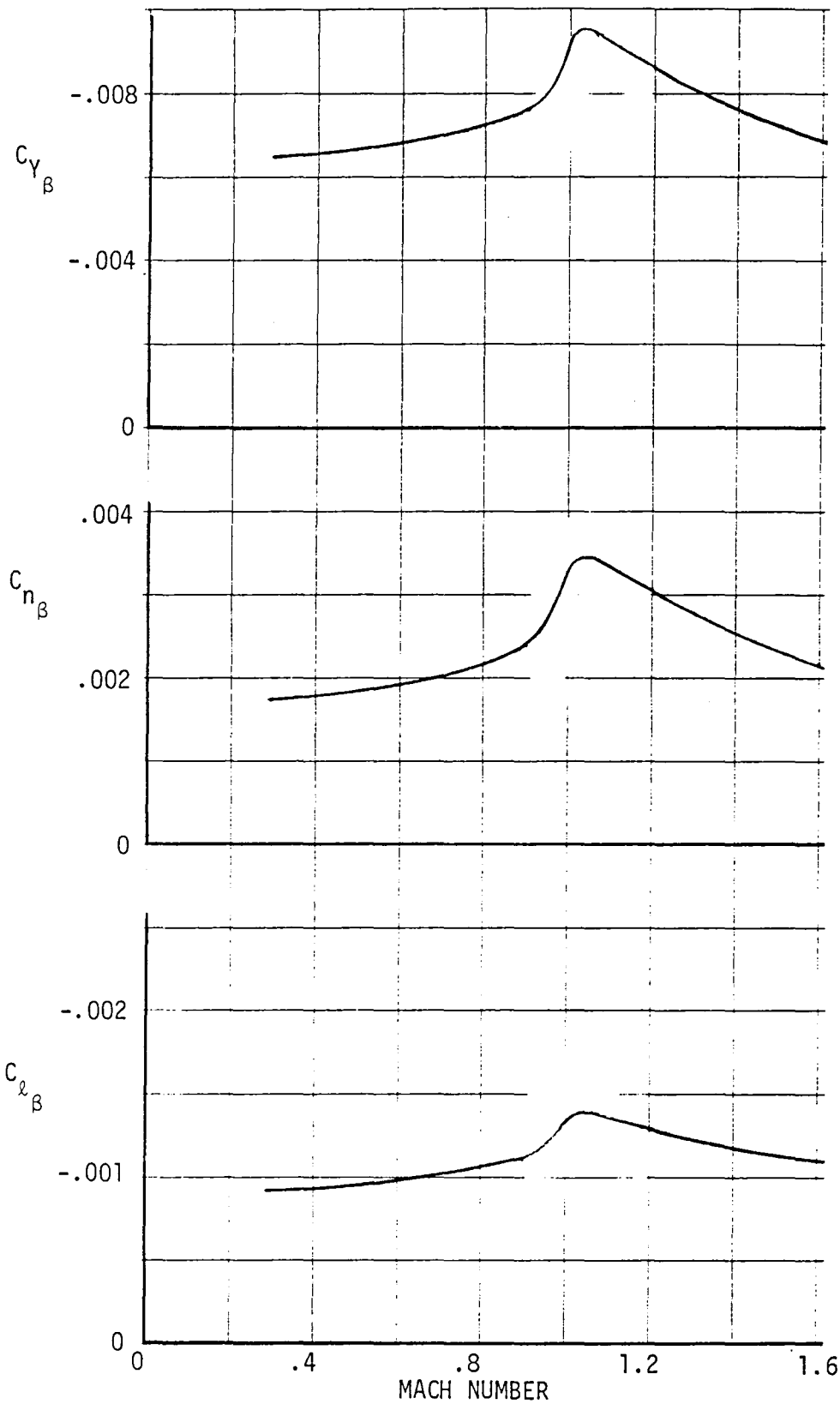

Figure 4-40 Alternate Configuration Static Directional Stability

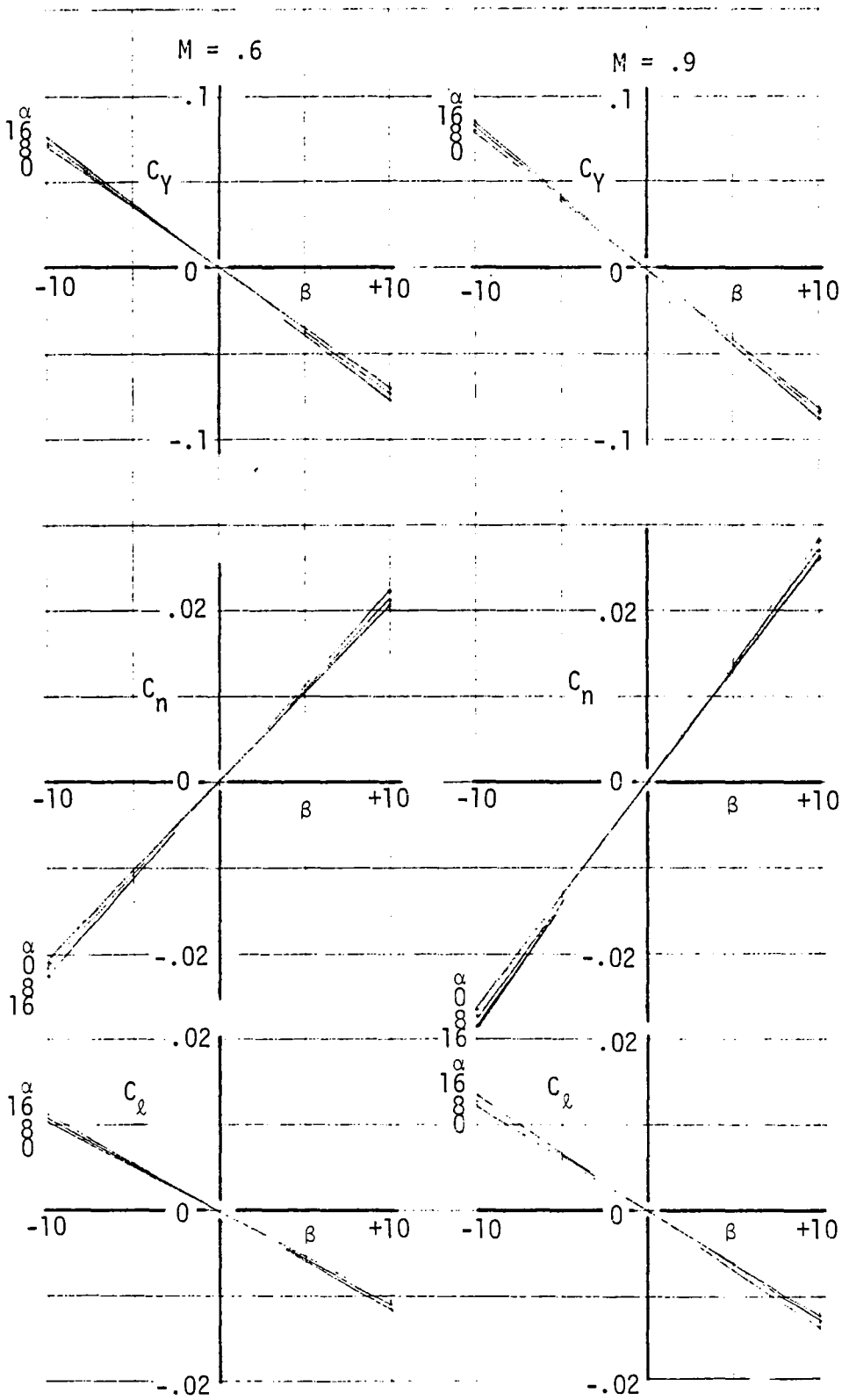

Figure 4-41a Alternate Configuration Directional Stability

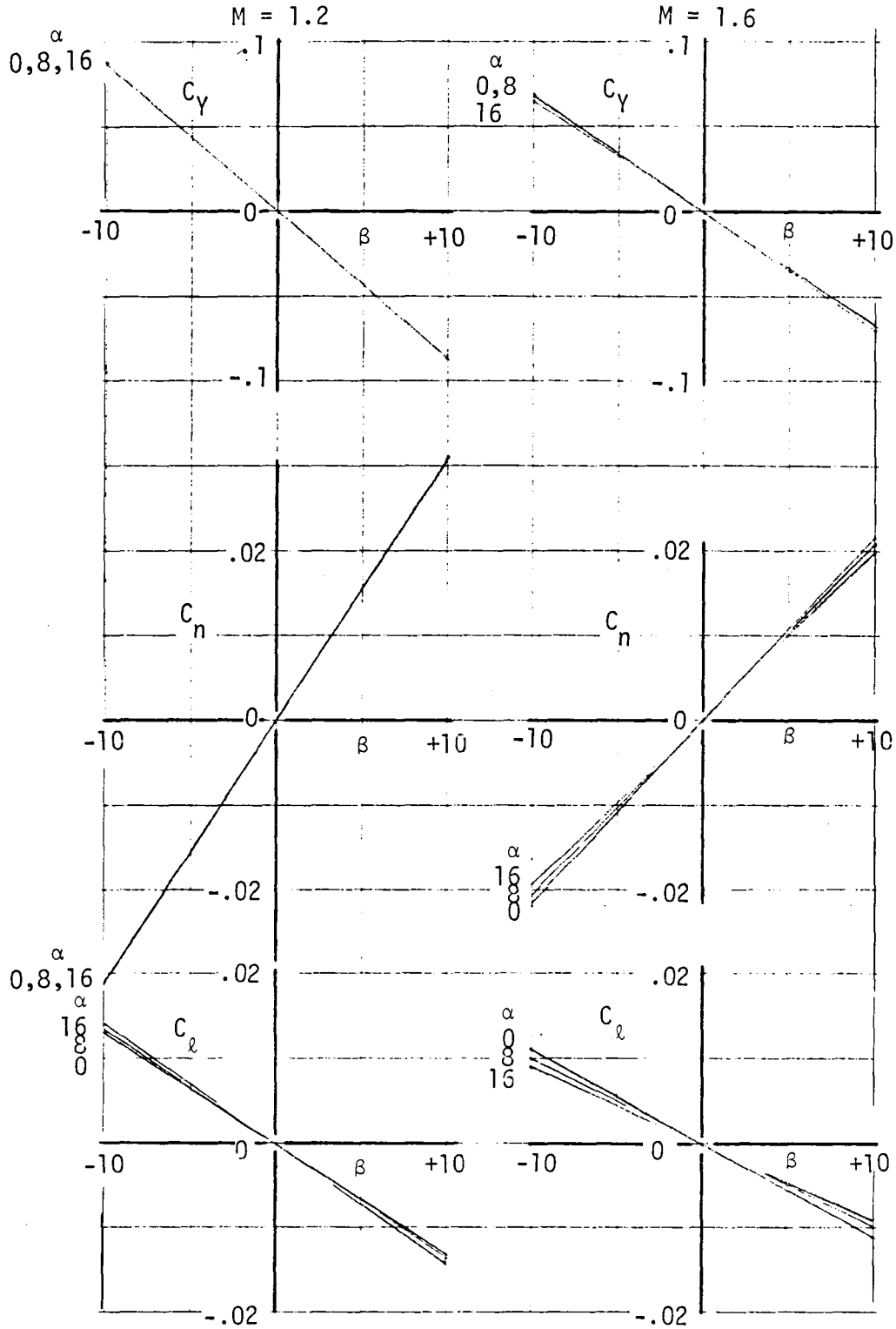

Figure 4-41b Alternate Configuration Directional Stability

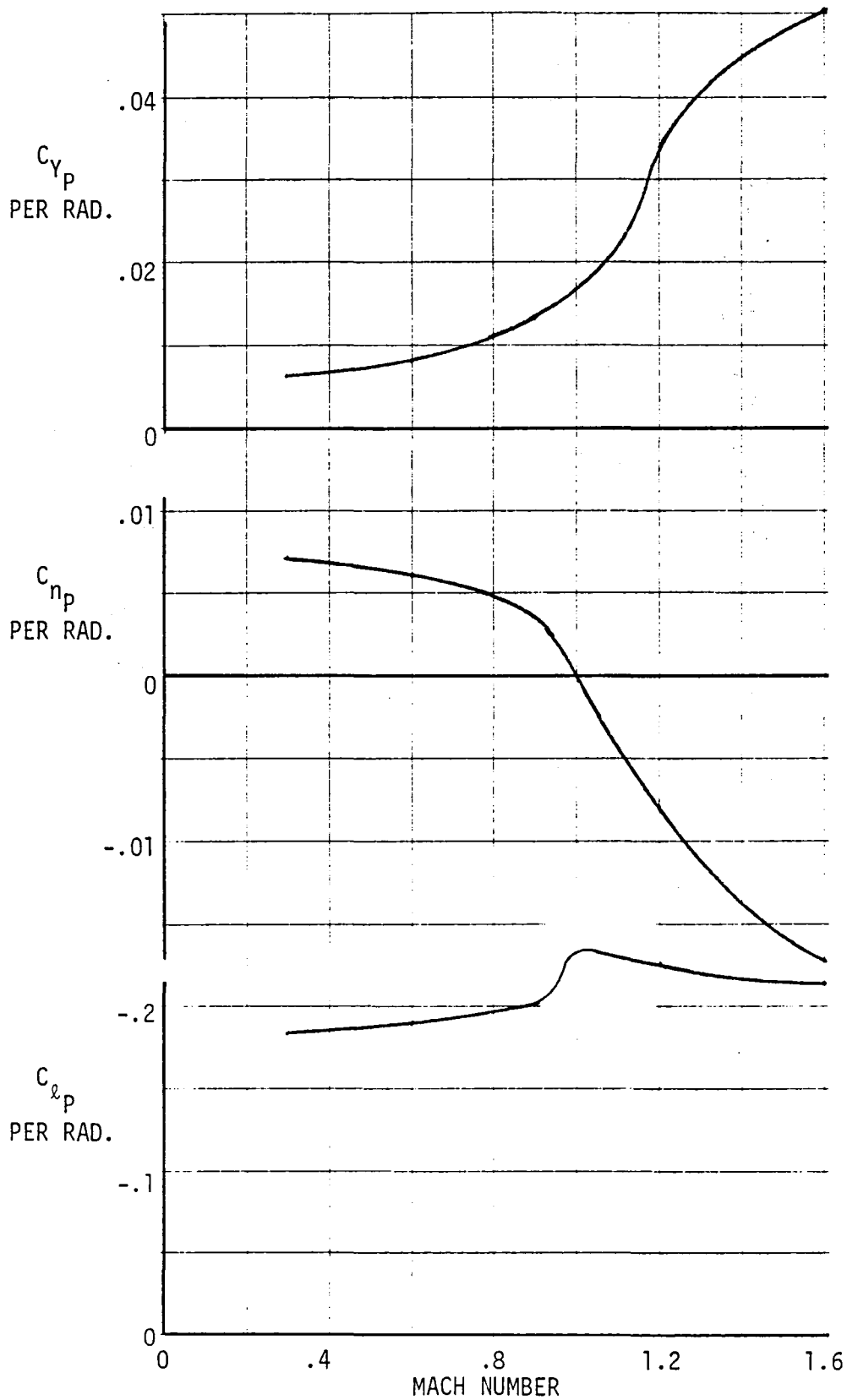

Figure 4-42 Alternate Configuration Rotary Derivatives

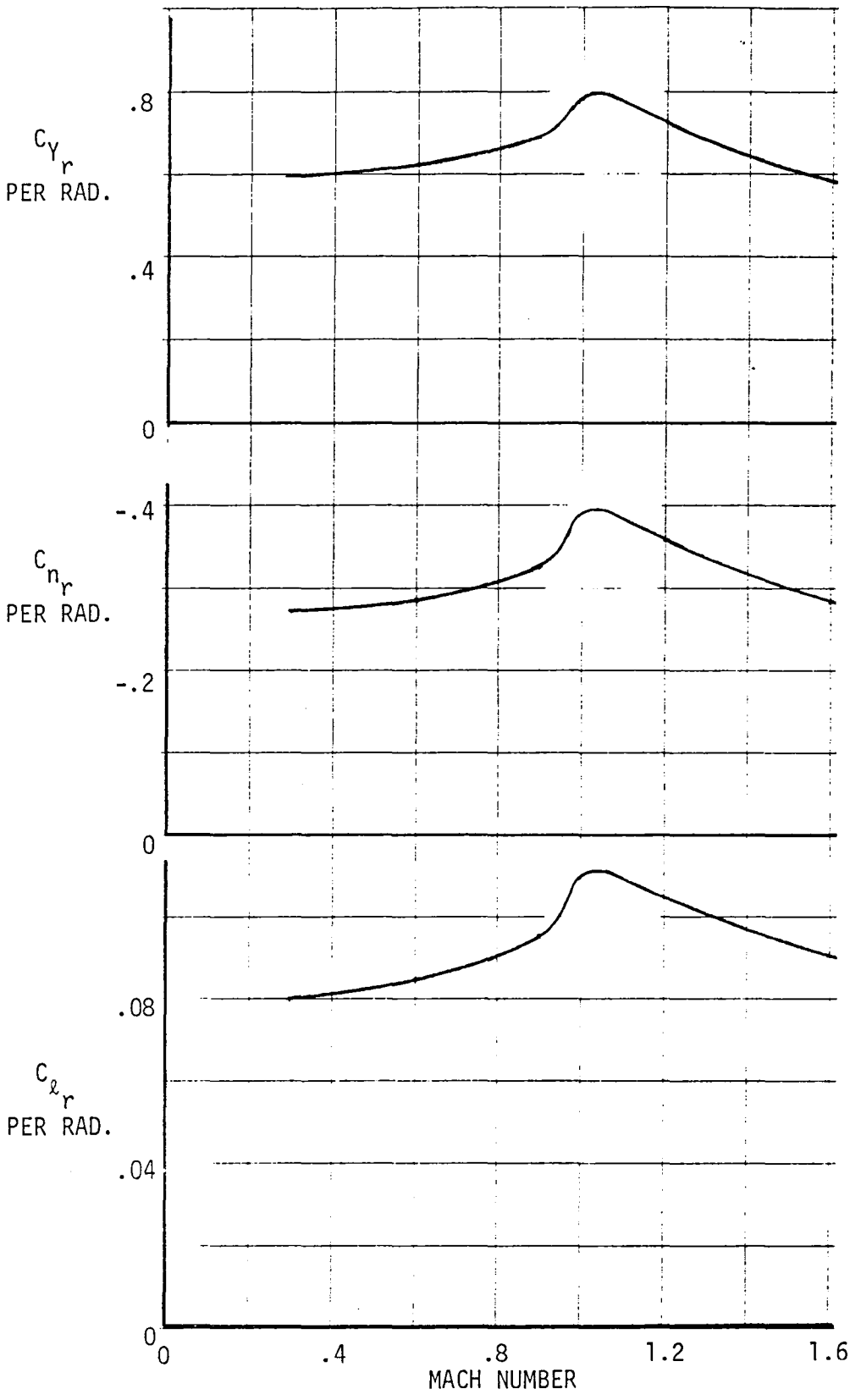

Figure 4-43 Alternate Configuration Yaw Rate Derivatives

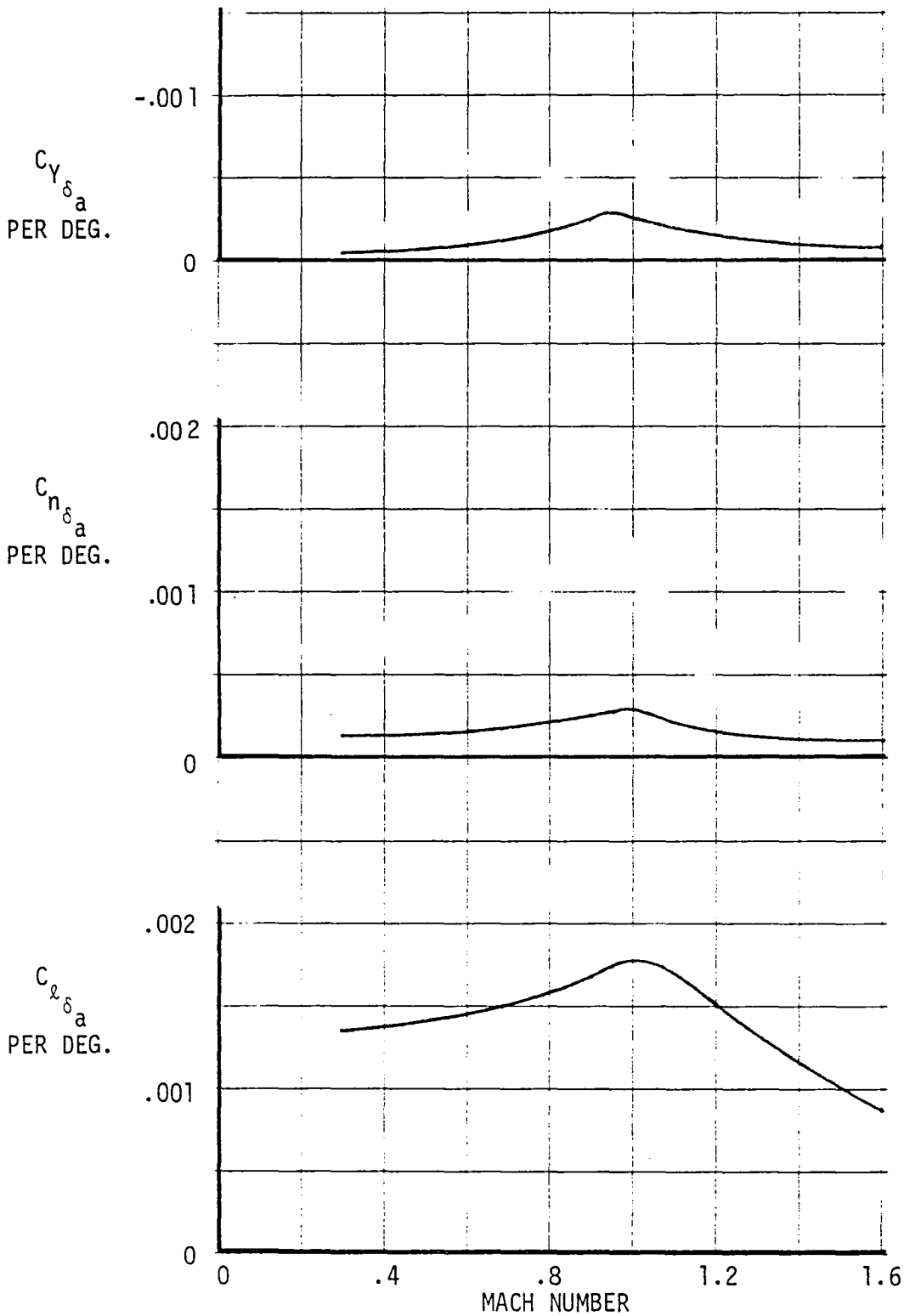

Figure 4-44 Alternate Configuration Lateral Control Effectiveness

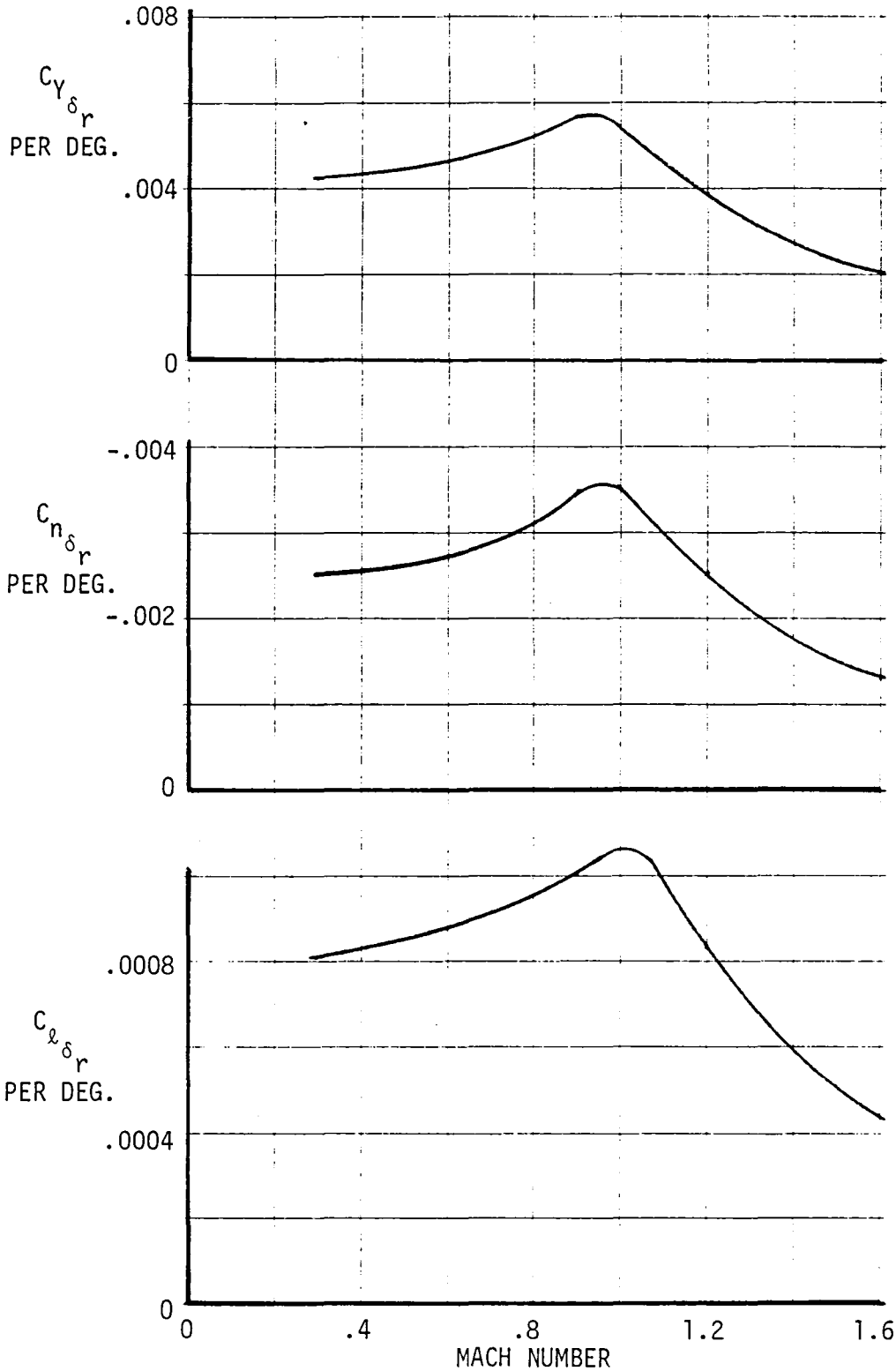

Figure 4-45 Alternate Configuration Rudder Effectiveness

4.6 ALTERNATE STOL/CONVERSION AND HOVER CHARACTERISTICS

STOL/Conversion - Lift and drag characteristics of the alternate configuration were developed using the methodology presented in section 4.3.1. In STOL the esssential difference between the baseline and alternate configurations is the reduced interference of the forward longitudinal augmenter on the aft lateral augmenter and the larger chordwise separation associated with the alternate configuration longitudinal augmenter.

Lift versus drag for augmenter angles of 25, 30, 40, and 50 degrees are shown in Figure 4-46 and 4-49, respectively. From Figure 4-47 it is noted that 37,000 pounds of lift can be developed at 100 knots and 30 degrees augmenter angle.

Hover Ground Effect - The discussion and data presented in Section 4.3 for the baseline configuration is applicable to the alternate design. However, it should be noted that different ground effects are expected from the variation in forward augmenter placement and wing planform. The maximum ground effect would be expected to be less. The loss in ground effect from gear extended down to gear static should also be diminished.

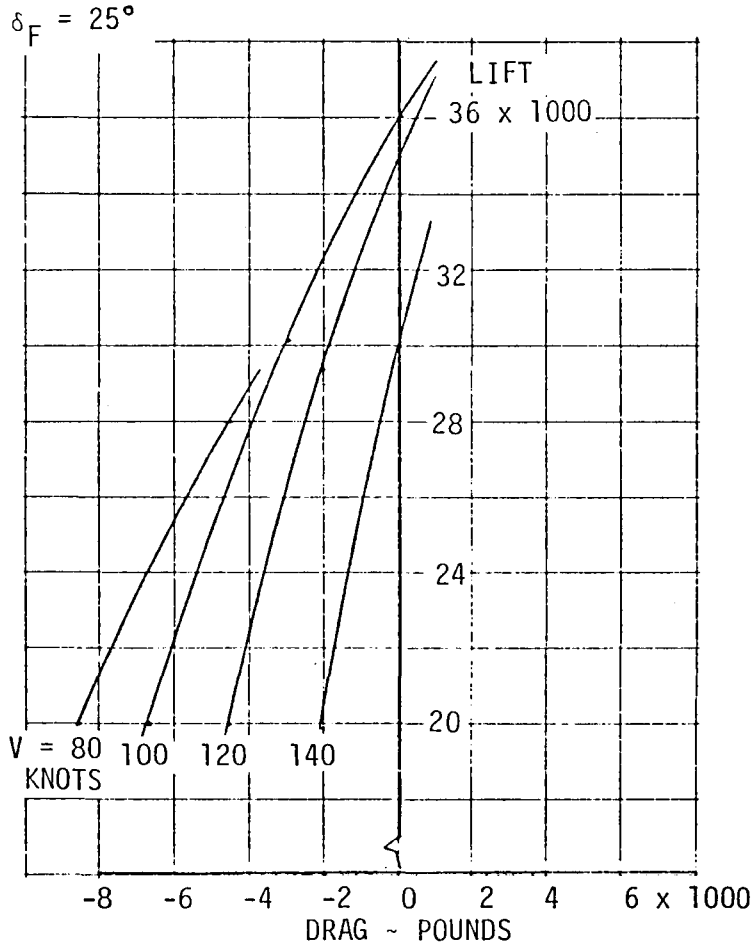

Figure 4-46. Alternate Configuration STOL Aero Characteristics

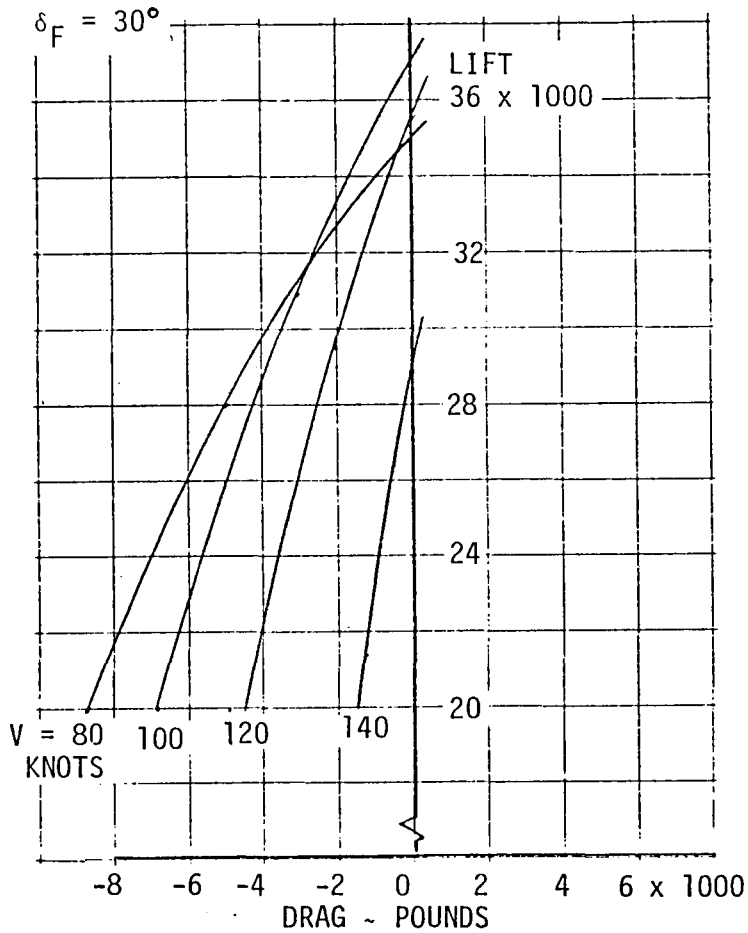

Figure 4-47. Alternate Configuration STOL Aero Characteristics

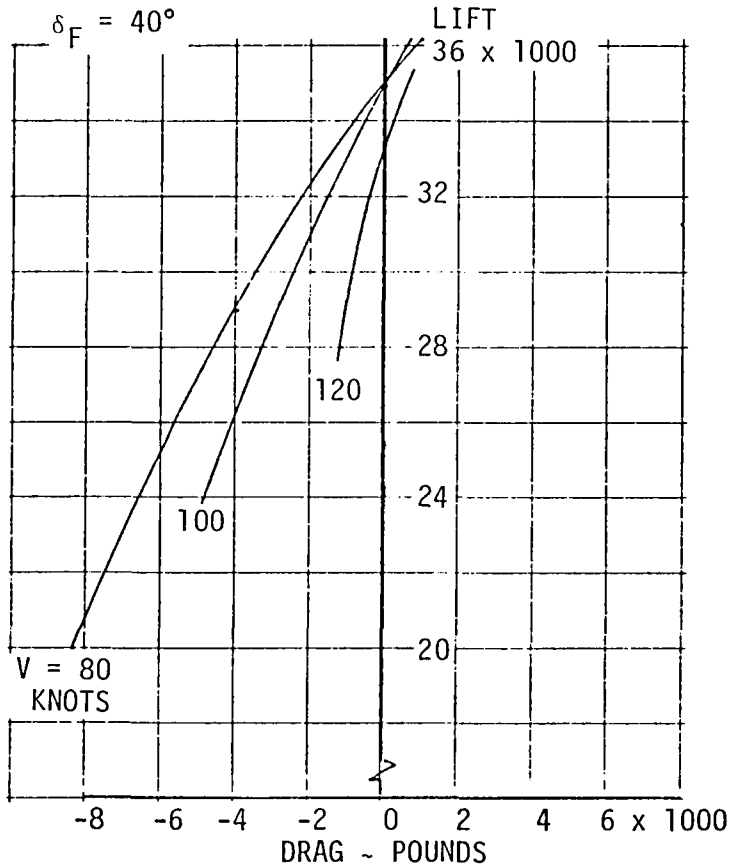

Figure 4-48. Alternate Configuration STOL Aero Characteristics

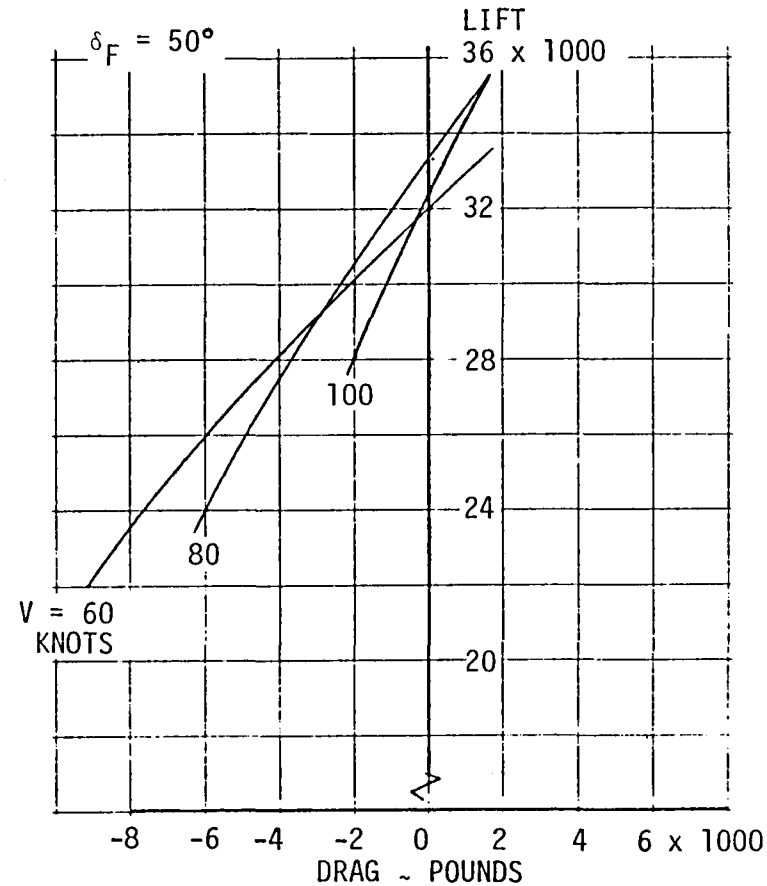

Figure 4-49. Alternate Configuration STOL Aero Characteristics

4.7 PROPULSION INDUCED EFFECTS

The propulsion system exhaust flow can have a significant effect on the aerodynamics of an air vehicle. This is particularly true if the jet exhausts near a lifting surface, e.g., over or under a wing or at a wing or horizontal tail trailing edge. In the up and away flight modes for the configurations of this study, the engine exhaust is well aft of the lifting surface trailing edge so any velocities induced on the aft fuselage by the jet exhaust would have an insignificant effect on aerodynamic characteristics. The propulsion system does have a second order effect on the high speed aerodynamic characteristics through the diverter valve. The diverter valve, as presently conceived, contributes to a rather steep boattailing of the aft fuselage and, thus, about 20 percent of the total configuration wave drag. In the hover and STOL flight modes the propulsion system exhaust is through the wing and does have a significant effect on the aerodynamic characteristics, enhancing the lift and providing rather complex but mostly favorable ground effects.

4.7.1 Hover Flight Mode

The vertical takeoff gross weight is determined in free air hover by allowing a reserve from the maximum lift for MIL-F-83300 type simultaneous control requirements plus 0.05 a/g vertical acceleration. The effect of these reserves are shown on Figures 6-10 and 6-28. The maximum lift is calculated from primary thrust and augmentation ratio. No adverse effects have been noted due to mutual interaction of fore and aft augmenters. An adverse interaction was suspected during full scale wing canard thrust augmented wing aircraft tests. Fuselage pressure measurements and a subsequent scale model force test, conducted specifically to investigate this phenomenon, both showed no negative lift or suckdown effect.

The net ground effects are shown in Figure 4-25 for a canard-wing configuration with spanwise fore and aft augmenters similar to the baseline configuration. It is noted that the full scale hot and 0.2 scale cold flow data agreed quite well. The loss in lift as the vehicle settles from wheel contact to the static (thrust off) height is due primarily to a loss in augmentation on the forward (low canard) augmenter of this configuration. This observation is corroborated by the wing-canard model pitching moment data at various heights above the ground shown on Figure 4-50. As the aircraft comes closer to the ground, increasing nose down pitching moment is encountered. Also, as noted on Figure 4-50, there is more than adequate pitch control power to overcome this ground effect. The present configurations have their forward augmenters higher above the ground than the low canard and in the same plane as the aft augmenter, so the ground induced nose down pitching moment and lift loss should be reduced from that shown.

The fountain on the wing-canard aircraft was found to act along a line between the wing and canard, shortly behind the wing leading edge-fuselage juncture. As the baseline aircraft has a similar spanwise augmenter arrangement and a single lifting surface, this fountain will have a great deal more area to work on and, thus, will produce a more

positive ground effect than that of the wing-canard aircraft. The alternate aircraft with its forward augmenters in a chordwise orientation will have less positive fountain effect than either of the other two configurations. Its fountains will be concentrated primarily on the fuselage.

In the presence of the ground, bank angle was found to induce an unstable rolling moment, as shown on Figure 4-51. The magnitude of this rolling moment is a function of height above the ground. It first appears as the aircraft descends to about 13 feet (half span) above wheel contact and increases as the aircraft descends further. The basic roll control in hover for all these designs is differential (L-R) wing diffuser angle. The data for wing roll control (square symbols) show the effect of using approximately 80 percent of the available wing roll control to counter a ten degree bank angle. These data indicate that the available roll control is reduced by ground proximity. As shown on Figure 4-51, the use of the canard (forward spanwise augmenter) provided satisfactory roll control at all ground heights.

4.7.2 Environmental Effects

The propulsion induced flow field in the presence of the ground that affects the aerodynamic characteristics could also reflect back on the engine through reingestion of the augmenter efflux. However, as noted in section 5.3, the primary and auxiliary inlets were placed on top of the fuselage to circumvent this potential problem. In addition, the wing shields the inlet from the augmenter efflux; and the augmenter efflux is relatively cool compared to direct thrust high lift systems, as shown on Figure 2-1.

The velocity profiles at ground level from an aircraft with forward and aft spanwise augmenters suspended 30 feet above the ground is shown on Figure 4-52. The velocities are under 100 ft/sec. and peak at 60 ft/sec. at most azimuths around the aircraft.

Sound pressure levels from XFV-12A augmenter tests are compared with direct thrust VTO concepts on Figure 4-53. It can be seen that the thrust augmenting ejector produces significantly lower noise levels than either of the other two VTO concepts.

4.7.3 STOL/Conversion Flight Mode

At forward speeds the thrust ejector augmented wing experiences a significant benefit from propulsion induced forces, namely, a very strong boundary layer control. This allows the use of large flap deflections, as high as 90 degrees with no separation, i.e., full potential lift is realized. A supercirculation effect, similar to that shown for jet flaps in Reference 4-3, should be present. However, since none has been identified in test data to date, it has not been included in the calculation of STOL or conversion performance. The contractor is pursuing the determination of this factor as rapidly as resources permit.

The interaction of two spanwise tandem thrust augmenting ejectors in a single lifting surface was expected to produce some unfavorable effect. In order to estimate this effect, an analysis method was conceived and checked out against limited wind tunnel data on a pair of equal span, very close coupled tandem augmenters. The lift was defined as:

$$C_L = C_{L_0} + \phi C_\mu \sin(\alpha + \delta)$$

where C_{L_0} is the theoretical potential lift which can be calculated by any one of several distributed singularity techniques. For these analyses simple bound vortices were used. These singularities were distributed over subpanels on the wing, flaps, body, and augmenter endplates with the requirement of zero flow velocity at the 3/4 chord of each local subpanel.

Because the jet plume from the forward augmenter precludes the lower half of the aft augmenter from "seeing" the freestream, some correction must be made. In order to account for this blanking effect, the input control point deflection angle was assumed to be half of the actual flap angle for determination of the net lift of the complete configuration. This assumption is based on the linear theory result that half the lift is generated on the lower surface and half on the upper surface. Excellent agreement of the calculated lift with experimental values is shown on Figure 4-54.

With lift coefficient calculable STOL/conversion performance can be determined from the drag equation:

$$C_D = -r\phi C_\mu + \frac{C_L^2}{\pi \mathcal{R}_e + 2\phi C_\mu} + \frac{\dot{m}V}{qS} + C_{D_0}$$

where $r = \cos(\alpha + \delta) + \frac{1}{2}\sin^2(\alpha + \delta)$
ϕ = static augmentation at δ
$\dot{m}$ = total secondary airflow through augmenters and engine
C_{D_0} = unseparated profile drag with the flaps down

A comparison of the estimated drag with experimental data is shown on Figure 4-55. Again, very good agreement is achieved with experimental data especially when experimental lift data are used in the drag equation.

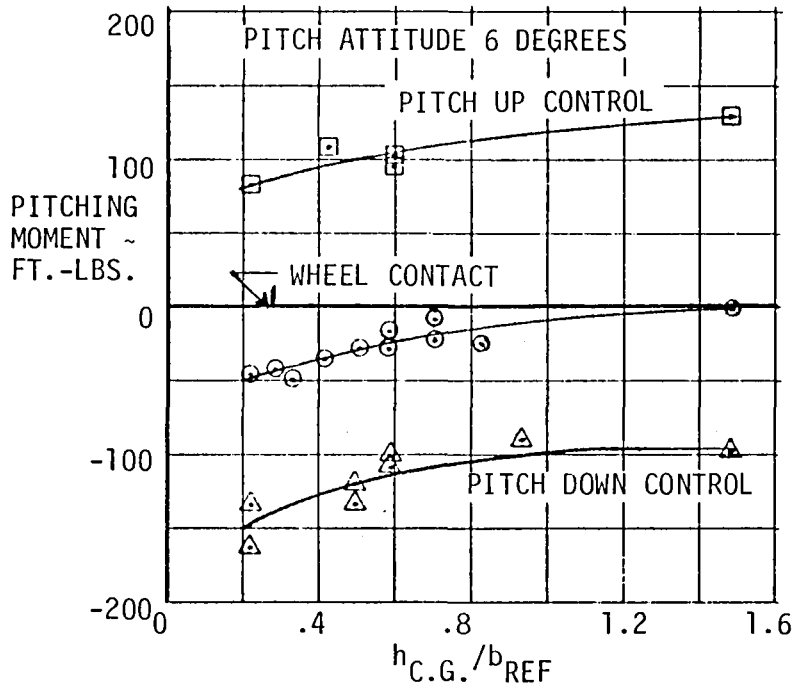

Figure 4-50. 0.2 Scale XFV-12A Pitching Moment in Ground Effect

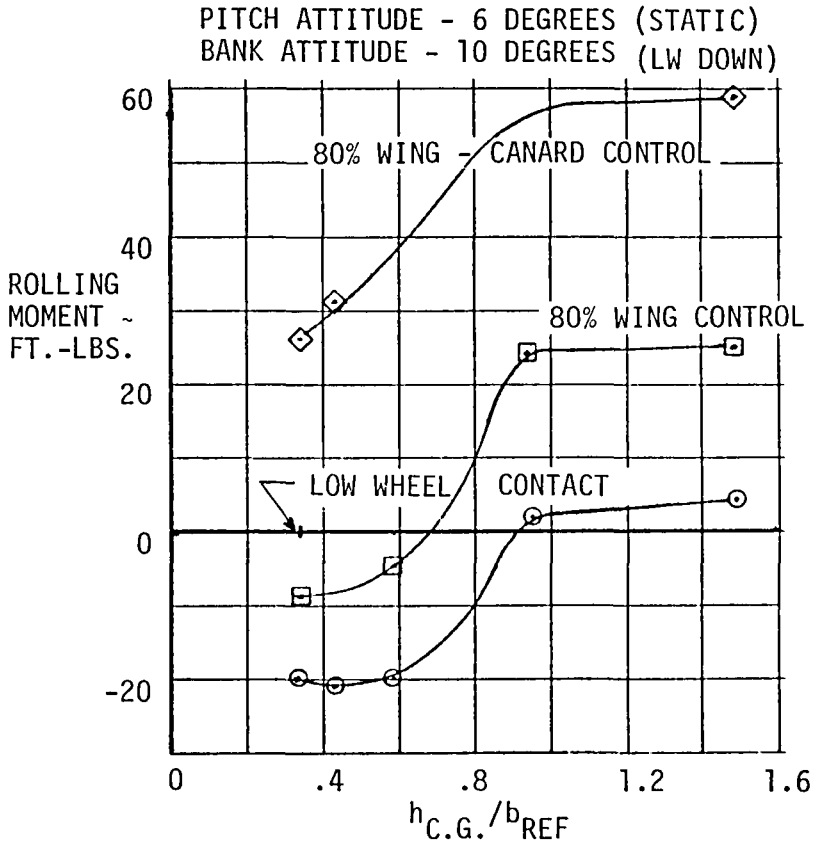

Figure 4-51. 0.2 Scale XFV-12A Rolling Moment in Ground Effect

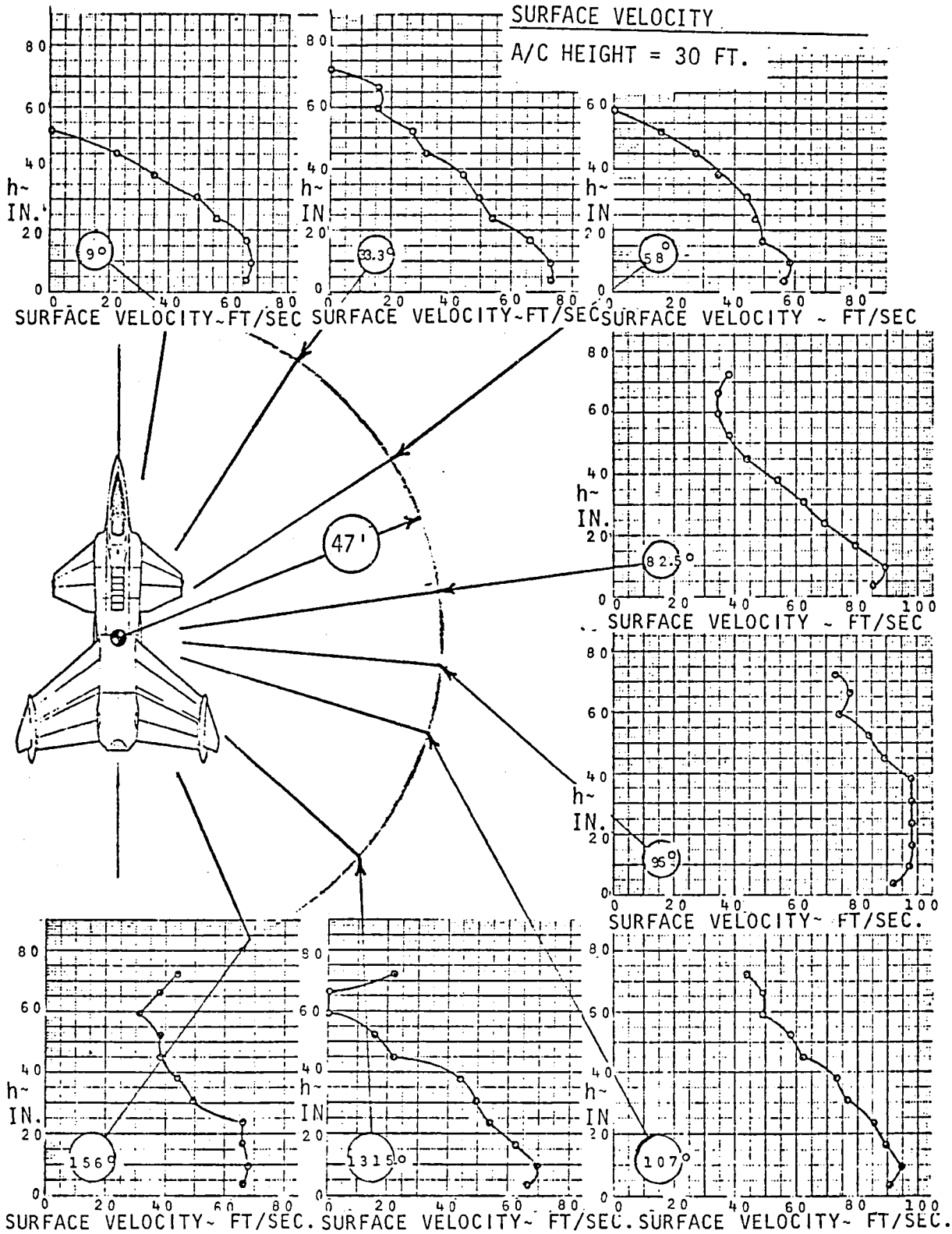

Figure 4-52 Footprint Air Velocity

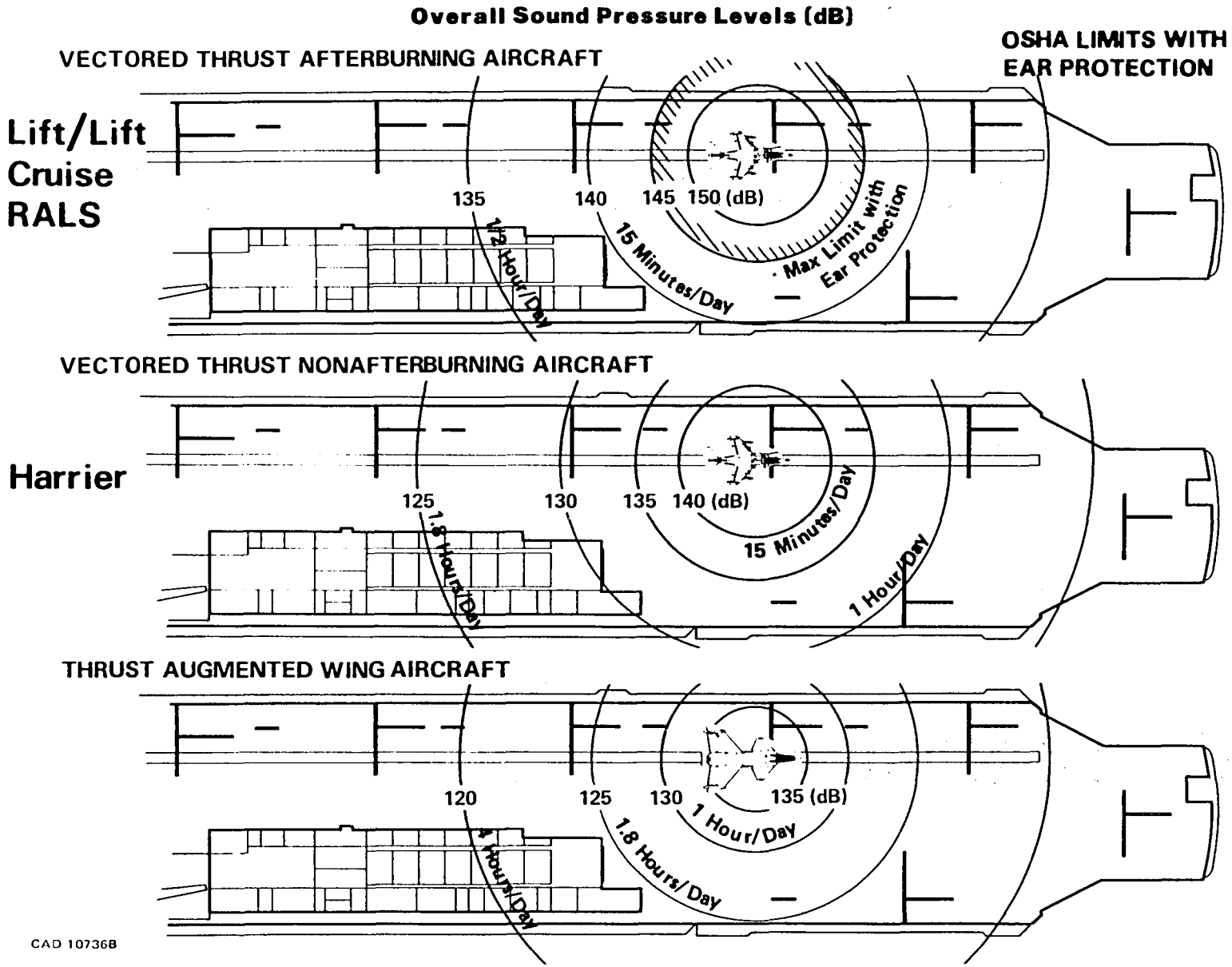

Figure 4-53 V/STOL Aircraft Acoustic Footprints

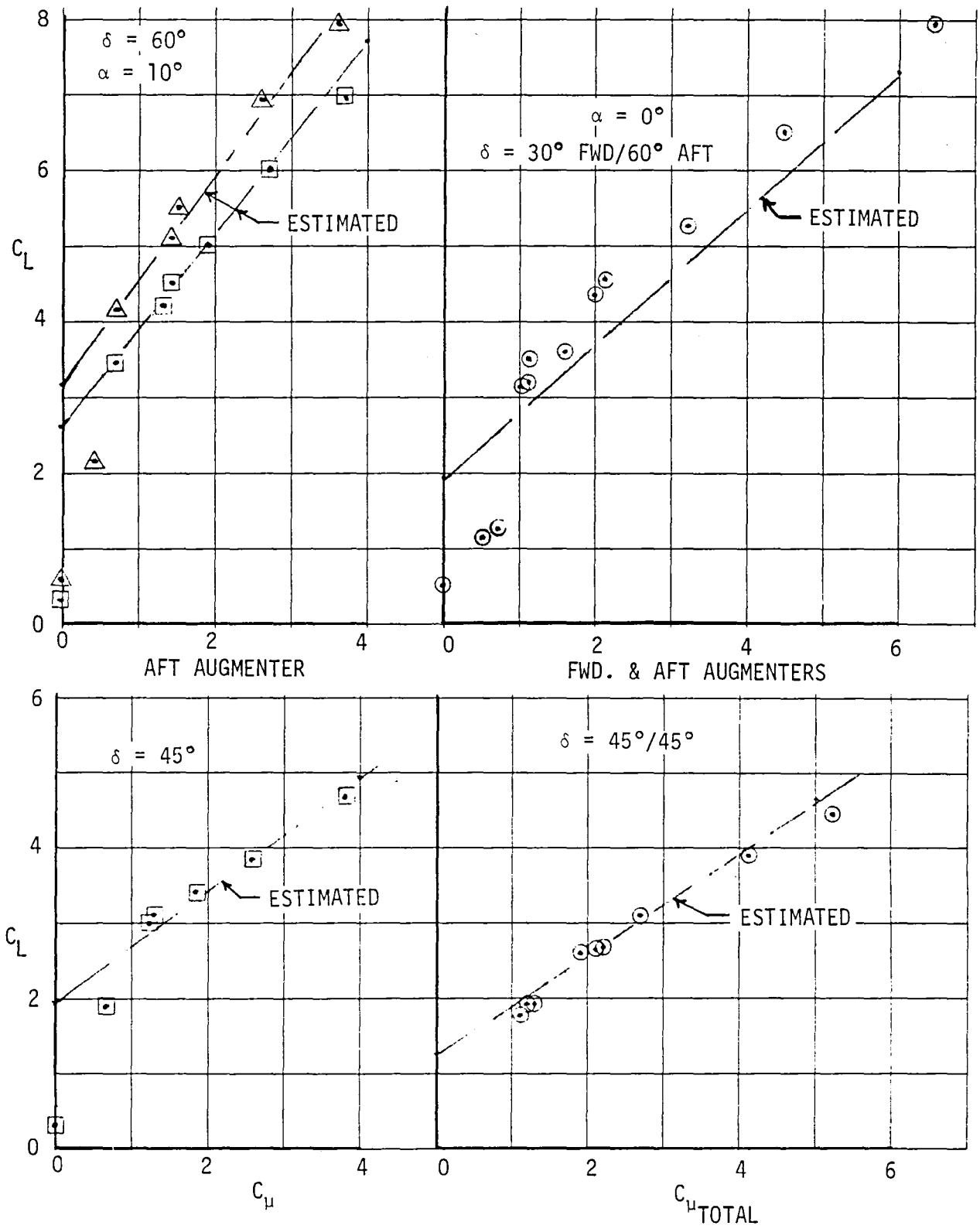

Figure 4-54. Calculated-Experimental STOL Lift Comparison

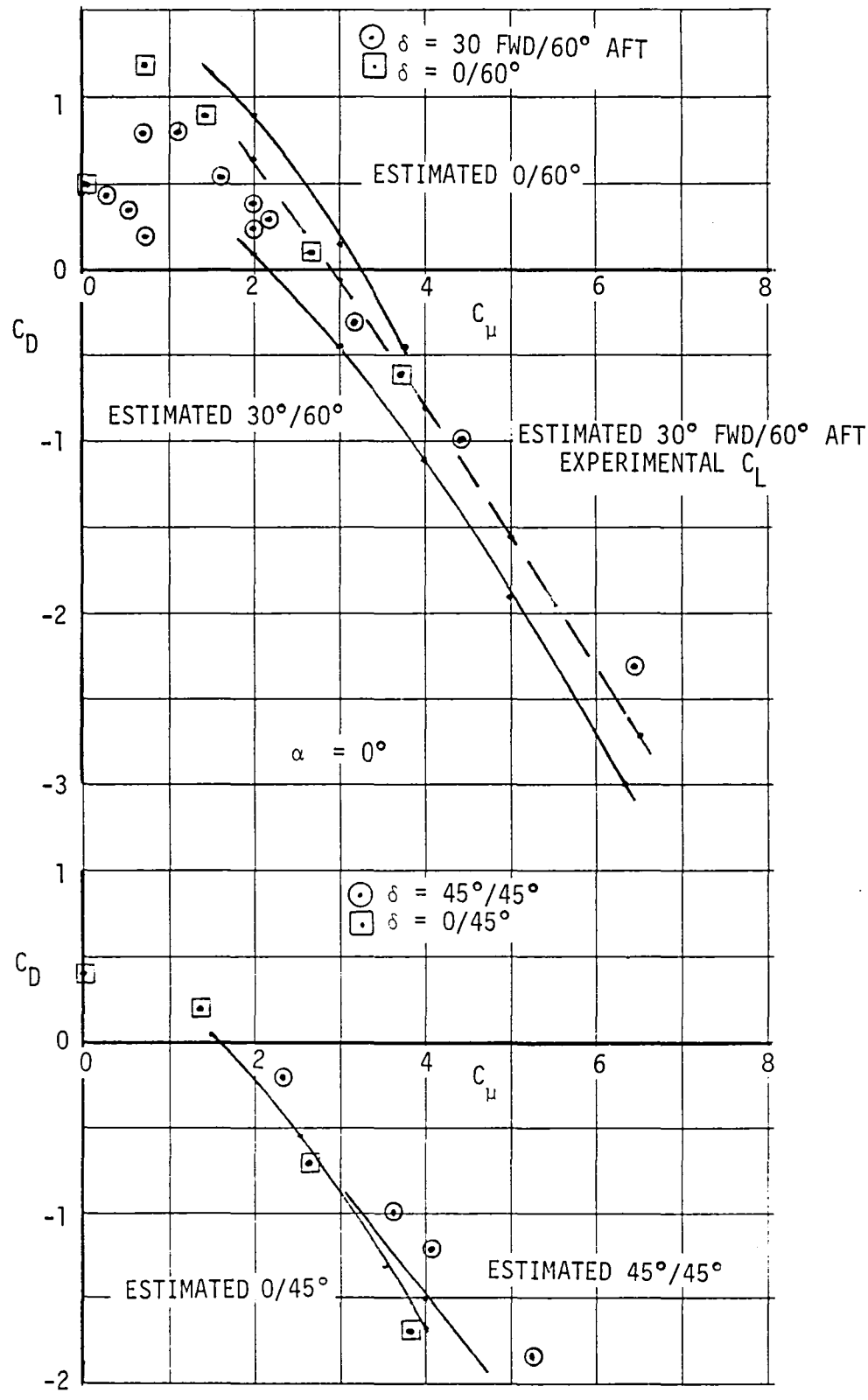

Figure 4-55. Calculated-Experimental STOL Drag Comparison

5.0 PROPULSION CHARACTERISTICS

5.1 ENGINE SELECTION

A parametric propulsion system analysis was undertaken to select the propulsion cycle. The Pratt and Whitney Aircraft JT69 Engine Family Performance Model parametric engine cycle computer deck CCD1178, dated 1 September 1980, was selected to conduct this analysis. The engine deck generates engine weights and dimensions in addition to engine performance.

All engines in the parametric study were mixed flow turbofans and were flat rated to a Tropical Day (90°F). The three engine cycle parameters that were varied were Turbine Inlet Temperature (TIT), Fan Pressure Ratio (FPR), and Overall Pressure Ratio (OPR). Bypass ratio is not an independent parameter when FPR is specified.

Factors influencing cycle parameter selection for an augmenter-type V/STOL aircraft include thrust to weight ratio, SFC at cruise, nozzle pressure ratio (P_{T7}/P_0), and nozzle mixed flow temperature (T_7). Augmenter nozzle pressure ratio should not be much greater than 3.0 for proper augmenter performance; therefore, the engine nozzle pressure ratio should be 3.3 - 3.6 to account for the ducting system pressure losses. Nozzle pressure ratio is essentially a direct function of FPR. A nozzle maximum mixed flow temperature of 1200°F was selected based on ducting material considerations.

Engine thrust to weight ratios versus nozzle pressure ratio and turbine inlet temperature for two overall pressure ratios are presented in Figure 5-1. As TIT increases, thrust to weight also increases. It was decided to limit TIT to 2800 degrees for the engine technology available in the projected time period for this aircraft.

It is desirable to have the augmenter ducts as small as possible. The engine exit airflow parameter $W_7\sqrt{T_7}/P_7$ directly affects ducting size and pressure losses. The airflow parameter is a function of nozzle pressure ratio only, as shown in Figure 5-2, and is independent of TIT and OPR. the higher the nozzle pressure ratio the smaller the ducts. The nozzle temperature, presented in Figure 5-3 is a function of nozzle pressure ratio and OPR but is independent of TIT. For the smallest size augmenter ducts with temperatures under 1200°F, the nozzle pressure ratio should be less than 3.75 and OPR equal 30. An OPR 30 engine has a lower thrust to weight ratio than an OPR = 20 engine (Figure 5-1), but the cruise SFC's are better for OPR = 30 (see Figure 5-4). The OPR = 30 engine offers a better tradeoff on SFC's than the higher thrust to weight of the OPR = 20 engine.

5.2 ENGINE DESCRIPTION

The engine parameters for the engine cycle selected for this study are presented in Figure 5-5.

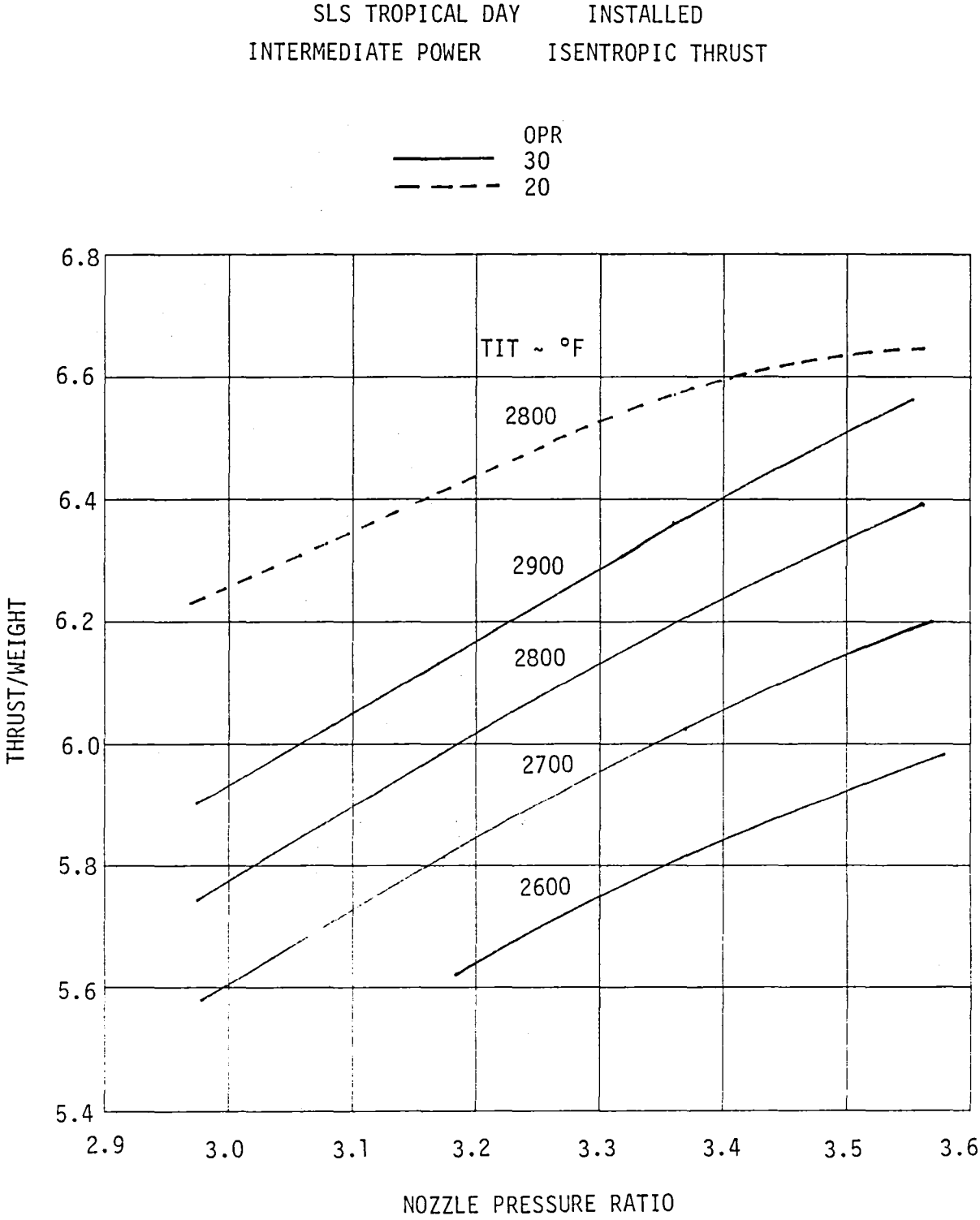

Figure 5-1 Engine Thrust to Weight Ratios

SLS TROPICAL DAY INSTALLED
ISENTROPIC THRUST = 20,000 LBS.

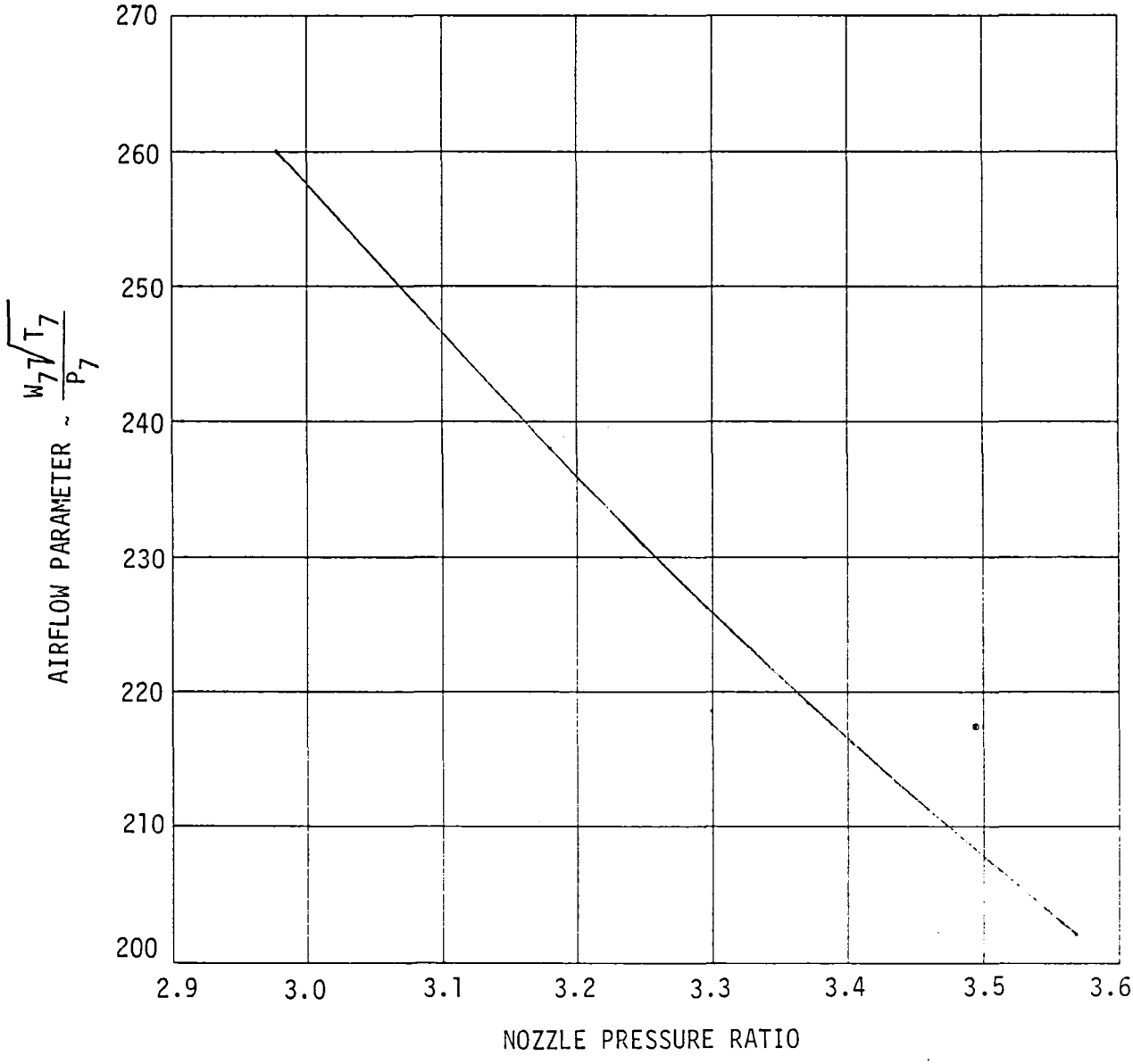

Figure 5-2 Duct Airflow Parameter

SLS TROPICAL DAY INSTALLED

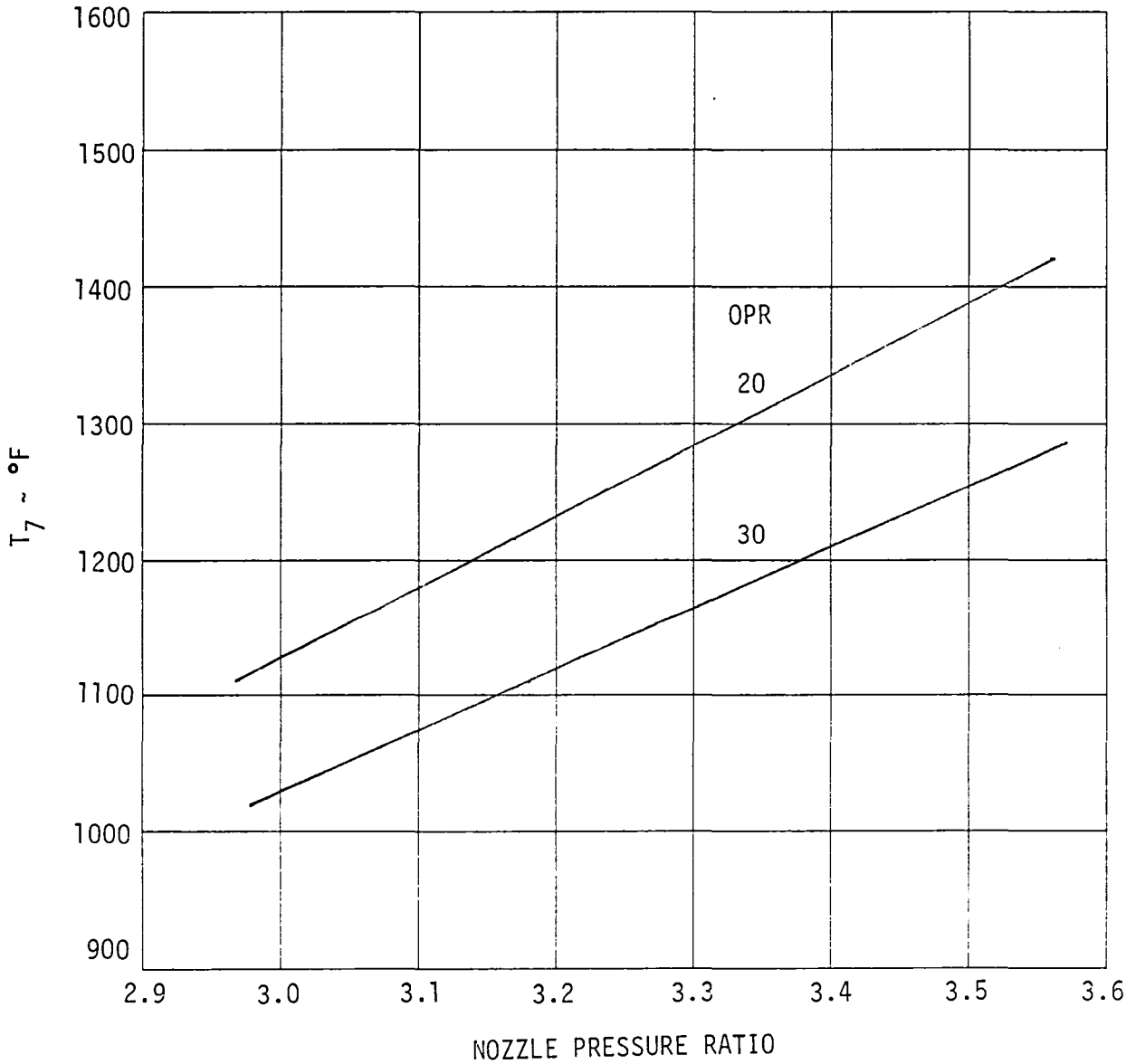

Figure 5-3 Nozzle Mixed Flow Temperature

M = 0.8 35,000 FEET
TIT = 2800 °F

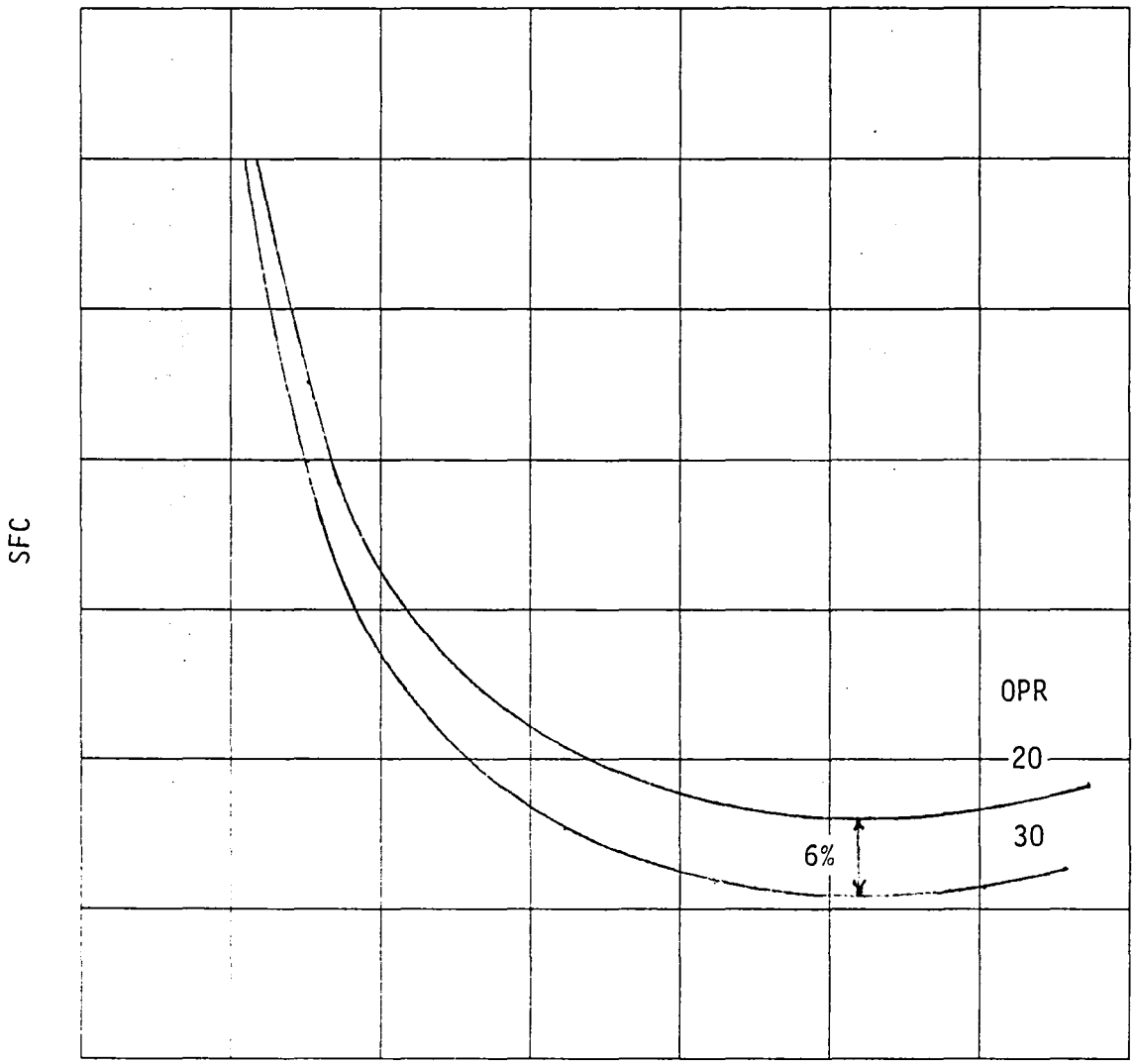

Figure 5-4 Cruise SFC Comparison

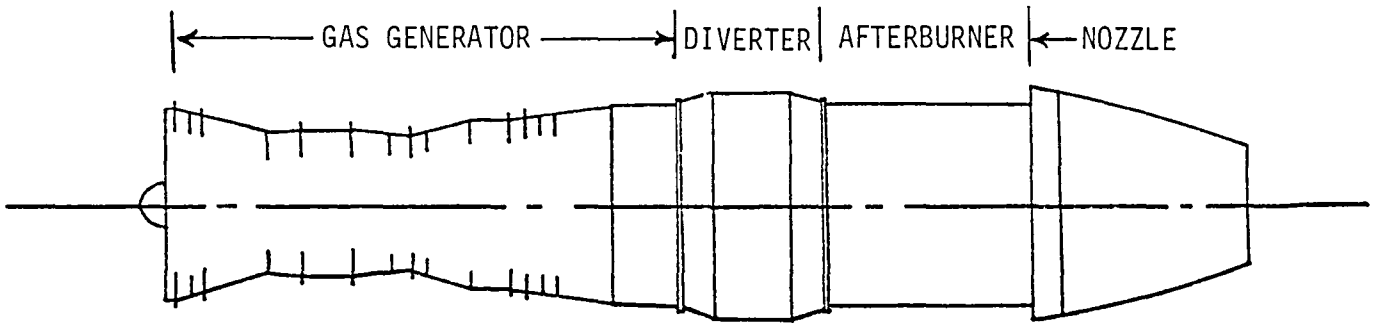

COMPUTER DECK NO. CCD 1178 - P&WA JT69 ENGINE

FAMILY PERFORMANCE MODEL - 1 SEPTEMBER 1980

MAX A/B - LBS.	33,880
INTERMEDIATE - LBS.	20,600
OVERALL PRESSURE RATIO	30.0
BYPASS RATIO	.506
MAX TURBINE INLET TEMPERATURE - °F	2,800

Figure 5-5 Engine Characteristics

5.3 AIR INDUCTION SYSTEM

The air induction system consists of a two-dimensional five-degree fixed ramp supersonic inlet designed with emphasis on acceleration to M = 1.6, a gradual S-bend diffuser to the engine face, and an auxiliary inlet for improved performance at V/STOL operating conditions.

The inlet is located on top of the fuselage, just aft of the canopy. This arrangement was selected primarily to minimize reingestion during VTO operation. Full scale tethered airplane tests of the XFV-12A which has vertical ramp side inlets, a bifurcated diffuser, plus an auxiliary inlet on top of the fuselage, indicated that little of the reingestion encountered entered via the top inlet, as reported in Reference 5-1 and shown in Figure 5-6.

The top mounted inlet has the following additional advantages: (1) lower radar signature to forward and lower sectors; (2) uncluttered lower fuselage for flexibilty in external stores arrangement; and (3) elimination of foreign object damage (FOD) to the engine from runway debris.

The auxiliary inlet, patterned after the successful XFV-12A design is located in the low flow velocity region of the diffuser. The auxiliary inlet doors provide a net flow area of 1192 square inches. Estimated inlet recovery at static conditions is presented in Figure 5-7, based on full scale XFV-12A data presented in Reference 5-1.

Limited subsonic Rockwell tests of an upper inlet were conducted in combination with various lifting surface configurations on a fighter fuselage configuration. A canard + strake configuration located ahead of and below the inlet was similar in orientation to the wing/inlet configurations of this study. Unpublished results of tests with this configuration indicated excellent pressure recovery at high angles of attack, as shown in Figure 5-8. These results are consistent with those of reference 5-2 which indicated that top-mounted inlets with proper lifting surface/forebody integration are competitive with fuselage-and wing-shielded inlets.

Estimated inlet performance for the five-degree fixed ramp supersonic inlet is presented in Figure 5-9 for high subsonic and supersonic flight (normal cruise) conditions. This estimate accounts for the oblique and normal shock losses and the diffuser losses. Pressure losses resulting from duct friction, turning and shock/boundary layer interaction are included in the estimated diffuser losses. A breakdown of the various losses in terms of the pressure recovery (1 - loss) is presented in Table 5-1. A comparison of the estimated pressure recovery with the recovery of four two-dimensional inlets is also shown on Figure 5-9. The F-107 inlet is above the canopy, Reference 5-3. The others are side inlets. The F11F-1F inlet ramp is fixed; the ramps of the others are variable which results in better performance at high supersonic speeds. The F11F-1F and the F-106 have bifurcated diffusers which would typically have higher pressure losses.

TABLE 5-1

INLET TOTAL PRESSURE RECOVERY COMPUTATION

5° FIXED RAMP

Mach No.	Oblique Shock Recovery	Normal Shock Recovery	Estimated Diffuser Recovery	Estimated Inlet Total Pressure Recovery
1.0	1.0	1.0	.965	.965
1.25	.9976	1.0	.965	.963
1.4	.9984	.9914	.965	.955
1.6	.9984	.9513	.965	.917
1.8	.9982	.8848	.965	.852
1.9	.9981	.846	.965	.815

Supersonic inlet recovery is enhanced by a ramp bleed system which removes most of the ramp boundary layer and reduces shock/boundary layer interaction. Pertinent inlet dimensional characteristics are:

Capture Area = 1106 $in.^2$
Throat Area = 940 $in.^2$
Inlet Lip Thickness = 0.5 in.

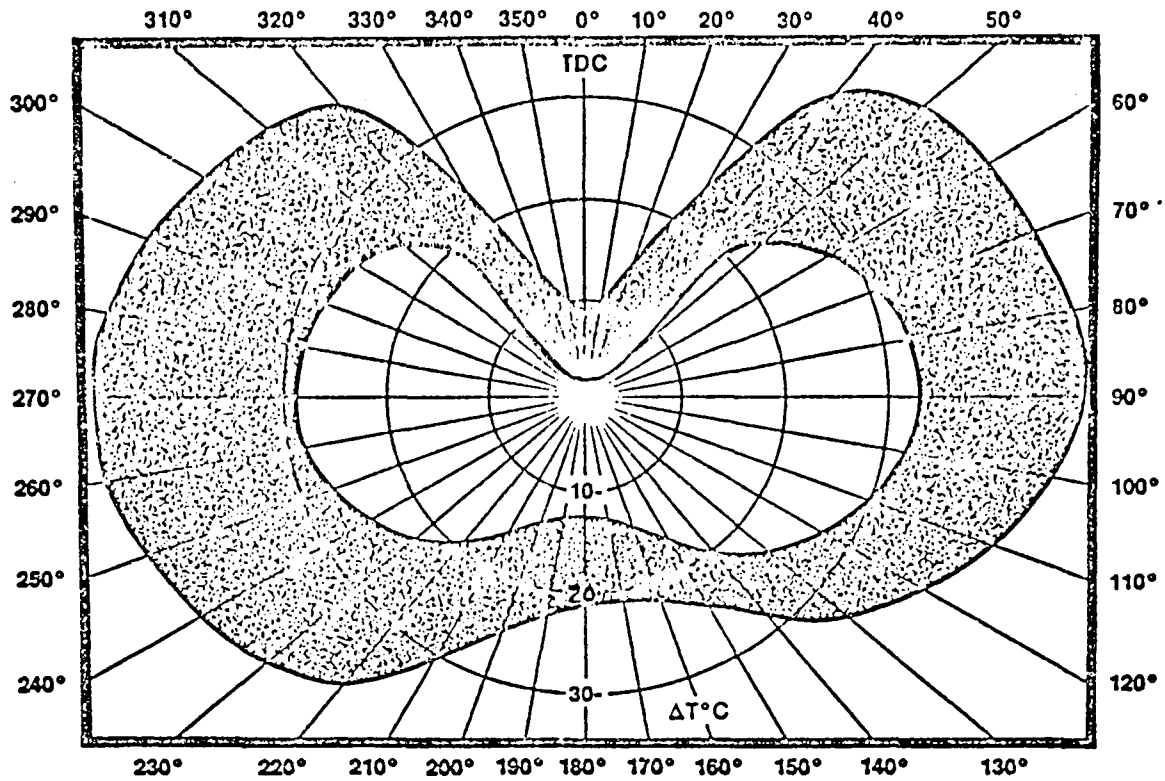

SPATIAL TEMPERATURE GRADIENTS AT XFV-12A ENGINE FACE
DURING REINGESTION 4 TO 7 SECONDS AFTER FLAP SWEEP

Figure 5-6 Reingestion Profile

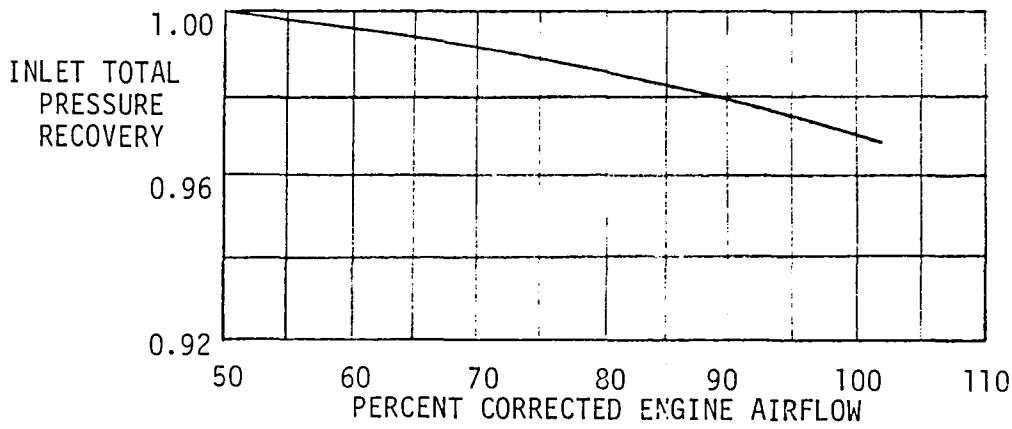

Figure 5-7 Inlet Pressure Recovery at Static Conditions

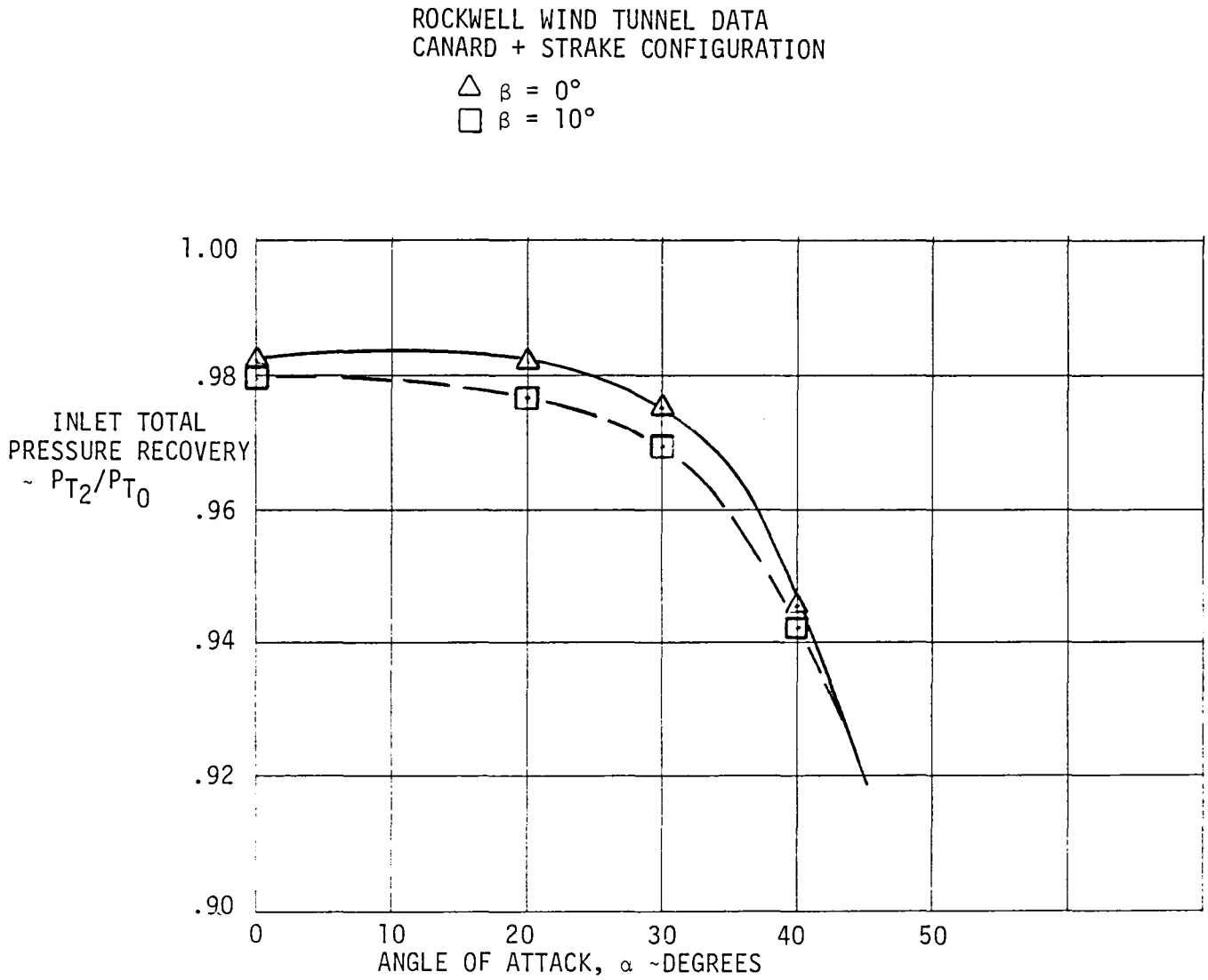

Figure 5-8 Effect of Forebody Surfaces on Inlet Total Pressure Recovery at Angles of Attack

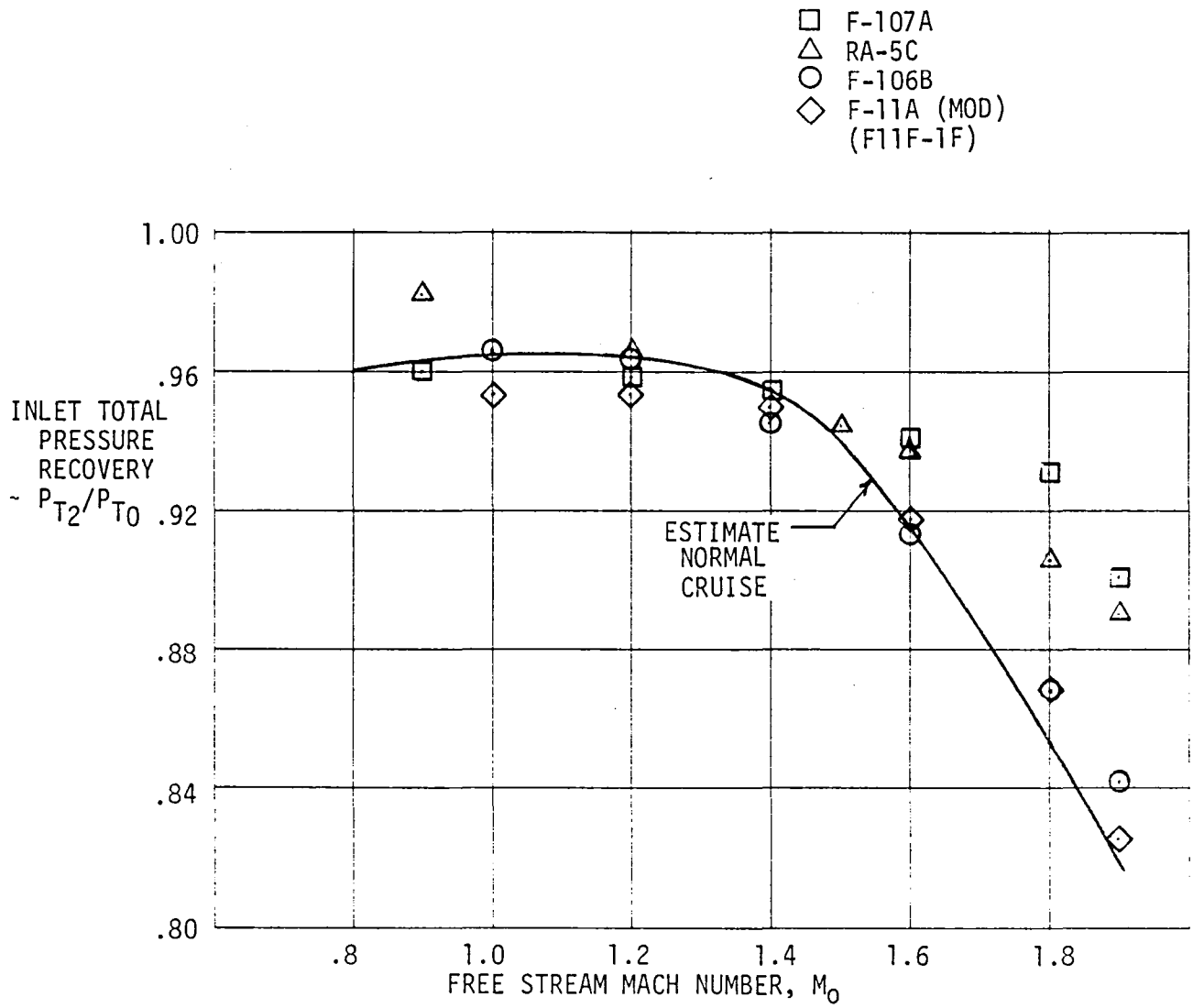

Figure 5-9 Estimated Inlet Pressure Recovery

5.4 EXHAUST NOZZLE - DIVERTER - DUCTING SYSTEM

The exhaust nozzle is of conventional convergent-divergent design to provide a full range of afterburning and non-afterburning performance over the complete conventional flight envelope. For vertical and STOL operation, flow to the nozzle is completely blocked by a diverter which directs all of the engine flow to the augmenter system.

Extensive diverter design, test, engine integration and development experience was obtained during the XFV-12A program. Initial development is described in Reference 5-4, with later experience summarized in Reference 5-5. Full scale fixed and operable diverter tests were conducted by both P&WA and Rockwell. P&WA conducted initial engine compatibility tests and pre- and post-test performance calibrations. Rockwell testing included 100-foot whirl rig tests in which the engine and diverter provided a variable gas supply for augmenter component tests. Static tests of the XFV-12A with the engine/diverter system installed and tethered aircraft tests at NASA Langley provided aircraft/engine/diverter integration and compatibility information.

Results of these tests demonstrated diverter durability and reliability, indicated that performance requirements were generally met or exceeded, and verified that engine operation, control and performance when exhausting into a diverter/augmenter system is satisfactory.

The aircraft tests also provided extensive experience with the engine to augmenter ducting system. There was no evidence of thermal or leakage problems, and pressure losses were at acceptable levels.

Pressure losses are held to a minimum by adhering to a maximum design Mach number of 0.3.

Bend radius criteria were obtained from Reference 5-6. Turning vanes are used in comparatively sharp bends and Mach numbers are reduced to .23 to improve the exit velocity distribution and reduce the pressure loss. For the XFV-12A, turning vane configurations and position were optimized using full scale models of feed duct components as described in Reference 5-4. Details of a typical feed system for a forward lateral augmenter and pitchpipe, and for an aft augmenter are shown in Figure 5-10.

Estimated duct pressure losses and the corresponding thrust losses for the pitch pipe, forward feed and aft feed systems are shown in the table below.

TABLE 5-2

DUCTING PRESSURE/THRUST LOSSES*

Pitch Pipe	Fwd Augmenter Feed	Aft Augmenter Feed
8% Flow	50% Flow	42% Flow
$\Delta P/P_T$ = 16.9%	$\Delta P/P_T$ = 21.3%	$\Delta P/P_T$ = 12.1%
$\Delta F_G/F_G$ = 6.9%	$\Delta F_G/F_G$ = 9.1%	$\Delta F_G/F_G$ = 4.7%

*These losses are in addition to the thrust loss assessed for system leakage estimated = 2% of total thrust.

5.5 PITCH REACTION CONTROL

Identical variable area nozzles located fore and aft provide pitch reaction control. Each convergent nozzle is fully variable from open to closed for optimal aircraft control. A sketch of the nozzle is shown in Figure 5-11. Estimated pressure losses for the pitch reaction control system are presented in Table 5-1 above.

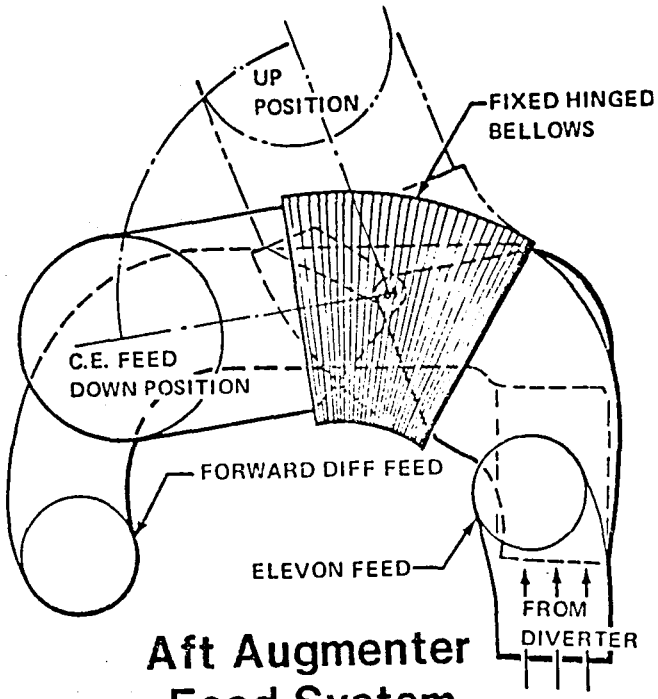

Aft Augmenter Feed System

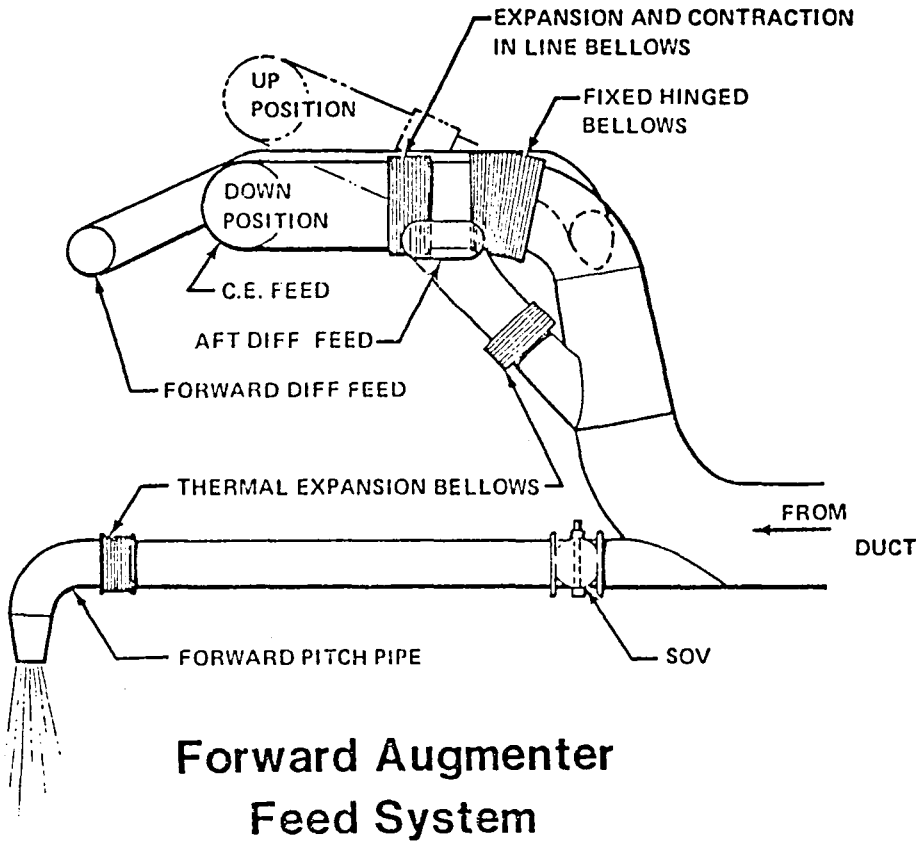

Forward Augmenter Feed System

Figure 5-10 Typical Feed Systems

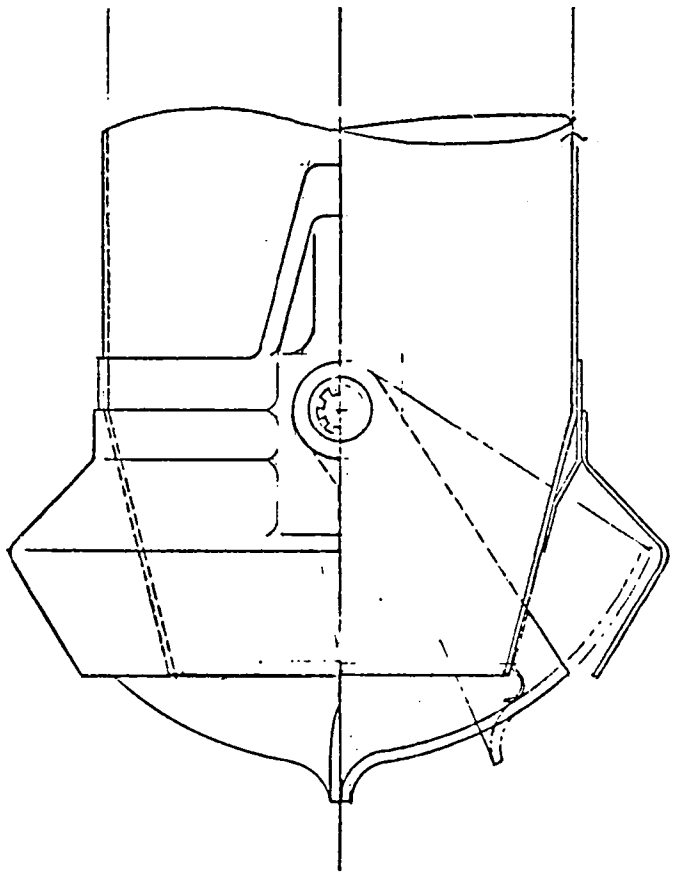

Figure 5-11 Pitch Reaction Control Nozzle

5.6 AUGMENTER SYSTEM

5.6.1 Principle of Thrust Augmentation

The additional thrust required to achieve VTOL performance is obtained by diverting the engine exhaust flow through thrust augmenting ejectors located in the wing of the aircraft. Each ejector consists of a duct, formed by a pair of blown flaps with endplates across their inboard and outboard ends, and a central nozzle. Entrainment by the primary exhaust jets draws a large quantity of air through the duct. The flaps redirect the entrained flow along the axis of the primary jets; in the process, a circulation is generated around the flap sections. Thus, the flaps may be viewed as wings "flying" in the velocity field of the entrained flow, so that a force analogous to the lift on a wing is developed on each of the flaps. It is this force which augments the thrust of the primary jets. By Newton's Law of action and reaction, an equal but opposite force increases the jet thrust. This process is described in greater detail in Reference 5-7.

The thrust augmentation ratio may, therefore, be defined as the ratio of the initial jet thrust, T, plus the force on the flaps, F, to the isentropic thrust of the primary jet mass;

$$\phi = \frac{T + F}{\dot{m}V}$$

The amount of thrust augmentation depends on the rate of jet entrainment, and the size, shape, and location of the flaps. These flap parameters are characterized by the ejector inlet area ratio, $A_{2/0}$, which is the ratio of the ejector inlet area to the primary nozzle exit area; the diffuser area ratio, $A_{3/2}$, which is the ratio of the ejector exit area to its inlet area; and the length ratio, L/W, which is the ratio of the flap chord to the inlet width.

In general, the thrust augmentation ratio increases with the length of the ejector, and the diffuser area ratio. The dependence of the thrust augmentation on these parameters is shown in Figure 5-12 for a fixed value of the inlet area ratio. The increase in augmentation with diffuser area ratio is limited by diffuser separation. Viscous losses limit the increase in augmentation with length, but this does not become important until the ratio of flap length to throat width (L/W) reaches a value of about 10, which is longer than most aircraft ejectors. The thrust augmentation also increases with the inlet area ratio, if the L/W ratio is constant; however, since the length of the ejector is limited by the necessity for ground clearance, there is an optimum inlet area ratio for each ejector of prescribed length. This optimum increases with the jet entrainment rate, so that it becomes doubly important to maximize this parameter.

5.6.2 Ejector Geometry

The aft augmenter on the baseline airplane is shown in cross section in Figure 5-13. The aft augmenter on the alternate airplane is

very similar to the one shown. The ejector duct is formed by forward and aft wing flaps, which also serve as feed ducts for the Coanda jets in the ejector inlet. These jets provide boundary layer control to prevent separation of the secondary flow in the suction peak at the leading edge of the flap, or in the more gradual pressure rise in the diffuser section. The central nozzle also serves as an upper surface close out door, when the flaps are retracted to form a conventional airfoil. Maximum ejector performance would utilize about 70 percent of the primary flow in the central nozzle. However, when duct losses are taken into consideration, the performance of the lift system is optimized with 65 percent of the flow in the centerbody nozzle.

The centerbody nozzle was designed to provide large entrainment rates, while providing a simple close out scheme, with no protrusions on the airfoil surface when the ejector was retracted. The nozzle exit consists of alternating lobes and spanwise slots. The alternating segments of the jet are deflected approximately 15 degrees from the axis of the ejector, in order to produce a system of streamwise vortices. These vortices enhance the turbulent entrainment and draw additional air through the ejector, thus increasing the augmentation.

The forward ejectors on the baseline airplane are similar to the aft ejectors. However, the forward ejector on the alternate configuration is parallel to the centerline of the airplane, as shown on Figure 3-4. A cross section of the forward ejector of the alternate configuration is shown on Figure 5-14. The same principles are used in the ejector as in the spanwise ejectors. The centerbodies are still oriented spanwise and have alternating lobes and spanwise slots, but they span the throat from diffuser surface to diffuser surface rather than being parallel to the diffuser surfaces. These short spanwise centerbodies are arranged in tandem so that they can be rotated aft to deflect the thrust during transition and close up to form the top surface of the augmenter. Coanda jets are provided for both inboard (fuselage side) and outboard diffuser surfaces. Only the outboard diffuser surface is moveable, and it retracts to form the lower surface of the augmenter and wing in conventional flight.

5.6.3 Ejector Performance

The expected performance of these ejectors has been determined from tests of similar ejectors. Although the geometry of a scale model can be made to duplicate the full size prototype, it is not possible to simultaneously match the Mach and Reynolds numbers, which are the relevant scaling parameters for aerodynamic testing. However, because the velocity of the prototype jet is large, the flow is turbulent and the effects of viscosity are small. In this case, changes in the Reynolds number only affect the very smallest scales of the turbulence, which do not interact directly with the secondary flow. According to this principle of asymptotic invariance, the Reynolds number is not a relevant parameter if its value is large. The effects of the primary jet temperature on its density and velocity are compensating, so that this effect can also be neglected. A more complete discussion of ejector scaling may be found in

Reference 5-8. Tests performed at Rockwell International with an exact scale ejector model matched the performance of the full scale ejector. The results of this test are shown in Figure 5-15. Thus, it is felt that by matching the Mach number of the prototype, scale model tests can be used to predict the performance of full size ejectors.

The characteristics of the aft ejectors on both airplanes are summarized in Table 5-3. The measured performance of scale model ejectors having similar geometry is shown in Figure 5-16. The lower curve describes the performance of an ejector which had a hypermixing nozzle without lobes, and the upper curve shows the performance of a nozzle with symmetric lobes on both sides. Since the proposed nozzles have asymmetric lobes, they may be expected to have performance in this range.

TABLE 5-3

EJECTOR CHARACTERISTICS

	BASELINE AFT	ALTERNATE AFT	BASELINE FORWARD	ALTERNATE FORWARD
Inlet Area Ratio	20.5	22.0	14.0	12.5
Length Ratio	1.5	1.5	1.6	1.4
Aspect Ratio	3.6	3.7	2.2	3.6
Augmentation Ratio	1.60	1.56	1.48	1.41

A configuration very similar to the forward ejector on the baseline airplane has been tested at model scale. The measured performance of this ejector is shown in Figure 5-17.

Full scale testing of a longitudinal augmenter similar to the alternate forward augmenter were conducted at NASA Ames for DeHavilland Aircraft.

The early tests of the DeHavilland V/STOL model (References 5-9 and 5-10) with a forward longitudinal augmenter indicated static augmentation ratios of 1.48. The gross thrust augmentation ratio, as defined for the DeHavilland configuration in Reference 5-10, is equal to the measured force (corrected for mass flow and base pressure effects), divided by the measured nozzle force. In the present study augmentation ratio is defined as the measured lift divided by the isentropic gross thrust at the nozzles. In order to provide a common basis for comparison, the data of Reference 5-10 were corrected for door configuration effects and the nozzle thrust coefficients.

The alternate configuration of this study uses fully articulated centerbodies that will develop maximum static augmentation and can also close out the wing nozzle surface to provide efficient wing-borne flight. In addition Coanda nozzles are used in the alternate design to ensure a fully developed augmenter with little or no areas of separation for large exit to inlet area ratios. The length to width ratio of the DeHavilland design (1.7) is somewhat larger than that of the alternate configuration (1.5). The alternate configuration has a larger exit area, so its static augmentation of 1.41 compared to the DeHavilland value of 1.48 should be readily achievable.

The articulated centerbodies of the alternate configuration can be tilted rearward to maximize either STOL lift or acceleration. In the DeHavilland design the fixed nozzles of the forward augmenter were twisted aft 12.5 degrees in order to provide adequate acceleration in the conversion mode (Reference 5-11).

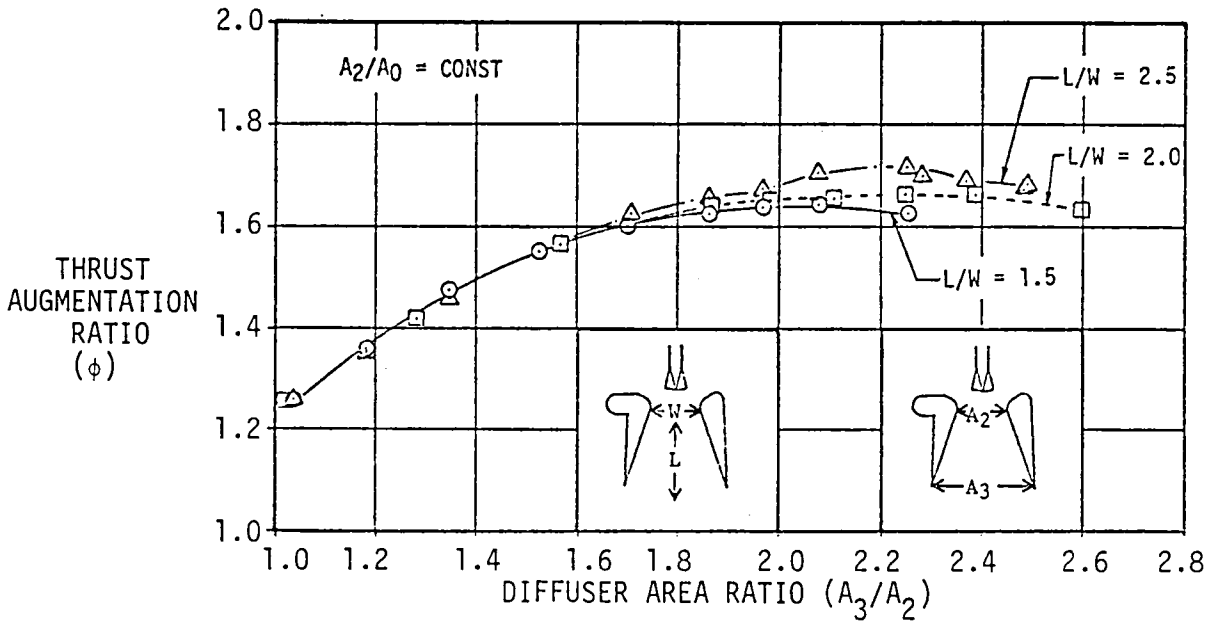

Figure 5-12. Effect of Flap Length and Diffuser Area Ratio on Thrust Augmentation Ratio

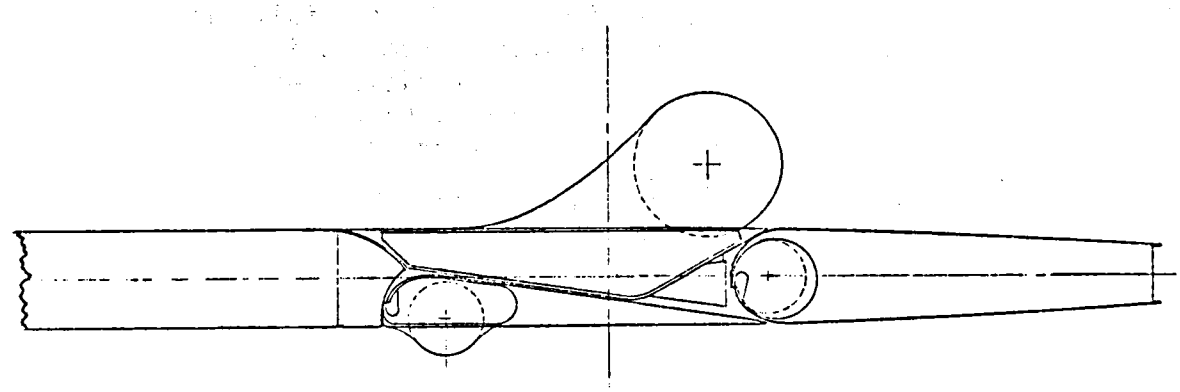

CLOSED

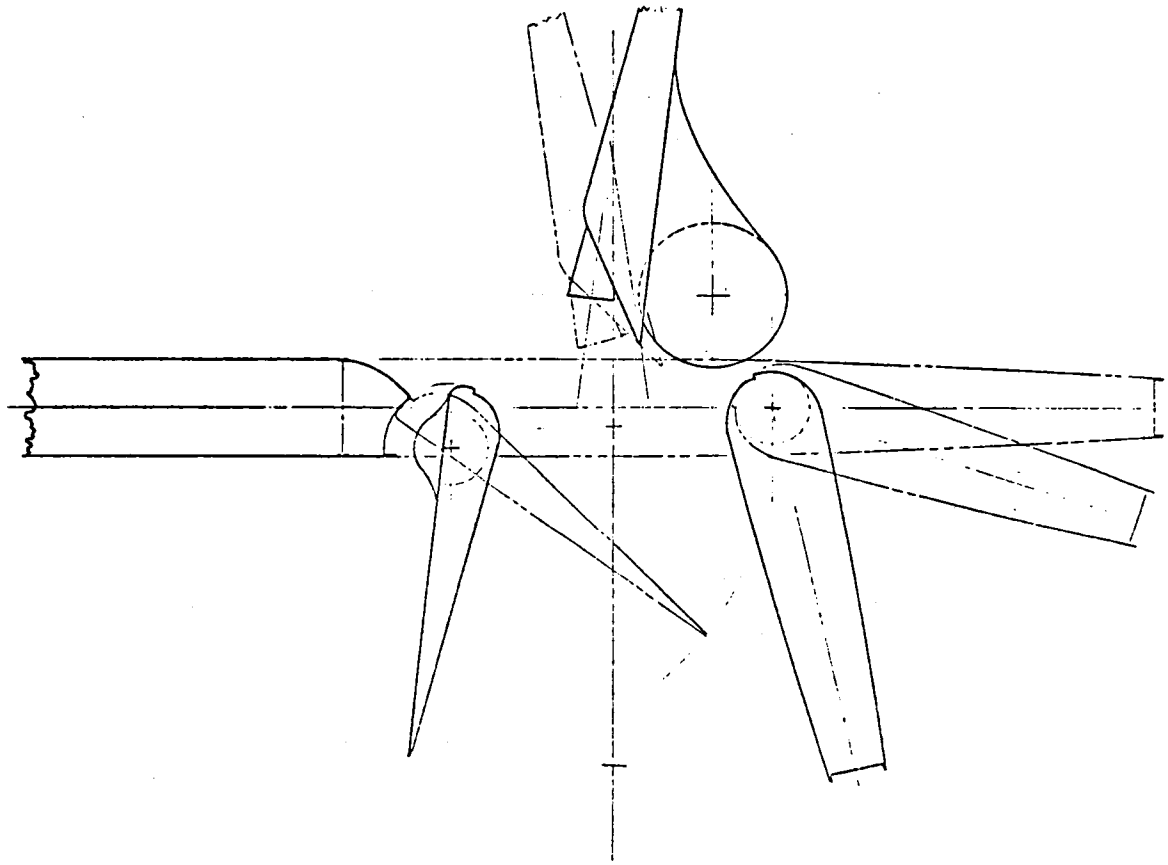

OPEN

Figure 5-13 Baseline Aft Augmenter Cross Section

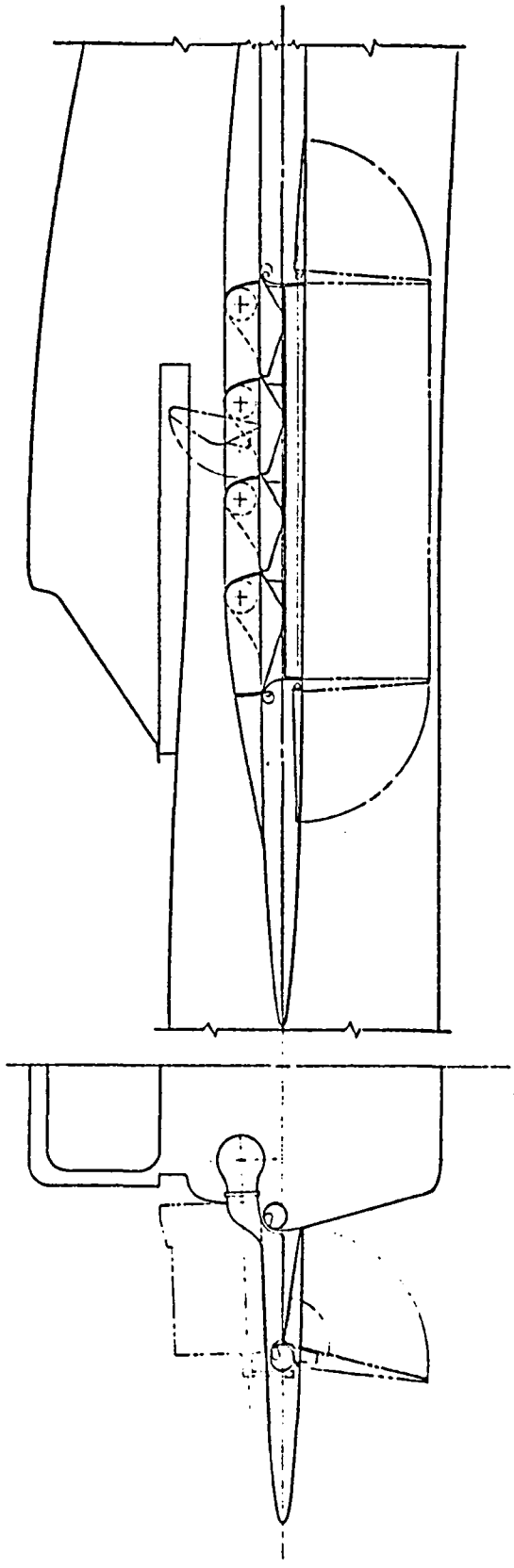

Figure 5-14 Forward Ejector - Alternate Configuration

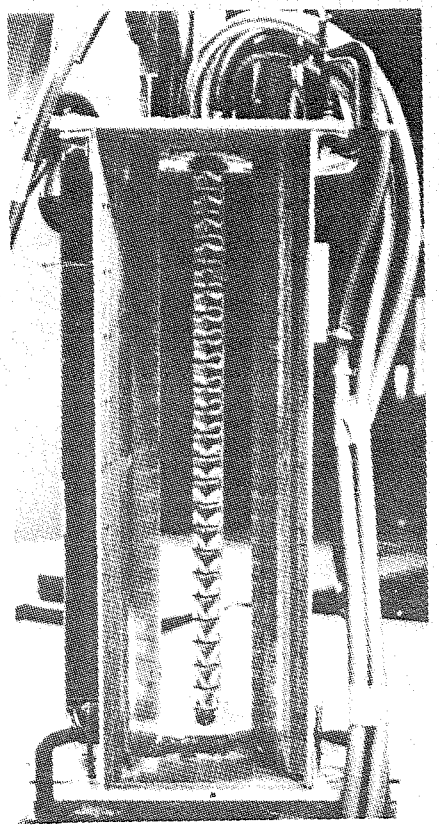

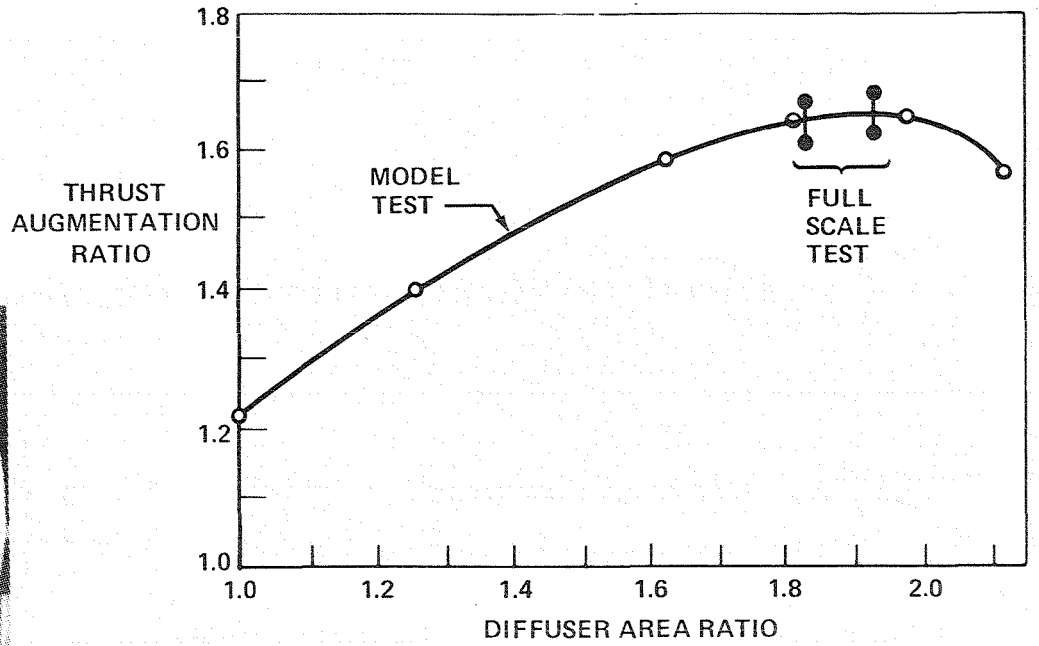

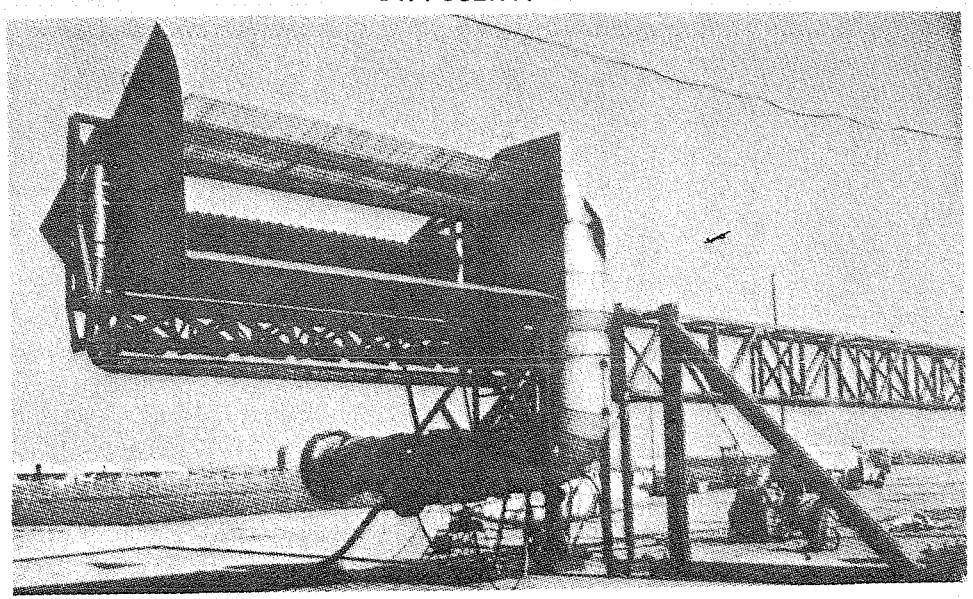

Figure 5-15 Scale and Full Size Ejectors

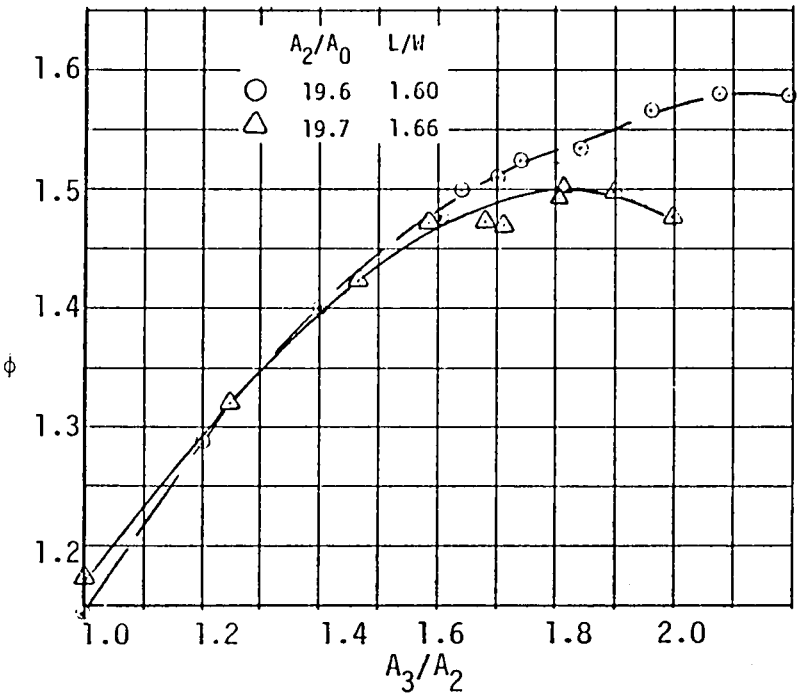

Figure 5-16. Measured Performance of 0.2 Scale Model Aft Ejectors

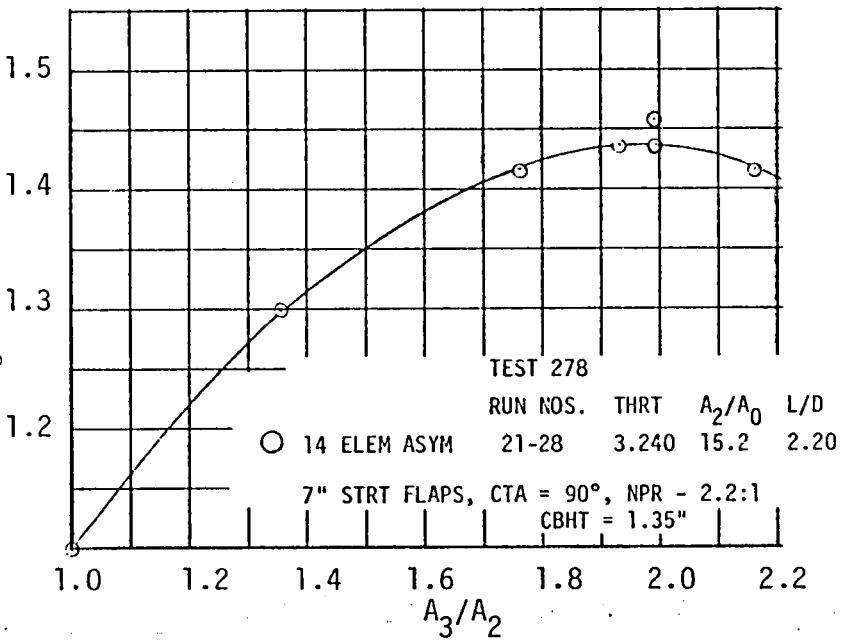

Figure 5-17. 14 Element Asymmetric Centerbody Nozzle Performance

5.7 INSTALLATION FACTORS

The Navy method for bookkeeping installed propulsion system performance is defined by the following equation:

$$NPF = F_G \cos(\alpha + \tau) - F_R - qS_{Ref}(\Delta C_{D_{Sub}} + \Delta C_{D_{AB}})$$

where:

- NPF - Net Propulsive Force
- F_G - Engine gross thrust
- α - Angle of attack
- τ - Longitudinal Thrust Line Inclination
- F_R - Ram Drag
- q - Dynamic Pressure
- S_{Ref} - Reference Wing Area for Aerodynamic Coefficients
- $\Delta C_{D_{Sub}}$ - Incremental Subcritical Inlet Spillage Drag Coefficient
- $\Delta C_{D_{AB}}$ - Incremental Nozzle/Afterbody Drag Coefficient that is a Function of Engine Throttle Position

This method includes all force components independent of engine power setting in the aircraft lift/drag characteristics and all force components which are functions of engine throttle setting and/or induction and exhaust system geometry in the installed propulsion system performance. The propulsion system performance in this report utilizes this equation with the exception of the nozzle/afterbody drag coefficient. The aerodynamic drag bookkeeping stops at the maximum engine exhaust nozzle diameter and the nozzle boatail drags are obtained from the engine computer deck. The NPF equation can be rewritten:

$$NPF = F_G \cos(\alpha + \tau) - F_R - qS_{Ref} C_{D_{Sub}} - F_{AB}$$

where:

F_{AB} - Engine Nozzle Boattail Drag

The terms F_G, F_R, and F_{AB} are obtained from the Pratt and Whitney engine cycle deck CCD 1178 as a function of altitude, Mach number, engine power setting, inlet pressure recovery, bleed, and horsepower extraction. The inlet pressure recovery curve is presented in Figure 5-9. Bleed and horsepower extraction are 50 lb/min. and 71 HP,

respectively. The terms α and τ are assumed to be 0.0; therefore, the cosine function is 1.0.

The theoretical inlet spillage drag is calculated at each flight condition for critical and subcritical operation. The theoretical values are multiplied by a "K" factor to obtain the actual values. The "K" factor is presented in Figure 5-18. The spillage drag at critical operation is included in the aero drag and the difference between critical and subcritical operation is included in the propulsion system performance. There is also an inlet ramp bleed but since it is not a function of engine throttle setting, it is included in the aero drag. Ramp bleed flows are presented in Figure 5-19. The drag coefficients for the inlet spillage drag at critical mass flow ratio and the ramp bleed flows are presented in Figure 4-3. The incremental inlet spillage drag coefficient is presented in Figure 5-20.

5.8 INSTALLED PROPULSION SYSTEM PERFORMANCE

The propulsion system performance is considered proprietary to Pratt and Whitney Aircraft and may be obtained from the engine performance computer deck CCD 1178-00.0 with the installation factors presented in this report.

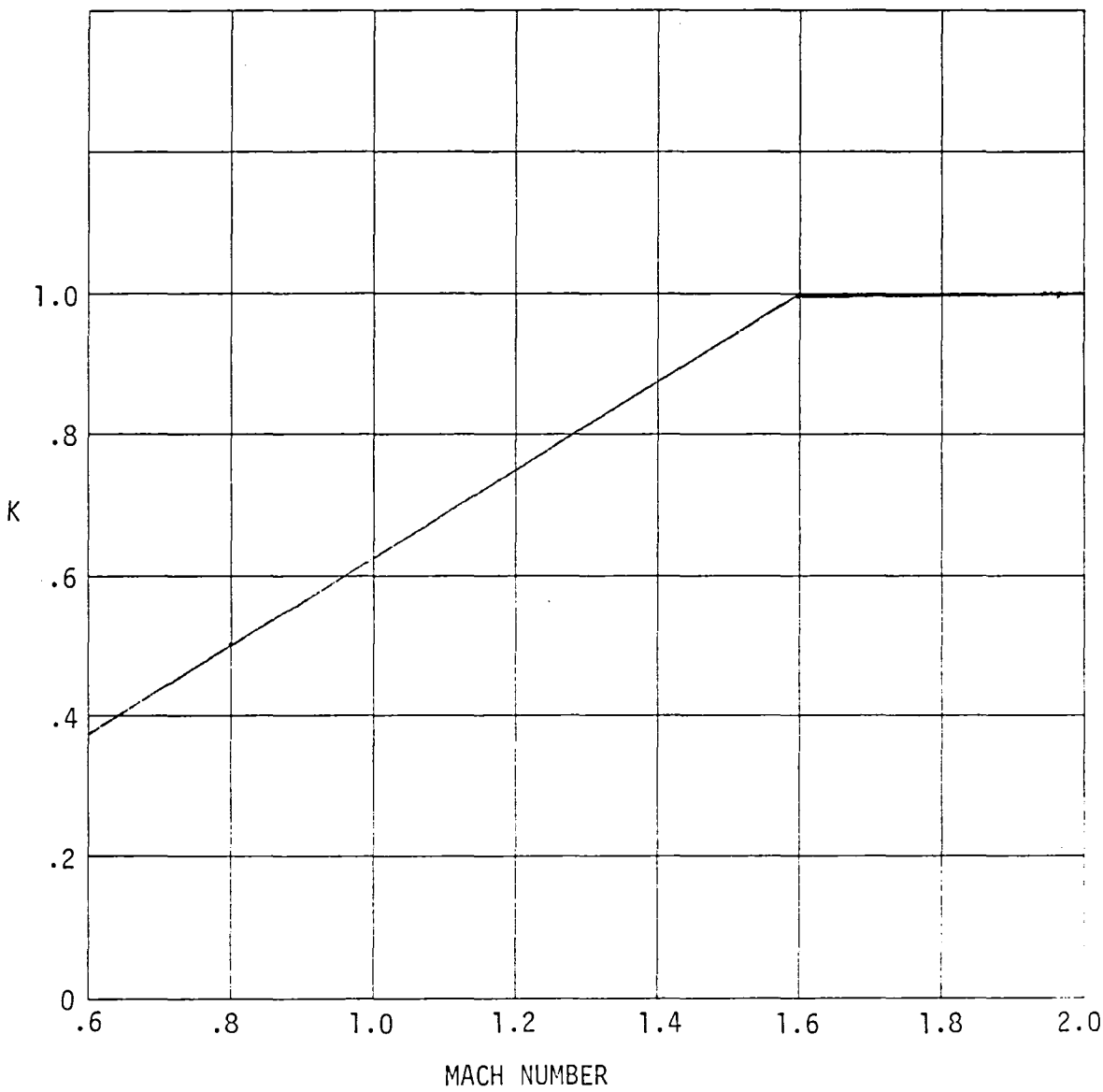

Figure 5-18 Spillage Drag Correction Factor

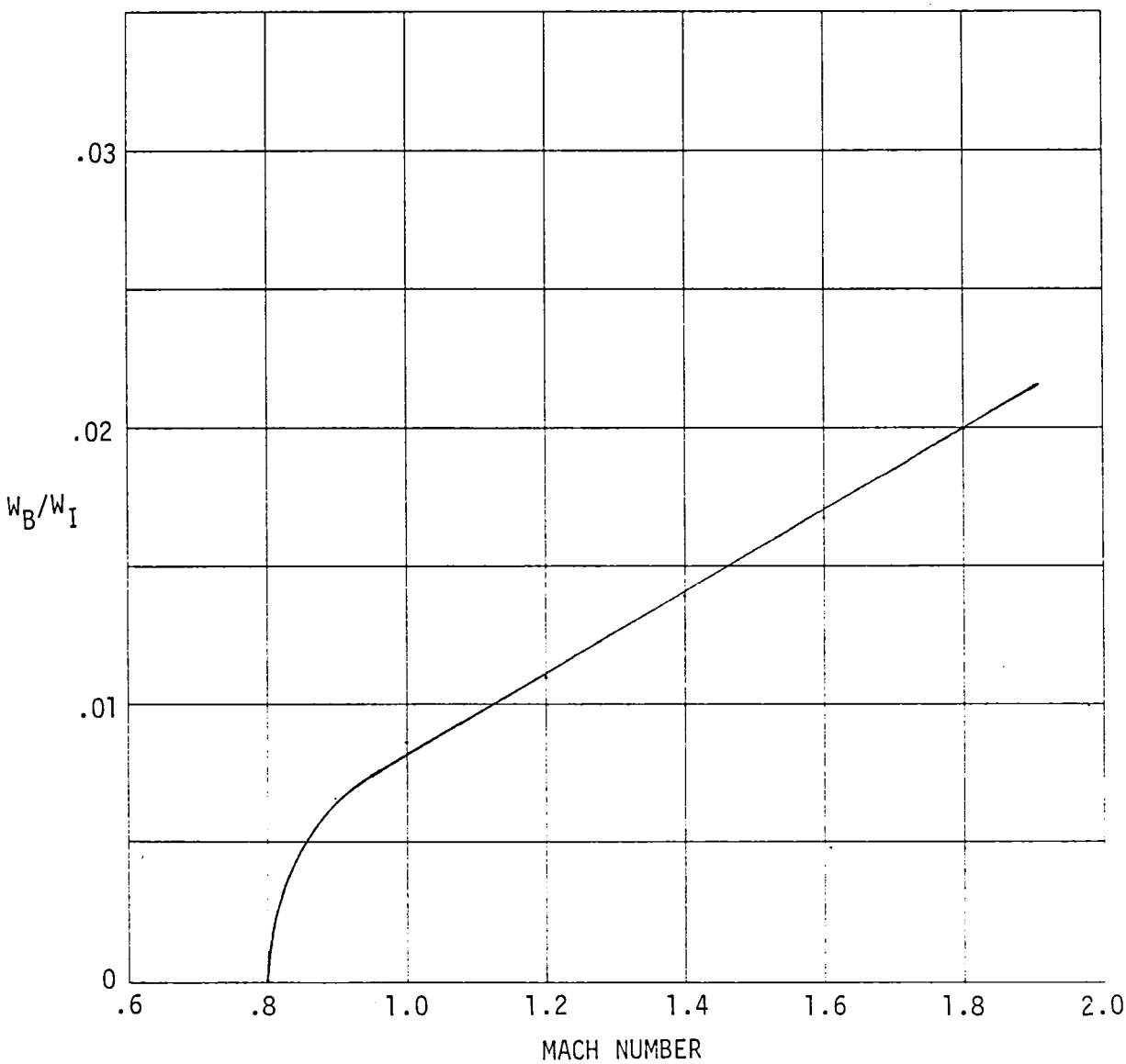

Figure 5-19 Inlet Ramp Bleed Air

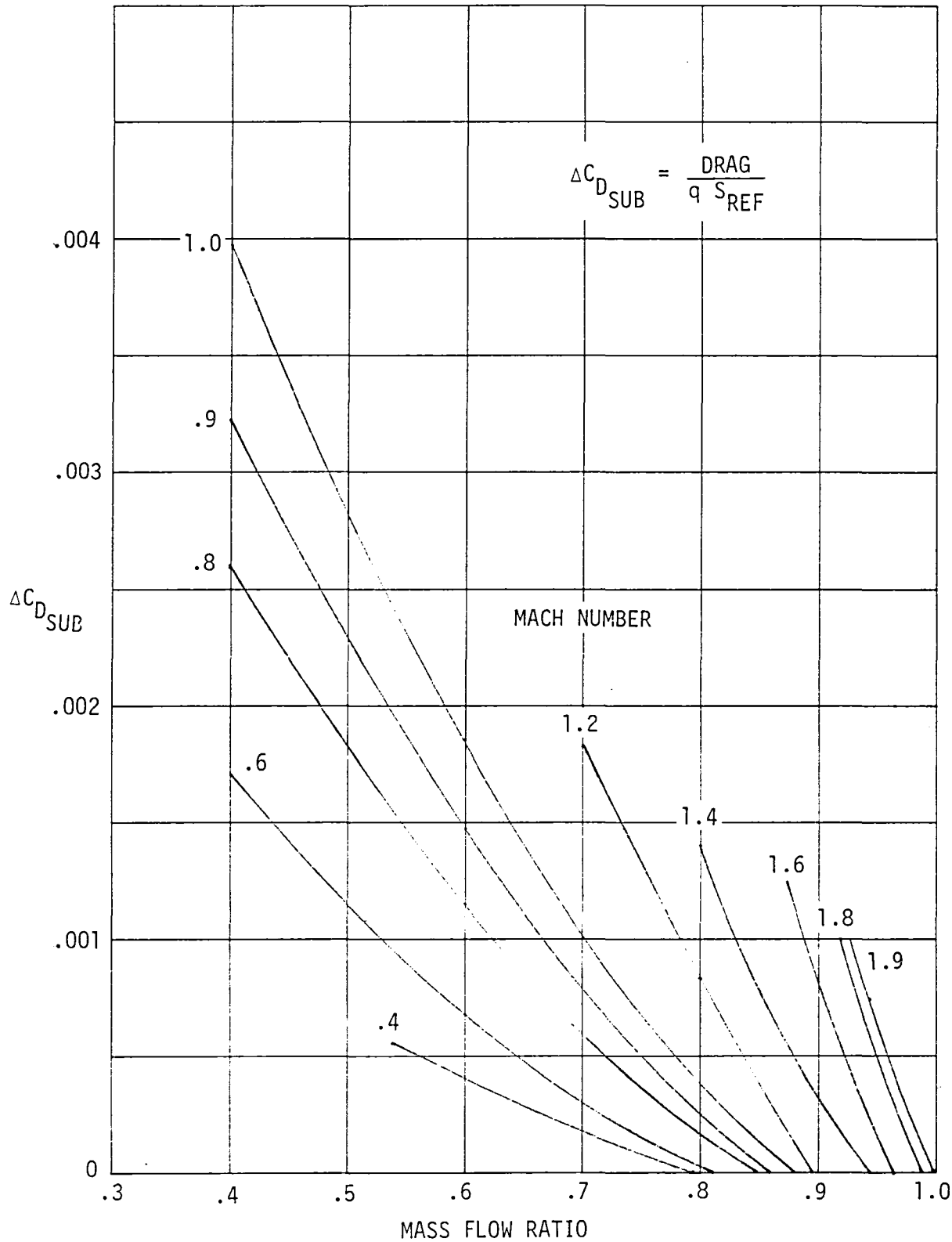

Figure 5-20' Incremental Subcritical Inlet Spillage Drag Coefficient

6.0 AIRCRAFT PERFORMANCE

6.1 BASELINE PERFORMANCE

6.1.1 Combat

The estimated performance was based on the profile and induced drag presented in Section 4.1.1. The combat weight upon which the performance is based is 22,022 pounds, and is defined as .88 x Vertical Takeoff Weight.

The flight envelope for the baseline aircraft with afterburner thrust is presented in Figure 6-1. The lower altitude Mach limit was based on the interceptor maximum design dynamic pressure of 1200 lb/sq ft. The higher altitude operating Mach number limit of 1.9 was established by the simple fixed ramp inlet optimized for flight at 1.6M. Because the aircraft has vertical lift capability, there is no low speed limit shown at the lower altitudes. The higher altitude low speed limit is based on the maximum lift coefficient of Figure 4-15.

Figures 6-2 through 6-4 present the specific excess power as a function of normal load factor ("g"). Curves are presented for maneuvering Mach numbers of .5M, .6M, .9M, 1.2M, and 1.6M for 10,000, 20,000, and 30,000 foot altitudes.

The acceleration characteristics from .8M to 1.6M are presented in Figure 6-5 for an operating altitude of 35,000 feet. The values of time, fuel used and distance covered to reach a given Mach number are shown.

6.1.2 Mission

The design missions are shown on Figure 6-6 for the baseline aircraft and are representative of both the VTO and STO requirements. Figure 6-7 presents a mission breakdown for the STO mission with full internal fuel.

Four subsonic missions are summarized in Figure 6-8. All missions assume a takeoff and landing reserve allowance equal to the design mission. Armament loadings and combat allowances are representative of the mission and are indicated in the summary. A breakdown of mission weights is presented in Section 3.2. The drag increments used for the various loading are presentd in Section 4.1.1.

The Combat Air Patrol mission is a 150 n.mi. radius mission achieved at best cruise altitude and velocity. The loiter on station is performed at best loiter velocity and an altitude of approximately 35,000 feet. Stores have been retained.

The Fighter Escort mission is a long range best cruise mission with final on station combat performed at an altitude of 10,000 feet. Initial and mid-mission climbs are performed at Intermediate Thrust as are all the subsonic mission climbs. Air-to-air missiles are retained.

The Interdiction mission is flown at best cruise altitude and speed with the exception of a 100 n.mi. sea level dash radius prior to combat. The dash Mach number is assumed to be .85M and the short range air-to-surface missiles are released at the target.

The Surface Strike mission is again a maximum radius of operation mission allowing a one hour loiter to be performed at the target. The loiter is flown at the best loiter speed at 20,000 feet altitude and is followed by release of the HARPOON missiles during combat.

6.1.3 Vertical Takeoff and Transition

The VTO lift budget for the baseline aircraft is shown in Figure 6-9. The budget is based on tropical day conditions and includes all duct losses and leakages. The maximum lift shown in the lift budget represents a maximum lift capability with zero control input and no vertical acceleration but is trimmed in pitch with the CG at F.S. 366.0. The lift with simultaneous control, in Figure 6-9, includes the lift reduction due to a control reserve equivalent to achieving the aircraft attitude changes in 1 second of 4 degrees pitch, 6 degrees roll, and 3 degrees yaw. These pitch, roll, and yaw angular values are recommended for use in VTOL aircraft by the U.S. Navy in place of the values currently specified in MIL-F-83300, the V/STOL Flying Qualities Specification. The VTO gross weight shown at the bottom of the lift budget is based on the capability to accelerate vertically with a lift to weight of 1.05, while maintaining the simultaneous control reserve.

The variation of lift capability with center of gravity is presented in Figure 6-10. The data of Figure 6-10 indicate how the lift is optimized for the takeoff CG of F.S 366.0. The slopes showing the reduction in lift as the CG moves forward are due to the forward augmenter and pitch reaction control operating at their maximum capacity and the additional trim being provided by reducing lift on the aft augmenter. The reduction in lift as the CG moves aft is due to the aft augmenter and aft pitch reaction control operating at their maximum capacity while the forward augmenter lift is reduced to provide the additional trim. The low slopes on the truncated portion of each curve reflect the difference in duct loss between the forward and aft pitch reaction control nozzle.

The ability to successfully transition to conventional flight speed is described by the acceleration capability along the flight path at the minimum augmenter mean flap deflection (where thrust diversion is initiated). Figure 6-11 presents the acceleration capability at a 25 degree mean augmenter flap deflection for the VTO takeoff weight. Adequate acceleration exists to perform complete transitions to conventional flight well beyond the minimum conventional flight speed of 1.05 V_{STO}. It is desirable to continue to accelerate to speeds greater than 1.05 V_{STO} in order to minimize the rotation required to achieve the conventional flight angle of attack at low speeds. The acceleration available at the higher speeds shown in Figure 6-11 makes that possible in level flight, and thus does not require diving the aircraft to complete the transition.

A transition is shown in Figure 6-12 initiated from a low speed accelerating condition at 60^{o} of mean flap. The transition was simply performed at a constant pitch angle of 5^{o} at the VTO gross weight. As seen in Figure 6-12 a climb has commenced at the start of mean flap reduction, and the aircraft continually accelerates past the point where the minimum augmenter deflection is reached. Initiation of thrust diversion is possible at any time after the minimum deflection is reached since, as shown in Figure 6-12, the airspeed has exceeded the stall speed (power-off).

It is also noted that the climb occurring after 25 seconds, in Figure 6-12, could be converted to a continued acceleration by pitching over to constant altitude. In that case, the maximum level flight speed would approach 150 KEAS.

6.1.4 Short Takeoff

Short takeoff distances for various length decks are shown in Figure 6-13. For the flat deck STO's it is assumed that the aircraft is rotated to an angle of attack that yields an a/g = .065 after the aircraft leaves the flat deck end. The STO's are all performed at a constant flap deflection.

A ski-jump takeoff point is also shown in Figure 6-13 with 20 knots wind-over-deck and a 20° ramp angle. The ski-jump deck run consts of a level deck section, a circular arc section and a short straight ramp section as shown in Figure 6-14. The horizontal distance used for the complete ski-jump was maintained at 400 feet.

The criteria employed for a ski-jump STO is the minimum rate-of-climb to be not less than zero. This criteria is suggested in Reference 6-1 and is considered a reasonable one. It is noted that a difference exists in the criteria for the ski-jump STO and the flat-deck STO's. The flat-deck STO require a rotation once off the deck to increase the lift. The rotation must be started and stopped at the proper angle of attack (at each weight) at the a/g = .065 point. Therefore, some altitude loss is assumed until the aircraft has reached the proper angle of attack and can convert the a/g to a climb or airspeed increase. This type of procedure is, of course, similar to conventional aircraft catapult takeoffs. If a no-sink (zero minimum rate-of-climb) criteria were applied to the flat deck STO's then the comparison between the curves of Figure 6-12 and the ski-jump would show a greater spread. It must be kept in mind, also, that a significant altitude increase occurs at the zero rate-of-climb condition for the ski jump STO. This is a bonus for takeoffs using the ski-jump technique.

A time history is shown in Figure 6-15 for a ski-jump takeoff. The ski-jump takeoff is performed in Figure 6-15 at a constant pitch angle off the end of the ramp which is a simple control task for the pilot An augmenter mean flap angle of 25 degrees was utilized for the baseline aircraft ski-jump STO since for the constraint of a 400 foot total takeoff distance this flap angle provided the required lift and drag characteristics for the airspeeds occurring at the ramp end.

The ramp angle of 20° used in the data of Figure 6-15 is considered a maximum practical value based on Reference 6-1. Figure 6-16 presents the takeoff weight variation with ramp angle for the baseline aircraft using a constant 400 foot deck length and the aforementioned criteria. Under the above conditions, it is apparent that 20° provides the best capability. However, under a different set of conditions, a lower ramp angle might be optimum.

At all gross weights equal or less than the VTO takeoff weight the aircraft can be landed vertically. Since the maximum landing design gross weight is less than the VTO takeoff weight, all landings can be made in the VTO mode. Landings in the conventional configuration are estimated to be similar to aircraft of the same weight range (without reverse thrust). An approach speed of 1.15 V_S = 112 KEAS results at the VTO takeoff weight.

6.1.5 Sensitivities

Mission sensitivities for the VTO mission are presented in Figure 6-17 and for the STO mission in Figure 6-18.

The empty weight variation for the VTO mission assumes a variation of fuel weight with the takeoff weight remaining constant. The empty weight variation affects a 63 n.mi. radius change per 1000 pounds weight change. A friction drag variation changes both the subsonic and supersonic phase of the DLI mission. A change of 20 drag counts (ΔC_D = .0020) changes the radius capability by 18 n.mi. A wave drag variation of 20 drag counts changes the mission radius by 12 n.mi.

Two weight variations are presented for the STO mission, Figure 6-18. The empty weight change affects only the weight at which the mission is flown and not the total fuel available. This results in a change of only 12 n.mi. per 1000 pounds of empty weight. If the fuel capacity is changed, the change per 1000 pounds of fuel is 48 n.mi. A 20 drag count change in the friction or wave drag affects the total radius of the STO missions by 32, or 24 n.mi, respectively.

The sensitivity of induced drag can best be reflected by the sensitivity of the sustained load factor as a function of speed. Figure 6-19 presents the sustained load factor for afterburning thrust at an altitude of 10,000 feet and the effect of a 20 percent increase in induced drag.

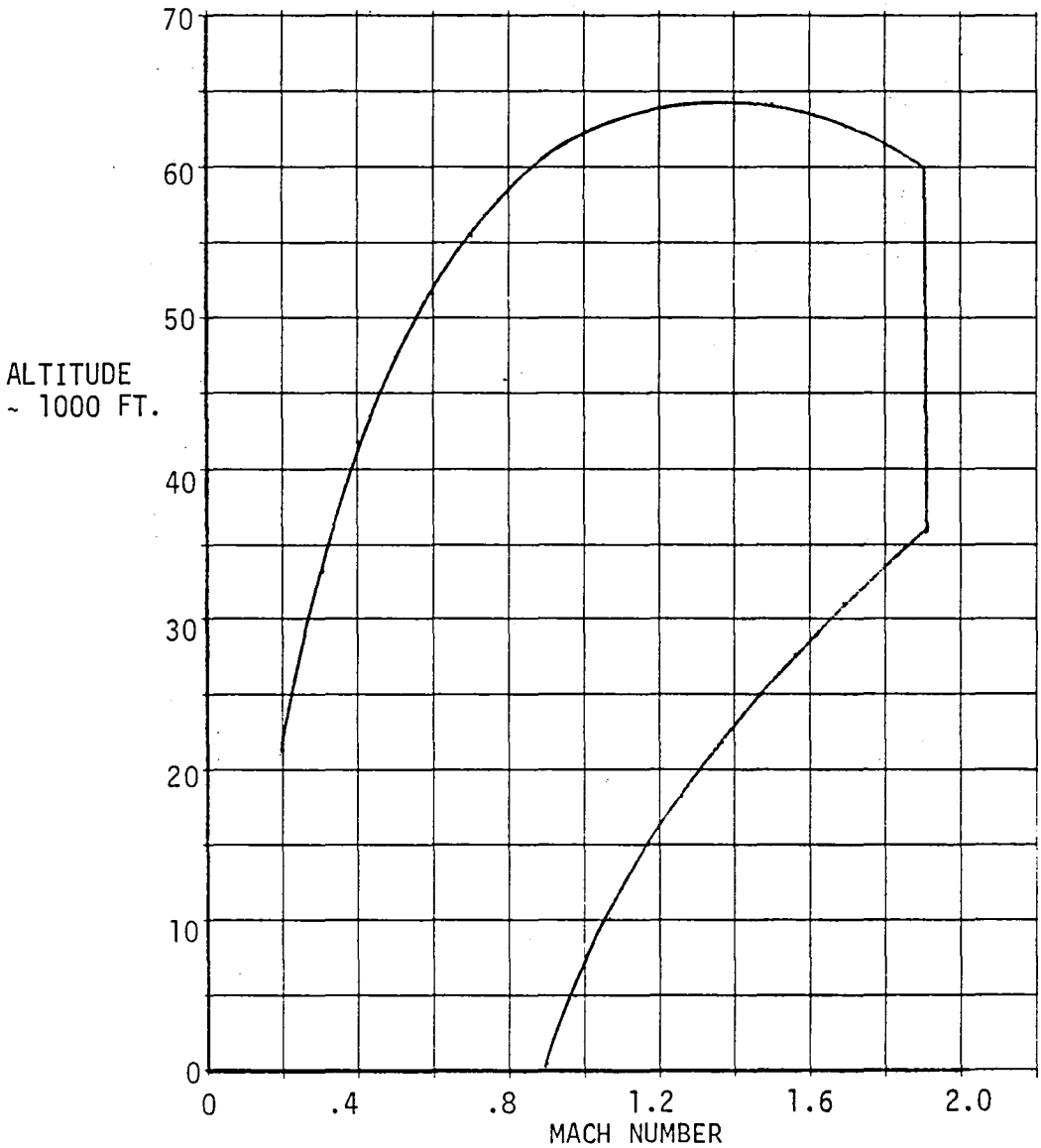

Figure 6-1 Baseline Speed-Altitude Flight Envelope

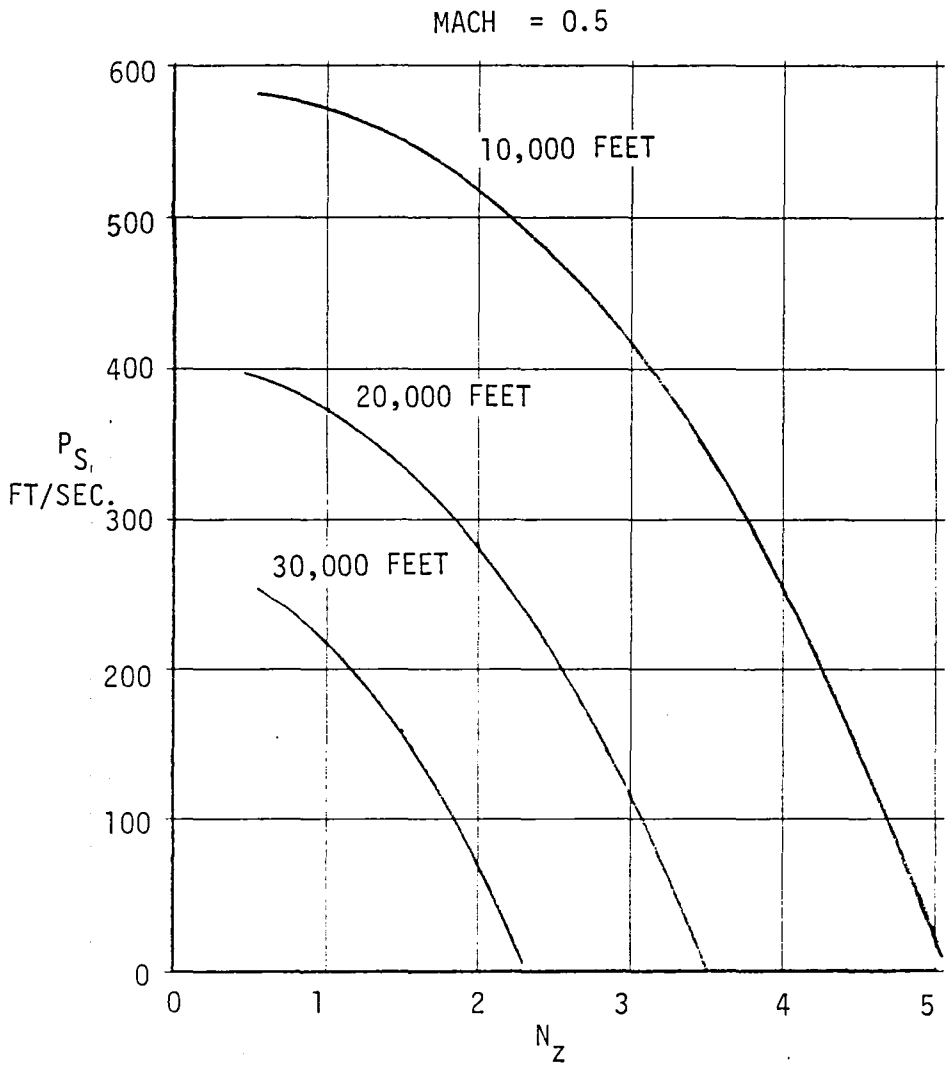

Figure 6-2 Baseline Specific Excess Power

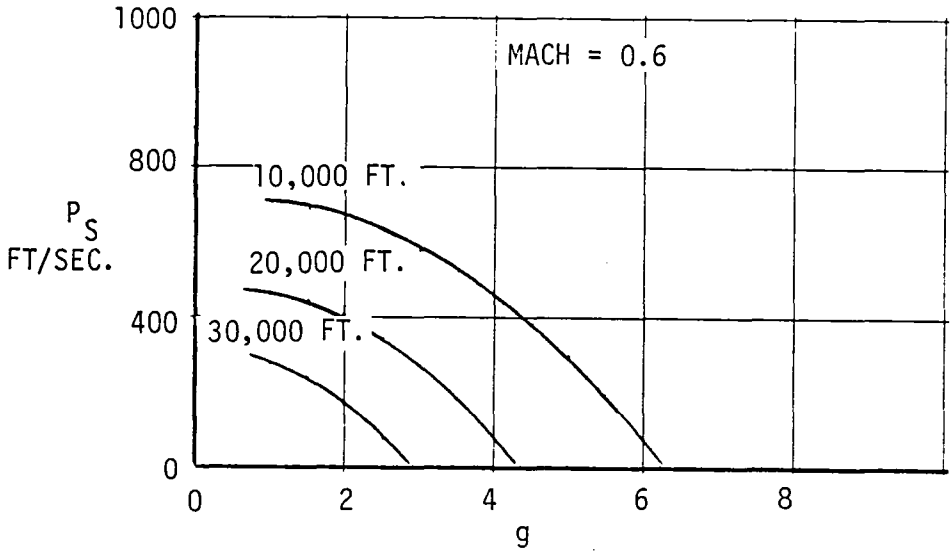

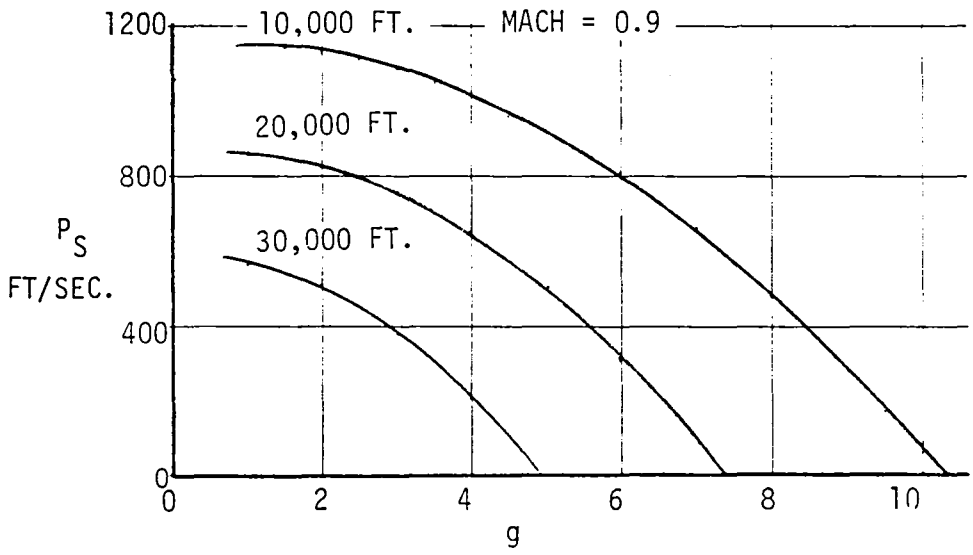

Figure 6-3 Baseline Specific Excess Power

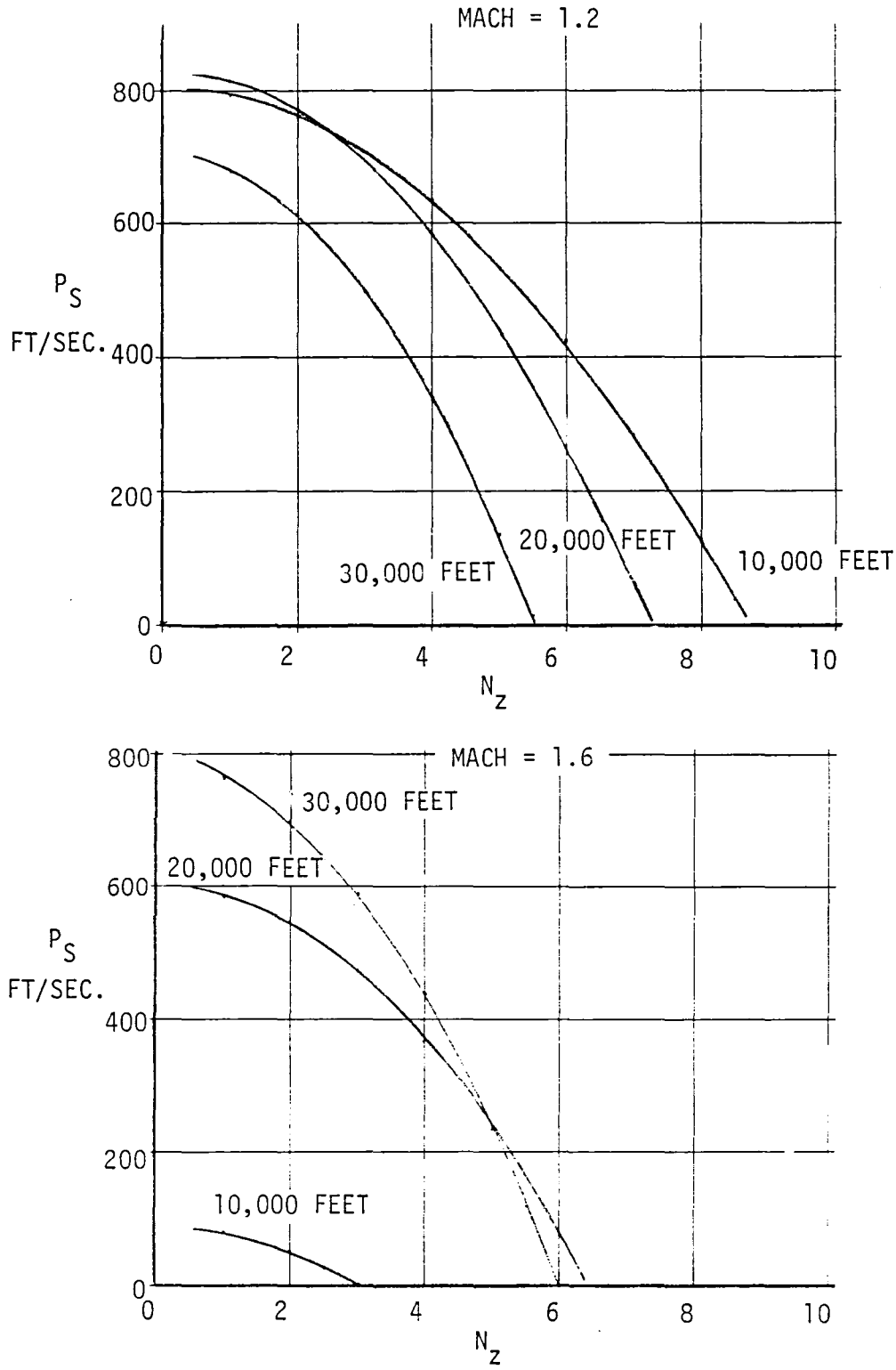

Figure 6-4 Baseline Specific Excess Power

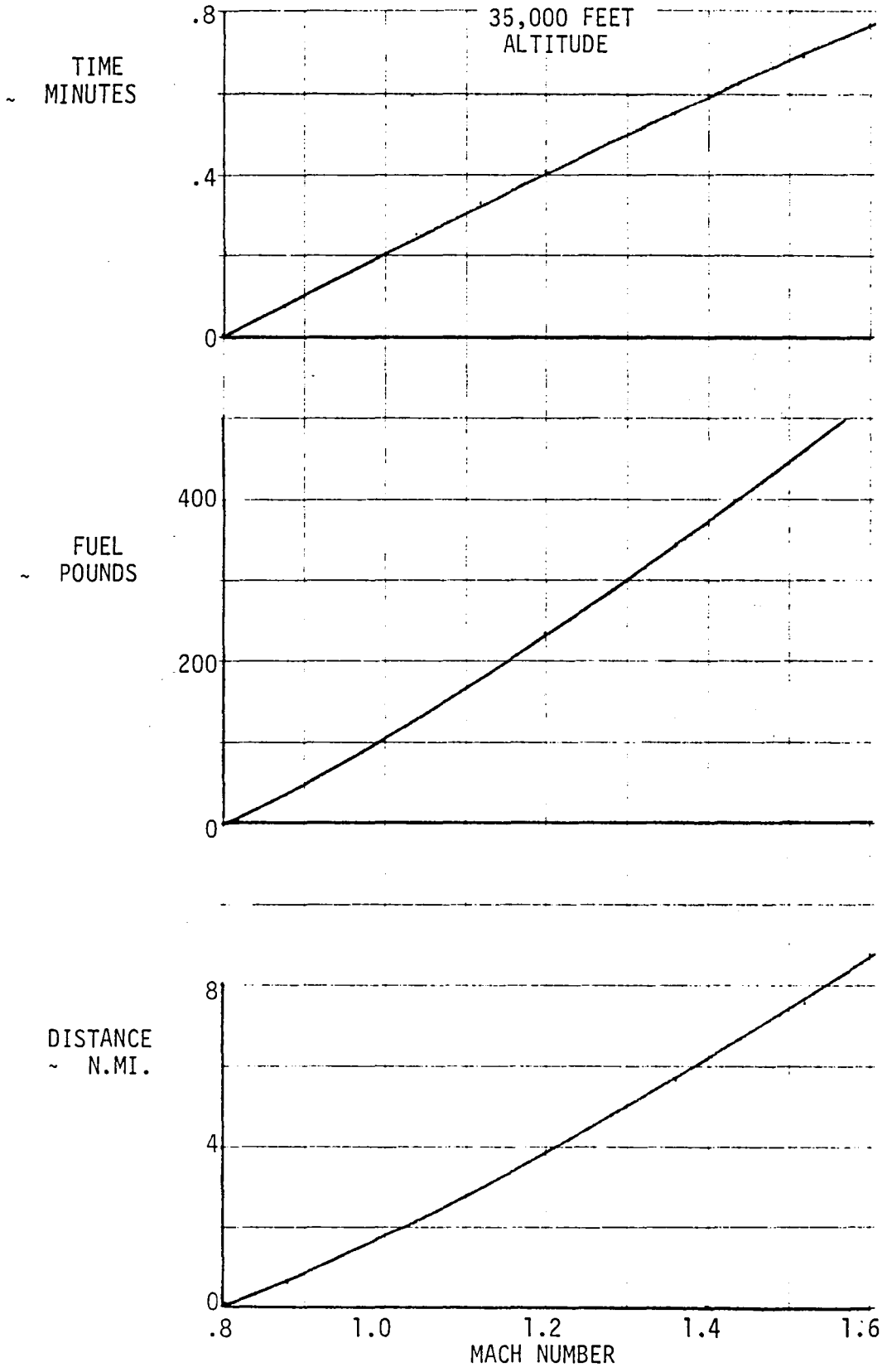

Figure 6-5 Baseline Supersonic Acceleration

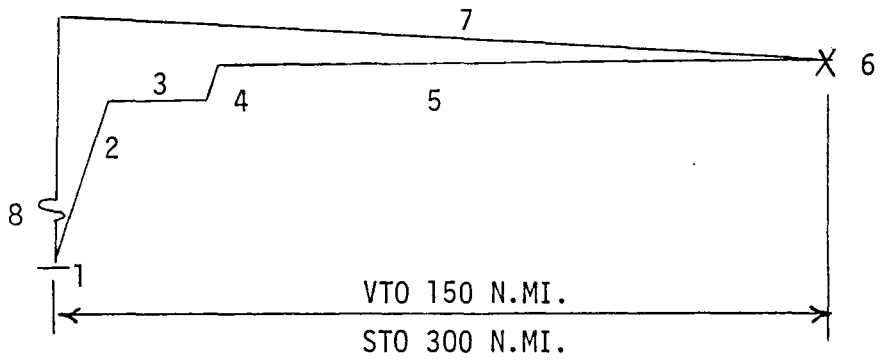

1. WARMUP, TAKEOFF, AND ACCELERATE TO CLIMB SPEED 4 MIN. IDLE PLUS 1.25 MIN. INTERMEDIATE
2. CLIMB TO 40,000 FT. MAX A/B
3. ACCEL. TO 1.6 MACH NUMBER @ 40,000 FT.
4. CLIMB @ 1.6 MACH TO 50,000 FT.
5. CRUISE @ 1.6 MACH @ 50,000 FT.
6. COMBAT 2 MIN. @ 1.6 MACH @ MAX A/B
7. CRUISE BACK TO BASE @ BEST CRUISE ALTITUDE AND VELOCITY (BCAV)
8. LANDING RESERVE (5% INITIAL FUEL + 10 MIN. LOITER AT SEA LEVEL)

Figure 6-6 Deck Launched Intercept Mission Profile

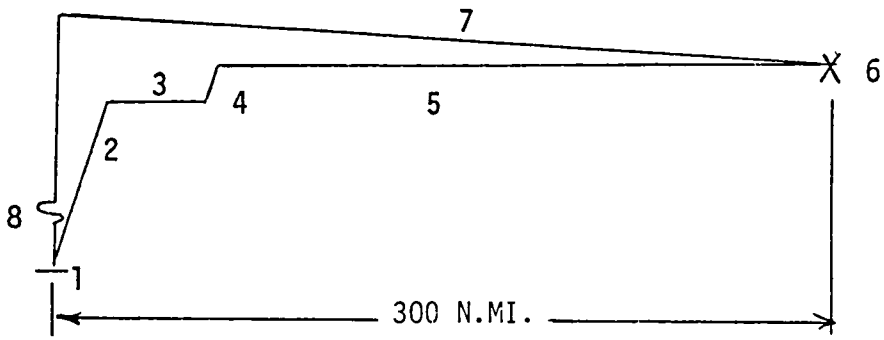

OPERATION	A/C WEIGHT LBS.	FUEL LBS.	DIST. N.MI.	TIME HRS.
1. WARMUP - TAKEOFF	29,598	413	0	.088
2. CLIMB TO 40,000 FT.	29,185	956	11	.020
3. ACCELERATE	28,229	731	16	.023
4. SUPERSONIC CLIMB	27,498	290	8	.008
5. SUPERSONIC CRUISE	27,208	3,417	265	.287
6. COMBAT	23,791	840	0	.033
7. RETURN CRUISE	22,951	1,366	300	.585
8. LANDING RESERVE	21,585	887	0	.167
	20,698			
TOTAL		8,900	600	1.21

Figure 6-7 STO DLI Mission Breakdown

COMBAT AIR PATROL

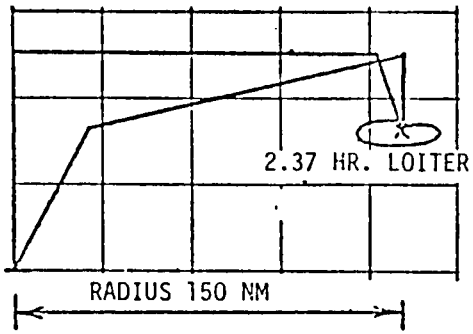

TOGW: 32,942 LBS.
FUEL:
INT: 8,900 LBS.
EXT: 2,720 LBS.
CMBT: 2 MIN - 1.5M - 35K A/B
ARMS: 4-AIAAM

FIGHTER ESCORT

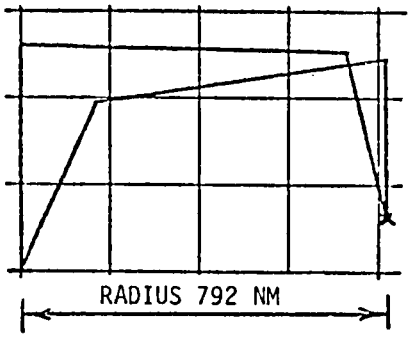

TOGW: 32,322 LBS.
FUEL:
INT: 8,900 LBS.
EXT: 2,720 LBS.
CMBT: 2 MIN. - 1.0M - 10K INT.
ARMS: 2-SRAAM
4-MRAAM

INTERDICTION MISSION

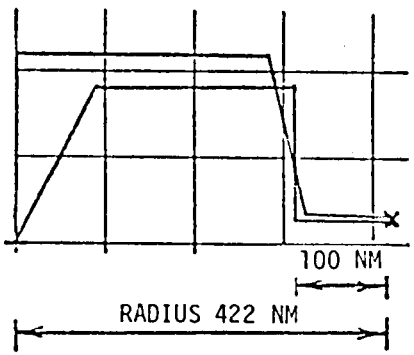

TOGW: 35,122 LBS.
FUEL:
INT. 8,900 LBS.
EXT. 2,720 LBS.
CMBT: 5 MIN. - .85M - SL INT.
ARMS: 2-SRAAM
4-SRASM

SURFACE STRIKE

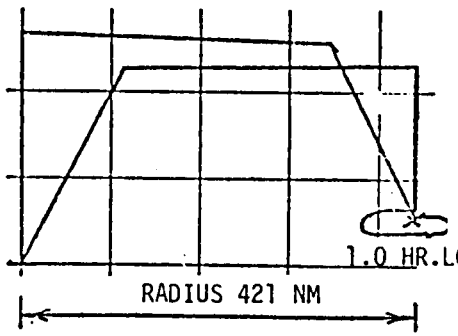

TOGW: 31,772 LBS.
FUEL:
INT: 8,900 LBS.
EXT: 1,360 LBS.
CMBT: 5 MIN. - .8M - 20K INT.
ARMS: 2-SRAAM
2-HARPOON

Figure 6-8 Baseline Subsonic Mission Capability

VTO LIFT BUDGET

ISENTROPIC GROSS THRUST	20,000 LBS.
LEAKAGE	400 LBS.
ISENTROPIC GROSS THRUST TO AUGMENTERS	19,600 LBS.
ISENTROPIC THRUST TO FORWARD AUGMENTER	9,800 LBS.
DUCT LOSSES	893 LBS.
FORWARD AUGMENTER NOZZLE ISENTROPIC THRUST	8,907 LBS.
FORWARD AUGMENTER LIFT (ϕ = 1.475)	13,138 LBS.
ISENTROPIC THRUST TO AFT AUGMENTER	8,232 LBS.
DUCT LOSSES AND LEAKAGE	388 LBS.
AFT AUGMENTER NOZZLE ISENTROPIC THRUST	7,844 LBS.
AFT AUGMENTER LIFT (ϕ = 1.595)	12,511 LBS.
ISENTROPIC THRUST TO PITCH REACTION CONTROL	1,568 LBS.
DUCT AND NOZZLE LOSSES AND LEAKAGE	108 LBS.
PITCH REACTION CONTROL NOZZLE ISENTROPIC THRUST	1,460 LBS.
MAXIMUM LIFT	27,109 LBS.
LIFT WITH SIMULTANEOUS CONTROL (4° θ, 6° ϕ, 3° ψ)	26,276 LBS.
VTO GROSS WEIGHT	25,025 LBS.

Figure 6-9 Baseline Aircraft Lift Budget - Tropical Day

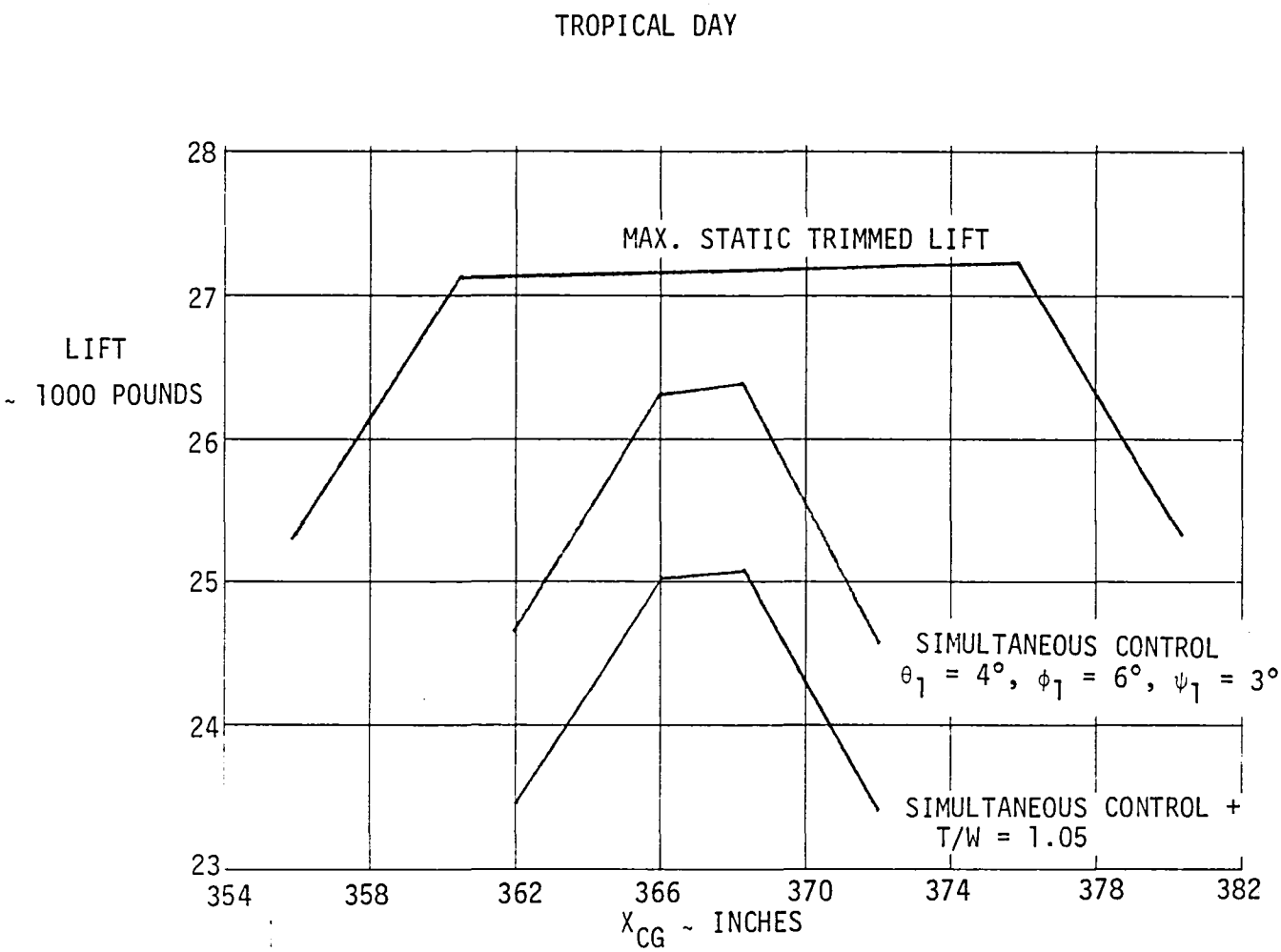

Figure 6-10 Baseline Aircraft - Vertical Lift Capability

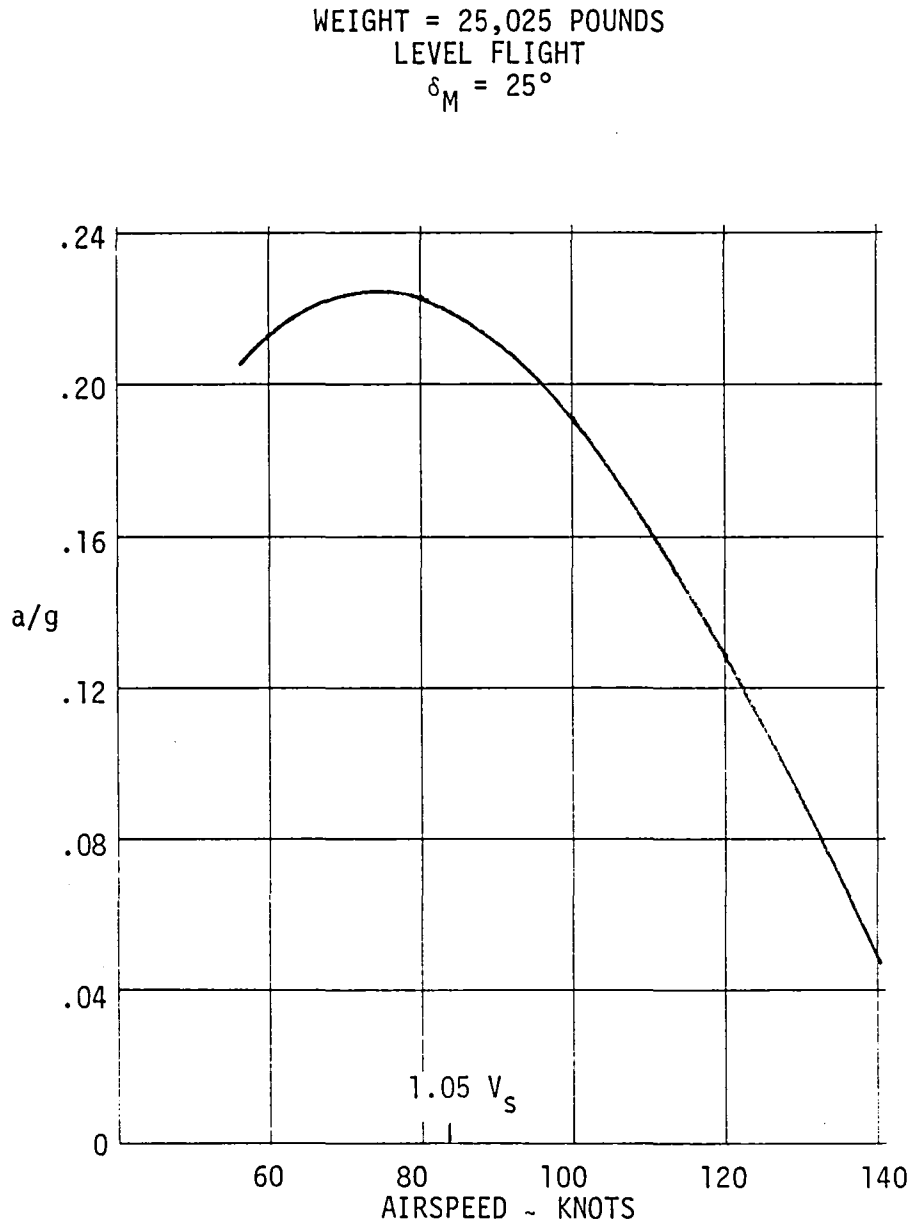

Figure 6-11 Baseline Aircraft Acceleration

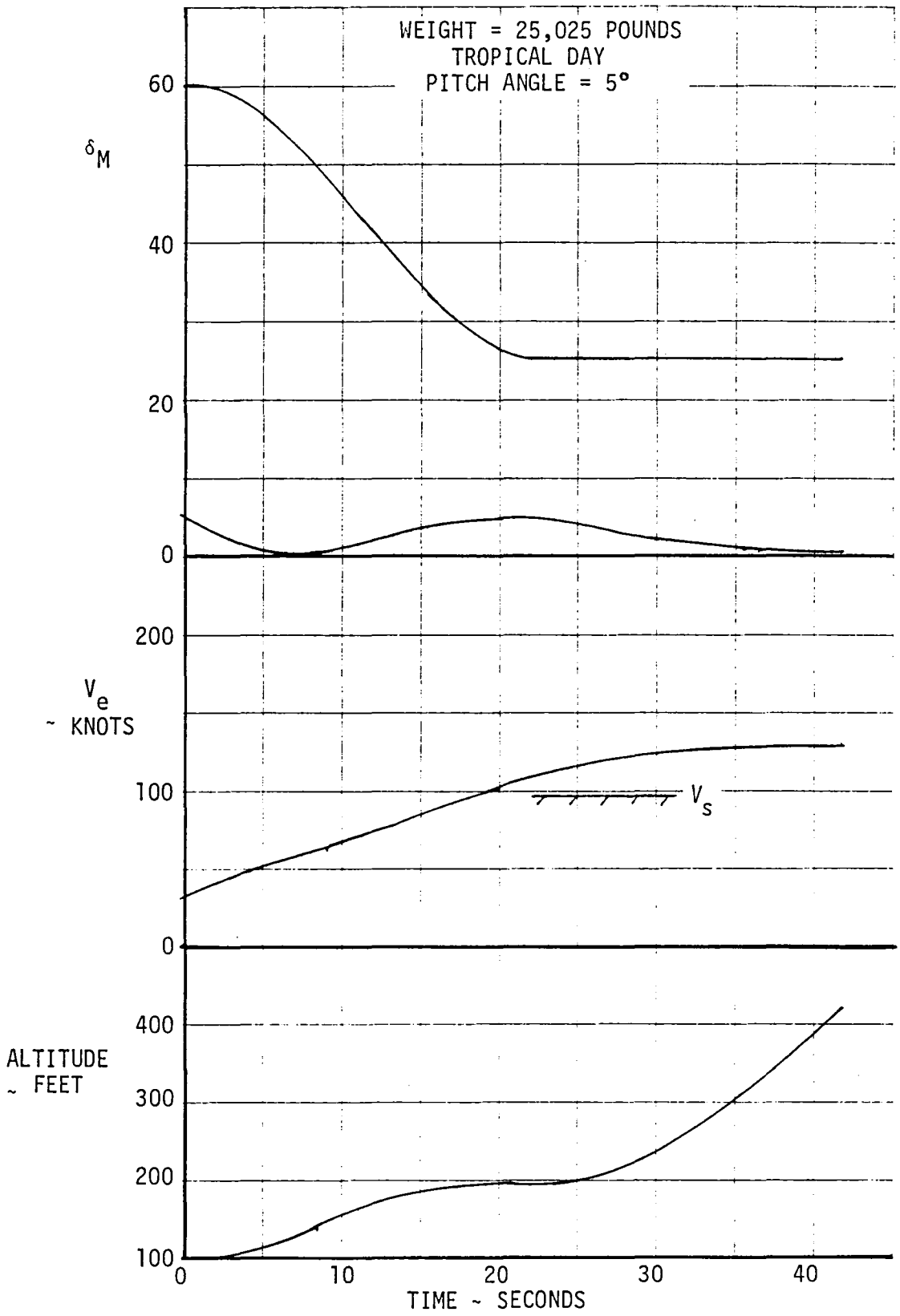

Figure 6-12 Baseline Aircraft Transition

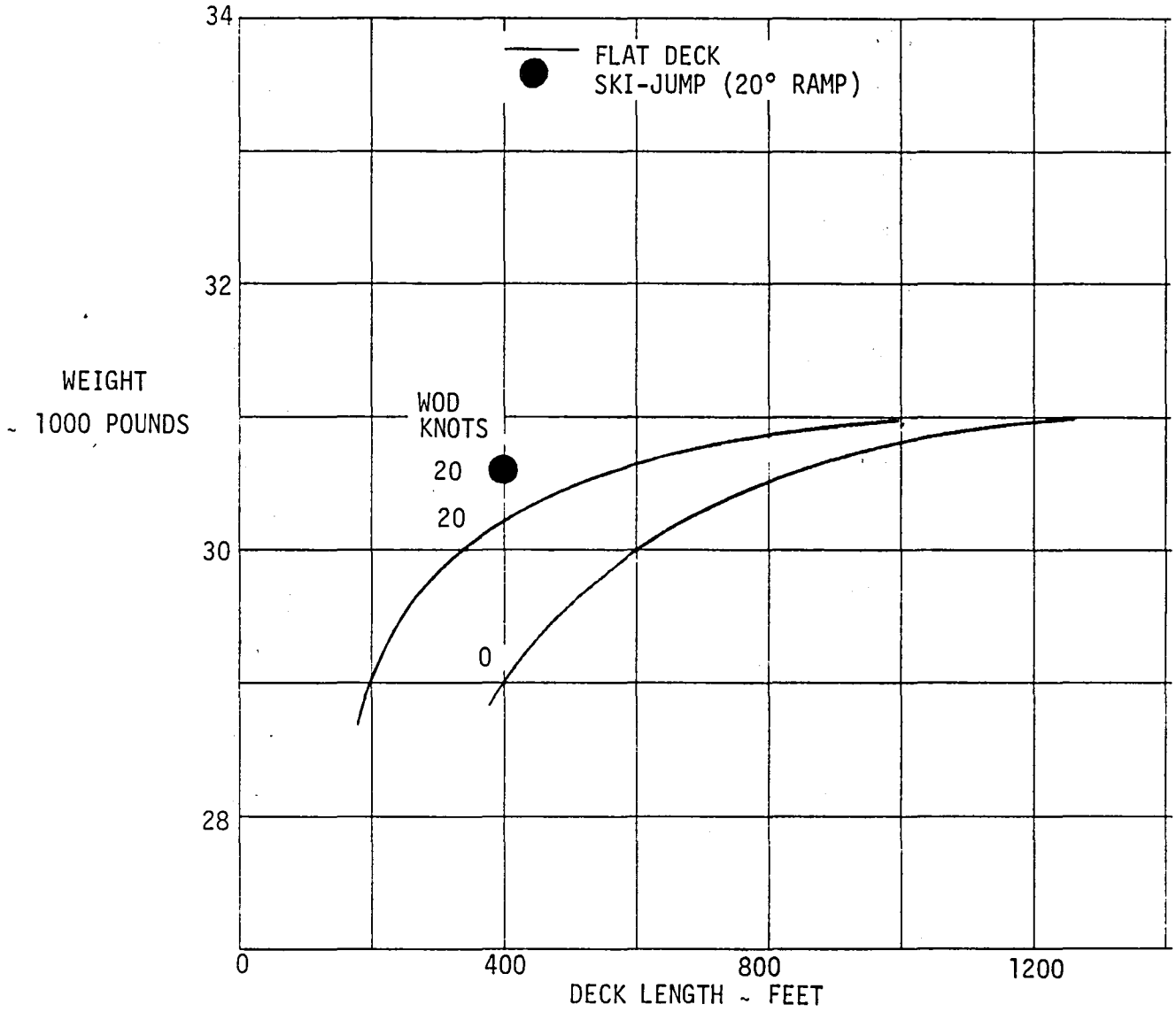

Figure 6-13 Takeoff Distance versus Deck Length for Baseline Configuration

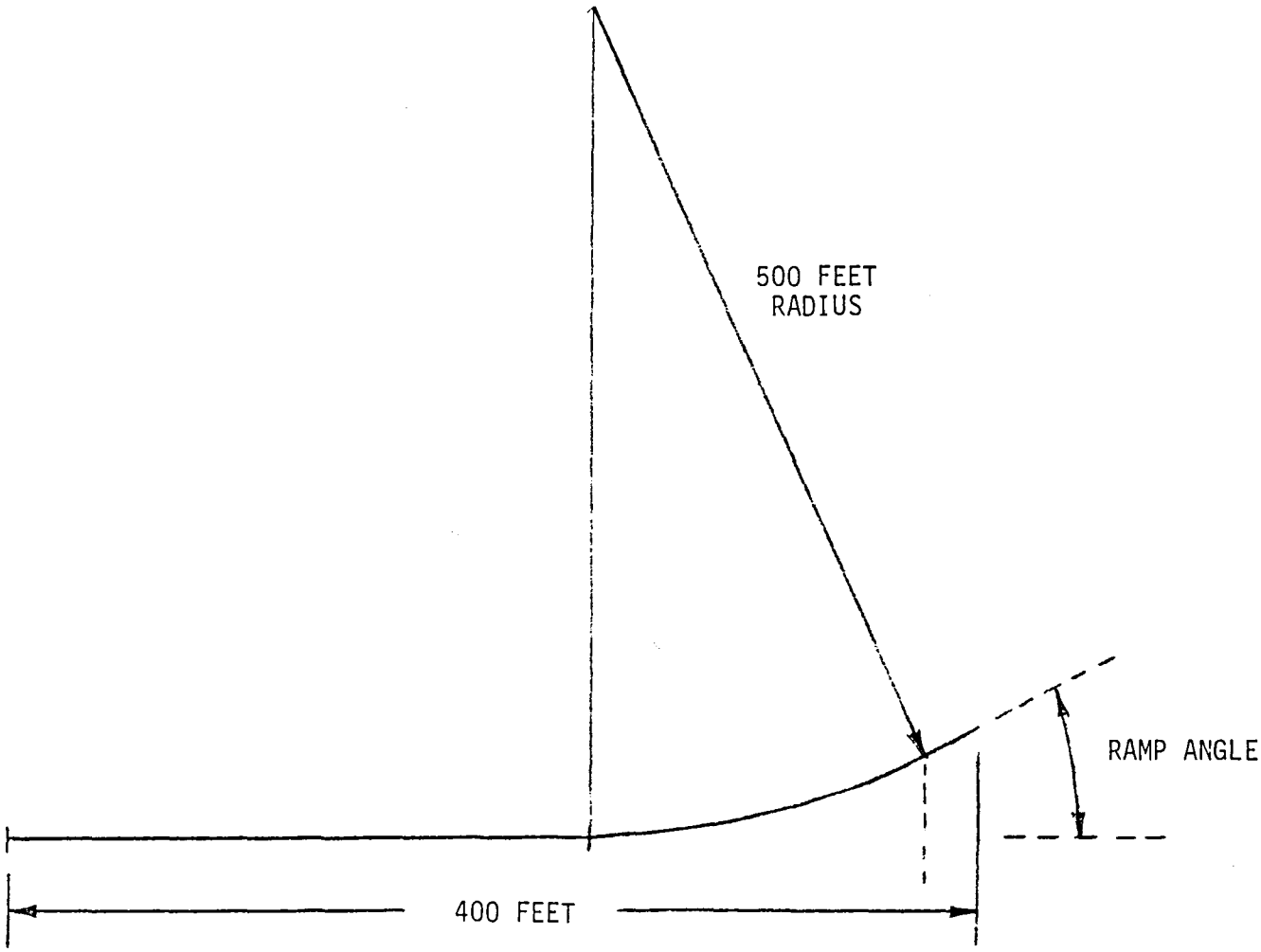

Figure 6-14 Ski-Jump Geometry

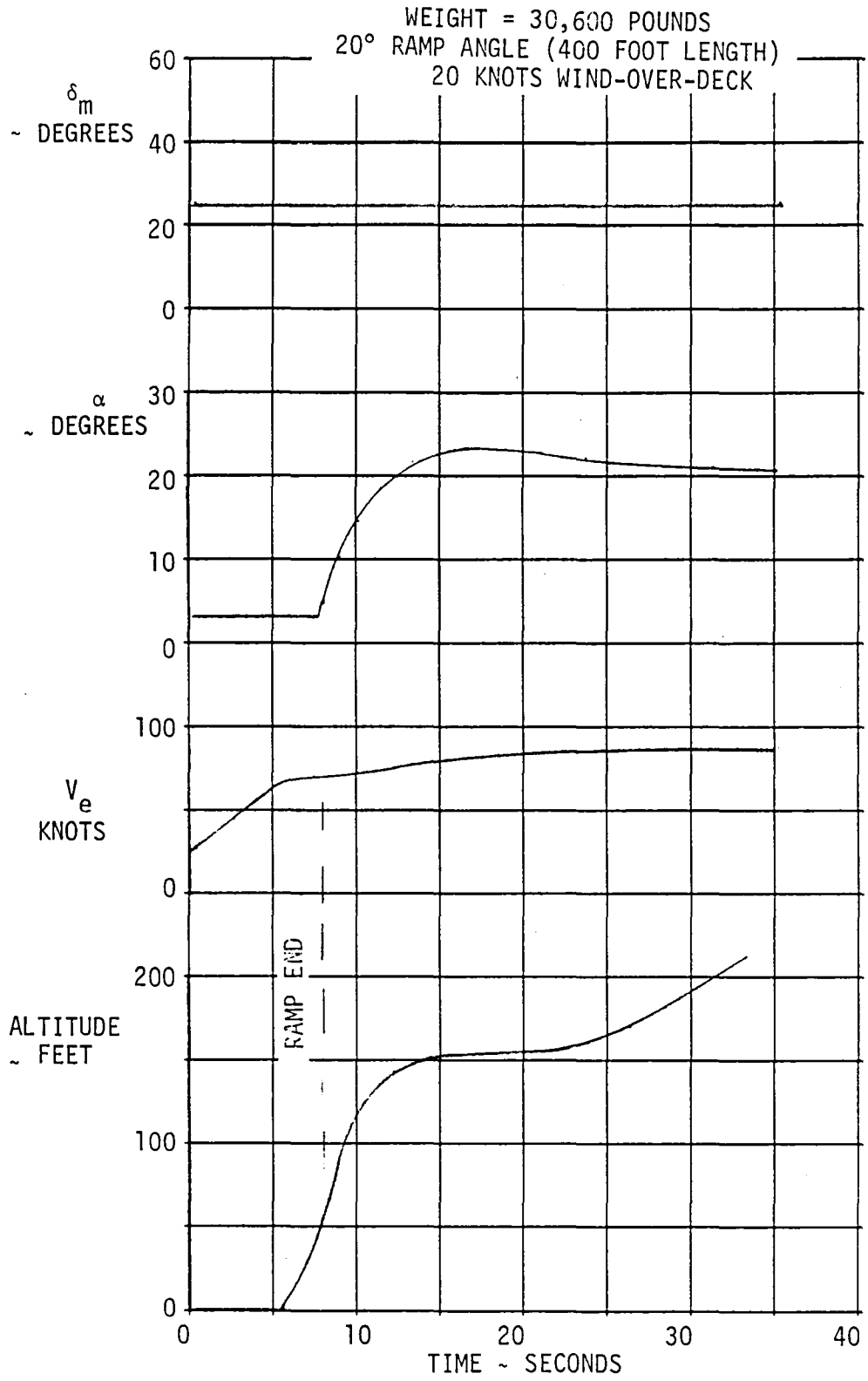

Figure 6-15 Ski-Jump Takeoff for Baseline Configuration

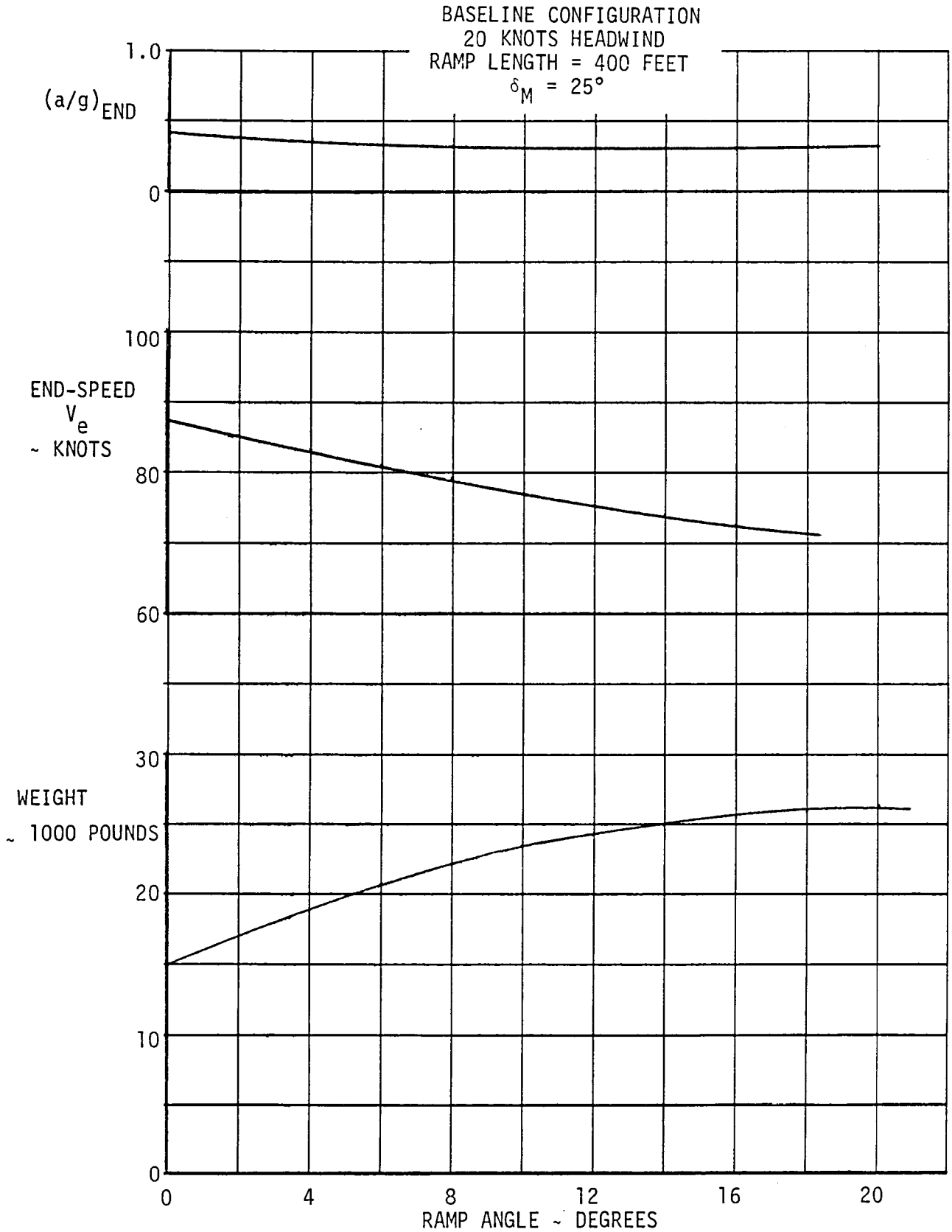

Figure 6-16 Ski-Jump Takeoff Variation with Ramp Angle

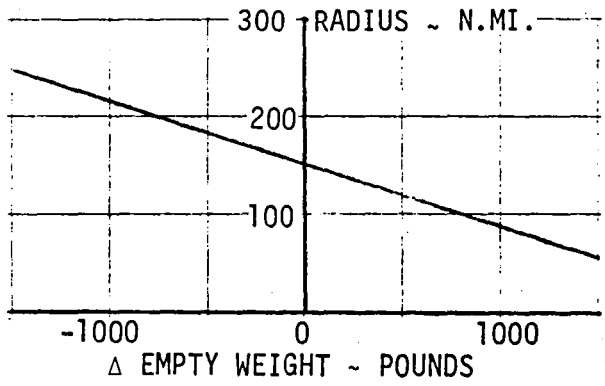

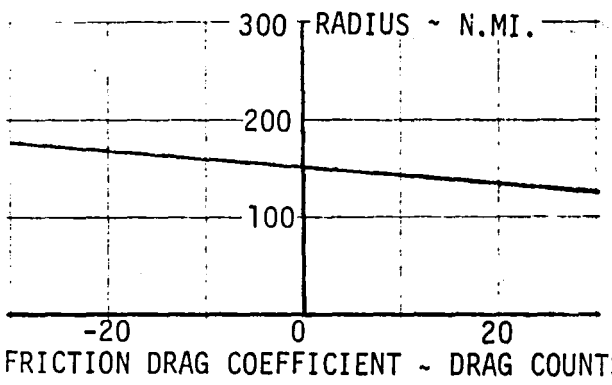

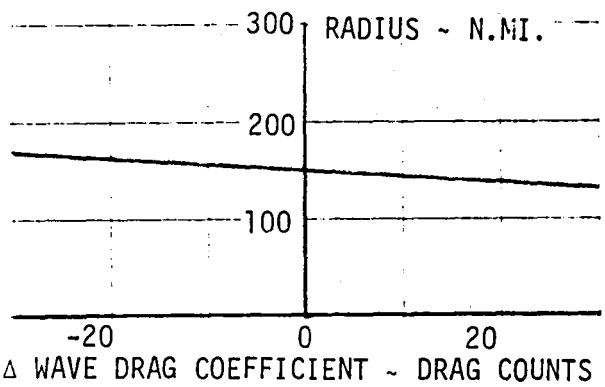

Figure 6-17 VTOL Mission Sensitivity

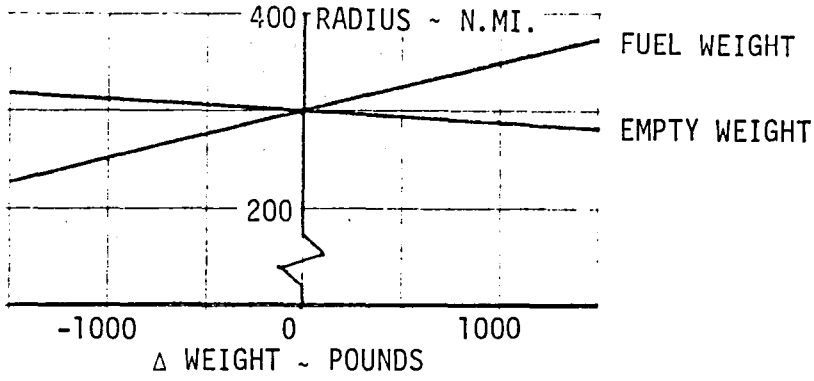

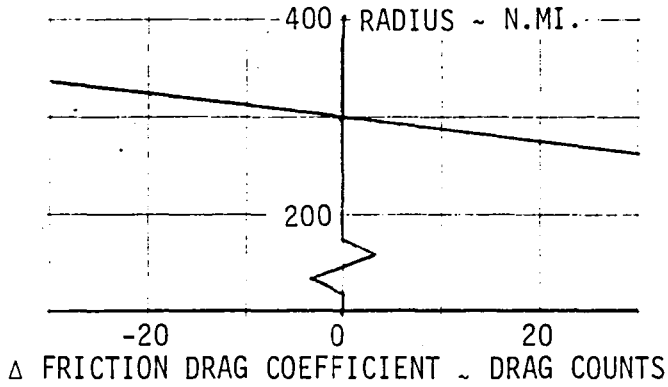

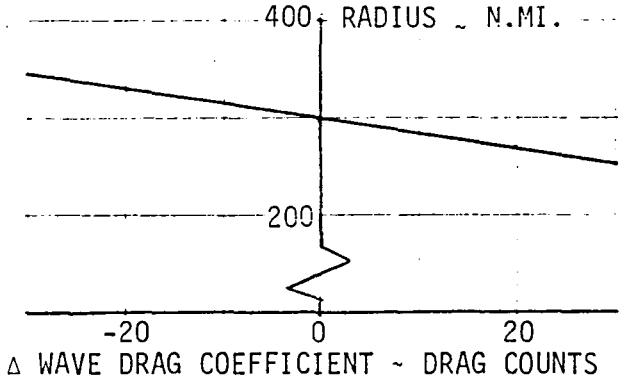

Figure 6-18 STOL Mission Sensitivities

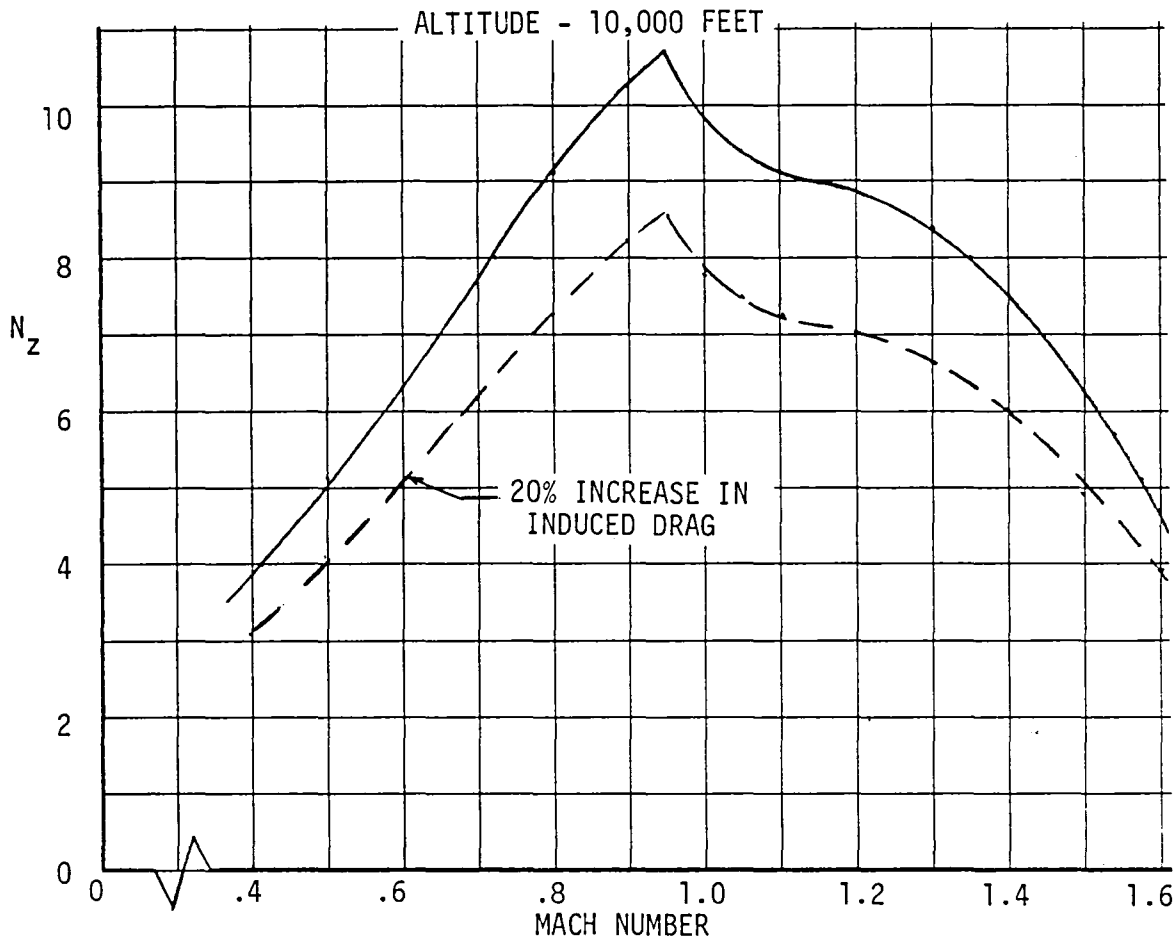

Figure 6-19 Baseline Configuration - Maneuver Load Factor versus Mach Number

6.2 ALTERNATE PERFORMANCE

6.2.1 Combat

The estimated aerodynamic characteristics for the alternate configuration are presented in Section 4.4.1 and were used in the determination of the following performance. The combat weight of the alternate (.88 VTOW) is 21,300 pounds. The flight envelope with afterburning thrust is presented in Figure 6-20. The dynamic pressure 1200 lbs/ft^2 and the Mach number limit of 1.9 are as previously defined for the baseline aircraft. Specific excess power versus load factor is presented in Figures 6-21 through 6-23 for .5M, .6M, .9M, 1.2M and 1.6M for altitudes of 10,000, 20,000, and 30,000 feet. A time history of the acceleration from .8 to 1.6M at 35,000 feet is shown in Figure 6-24 for the alternate configuration.

6.2.2 Mission

The Design Deck Launched Intercept mission used is the same as that previously presented for the baseline aircraft. A mission breakdown for the STO mission is presented in Figure 6-25. The subsonic mission performance capability is pesented in Figure 6-26, and is based on a usable internal fuel capacity of 8225 pounds. All missions are identical to those described in Section 6.1.2.

6.2.3 Vertical Takeoff and Transition

The VTO lift budget for the alternate aircraft is shown in Figure 6-27. The same conditions are used in determining the budget as for the baseline aircraft. The main difference between the two aircraft lift systems is the slightly lower augmentation ratios for the alternate aircraft, and this is the reason for the lower VTO lift capability. The variation of lift capability C.G. is given in Figure 6-28.

The acceleration capability at the minimum augmenter deflection is presented in Figure 6-29 and is similar to the baseline configuration. Adequate acceleration exists for good transition characteristics.

The transition is shown in Figure 6-30 performed similarly as for the baseline aircraft described in previous sections. The alternate aircraft has better STOL aerodynamics than the baseline, and with a lower VTO weight, the transition is accomplished even more handily than the baseline.

6.2.4 Short Takeoff

The alternate aircraft STO deck lengths are presented in Figure 6-31. Due to the lower drag characteristics of the alternate configuration a higher flap deflection can be used. All the takeoffs shown in Figure 6-31 are based on the use of the minimum augmenter mean flap deflection while on the deck and deflected to 50° (at 25°/second) after leaving the deck. The ski-jump point shown in Figure 6-31 uses a 10° ramp. No attempt to examine the gross weight variation with ramp angle was performed for the alternate configuration since the goal takeoff weight was achieved at 0 knots of wind at a reasonable ramp angle. The same remarks as for the baseline aircraft regarding the criteria differences between the flat deck STO's and the ski-jump STO apply to the alternate.

A time history for the ski-jump takeoff of the alternate aircraft is shown in Figure 6-32. For comparison a takeoff from a flat deck with no rotation of pitch angle to increase angle of attack is included in Figure 6-32 to indicate the altitude difference under identical procedures.

The alternate aircraft can also land vertically at all weights equal or less than the VTO gross weight. In the conventional configuration, the approach speed at 1.15 V_S is 109 KEAS at the VTO gross weight.

6.2.5 Sensitivities

Mission sensitivity for the VTO mission for the alternate configuration is presented in Figure 6-33. An empty weight variation which in turn causes a fuel variation results in a 71 n.mi. change in radius for each 1000 pound change. Changes in friction or wave drag of 20 counts (ΔC_D .0020) effect a change in mission radius of 19 and 13 n.mi., respectively.

The STO mission sensitivity is presented in Figure 6-34. Varying the empty weight of the aircraft causes a variation in radius of 13 n.mi. for each 1000 pound change. The fuel capacity causes a 54 n.mi. radius change for each 1000 pound. Mission sensitivity to friction or wave drag of 20 drag counts are 34 and 25 n.mi., respectively.

It is estimated that the wing base drag can be eliminated with the proper trailing edge treatment (Section 4.4.1). The skin friction sensitivity curve can be used to estimate the effect of variations in base drag. It is expected that the range of friction drag coefficient shown on Figures 6-33 and 6-34 cover the appropriate range of uncertainty of the base drag (Figure 7-2).

The maneuvering capability of the alternate configuration is presented in Figure 6-35 for an altitude of 10,000 feet. The effect of a 20 percent induced drag increase is presented to reflect its sensitivity.

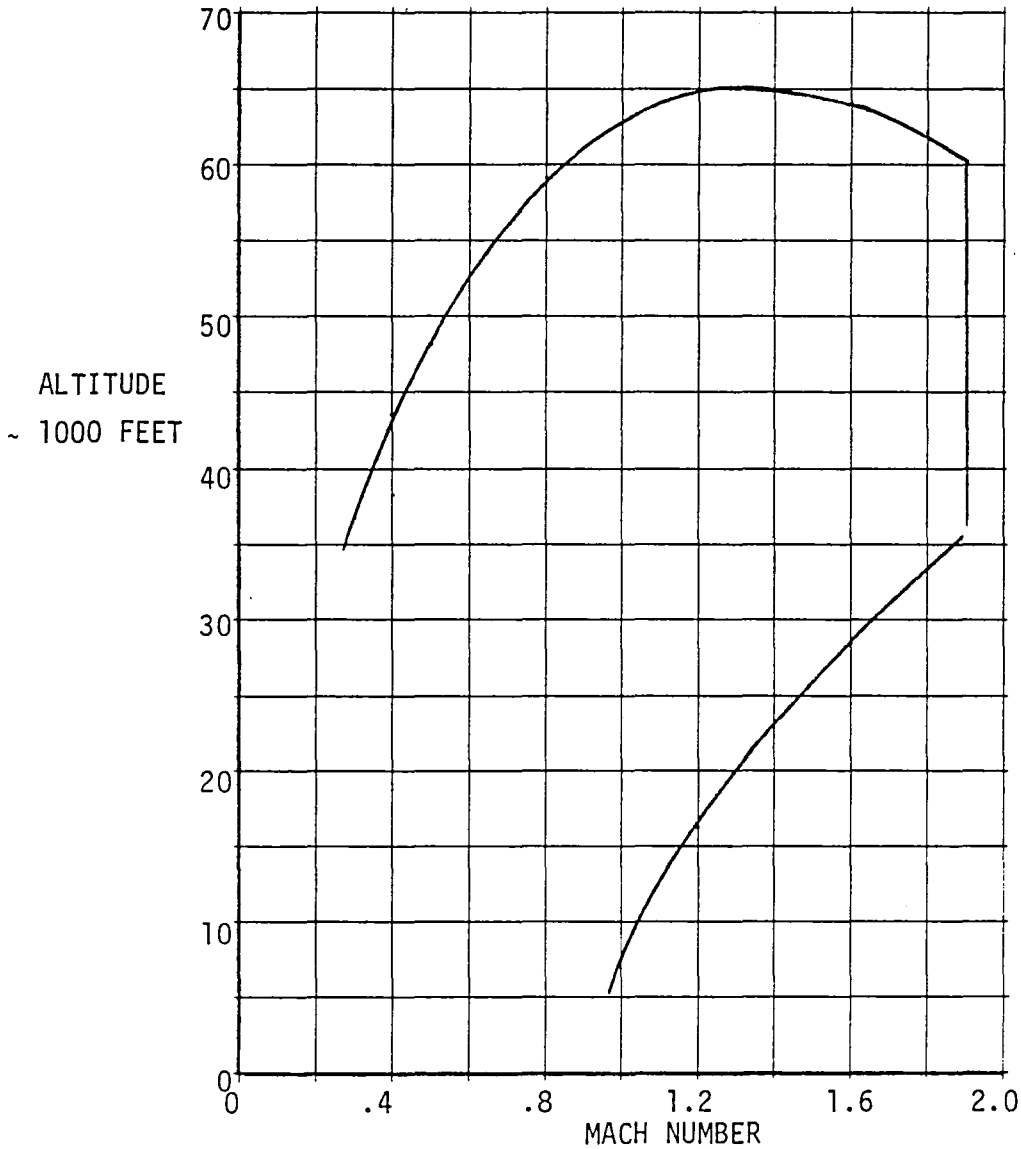

Figure 6-20 Alternate Speed-Altitude Flight Envelope

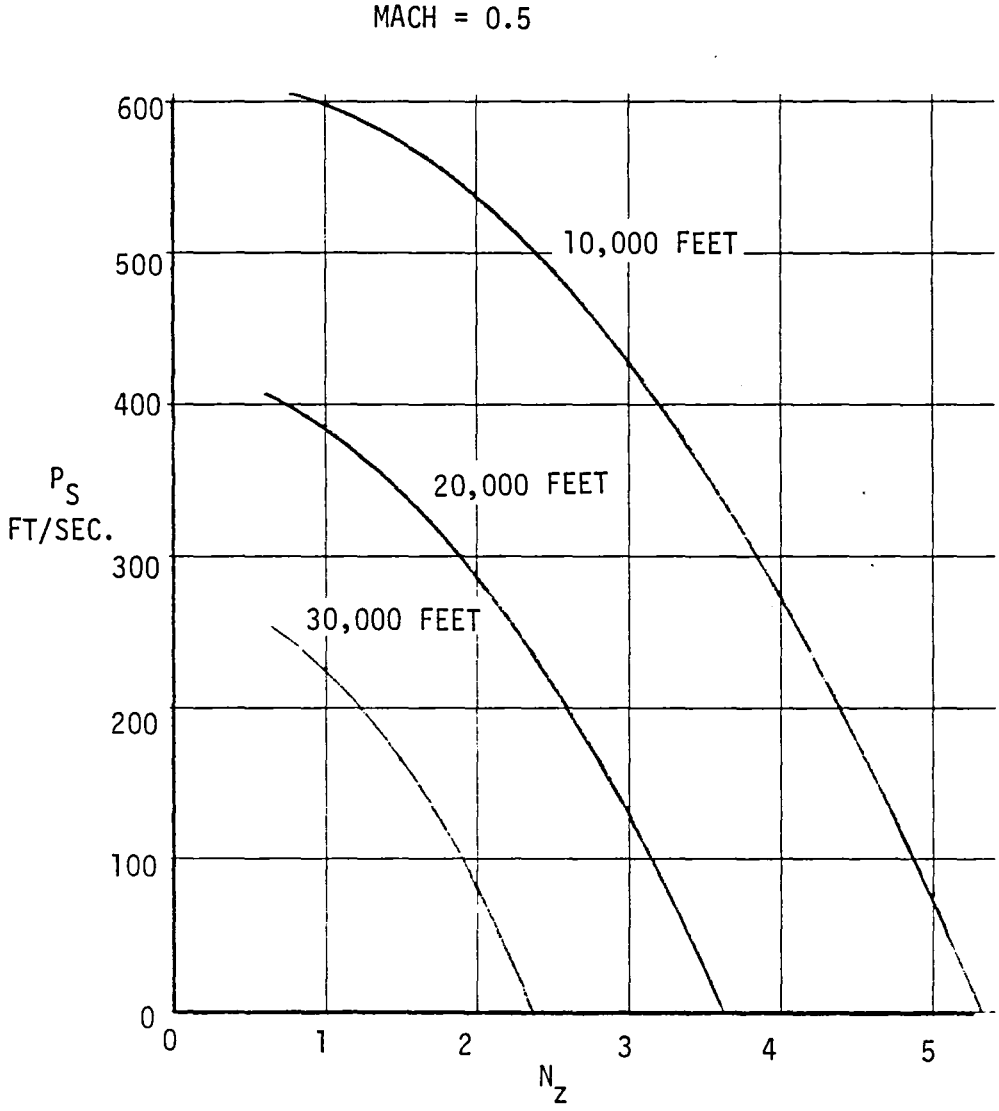

Figure 6-21 Alternate - Specific Excess Power

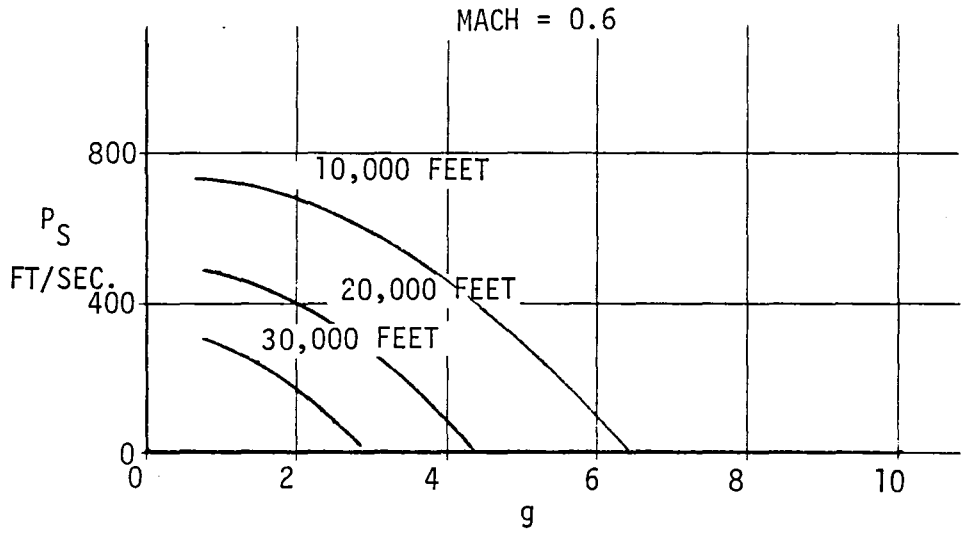

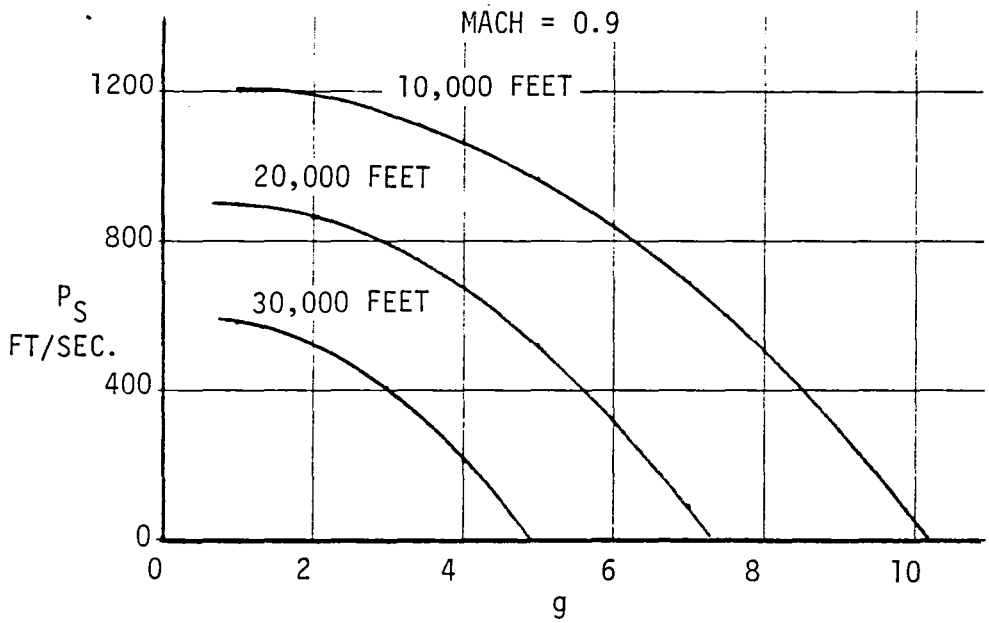

Figure 6-22 Alternate - Specific Excess Power

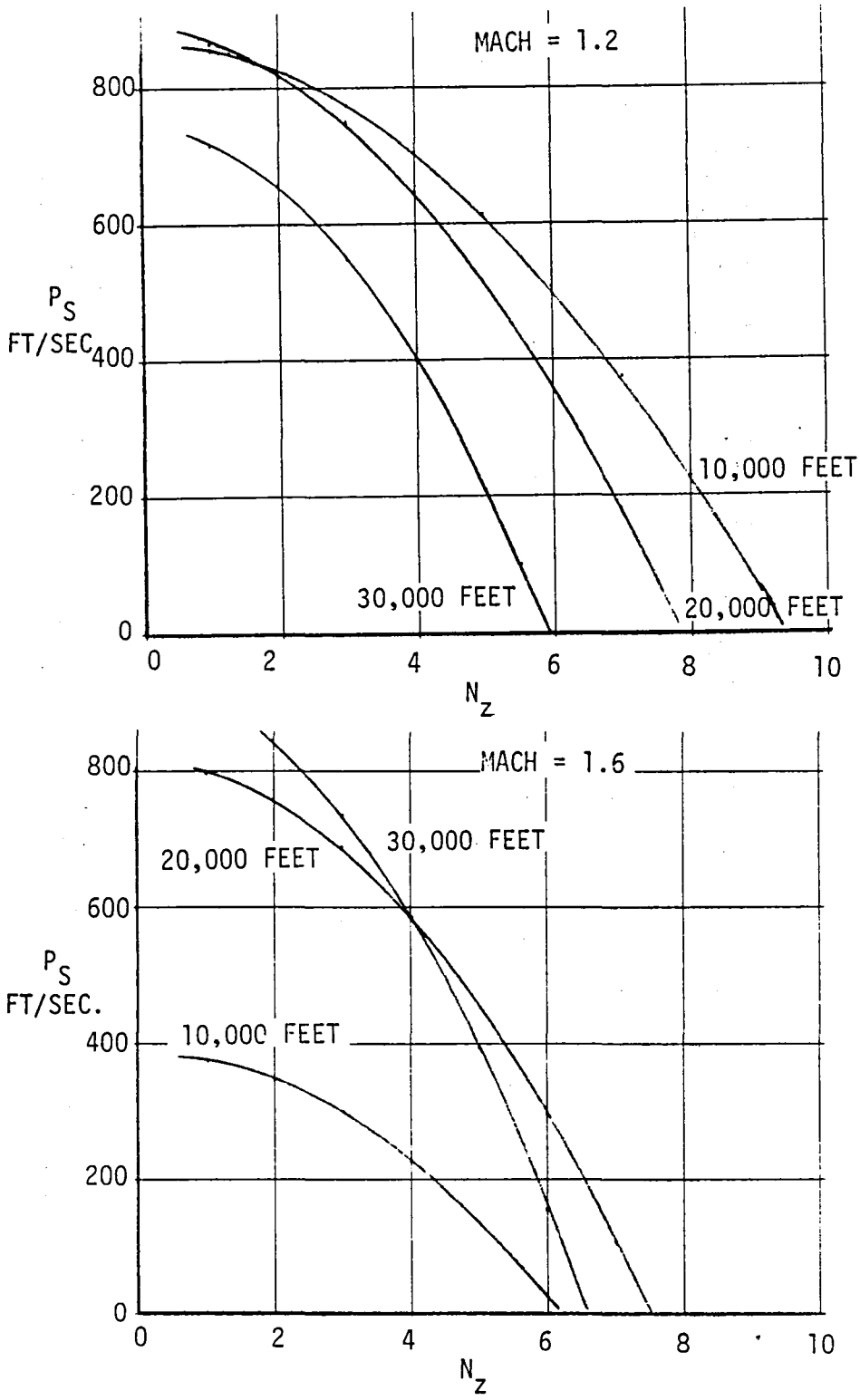

Figure 6-23 Alternate - Specific Excess Power

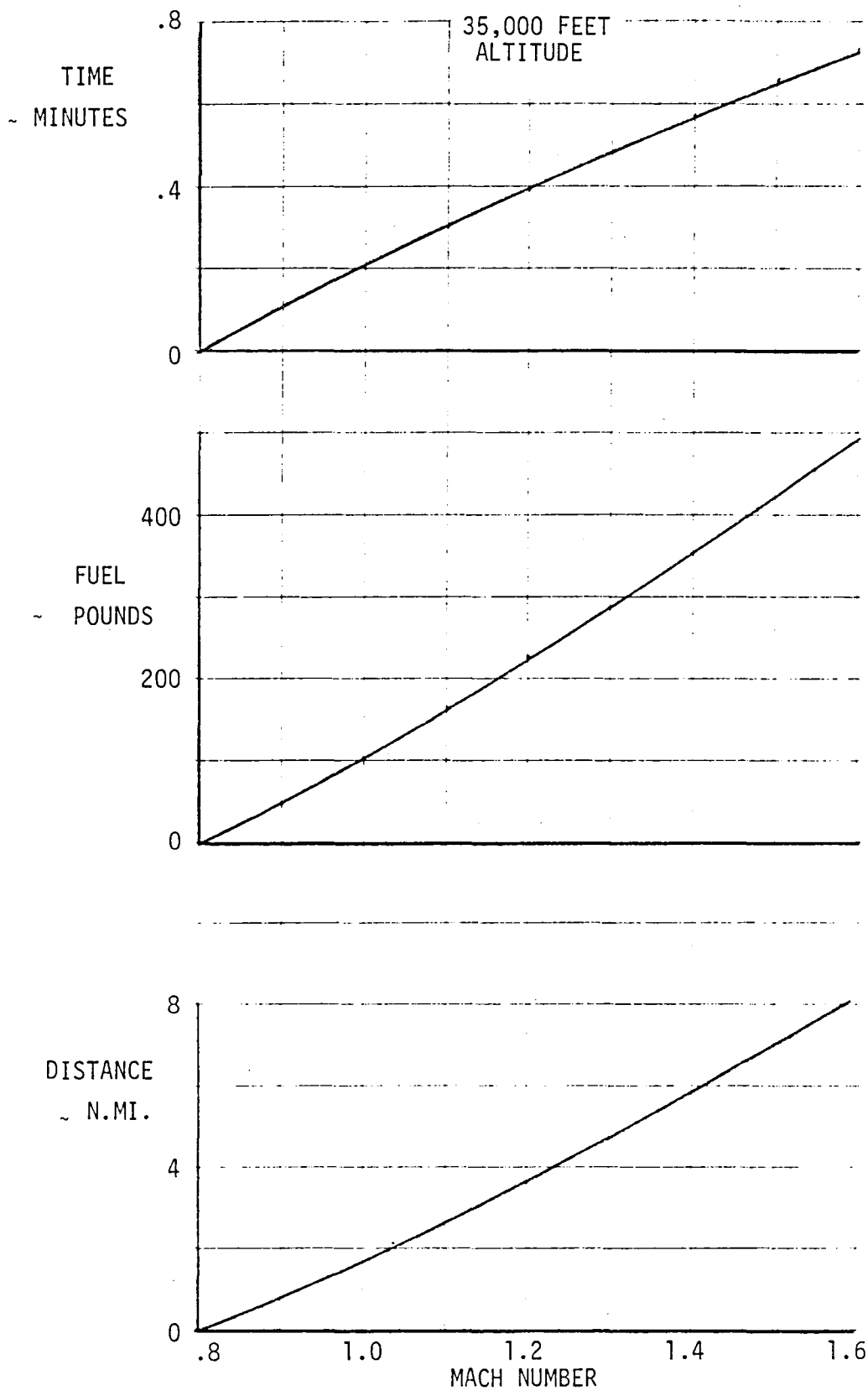

Figure 6-24 Acceleration Time History - Alternate Configuration

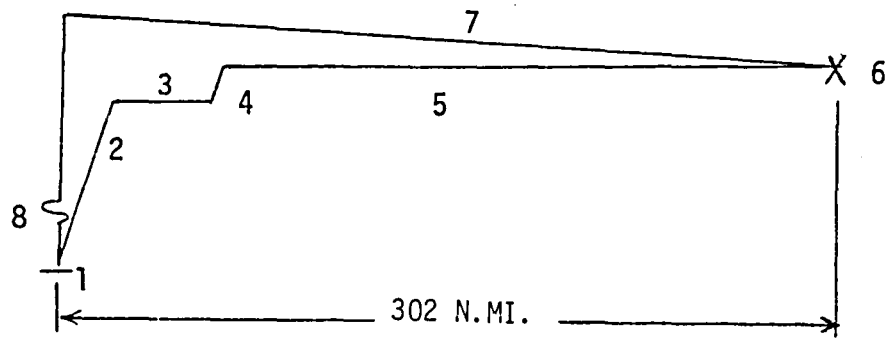

OPERATION	A/C WEIGHT LBS.	FUEL LBS.	DIST. N.MI.	TIME HRS.
1. WARMUP - TAKEOFF	28,489	413	0	.088
2. CLIMB TO 40,000 FT.	28,076	909	10	.018
3. ACCELERATE	27,167	676	15	.022
4. SUPERSONIC CLIMB	26,491	242	7	.008
5. SUPERSONIC CRUISE	26,249	2,953	270	.293
6. COMBAT	23,296	840		.033
7. RETURN CRUISE	22,456	1,354	302	.587
8. LANDING RESERVE	21,102	838	0	.167
	20,264			
TOTAL		8,225	604	1.22

Figure 6-25 STO Mission Breakdown Alternative

COMBAT AIR PATROL

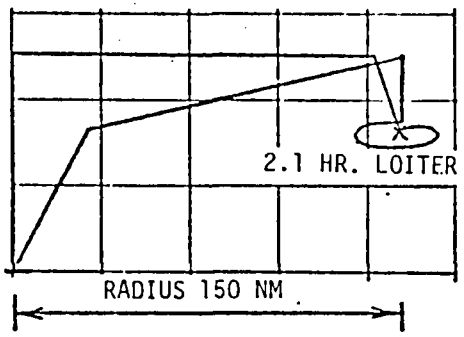

TOGW: 31,833 LBS.
FUEL:
INT: 8,225 LBS.
EXT: 2,720 LBS.
CMBT: 2 MIN. - 1.5M - 35K A/B
ARMS: 4-AIAAM

FIGHTER ESCORT

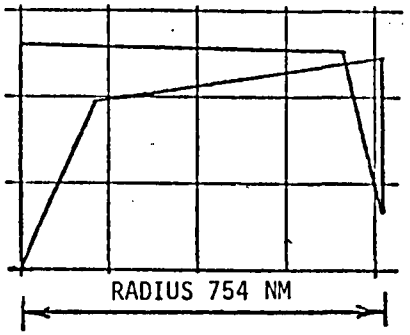

TOGW: 31,213 LBS.
FUEL:
INT: 8,225 LBS.
EXT: 2,720 LBS.
CMBT: 2 MIN. - 1.0M - 10K INT.
ARMS: 2-SRAAM
4-MRAAM

INTERDICTION MISSION

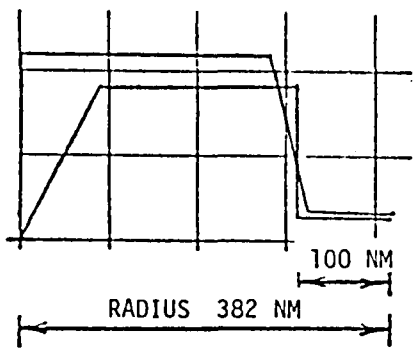

TOGW: 34,013 LBS.
FUEL:
INT. 8,225 LBS.
EXT. 2,720 LBS.
CMBT: 5 MIN. - .85M - SL INT.
ARMS: 2-SRAAM
4-SRASM

SURFACE STRIKE

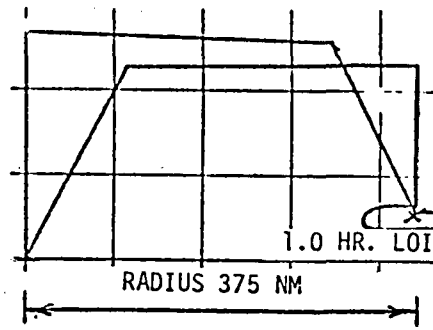

TOGW: 30,663 LBS.
FUEL:
INT: 8,225 LBS.
EXT. 1,360 LBS.
CMBT: 5 MIN. - .8M - 20K INT.
ARMS: 2-SRAAM
2-HARPOON

Figure 6-26 Alternate Subsonic Mission Capability

VTO LIFT BUDGET

ISENTROPIC GROSS THRUST	20,000 LBS.
LEAKAGE	400 LBS.
ISENTROPIC GROSS THRUST TO AUGMENTERS	19,600 LBS.
ISENTROPIC THRUST TO FORWARD AUGMENTER	9,800 LBS.
DUCT LOSSES	893 LBS.
FORWARD AUGMENTER NOZZLE ISENTROPIC THRUST	8,907 LBS.
FORWARD AUGMENTER LIFT (ϕ = 1.41)	12,559 LBS.
ISENTROPIC THRUST TO AFT AUGMENTER	8,232 LBS.
DUCT LOSSES AND LEAKAGE	388 LBS.
AFT AUGMENTER NOZZLE ISENTROPIC THRUST	7,844 LBS.
AFT AUGMENTER LIFT (ϕ = 1.56)	12,237 LBS.
ISENTROPIC THRUST TO PITCH REACTION CONTROL	1,568 LBS.
DUCT AND NOZZLE LOSSES AND LEAKAGE	108 LBS.
PITCH REACTION CONTROL NOZZLE ISENTROPIC THRUST	1,460 LBS.
MAXIMUM LIFT	26,256 LBS.
LIFT WITH SIMULTANEOUS CONTROL (4° θ, 6°ϕ , 3° ψ)	25,515 LBS.
VTO GROSS WEIGHT	24,300 LBS.

Figure 6-27 Alternate Aircraft Lift Budget - Tropical Day

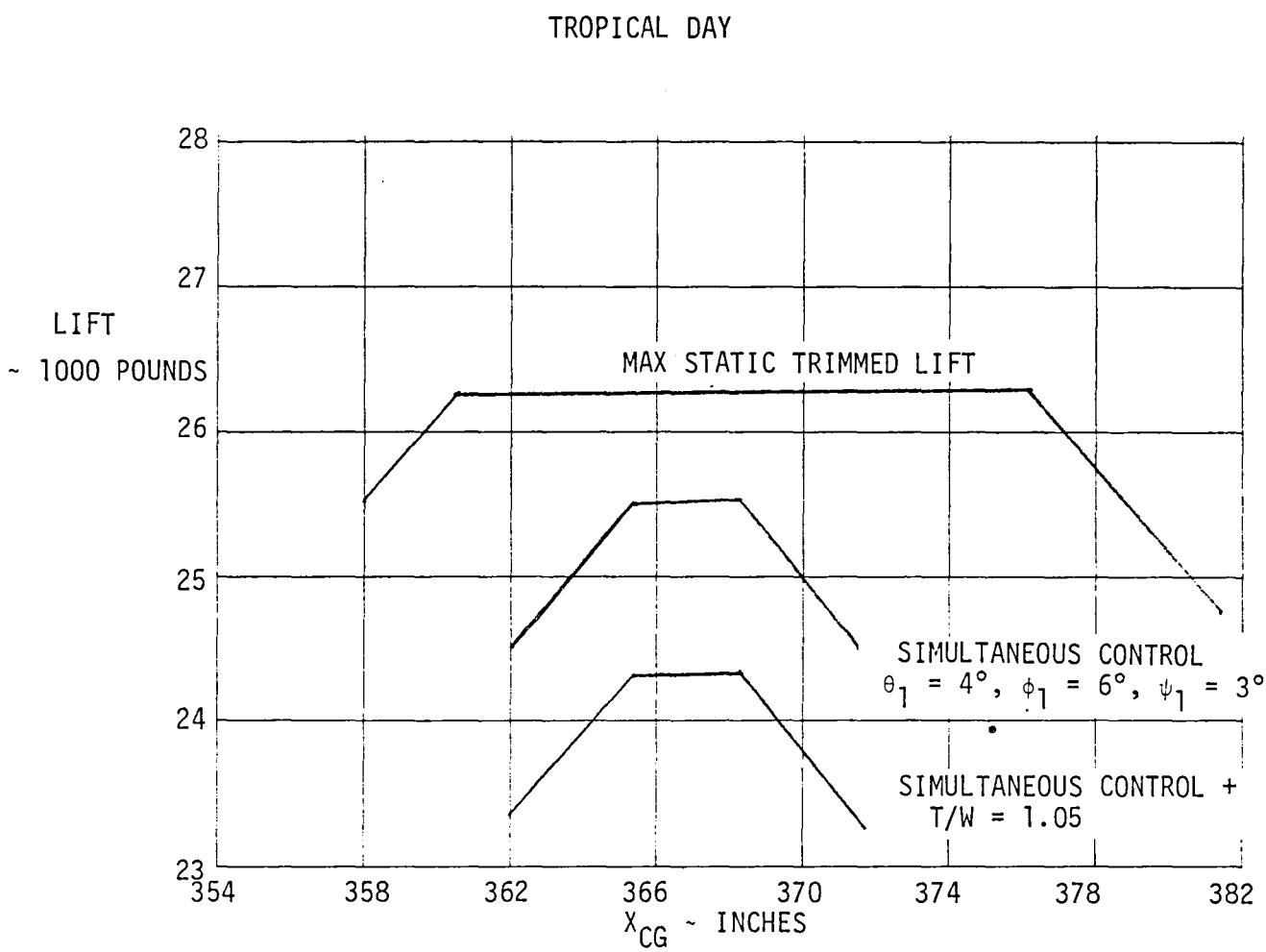

Figure 6-28 Alternate Aircraft - Vertical Lift Capability

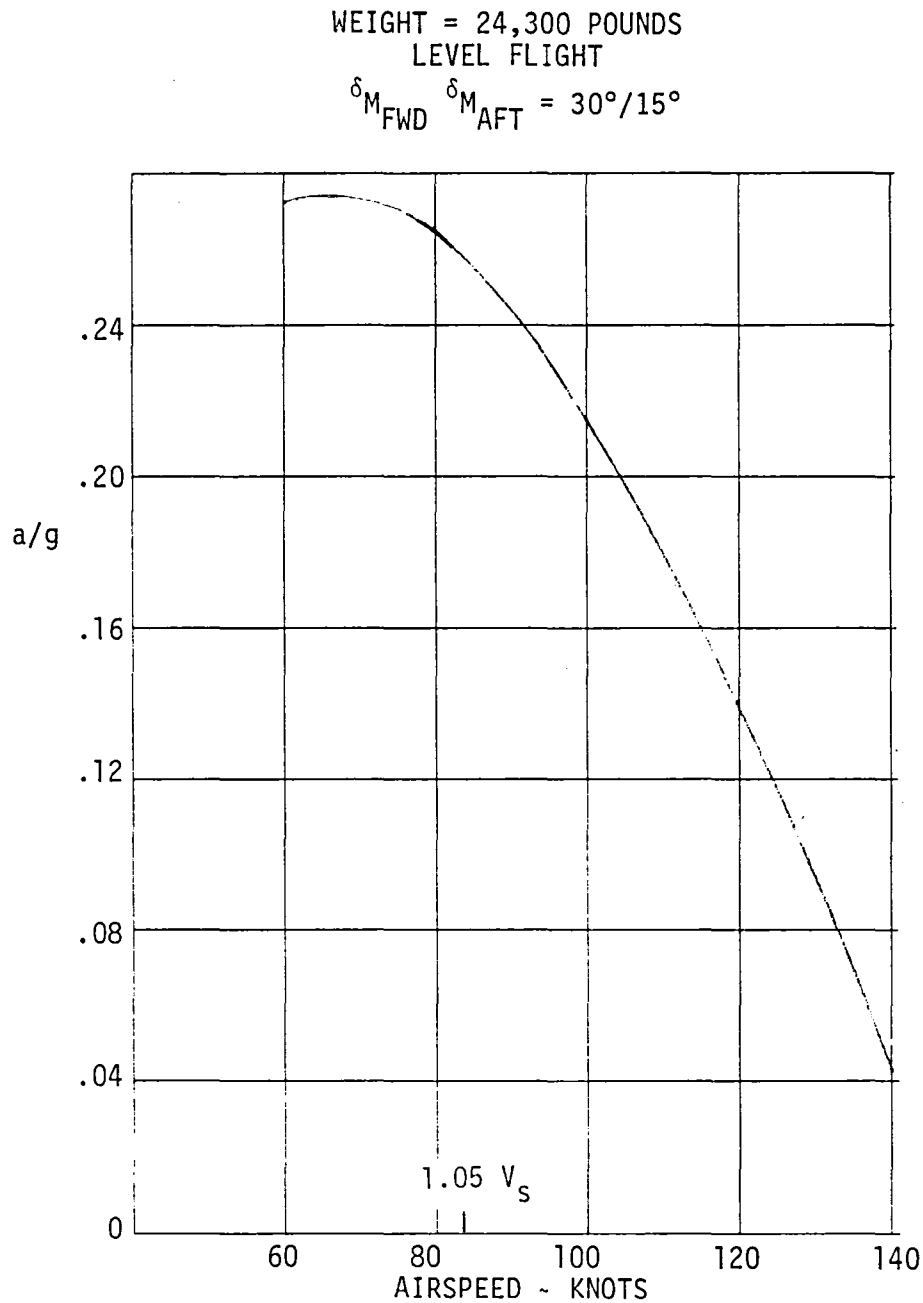

Figure 6-29 Alternate Aircraft Acceleration

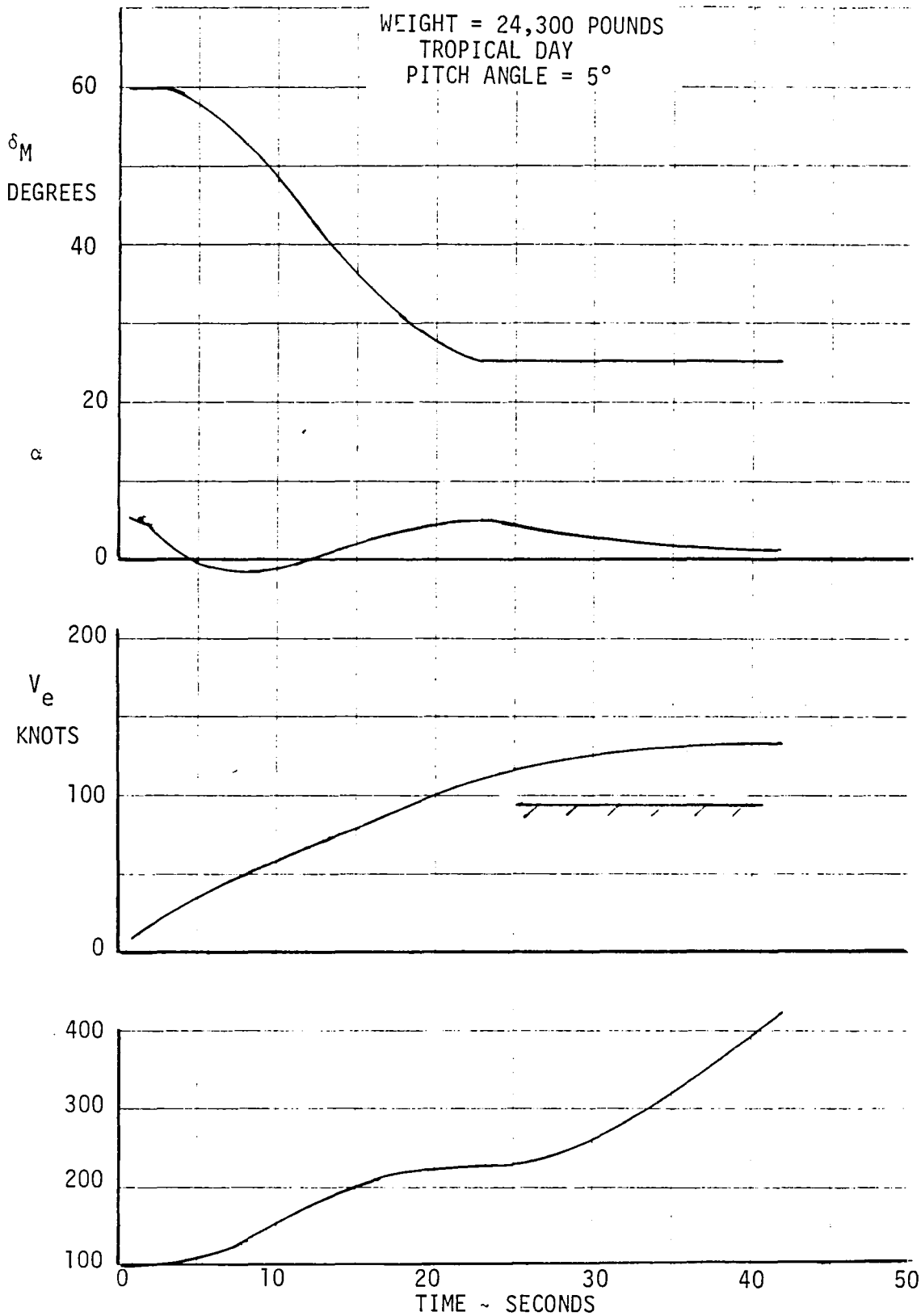

Figure 6-30 Alternate Aircraft Transition

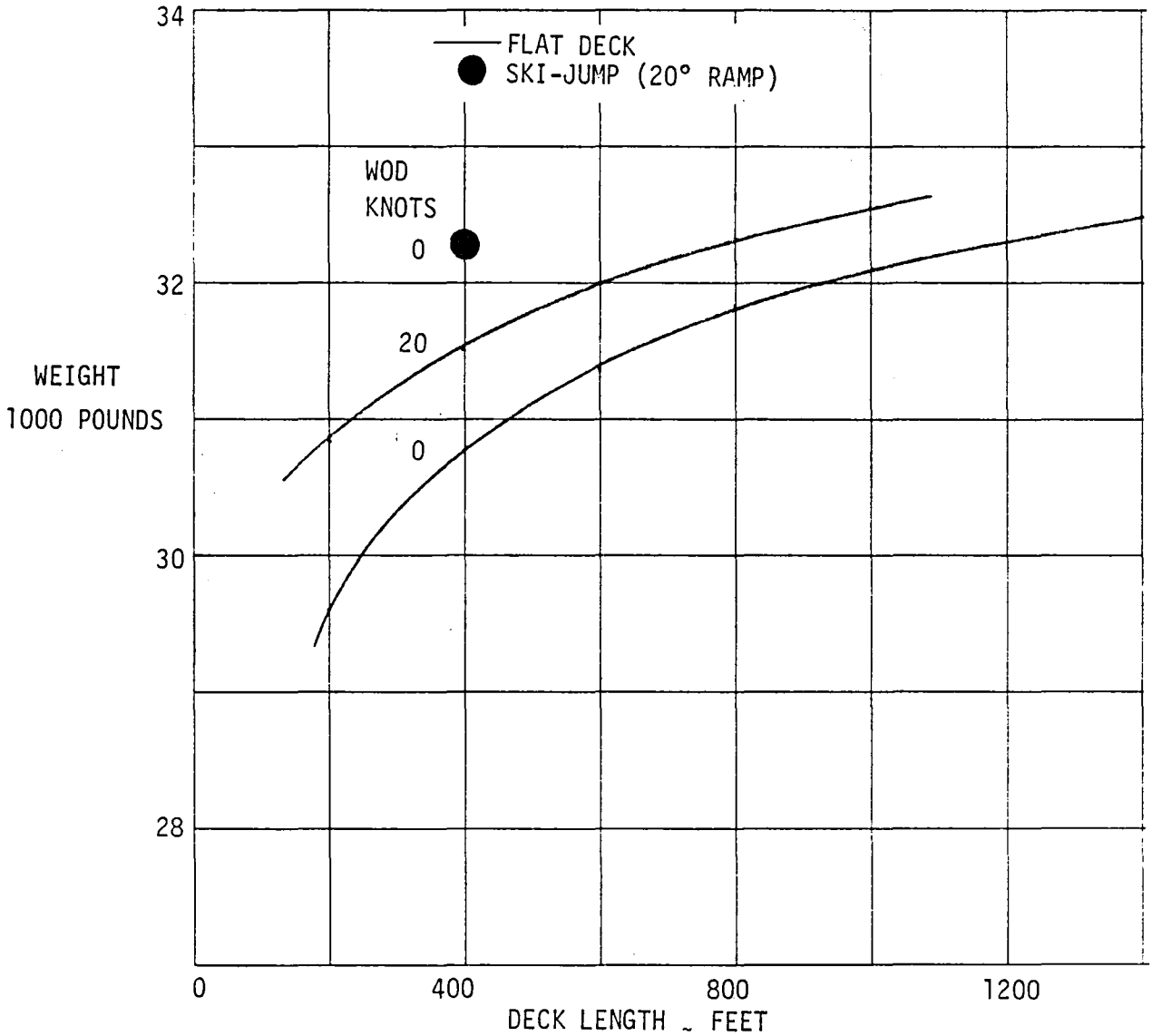

Figure 6-31 Takeoff Distance versus Deck Length for Alternate Configuration

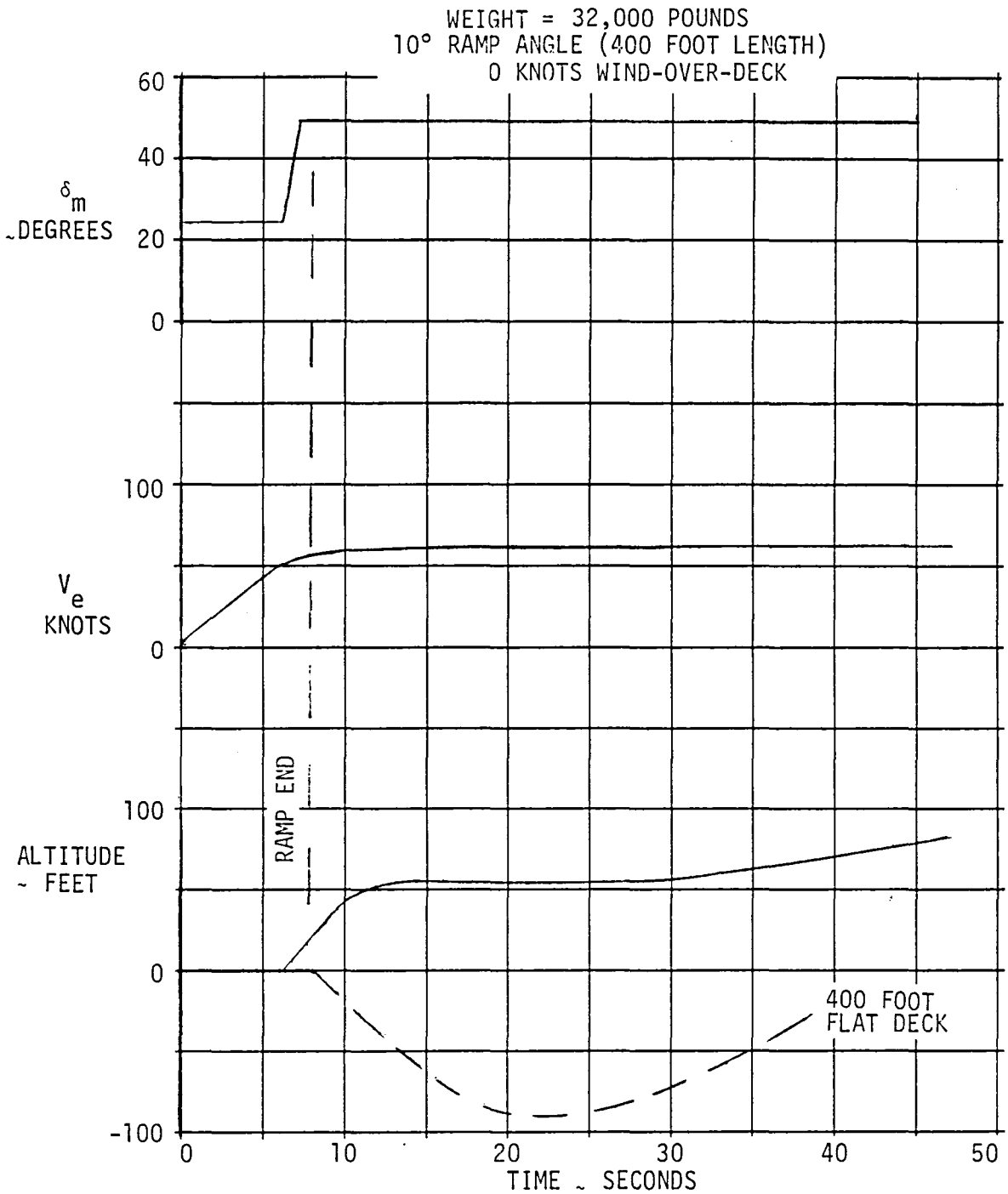

Figure 6-32 Ski-Jump Takeoff for Alternate Configuration

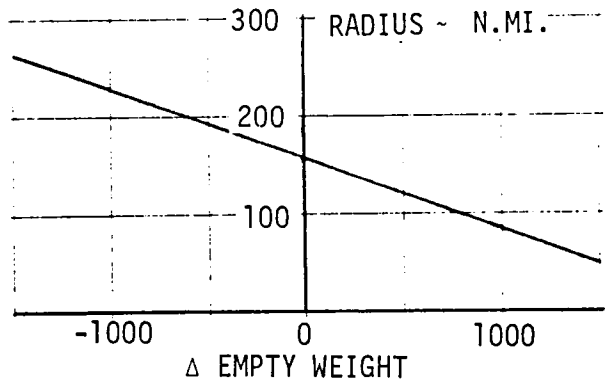

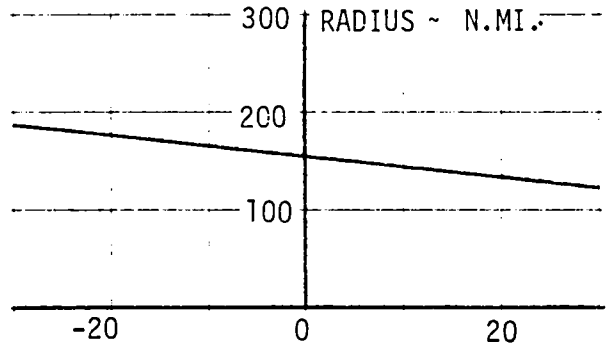

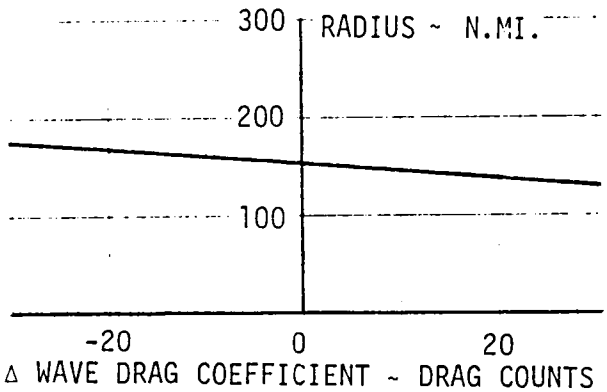

Figure 6-33 VTOL Mission Sensitivities - Alternate Configuration

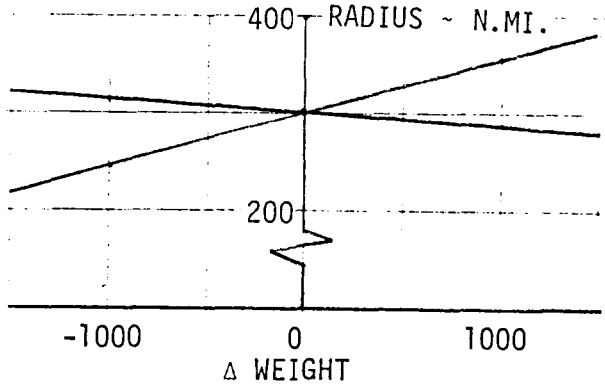

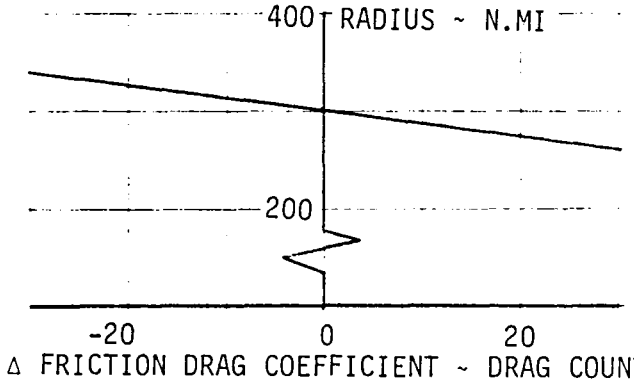

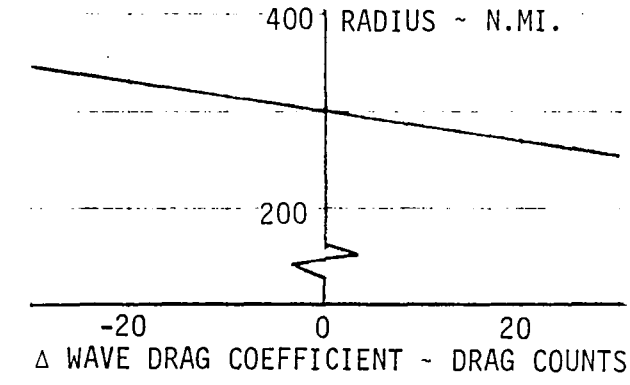

Figure 6-34 STOL Mission Sensitivities - Alternate Configuration

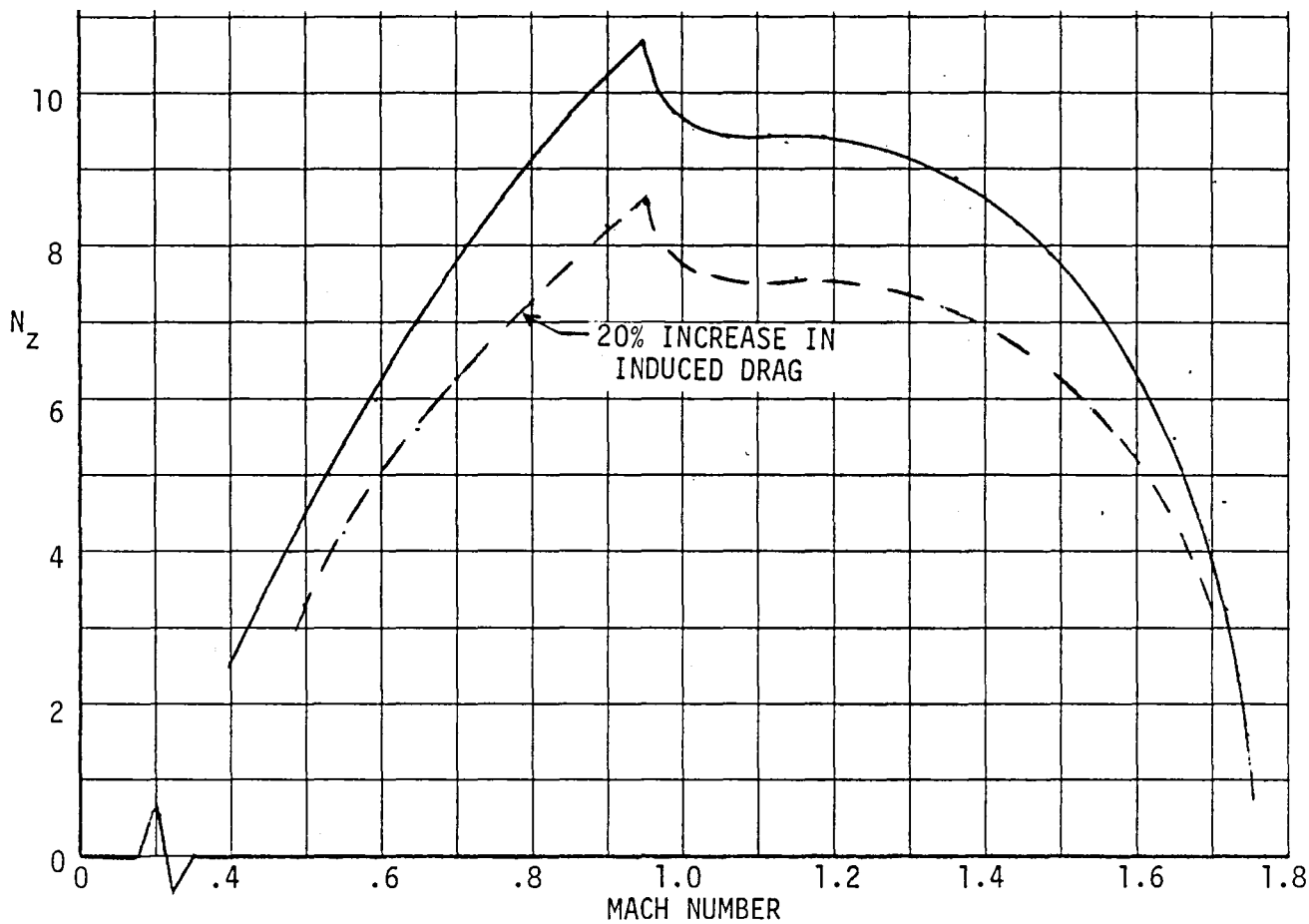

Figure 6-35 Maneuvering Load Factor Versus Mach Number
Alternate Configuration

7.0 AERODYNAMIC UNCERTAINTIES

7.1 SELECTION

The primary purpose of this study has been to identify areas or concepts of aerodynamic or aero/propulsion design that require additional research to provide confidence for their use in the successful design of future high speed V/STOL and conventional aircraft. To accomplish this end, the relative sensitivity of the aircraft concepts to various aerodynamic parameters was first determined. Then the confidence in predicting those parameters having the largest effect on the concept design was determined. Finally, those parameters and concepts having the greatest effect on the success of the design and the largest uncertainty in the accuracy of their quantification were selected for further research.

The most significant performance sensitivities are presented in sections 6.1.5 and 6.2.5. It can be seen that both zero lift drag and wave drag have a significant effect on the capability to perform the design missions. A small increase in drag would increase the fuel required to perform the mission and on the VTO mission this would mean an increased engine size to provide the vertical lift with a subsequent additional increase in fuel and drag. The resultant snowball effect can become significant. STO missions are less sensitive to weight but the increased fuel and tankage weight could be felt by the maximum sustained load factor requirements, and again a snowballing effect would be encountered. An increase in weight would be magnified by the load factor and require increased thrust and thus engine size and thus more fuel and weight. The snowballing effect on the STO mission would be expected to be less than that encountered with the VTO mission.

The effect of trimmed drag-due-to-lift was found to be small on the mission sensitivity but to have a rather large effect on the maximum sustained load factor, as shown in sections 6.1.5 and 6.2.5. As noted above a snowballing effect on aircraft size occurs with increasing engine size. The small effect on mission sensitivity can be explained by the fact that the aircraft is operating well below its maximum lift to drag ratio as shown in sections 4.1.1 and 4.4.1. Previous studies have shown that the supersonic cruise range could be increased slightly by increasing the cruise altitude to 55,000 feet, but this would require the pilot to wear a full pressure suit. Cruise at altitudes above 55,000 feet requires more fuel to climb than is saved by the higher altitude cruise.

High angle of attack characteristics affect the design directly in that they must be controllable for a successful aircraft design and indirectly by affecting the trim drag through the allowable amount of instability that can be handled.

From these investigations the most significant uncertainties were determined to be:

Base drag of two-dimensional blunt bases (subsonic-transonic-supersonic).

Wave drag of configurations with substantial lateral volume.

High angle of attack stability and control characteristics.

Canard trimmer-wing leading edge-inlet interference.

Drag-due-to-lift of variable camber configurations.

Effectiveness of wing tip mounted vertical tails on wings with highly swept leading edges.

High inlet operation at high angle of attack
- Effect of canopy proximity
- Effect of fuselage shape
- Effect of wing root shielding.

STOL aerodynamic characteristics of thrust augmenters.

7.2 DESCRIPTION

Several probable uncertainties were identified by experienced judgement in the initial proposal. Others have been identified during the study as the concept development and analysis progressed. The development of the concept also relegated some of the previously determined uncertainties, such as effect of wing leading edge droop and vortex flaps, to a lesser level of significance; while raising trim and destabilizing concepts, such as canards, to a higher level of importance.

7.2.1 Blunt Based Airfoil Drag

The use of a longitudinal or chordwise augmenter in the alternate aircraft allowed greater flexibility in wing planform design and lifting and control arrangements. The significantly further forward center of lift provided by the longitudinal augmenter vice the forward lateral augmenter of the baseline aircraft permitted the aft augmenter to be moved aft and incorporate the elevon as the aft diffuser flap. This bit of synergism reduced weight and increased lift in STOL.

In order to keep the wave drag down with the relatively steep boattail created by having the augmenter so close to the trailing edge, the airfoil contours were faired to a blunt trailing edge (about 60 percent of the maximum thickness). The blunt trailing edge must then be treated to keep the total drag to a minimum throughout the flight envelope of the aircraft. Calculations using far field wave drag theory, References 7-1 and 7-2, indicated significant reductions in wave drag could be achieved by fairing the airfoil to a blunt trailing edge with a two-dimensional stream tube. This was especially effective at the lower Mach numbers, as shown on Figure 7-1. However, when the estimated base drag, from the Rockwell Missile Drag Manual, for a square two-dimensional base end was taken into account most of the benefit disappeared. As can be seen the optimum bluntness, including base drag, is about 20 percent of the maximum airfoil thickness. Without base drag substantial reductions

in wave drag are realized by blunting the airfoil up to about 80 percent of its maximum thickness. A value of 60 percent bluntness was selected for the alternate configuration as this was the point where the benefits of drag reduction versus bluntness began tapering off.

Investigations by Nash, Reference 2-4, and the contractor have indicated the base drag of blunt based wings can be all but eliminated with proper trailing edge treatment and in some cases a thrust produced, as shown on Figure 7-2. These data are the results of contractor conducted wind tunnel tests in the Cornell Aeronautical Laboratory eight foot transonic wind tunnel on a semi span wing panel with a splitter plate on the trailing edge. Other promising concepts for base drag reduction that have also displayed benefit are shown on Figure 7-3. The proper combination of these concepts should be able to improve on the results of Figure 7-2.

7.2.2 Wave Drag

The lateral distribution of volume inherent with spanwise augmenters renders the linear far field wave drag theory suspect. This theory was developed to analyze configurations with long slender fuselages and thin wings. It resolves the cross sectional area distribution along any Mach plane cut through the aircraft into an equivalent body of revolution for analysis. Any relatively sudden changes in cross sectional area, e.g., wing leading edges aligned with the Mach plane, can be either under or over predicted, depending on where they fall relative to the Mach plane cuts. If a Mach plane cut falls right on a wing leading edge the resultant sudden increase in area would violate the linear theory constraints, and the wave drag would be over-predicted. If on the other hand a wing leading edge aligned with the Mach plane falls in the middle of two successive cuts the wave drag would probably be under-predicted. Studies, such as Reference 7-3, have shown 10 to 20 percent differences between test and theory depending on the geometry techniques used. Similarly, contractor analyses of Rockwell supersonic fighter and attack aircraft have indicated some erratic trends with Mach number that did not show up in wind tunnel or flight test.

7.2.3 High Angle of Attack/Stabilty/Control/Trim Drag

The high angle of attack characteristics, subsonic longitudinal instability, control power and trimmed drag due-to-lift are interrelated. High angle of attack stability and control characteristics are not readily predictable with any existing method. Local flow separation and vortex interactions can significantly alter the stability and control characteristics at high angles of attack. Limited wind tunnel data on configurations similar to the baseline and alternate aircraft are presented on Figures 7-4 and 7-5, respectively. These data were obtained from IR D testing just prior to the initiation of this study. The data show a mild pitch up before the stable stall. Both configurations exhibited positive stability from stall to 90 degrees angle of attack. This pitch up, followed by a stable stall, creates the potential for a

deep stall if control power is not adequate. Both baseline and alternate configurations were designed to be unstable control configured vehicles at subsonic speed and as nearly neutrally stable as possible at supersonic speeds. At subsonic speeds this concept provides essentially an automatic camber input with trim. That is, increasing angle of attack (lift) requires increasing amounts of elevon trailing edge down deflection to trim the increasing aircraft nose up pitching moment generated by the unstable configuration. This subsonic effect is maximized and the supersonic trim drag minimized at center-of-gravity positions providing subsonic instability levels of 10 to 12 percent MAC, as shown on Figure 7-6. However, high angle of attack pitch up considerations, such as those shown on Figures 7-4 and 7-5 along with estimated full aircraft nose down pitch control power, limit the maximum allowable instability to about five percent MAC. At instability levels greater than five percent MAC analyses indicate the ability to pitch the aircraft nose down from a high angle of attack condition would become marginal to unsatisfactory. The highly swept wing tips of the wind tunnel model configurations, which are throught to be the major culprit in the pitch-up, have been greatly modified and some washout tip twist incorporated for the present study configurations; but, the fact remains that the only satisfactory method to determine the effect of these planform changes on the high angle of attack characteristics is through wind tunnel test.

7.2.4 Canard Trimmer - Wing Leading Edge - Inlet Interference

One means of increasing longitudinal control power throughout the aircraft flight envelope would be to install a small all-moveable canard trimmer on the forward fuselage. This device could also be used to effectively increase longitudinal instability and thus reduce trim drag, as shown on Figure 7-6. It would obviously be desirable to install the canard as far forward on the fuselage as possible; however, the location and spread of its wake relative to the wing and inlet at various flight conditions would have to be determined so that it could be satisfactorily positioned. If it had to be moved under the wing root leading edge to shield its wake from the inlet the mutual interference effects of the wing and canard would have to be investigated. These considerations cannot presently be accurately determined from existing methods.

7.2.5 High Inlet Operation At High Angles of Attack

The use of inlets mounted on top of the fuselage has been avoided in high performance aircraft design due to the uncertain effects of body upwash and vortices on inlet performance. This is primarily a concern at the moderate to high angles of attack encountered in maneuvering. Inlets mounted on top of the fuselage are attractive for VTOL aircraft in that they minimize engine exhaust reingestion which is a major source of VTO performance degradation. They would also be attractive as a stealth benefit especially for ground attack. The effects on the inlet of wing inboard planform, canopy shape, fuselage nose length and cross section all add to the uncertainty, especially at high angles of attack. The capability of the engine inlet to operate efficiently at low and high angles of attack at subsonic speeds and at supersonic speeds is paramount to the success of any fighter concept.

A lifting surface located below the inlet with its leading edge ahead of the inlet can provide excellent inlet operation at high angles of attack, as shown on Figure 5-8. These data were obtained on a small scale model and had a canard with a leading edge strake mounted below the high inlet. The configuration of the wing root leading edge-fuselage juncture could have a significant effect on the flow field provided to the inlet. Also the effects of canopy proximity and shape could have significant effects on the quality of the flow field at the inlet. The effects of configuration on this complex flow field can only be determined through wind tunnel test.

7.2.6 Wing Tip Mounted Vertical Tails on Highly Swept Wings

Wing tip mounted vertical tails can provide many synergistic benefits to the aircraft design. Some of these benefits are good high angle of attack directional stability, reduced drag due to lift, improved longitudinal stability and a reduction in the aerodynamic center shift between subsonic and supersonic speeds. These benefits were evaluated in wind tunnel tests of the XFV-12A technology prototype, as reported in Reference 7-4 and are shown on Figure 7-7. Recent high angle of attack tests with a small model have indicated a breakdown of these beneficial effects on highly swept clipped delta wings at low angles of attack, as shown on Figure 7-8. Larger more accurately scaled model tests should be run to determine the cause of this early breakdown in wing tip mounted vertical tail effectiveness and to evaluate the effect of vertical tail cant angle so that their many synergistic benefits can be realized.

7.2.7 STOL Aerodynamic Characteristics of Thrust Augmenters

The STO characteristics of multiple thrust augmenting ejector configurations are still in some doubt. The contractor was able to predict the XFV-12A characteristics with a fair degree of confidence since wind tunnel data were available on the configuration. There was still some doubt regarding the effect of augmenter ram drag and thrust recovery. Attempts to extrapolate that data to the configurations analyzed herein proved futile and new methods had to be devised as discussed in section 4.3. These data were based on very limited tests with two full span tandem augmenters in very close proximity to each other. As can be seen the baseline configuration STO performance is rather severely penalized using these analyses. Although not a subject for Phase II, a general investigation of the performance of various arrangements of thrust augmenting ejectors at forward speed would add greatly to the capability to design this class of aircraft

7.3 UNCERTAINTY RESOLUTION

In order to resolve these uncertainties, it is proposed to conduct wind tunnel tests from low subsonic speeds to M = 2.0 on a full span sting mounted model. The baseline configuration will be the nucleus of the proposed model. This model will consist of a basic fuselage, wing, airflowing inlet, vertical tails on the fuselage, rudders, and wing trailing edge control surfaces. These components are illustrated in Figure 7-9.

The variations to this basic configuration required to resolve the defined uncertainties consist of those additional items illustrated on Figure 7-9 and/or discussed below.

An alternate configuration wing with three blunt trailing edge shape modifications.

Vertical tails mounted on the wing at the outboard end of the aft augmenters with the wing tips removed.

Changes in wing tip vertical tail cant angle (i.e., dihedral) to alter interaction effects and the input to stability about all three aircraft axies as well as the drag due to lift. Only the upper verticals will be changed. The lower verticals, although contributing to stability, also serve as augmenter end walls and cannot be readily changed.

A fuselage plug near the inlet to lengthen the fuselage nose and to increase the distance between canopy and inlet to determine the change in inlet recovery.

Fuselage strakes alongside the nose to alter the characteristics at high angles of attack and to improve inlet flow.

The chord length of the elevon will be changed to quantify this effect on aerodynamic interaction with the vertical tails as well as control sensitivity and control power.

An all-moveable canard at two longitudinal locations on the fuselage. This canard will have dihedral yet to be determined.

An alternate canopy shape intended to improve inlet flow while maintaining good pilot vision. This change may be combined with the fuselage plug.

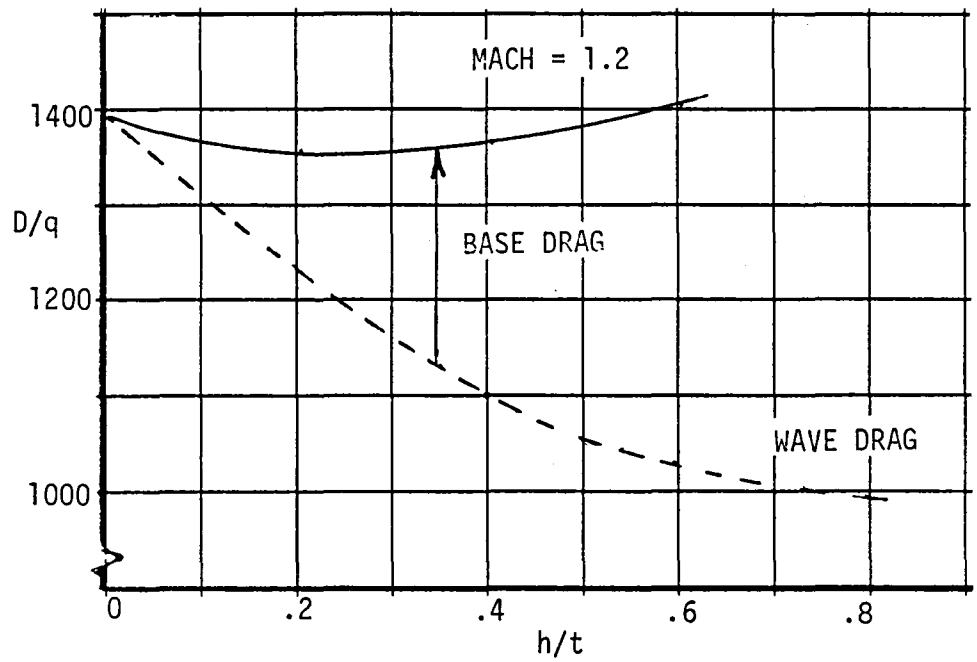

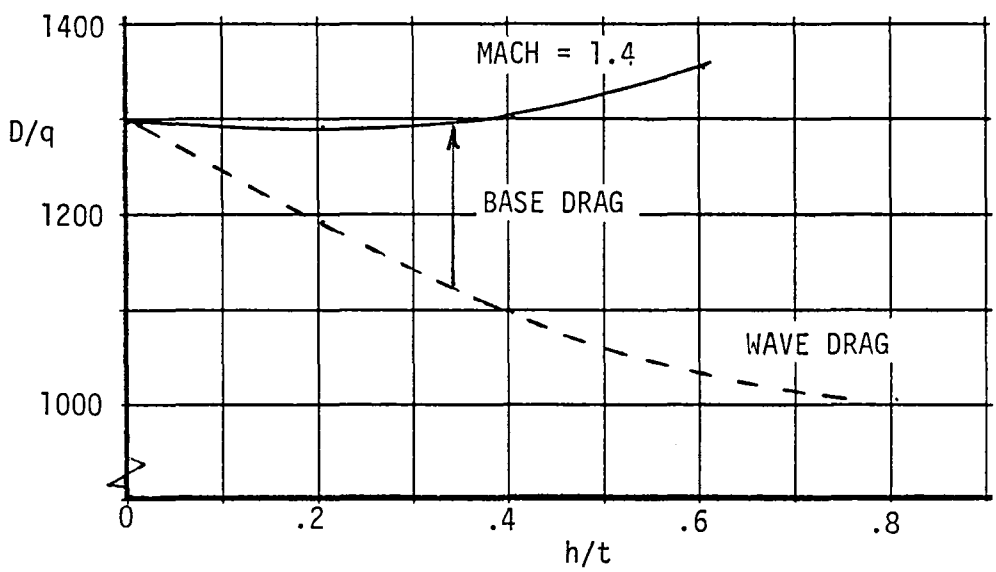

Figure 7-1a Effect of Wing Trailing Edge Bluntness on Pressure Drag - Alternate Configuration

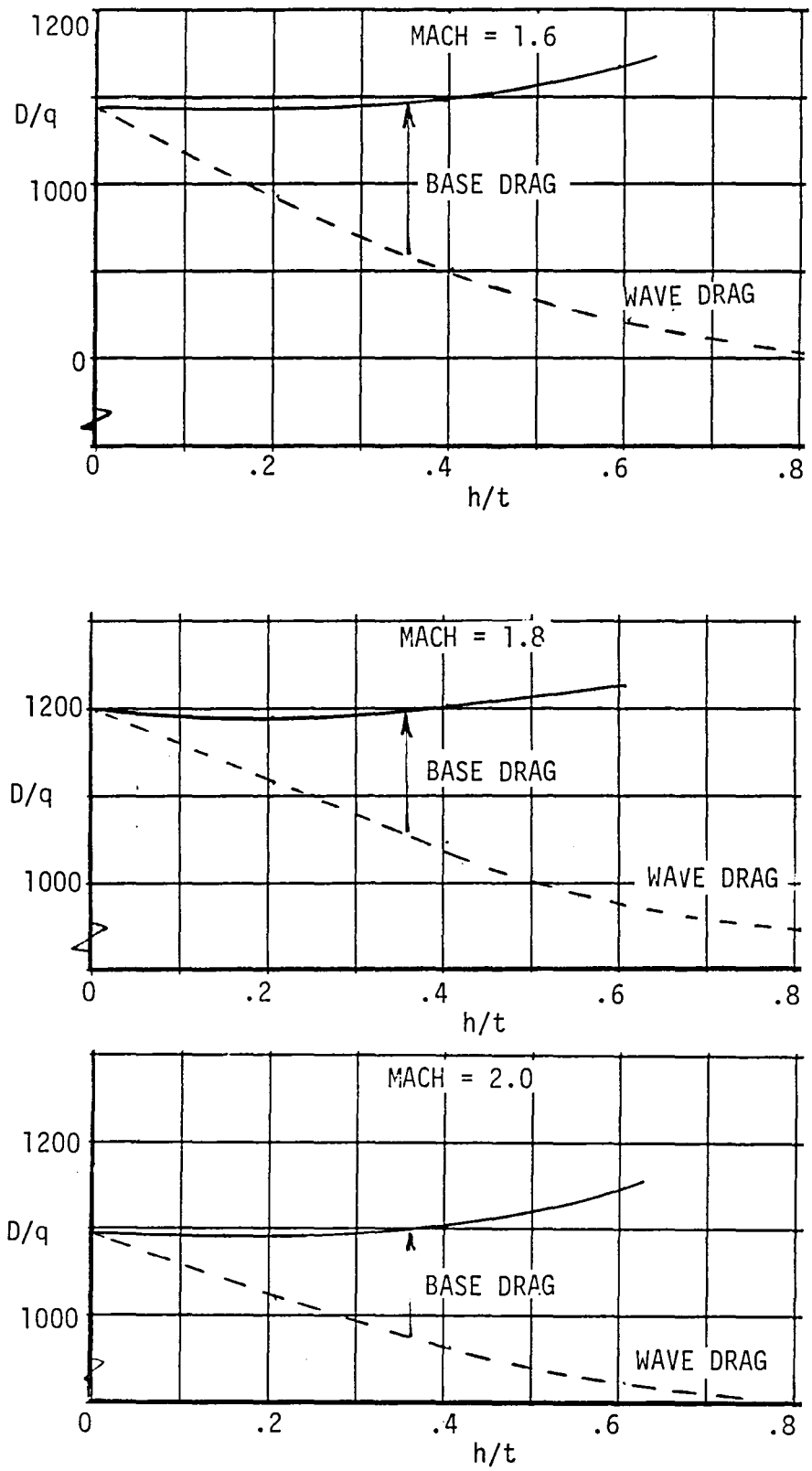

Figure 7-1b Effect of Wing Trailing Edge Bluntness on Pressure Drag - Alternate Configuration

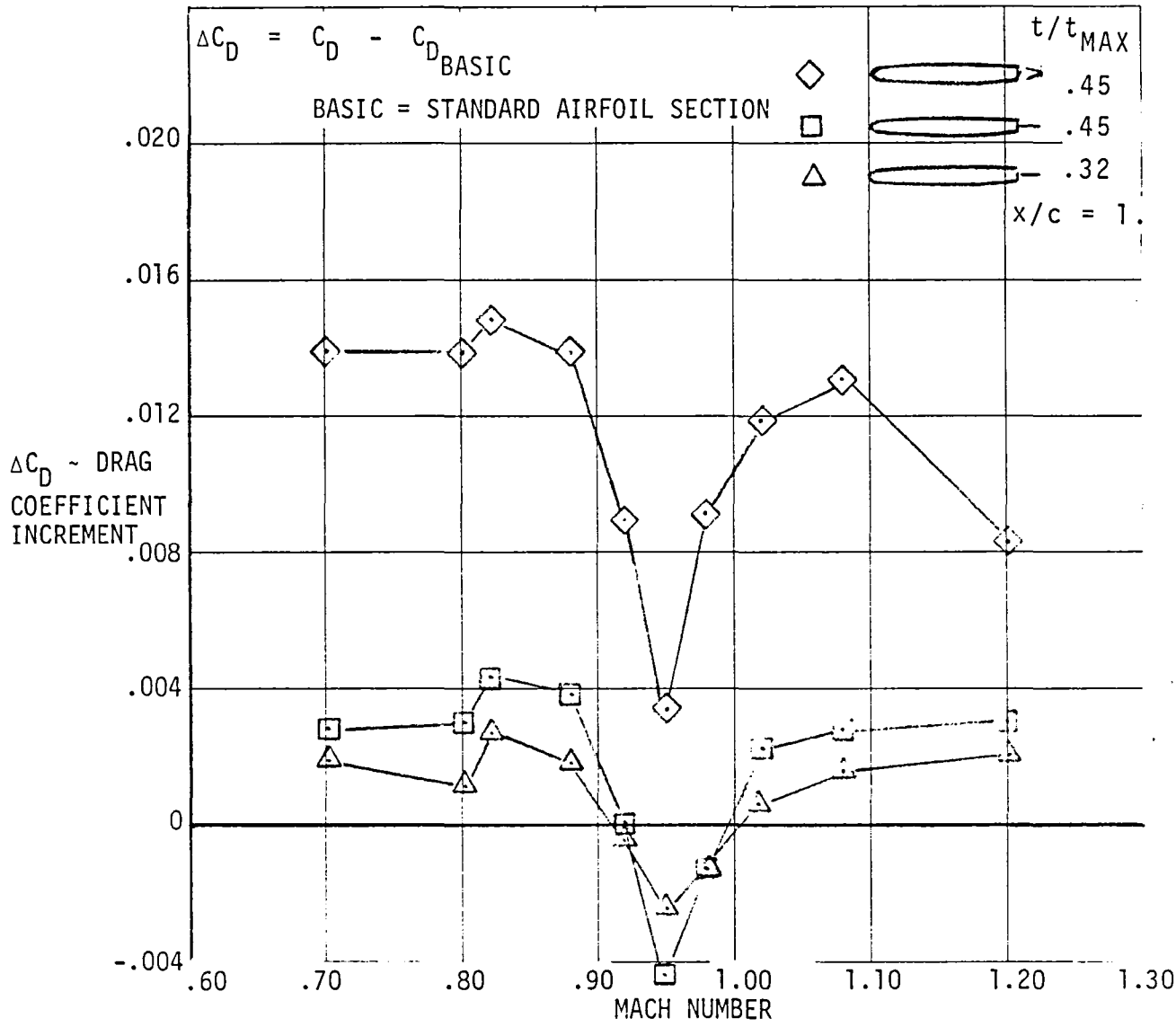

Figure 7-2 Effect of Airfoil Blunt Trailing Edge

SPLITTER PLATE

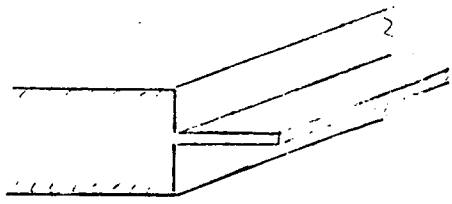

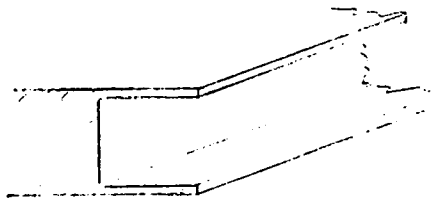

TRAILING EDGE CAVITY

VENTILATED TRAILING EDGE CAVITY

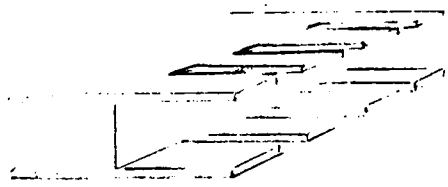

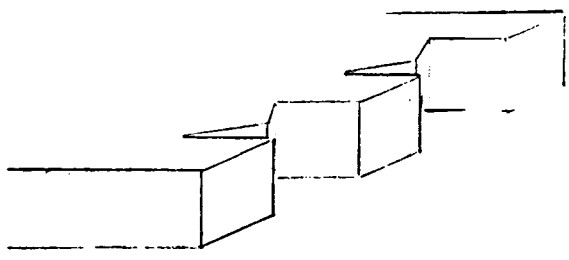

BROKEN TRAILING EDGE

Figure 7-3 Drag Alleviation Concepts

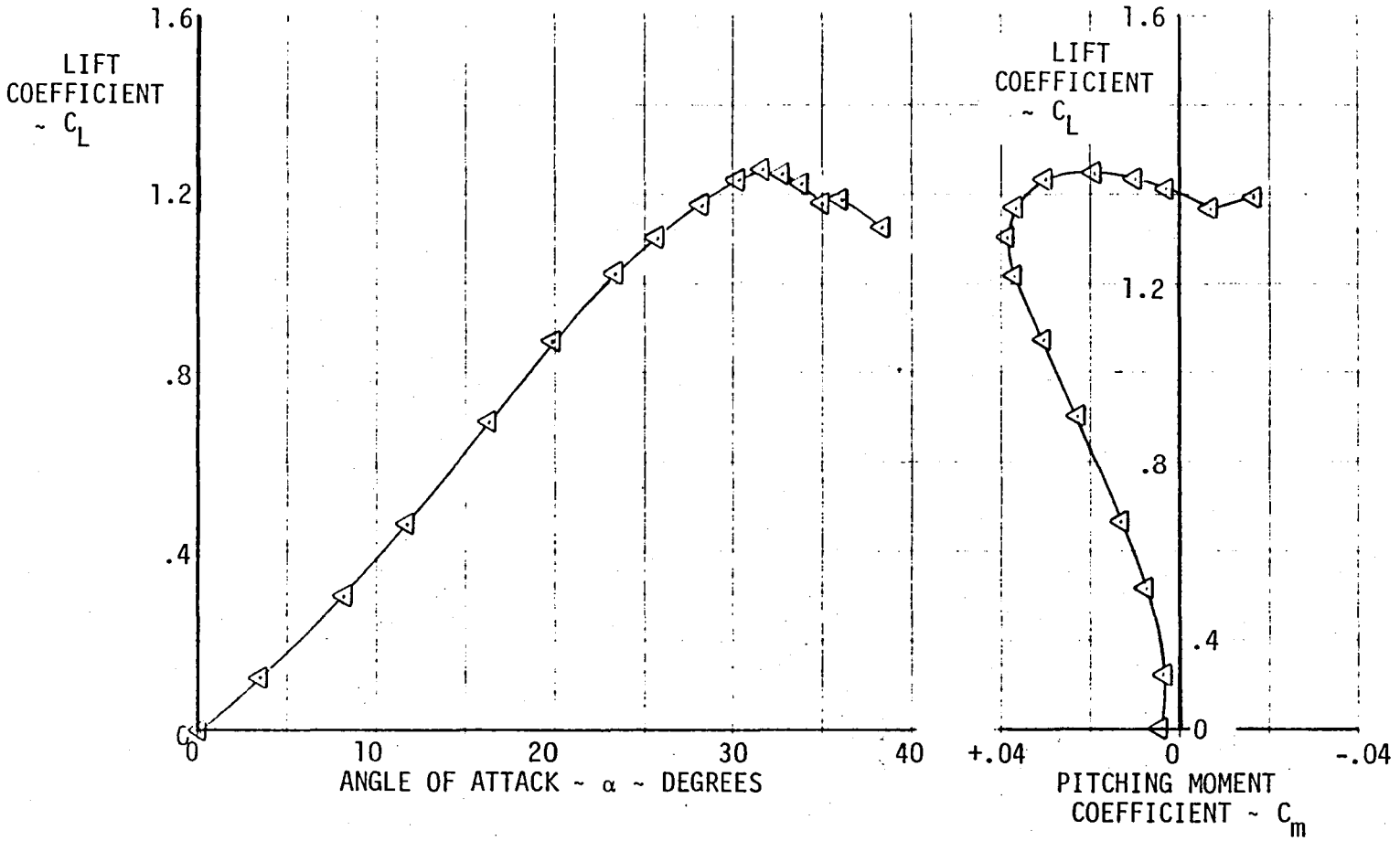

Figure 7-4 -035C High Angle of Attack Characteristics

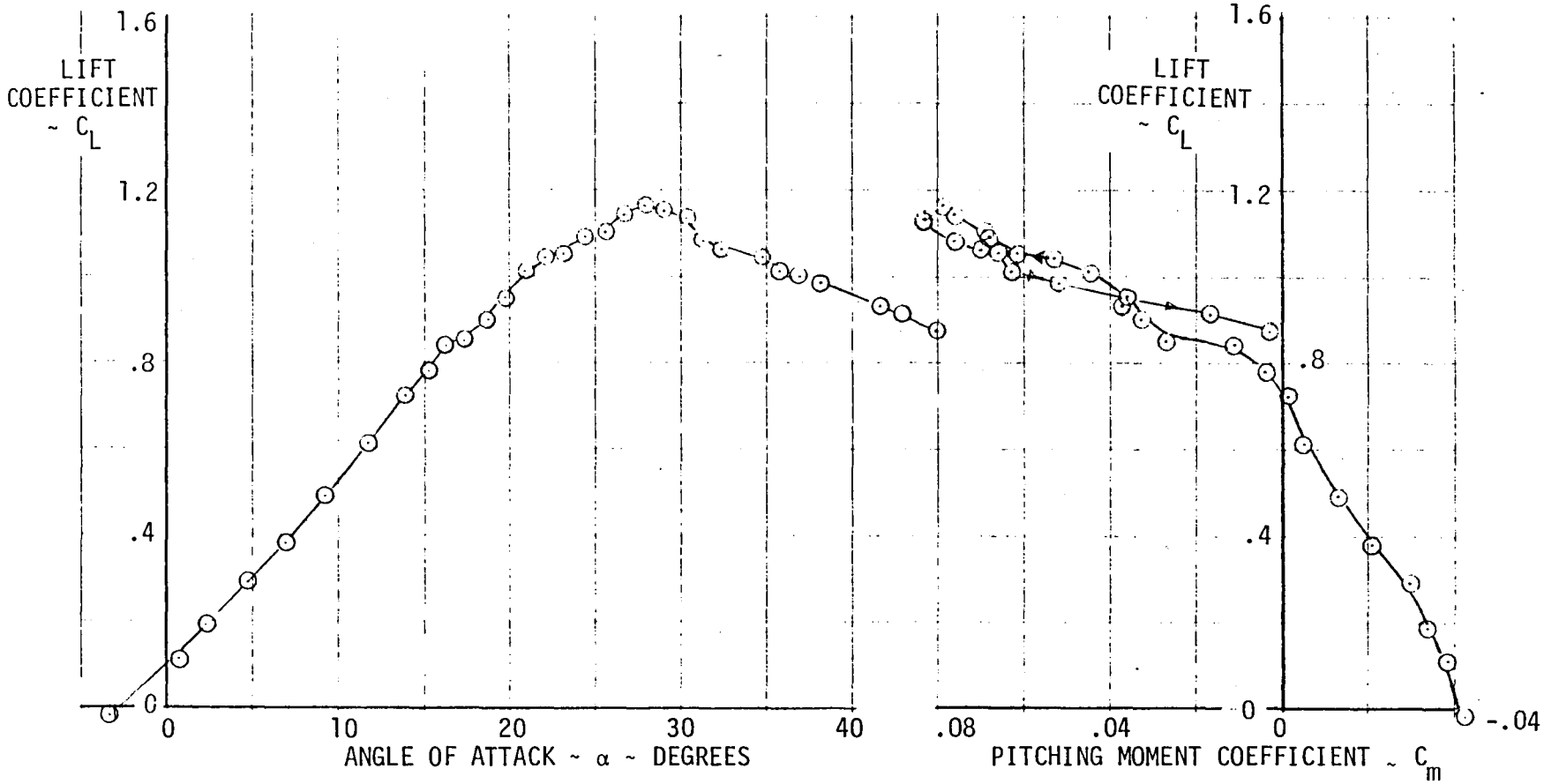

Figure 7-5 Supercruiser High Angle of Attack Characteristics

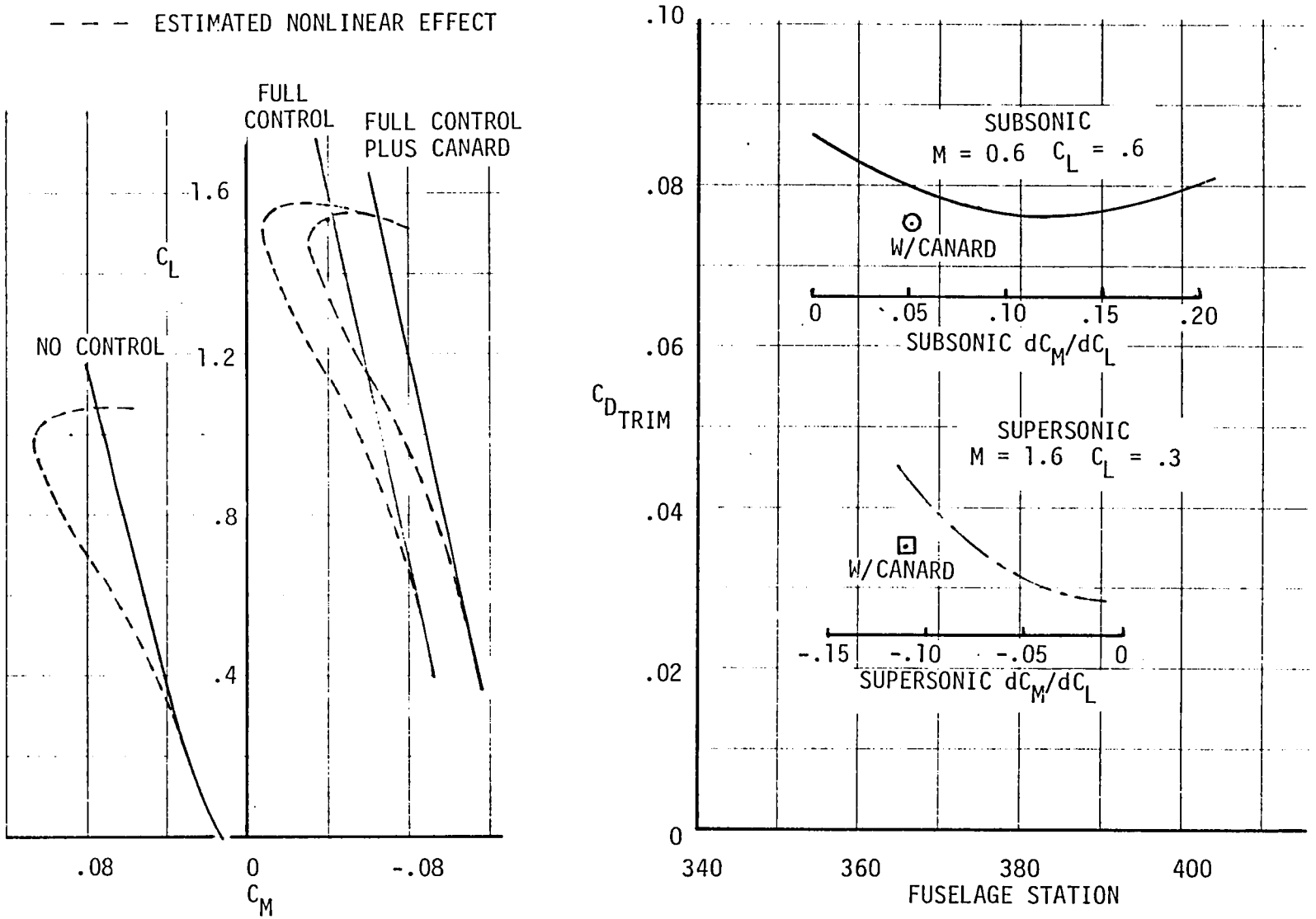

Figure 7-6 Canard Trimmer Benefits

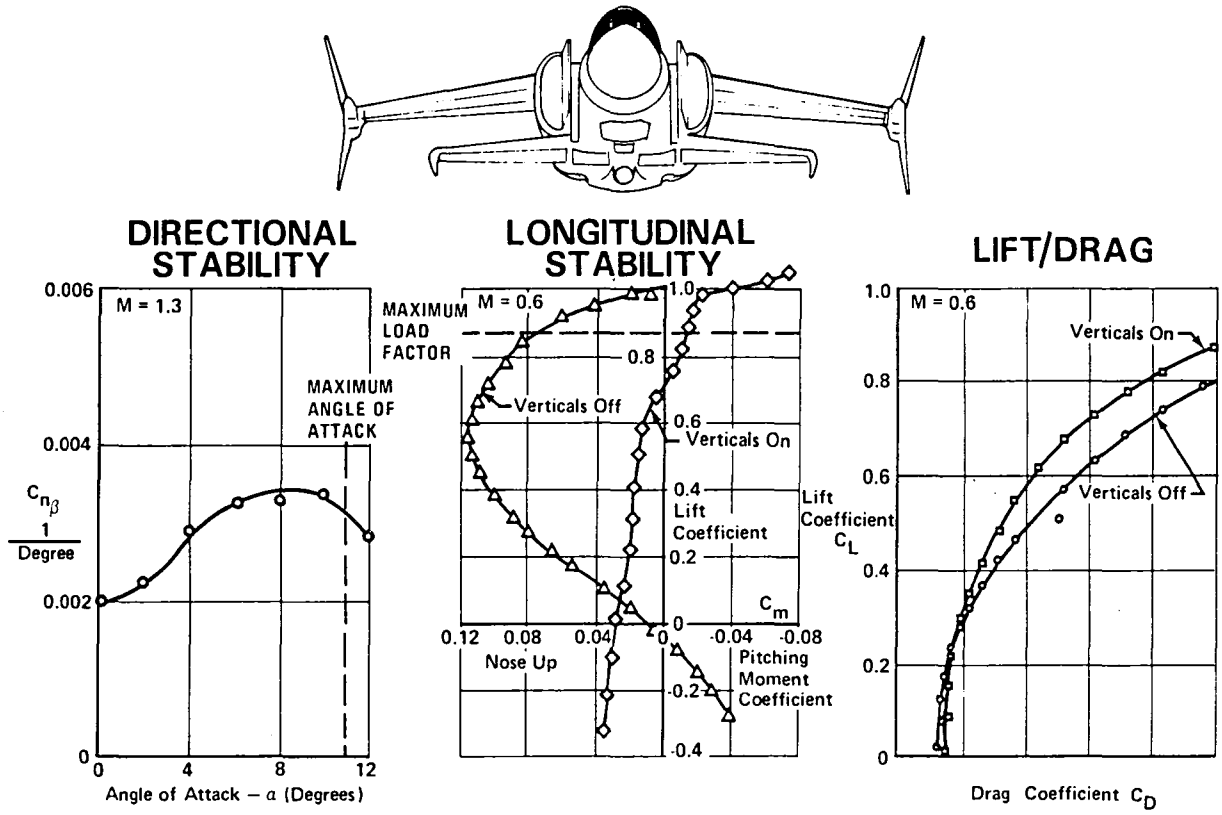

Figure 7-7 Favorable Effects of Outboard Vertical Tails

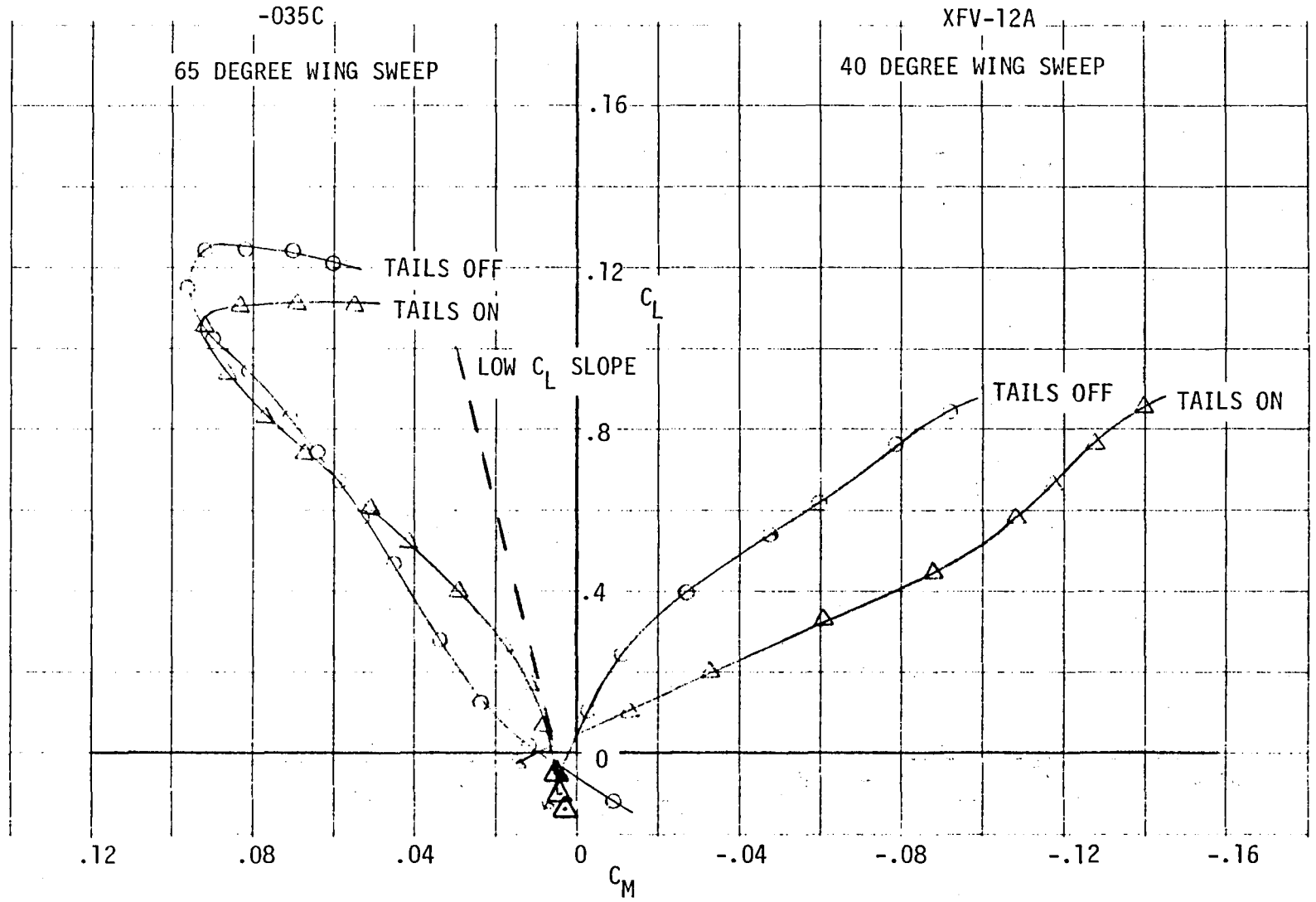

Figure 7-8 Effect of Wing Sweep on Wing Tip Vertical Tails

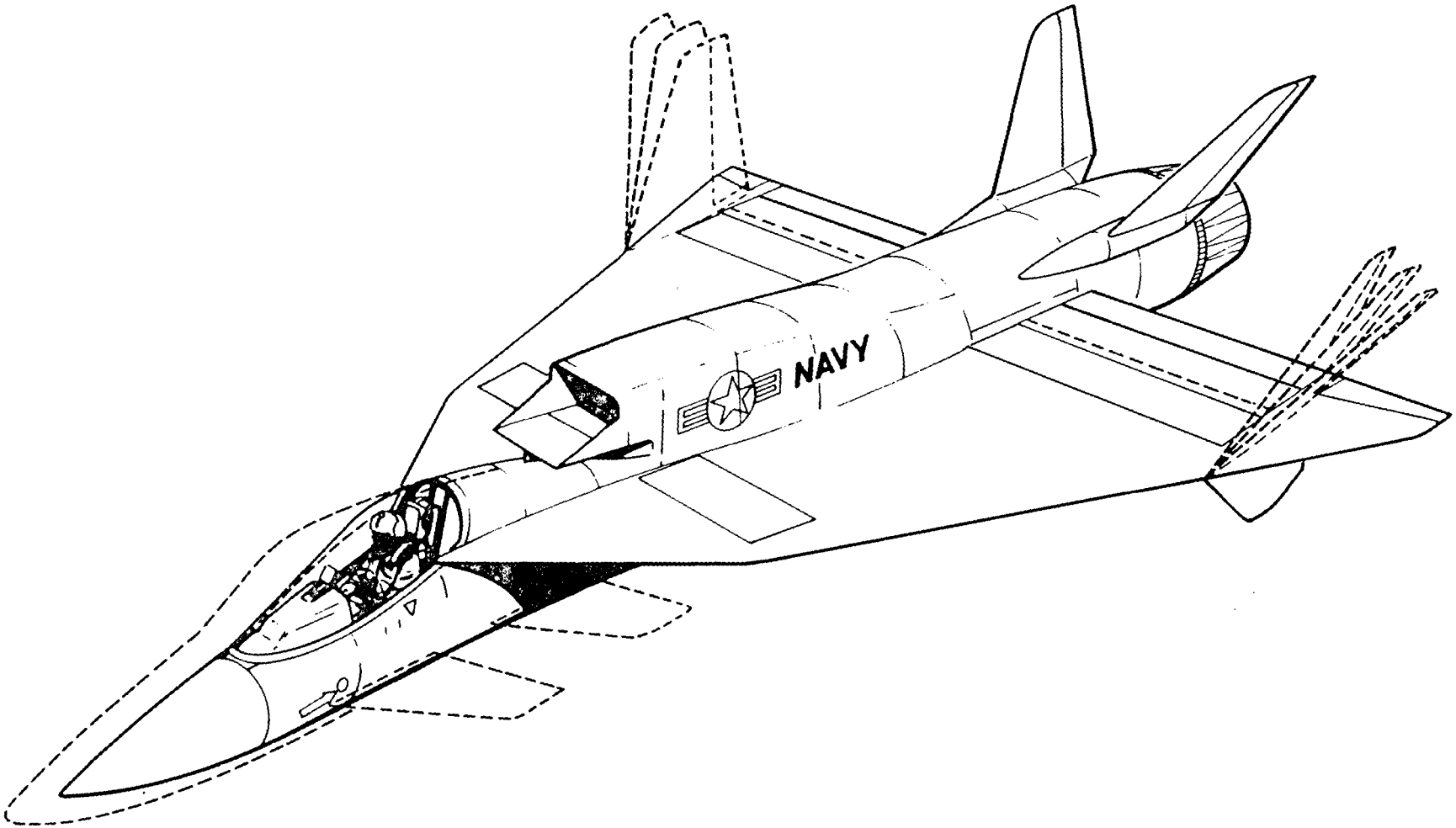

Figure 7-9 Configuration Variations

8.0 PROPOSED RESEARCH PROGRAM

8.1 OBJECTIVES

The basic objective of this proposed research program is the investigation of areas of aerodynamic uncertainty for which analytical methods are not available or their accuracy is suspect. The ultimate result is to enhance and expand the aerodynamic data base so that future high performance aircraft can be conceived and developed with a high degree of confidence in the success of the final article. In pursuit of the basic objective this research program will:

Explore the aerodynamic and aero/propulsion uncertainties identified in the Phase I study.

Assess the accuracy of analytical empirical methods.

Explore aerodynamic configuration components and arrangements that have the potential to enhance future Navy fighter/attack aircraft.

8.2 WIND TUNNEL MODEL SIZE

The proposed wind tunnel test program for Phase II of this study will utilize a flow-through duct, sting mounted model. Conceptual design studies based upon the final basic and alternate aircraft designs, Figures 3-1 and 3-4, have been conducted. These studies have concluded that an 8.5 percent model scale will offer the optimum model for resolution of aerodynamic uncertainties arising from analytical studies. A discussion of the scale selection criteria is contained in the following paragraphs.

8.2.1 Model Sizing Criteria

Compact-Multi Mission Propulsion Simulator Requirements - While the initial wind tunnel program will utilize flow through ducts, more definitive studies to follow would best be performed utilizing an on-board propulsion simulator able to simultaneously provide correct inlet flow and exhaust pressure ratios. An existing unit, currently undergoing preliminary tests at NASA Ames, would be used for this purpose. To correctly scale the aircraft design airflow of 280 lb/sec, the 1.65 lb/sec simulator would require a model scale shown below

$$\text{Scale Factor} = \sqrt{\frac{1.65}{280}} = 7.7 \text{ percent}$$

The physical dimensions of the simulator were obtained from the manufacturers of the unit.[a] While a detailed engineering study would be required of the proposed installation, it was highly doubtful that the simulator together with high pressure supply and bleed ducts could be accommodated in a 7.7 percent model without major compromise of the external aircraft scaled lines. Using a modest allotment for model wall thickness, it was estimated a model scale of 8.5 percent would be required

[a] Tech Development, Inc., Dayton, Ohio, Model 1230 - Simulator Drawing No. E19200.

to retain the integrity of external contours. At this scale, approximately 81 percent of inlet flow would be attained.

Model Blockage - Tunnel Wall Interference - For low speed testing, presence of the tunnel walls affect the data measured. To minimize corrections model frontal areas are historically limited to 0.5 percent of the tunnel cross sectional area and model spans to less then 70 percent of tunnel widtn (References 8-1 and 8-2). The 12 foot tunnel (cross-sectional area = 100.3 sq ft) would allow a maximum model scale of 10.3 percent. Model span is less critical.

The transonic tunnel with vented walls acts to relieve wall effects. However, too large a model overcomes the ventilating effect. For the 11 foot transonic tunnel, the limiting size has been specified as a model with lifting area no larger than three percent of the tunnel cross section area. This would allow a model scale of 8.1 percent.

As a compromise, 8.5 percent scale was selected. The slight exceeding of the three percent lifting area criteria in the 11 foot tunnel is offset by the very small model span and aspect ratio which should have a favorable influence on wall effects. Using this scale, the supersonic shock patterns were investigated. Figure 8-1 shows the 9 x 7-foot tunnel installation and associated shock angles. Reflected waves, which could influence model pressure distributions and resultant measured loads, are located well aft of the model metric surfaces for this model size.

8.2.2 Model Support/Base End Treatment

To further assure that the 8.5 percent scale was satisfactory for the proposed wind tunnel program, detailed model layouts were made. The design guidelines were as follows:

1. Existing stings of sufficient size to accommodate expected running loads in all three tunnels and starting loads in the 9 X 7-foot tunnel should be used.

2. A 2.5 inch internal balance of at least 17.3 inches length should be accommodated.

3. The flow through duct should be provided an exit area at least 110 percent of the throat area to obtain maximum possible internal flow and maintain flow stability.

4. The scaled aircraft lines should be retained.

The results of the model layouts are shown in Figure 8-2. The Rockwell Task MK X balance is shown for illustration. This balance is one of 11 balances of this size owned by Rockwell (see Table 8-1) and in conjunction with the Ames balance inventory assures that the load ranges will be well matched to final selected test conditions. All external lines are preserved. In addition, sufficient internal room exists for scanivalve instrumentation to accommodate up to 192 individual pressure measurements.

Since all design criteria could be met and the model scale generally satisfied requirements for minimum interference, it was concluded that an 8.5 percent scale would be an optimal model size for the proposed test program.

TABLE 8-1

ROCKWELL BALANCES (2.5-INCH DIAMETER)

BALANCE	DIAMETER (IN.)	LENGTH (IN.)	RATED LOADS			
			N1 AND N2 EACH (LB)	Y1 AND Y2 EACH (LB)	C (LB)	RM (IN.-LB)
3161-B	2.5	15.000	1,000	500	200	2,000
Task MK IA	2.5	13.400	1,000	500	250	2,000
Task MK IIIC	2.5	13.640	1,400	700	280	2,000
Task MK VIIC	2.5	17.310	2,500	1,250	300	4,000
Task MK IX	2.5	15.740	1,500	750	200	4,000
Task MK XA	2.5	17.312	5,500	1,750	1,250	6,000
Task MK XIVB	2.5	16.137	4,500	2,250	700	3,800
Task MK XXV	2.5	17.312	5,500	2,750	1,250	5,000
Task MK XXVI	2.5	16.297	2,500	1,250	300	3,000
Task MK XXIX	2.5	16.477	2,500	1,250	300	3,000

8.3 WIND TUNNEL MODEL HARDWARE

8.3.1 Model Variables

A review has been conducted of the wind tunnel model variables required to address uncertainties in the proposed Phase II test program. With one exception noted below, the variables are the same as those outlined in the proposal document for the present Phase I study (Reference 8-3).

The recommended model variables include:

Fuselage Group -

- Baseline Ducted Fuselage
- Variable Canopy Shape (2)
- Variable Forebody Shape (2)
- Extended Length Forebody (Constant Cross Section Plug Added to Baseline Fuselage)
- Removeable Forebody Strake (1)
- Canard Longitudinal Position (2)

Wing Group -

- Wing Planform (2-Basic and Alternate) Control Surfaces will be provided for both wings
- Wing Leading Edge Vortex Flap (1 Deflection)
- Elevon - 2 Segment - Extended Chord (5 Deflections)
- Elevon - 2 Segment - Short Chord (3 Deflections)
- Elevon - Blunt Trailing Edge with Alternate Training Edge Treatment (3 Deflections)

  Note: The blunt trailing edge elevon is an addition to the model variable list. A wing leading edge droop has been deleted.

8.3.2 Wind Tunnel Model Instrumentation

The proposed model instrumentation is outlined below. No changes in instrumentation requirements have been made from those outlined in the Phase I proposal (Reference 8-3).

- Internal 2.5 inch diameter balance. NASA Ames will supply this balance or a Rockwell owned unit may be substituted.
- A scanivalve type multiple pressure scanning device will be located in the fuselage. NASA Ames will supply this equipment or a Rockwell unit may be selected from present inventory.
- Wing Surface Pressure Taps. The number of orifices will be determined at the beginning of the Phase II contract.
- Flow-through duct exit pressure rake for internal drag determination. Rake will be sting mounted and will be calibrated in the laboratory prior to testing.
- Engine inlet pressure rake-fuselage mounted-removable. This rake will not be used while aerodynamic force data is being collected.
- Dynamic pressure transducers on each wing planform for wing buffet detection.

8.3.3 Model Support Hardware

Existing NASA Ames wind tunnel stings will be used if possible. The model base will accommodate sting sizes up to 2.75-inches diameter. Should studies at the beginning of Phase II indicate the requirement for special stings, the contractor will design and fabricate this hardware. Model angle of attack and yaw requirements in the 11-foot and 9 X 7-foot wind tunnels will require a single bent sting support (see Figure 8-3). The 12-foot tunnel will require an adapter to extend the basic support system angle of attack capabilities for select configurations.

8.4 WIND TUNNEL TEST PLAN

8.4.1 General

A detailed discussion of the contractor's approach to the wind tunnel program was originally presented in Reference 8-3 (see pp 2-56 to 2-66). This discussion covered model design and fabrication approach, model and support dimensional verification, documentation and report contents, coordination schedules with NASA personnel and a detailed breakdown of personnel support during the test phase. There are no changes to the general approach to the proposed Phase II tests.

8.4.2 Wind Tunnel Test Program

A preliminary proposed test plan is shown in Table 8-2. Tests are planned in the Ames 12 foot, 11 foot, and 9 x 7 foot wind tunnels to resolve the uncertainties and to obtain a complete set of stability and control data on the baseline and alternate configurations. It is planned to begin in the 12 foot tunnel in order to obtain preliminary data at low speed so as to have data on which to base the test run schedule in the 11 foot tunnel, which will be the second test scheduled.

The proposed program (Table 8-2) is presented in tabular form, grouped as described below.

- Group 1 is a Mach number series to moderate angles of attack to assess the basic drag and stability characteristics of the baseline and alternate configurations.
- Group 2 is a limited Mach number series at moderate angles of attack to assess the drag reduction potential of various wing trailing edge treatments.
- Group 3 is a complete Mach number series at moderate angles of attack to assess basic stability and control and trim drag characteristics.
- Group 4 is a subsonic Mach number series to high angles of attack to assess stability and control characteristics.
- Group 5 is a Mach number series to high angles of attack subsonically and transonically, to moderate angles of attack supersonically to assess inlet performance and the interference effects of various components on inlet performance.
- Group 6 is a limited Mach number series to high angles of attack subsonically and moderate angles of attack supersonically to assess the benefits of wing tip mounted vertical tails.

TABLE 8-2

TEST PROGRAM - MODEL NOMENCLATURE

B_1 - BASELINE FUSELAGE

B_2 - FUSELAGE, EXTENDED LENGTH

B_3 - FUSELAGE - ALTERNATE FOREBODY SHAPE

St_1 - FUSELAGE STRAKE

K_1 - CANOPY - BASELINE

K_2 - CANOPY - ALTERNATE

r_1 - INLET PRESSURE RAKE

δ_a - AILEVATOR DEFLECTION ANGLE

δ_c - CANARD INCIDENCE ANGLE

δ_e - ELEVON DEFLECTION ANGLE

δ_R - RUDDER DEFLECTION ANGLE

W_1 - WING - BASELINE

W_2 - WING - ALTERNATE

W_3 - WING - BASELINE WITH TIPS REMOVED

E_1 - ELEVON/AILEVATOR - SHORT CHORD

E_2 - ELEVON/AILEVATOR - EXTENDED CHORD

E_3 - ELEVON - BLUNT TRAILING EDGE - BASIC

E_4 - ELEVON - BLUNT TRAILING EDGE - #2

E_5 - ELEVON - BLUNT TRAILING EDGE - #3

E_6 - ELEVON - BLUNT TRAILING EDGE - #4

F_1 - LEADING EDGE VORTEX FLAPS

V_1 - VERTICAL TAIL - FUSELAGE MOUNTED

V_2 - VERTICAL TAIL - WING TIP MOUNTED - CANT ANGLE #1

V_3 - VERTICAL TAIL - WING TIP MOUNTED - CANT ANGLE #2

V_4 - VERTICAL TAIL - WING TIP MOUNTED - CANT ANGLE #3

R_1 - RUDDER

C_1 - CANARD - FORWARD FUSELAGE STATION

C_2 - CANARD - AFT FUSELAGE STATION

GROUP	CONFIGURATION	$\alpha°$	$\beta°$	$\delta_c°$	$\delta_R°$	$\delta_a°$	$\delta_e°$	MACH NUMBER 0.2	0.6	0.8	0.9	1.2	1.4	1.6	1.8
1	B_1K_1	VAR	0					X	X	X	X	X	X	X	X
	$B_1K_1V_1R_1$	VAR	0		0			X	X	X	X	X	X	X	X
	$B_1K_1W_1E_1V_1R_1$	VAR	0		0	0	0	X	X	X	X	X	X	X	X
	$B_1K_1W_2E_3V_1R_1$	VAR	0		0	0	0	X	X	X	X	X	X	X	X

TABLE 8-2 Continued

TEST PROGRAM

GROUP	CONFIGURATION	$\alpha°$	$\beta°$	$\delta_c°$	$\delta_R°$	$\delta_a°$	$\delta_e°$	MACH NUMBER 0.2	0.6	0.8	0.9	1.2	1.4	1.6	1.8
2	$B_1K_1W_2E_4V_1R_1$	VAR	0	–	0	0	0		X		X	X		X	
	$B_1K_1W_2E_5V_1R_1$	↓	↓	↓	↓	↓	↓		X		X	X		X	
	$B_1K_1W_2E_6V_1R_1$								X		X	X		X	
3	$B_1K_1W_1E_1V_1R_1$	VAR	0	-	0	0	10	X	X	X	X	X	X	X	X
		↓	↓	↓	↓	↓	20	X	X	X	X				
							30	X	X	X	X				
							-10					X	X	X	X
							-20					X	X	X	X
						±10	0	X	X	X	X	X	X	X	X
						±20	0	X	X	X	X	X	X	X	X
						30	30	X							
						±30	0	X	X	X	X	X	X	X	X
		0	VAR		0	0	0	X	X	X	X	X	X	X	X
		VAR	5°		0	0		X	X	X	X	X	X	X	X
	$B_1K_1W_2E_3V_1R_1$	VAR	0	-	0	0	10	X	X	X	X	X	X	X	X
		↓	↓	↓	↓	↓	20	X	X	X	X	X	X	X	X
							30	X	X	X	X	X	X	X	X
						±10	0	X	X	X	X	X	X	X	X
						±20	0	X	X	X	X	X	X	X	X
						±30	0	X	X	X	X	X	X	X	X
		0	VAR	-	0	0	0	X	X	X	X	X	X	X	X
		VAR	5°	-	0	0	0	X	X	X	X	X	X	X	X
	$B_1K_1W_1E_2V_1R_1$	VAR	0	-	0	0	1	X	X	X	X	X	X	X	X
		↓	↓	↓	↓	0	10	X	X	X	X	X	X	X	X
						0	20	X	X	X	X	X	X	X	X
						0	30	X	X	X	X	X	X	X	X
		0	VAR	-	0	0	0	X	X	X	X	X	X	X	X
		VAR	5°	-	0	0	0	X	X	X	X	X	X	X	X

							10	X	X	X	X				
							20	X	X	X	X				
							30	X	X	X	X				
	$B_1K_1W_1E_1V_1R_1$	VAR	0	-	10	0	0	X	X	X	X	X	X	X	X
					20			X	X	X	X	X	X	X	X
					30			X	X	X	X	X	X	X	X
					0	±10		X	X	X	X	X	X	X	X
					0	±20		X	X	X	X	X	X	X	X
	$B_1K_1W_2E_3V_1R_1$	VAR	0	-	10	0	0	X	X	X	X	X	X	X	X
					20			X	X	X	X	X	X	X	X
					30			X	X	X	X	X	X	X	X
					0	±10		X	X	X	X	X	X	X	X
					0	±20		X	X	X	X	X	X	X	X
	$B_1K_1W_1E_1C_1V_1R_1$	VAR	0	0	0	0	0	X	X	X	X	X	X	X	X
				-15				X							
				-30				X							
				-30	0	+30	30	X							
	$B_1K_1W_1E_1C_2V_1R$	VAR	0	0	0	0	0	X	X	X	X	X	X	X	X
				-15				X							
				-30				X							
				-30	0	30	30	X							
	$B_1K_1St_1W_1E_2V_1R_1$	VAR	0	-	0	0	0	X	X	X	X	X	X	X	X
			5	-	0	0	0	X	X	X	X				
4	$B_1K_1W_1E_1V_1R_1$	VAR	0	-	0	0	0	X							
	$B_1K_1W_1E_1V_1R_1$	VAR	10	-	0	0	0	X							
	$B_1K_1W_1E_1V_1R_1$	VAR	0	-	0	30	30	X							

TABLE 8-2 Continued

TEST PROGRAM

GROUP	CONFIGURATION	$\alpha°$	$\beta°$	$\delta_c°$	$\delta_R°$	$\delta_a°$	$\delta_e°$	MACH NUMBER 0.2	0.6	0.8	0.9	1.2	1.4	1.6	1.8
4	$B_1K_1W_2E_3V_1R_1$	VAR	0	-	0	0	0	X							
		VAR	10	-	0	0	0	X							
		VAR	0	-	0	30	30	X							
5	$B_1K_1W_1E_1V_1R_1r_1$	VAR	0	-	0	0	0	X		X	X	X		X	
		10	VAR	-	↓	↓	↓	X			X	X			
		20	VAR	-				X							
	$B_1K_1W_1E_1C_1V_1R_1r_1$	VAR	0	0				X		X	X	X		X	
		10	VAR	0				X			X	X			
		20	VAR	0				X							
	$B_1K_1W_1E_1C_2V_1R_1r_1$	VAR	0	-	0	0	0	X			X	X		X	
		10	VAR	-	0	0	0	X			X	X			
		20	VAR	-	0	0	0	X			X	X			
	$B_1K_2W_1E_1V_1R_1r_1$	VAR	0					X		X	X	X		X	
		10	VAR					X			X	X			
		20	VAR					X							
	$B_1K_1W_2E_1V_1R_1r_1$	VAR	0					X		X	X	X		X	
		10	VAR					X			X	X			
		20	VAR					X							
	$B_2K_1W_1E_1V_1R_1r_1$	VAR	0					X		X	X	X		X	
		10	VAR					X			X	X			
		20	VAR					X							
	$B_1K_1St_1W_1E_2V_1R_1r_1$	VAR	0					X		X	X	X		X	
		10	VAR					X			X	X			
		20	VAR	↓	↓	↓	↓	X							
	$B_3K_1W_1E_1V_1R_1r_1$	VAR	0	-	0	0	0	X		X	X	X		X	
		10	VAR	-	0	0	0	X			X	X			
		20	VAR	-	0	0	0	X			X	X			

TABLE 8-2 Concluded

TEST PROGRAM

GROUP	CONFIGURATION	$\alpha°$	$\beta°$	$\delta_c°$	$\delta_R°$	$\delta_a°$	$\delta_e°$	MACH NUMBER 0.2	0.6	0.8	0.9	1.2	1.4	1.6	1.8
6	$B_1K_1W_3E_1$	VAR	0	-		0	0	X	X		X	X		X	
	$B_1K_1W_3E_1$	VAR	5	-		0	0	X	X		X	X		X	
	$B_1K_1W_3E_1V_2R_1$	VAR	0	-	0	0	0	X	X		X	X		X	
	$B_1K_1W_3E_1V_2R_1$	VAR	5	-	0	0	0	X	X		X	X		X	
	$B_1K_1W_3E_1V_3R_1$	VAR	0	-	0	0	0	X							
	$B_1K_1W_3E_1V_3R_1$	VAR	5	-	0	0	0	X							
	$B_1K_1W_3E_1V_4R_1$	VAR	0	-	0	0	0	X							
	$B_1K_1W_3E_1V_4R_1$	VAR	5	-	0	0	0	X							

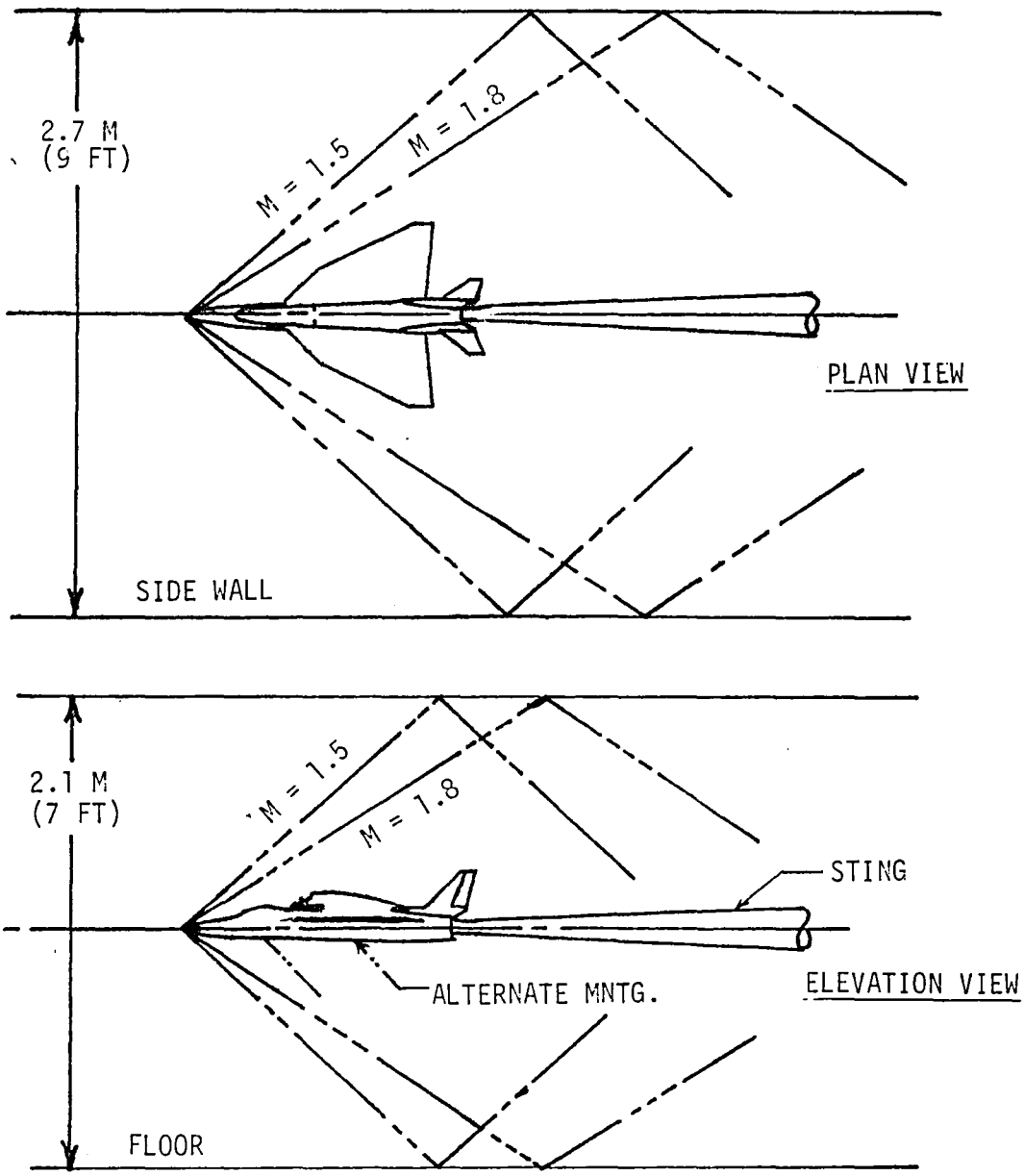

.085 SCALE BASELINE MODEL
AMES 9 x 7 WIND TUNNEL ENVELOPE

Figure 8-1 Shock Rhombus with 8.5 Percent Scale Model Installed in Ames 9 x 7 Foot Wind Tunnel

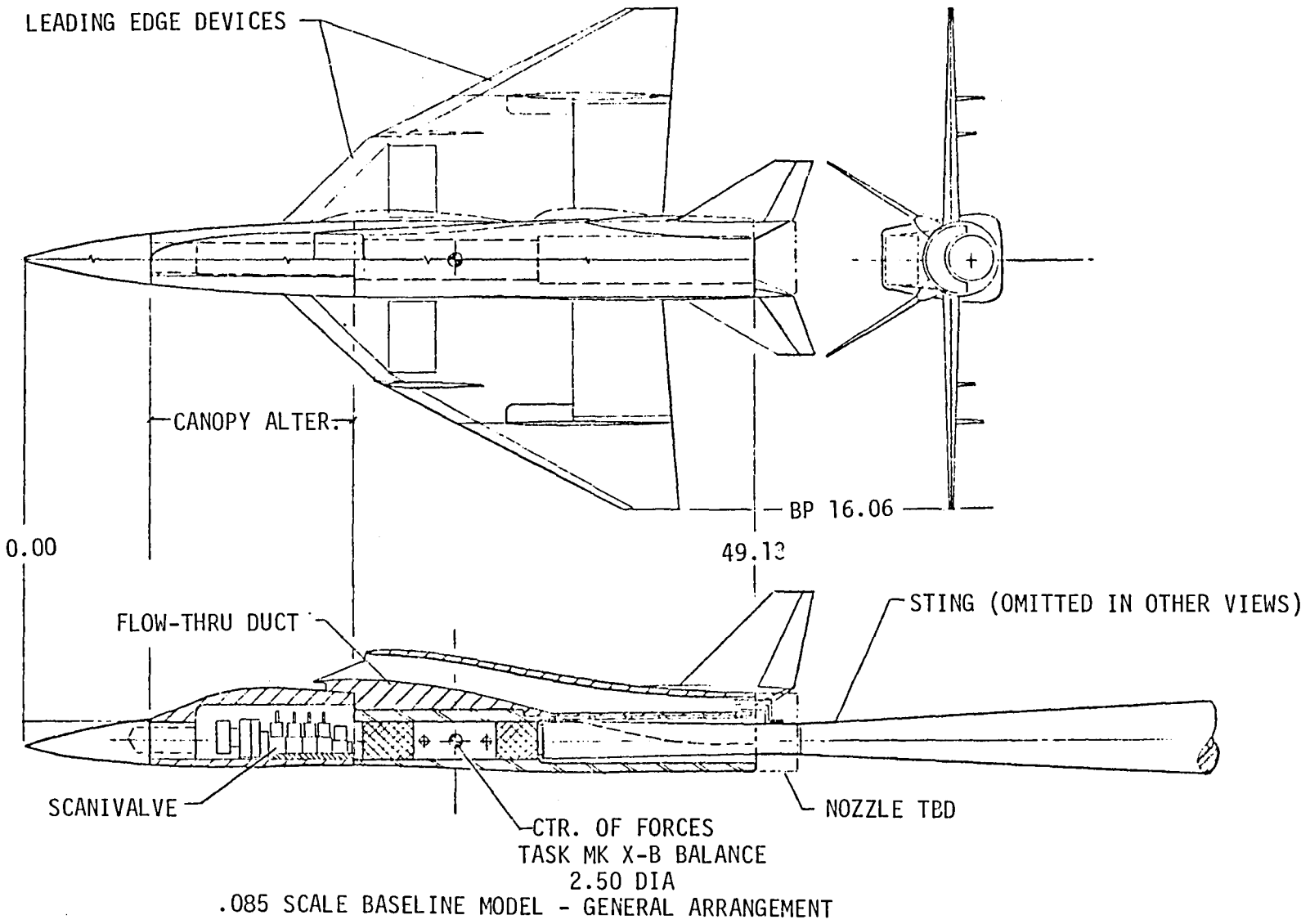

Figure 8-2 Wind Tunnel Model Details

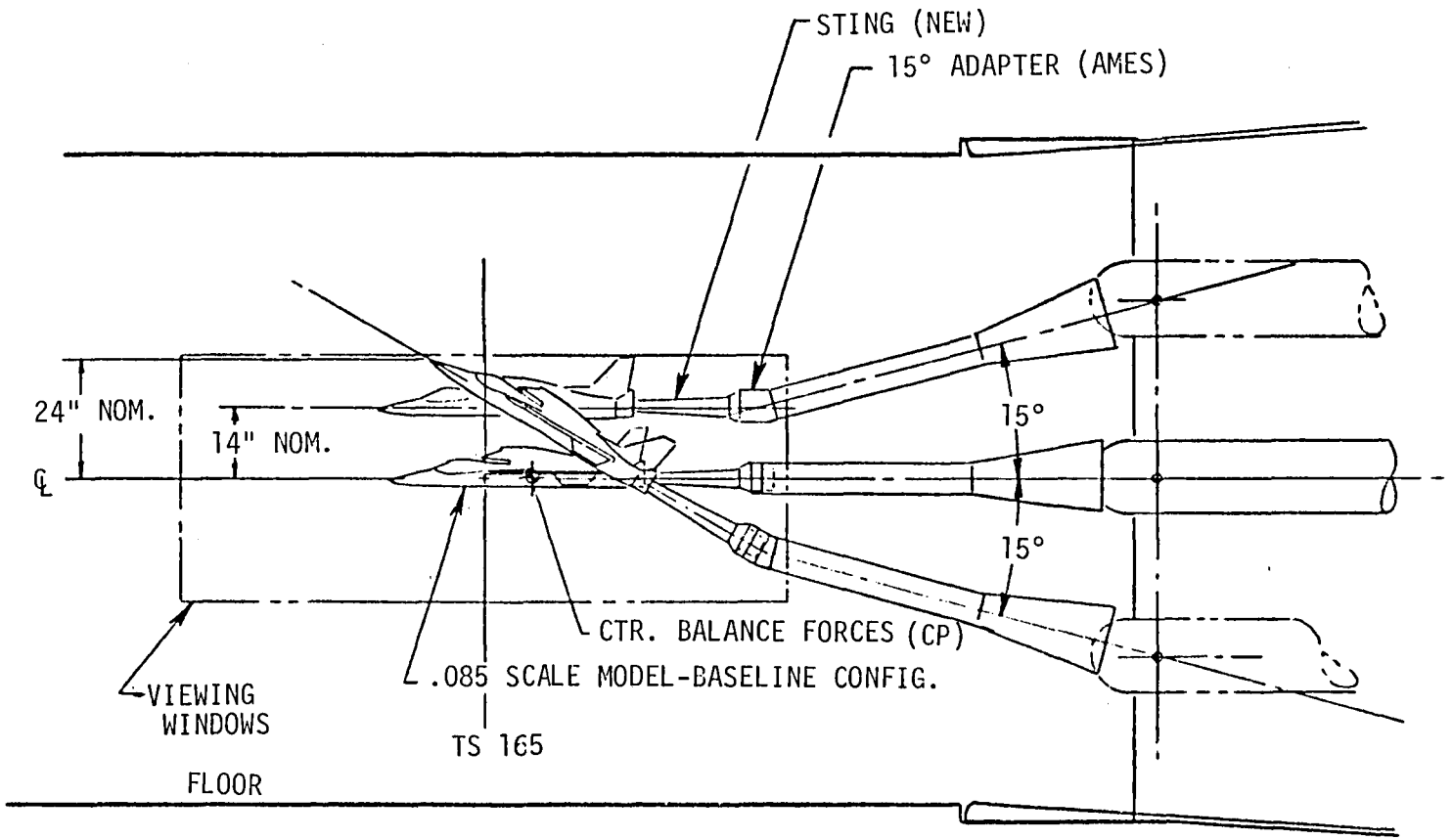

Figure 8-3 Ames 11 x 11 Foot Transonic Test Section Installation

9.0 CONCLUSIONS

The potential of a pair of thrust augmenter wing supersonic V/STOL aircraft concepts designed to fulfill the Navy fighter/attack role has been studied in some detail. Systems and structural investigations were carried out to the extent necessary to ensure a credible design. These studies determined the following:

1. Thrust augmented wing aircraft provide feasible configurations to satisfy the post 1990 shipboard V/STOL fighter/attack requirement.

2. The alternate configuration (with the longitudinally oriented forward augmenter) provided performance superior to that of the baseline configuration and greater flexibility in design. In order to achieve this capability, the wing base drag must be eliminated, which limited test data show is possible.

3. Uncertainties in the prediction accuracy of friction, wave base, and trimmed drag and the stability and control characteristics at high angles of attack all have a significant impact on the design of the aircraft.

4. The high angle of attack longitudinal stability and control characteristics cannot be predicted by available methods.

5. The use of a top of the fuselage mounted inlet provides advantages in reingestion, stealth, and FOD but operation behind a canopy and forward fuselage produce unknowns that must be evaluated in test. Lifting surface shielding of top mounted inlets with fuselage strakes has been shown to greatly enhance their performance.

6. Auxiliary trimming devices such as canards can be used to reduce the trimmed drag-due-to-lift at subsonic and supersonic speeds and enhance the control power throughout the flight envelope.

7. Vertical tails mounted on the wing tips can be used to increase longitudinal and directional stability, reduce drag-due-to-lift (increase effective aspect ratio), and reduce the aerodynamic center shift between subsonic and supersonic speeds. They can also be used to significantly reduce wing span for improved carrier deck spotting. However, limited wind tunnel data indicate that their benefits disappear on wings with high leading edge sweep angles.

8. Additional low speed testing is required to enable satisfactory prediction and refinement of the STO/Conversion characteristics of closely coupled tandem augmenters.

10.0 REFERENCES

1 W. P. Nelms: "Studies of Aerodynamic Technology for VSTOL Fighter/Attack Aircraft." AIAA Paper 78-1511, AIAA Aircraft Systems and Technology Conference, Los Angeles, California, August 21-23, 1978.

1-1 J. R. Lummus et al.: "Study of Aerodynamic Technology for VSTOL Fighter/Attack Aircraft." NASA CR-152128, 1978.

1-2 W. R. Burhans et al.: "Study of Aerodynamic Technology for VSTOL Fighter/Attack Aircraft." NASA CR-152129, 1978.

1-3 S. H. Brown et al.: "Study of Aerodynamic Technology for VSTOL Fighter/Attack Aircraft - Horizontal Attitude Concept." NASA CR 152130, 1978.

1-4 Gerhardt, H. A., and Chen, W. S., "Study of Aerodynamic Technology for V/STOL Fighter/Attack Aircraft - Vertical Attitude Concept," NASA CR152131, dated May 1978.

1-5 H. H. Driggers et al.: "Study of Aerodynamic Technology for VSTOL Fighter/Attack Aircraft." NASA CR-152132, 1978.

1-6 Tyler, J. T., "An Assessment of Sea Based Air Master Study," AIAA Paper 80-1820, AIAA Aircraft Systems Meeting, Anaheim, California, August 4-6, 1980.

1-7 Bonner, E., Clever, W., and Dunn, K., "Aerodynamic Preliminary Analysis System II," NASA CR 165627, April 1981.

1-8 "USAF Stability and Control Digital DATCOM," AFFDL-TR-79-3032, April 1979.

2-1 Torenbuk, E., "Synthesis of Subsonic Airplane Design," Delft University Press, 1976.

2-2 Cleary, J. W., and Stevens, G. L., "The Effects at Transonic Speeds of Thickening the Trailing Edge of a Wing With a 4 Percent Thick Circular Arc Airfoil," NACA RM A51J11, October 1951.

2-3 Dugan, D. W., "Effects of Three Types of Blunt Trailing Edges on the Aerodynamic Characteristics of a Plane Tapered Wing of Aspect Ratio 3.1, With a 3 Percent Thick Biconvex Section," NACA RM A52E01, May 1952.

2-4 Nash, J. F., "A Discussion of Two Dimensional Turbulent Base Flow," Aeronautical Research Council R. and M. No. 3468, 1967.

4-1 Feagen, R. C., and Morrison, W. D., "Delta Method, An Empirical Drag Buildup Technique," Lockheed-California, NASA CR 15171, December 1978.

4-2 Raymer, Daniel P., "Developing an Aircraft Configuration Using a Minicomputer," Astronautics and Aeronautics Magazine, November 1979.

4-3 McCormick, B. W., Jr., "Aerodynamics of V/STOL Flight," Academic Press, New York-London 1967.

5-1 W. Walter and J. DeLany, "Stability Analysis of YF401 Engine in a XFV-12 Aircraft," AIAA-80-1246, July 1980.
5-2 T. L. Williams, W. P. Nelms, D. Smeltzer, "Top-Mounted Inlet System Feasibility for Transonic-Supersonic Fighter Aircraft," NASA TM 81292, April 1981.
5-3 W. R. Haagenson, et al., "Correlation between F-107A Airplane Flight Test and Model Data of Air Induction System Parameters," WADC TR59-440, July 1959.
5-4 Swavely, C. E., "Engine Flow Diverter System for the XFV-12A Prototype Aircraft," AIAA-74-1194, October 1974.
5-5 J. T. DeLany and G. M. Jenkins, "XFV-12A Propulsion System Development," ASME-76-GT-125, March 1976.
5-6 "SAE Aerospace Applied Thermodynamics Manual," October 1969.
5-7 Bevilaqua, P. M.," Lifting Surface Theory for Thrust Augmenting Ejectors," AIAA Journal May 1978, pp 475-480, May 1978.
5-8 Bevilaqua, P.M., and Combs, C. P., "Theory and Practice of Ejector Sealing," Proceedings at the Ejector Workshop for Space Applications, Dayton, Ohio, August 2-5, 1981.
5-9 Garland, D. B., "Phase 1 Wind Tunnel Tests of the J-97 Powered External Augmentor V/STOL Model," DeHavilland Report DHC-DND79-4 (NASA CR 152255), July 1980.
5-10 Garland, D. B., "Static Tests of the J-97 Powered, External Augmentor V/STOL Wind Tunnel Model," DeHavilland Report DHC-DND77-4 (NASA CR 152403), February 1978.
5-11 Garland, D. B., and Harris, J. L., "Phase 2 and 3 Wind Tunnel Tests of the J-97 Powered, External Augmentor V/STOL Model," DeHavilland Report DHC-DND 80-1 (NASA CR 152380), March 1980.

6-1 Fozard, J. W., "Ski-Jump - A Great Leap for Tactical Air Power," British Aerospace, Kingston-Brough Division, 1979.

7-1 Lomax, H., "The Wave Drag of Arbitrary Configurations in Linearized Flow as Determined by Areas and Force in Oblique Planes," NACA RM A55A18, 1955.
7-2 Jones, R. T., "Theory of Wing Body Drag at Supersonic Speeds," NACA TR1284, 1956.
7-3 Lamb, Milton, and McLean, F. Edward, "Evaluation of Techniques for Numerical Representation and Prediction of the Longitudinal Aerodynanic Characteristics of Supersonic Fighters," NASA TMX 2283, June 1971.
7-4 Mark, L., and DeHart, J., "High Speed Aerodynamic Design of an Innovative V/STOL Canard-Wing Configuration," AIAA Paper 76-910, AIAA Aircraft Systems and Technology Meeting, Dalls, Texas, September 27-29, 1976.

8-1 Pope, A., "Wind Tunnel Testing," John Wiley and Sons, 1954, New York, N.Y.
8-2 Pankhurst, R. C. and Holder, D. W., "Wind Tunnel Technique," Pitman and Sons, Ltd., London, 1948.
8-3 Anon, "Proposal For Study of Aerodynamic Technology for Single-Cruise-Engine V/STOL Fighter/Attack Aircraft," Rockwell Report NR80H-80, dated September 1980.

1. Report No.	2. Government Accession No.	3. Recipient's Catalog No.
NASA CR166270		

4. Title and Subtitle	5. Report Date
STUDY OF AERODYNAMIC TECHNOLOGY FOR SINGLE-CRUISE-ENGINE V/STOL FIGHTER/ATTACK AIRCRAFT	FEBRUARY 1982
	6. Performing Organization Code

7. Author(s)	8. Performing Organization Report No.
LEON MARK	NR81H-100
	10. Work Unit No.

9. Performing Organization Name and Address	11. Contract or Grant No.
ROCKWELL INTERNATIONAL 4300 E. FIFTH AVENUE P.O. BOX 1259 COLUMBUS, OHIO 43216	NAS2-11002
	13. Type of Report and Period Covered
12. Sponsoring Agency Name and Address NATIONAL AERONAUTICS & SPACE ADMINISTRATION, WASHINGTON DC 20546 DAVID TAYLOR NAVAL SHIP R&D CENTER, CARDEROCK, MD. 20034 NAVAL AIR SYSTEMS COMMAND, WASHINGTON, D.C. 20361	CONTRACTOR FINAL REPORT JUNE 1981 TO FEBRUARY 1982
	14. Sponsoring Agency Code RTOP 505-43-01

15. Supplementary Notes

TECHNICAL MONITORS: D.A. DURSTON/W.P. NELMS, NASA-AMES, MAIL STOP 227-2, MOFFETT FIELD CA 94035
(415)965-5855/5879, FTS 448-5855/5879
POINT OF CONTACT: J. H. NICHOLS, JR., DTNSRDC
POINT OF CONTACT: M. W. BROWN, NAVAIR

16. Abstract

Conceptual designs and analyses were conducted on two V/STOL supersonic fighter/attack aircraft. These aircraft feature low footprint temperature and pressure thrust augmenting ejectors in the wings for vertical lift, combined with a low wing loading, low wave drag airframe for outstanding cruise and supersonic performance.

Aerodynamic, propulsion, performance, and mass properties were determined and are presented for each aircraft. Aerodynamic and Aero/Propulsion characteristics having the most significant effect on the success of the up-and-away flight mode were identified, and the certainty with which they could be predicted was defined. A wind tunnel model and test program are recommended to resolve the identified uncertainties.

17. Key Words (Suggested by Author(s))	18. Distribution Statement
V/STOL Fighter/Attack Aerodynamics Thrust Augmenter Wing Clipped Delta Wing	~~FEDD Distribution~~ Subject Category 02

19. Security Classif. (of this report)	20. Security Classif. (of this page)	21. No. of Pages	22. Price*
UNCLASSIFIED	UNCLASSIFIED	234	

Available: NASA's Industrial Applications Centers

End of Document